Normandie Université

THÈSE

Pour obtenir le diplôme de doctorat

Spécialité GENIE CIVIL

Préparée au sein de l'Université de Caen Normandie

Béton Biosourcé Isolant Semi-structurel et Etanche à l'eau

Présentée et soutenue par
Abdelrahman MOHAMAD

Thèse soutenue le 9/11/2021 devant le jury composé de		
M. Gilles ESCADEILLAS	Professeur, LMDC / INSA Toulouse	Rapporteur
Mme Siham KAMALI-BERNARD	Maître de conférences HDR, INSA Rennes	Rapportrice
Mr. Frédéric BECQUART	Maitre de conférences, IMT Lille Douai	Examinateur
Mme Fouzia KHADRAOUI	Enseignante chercheure, ESITC Caen	Co-encadrante
Mr. Mohamed BOUTOUIL	Directeur de Recherche, ESITC Caen	Directeur de Thèse
Mr. Daniel CHATEIGNER	Professeur, Université Caen Normandie CRISMAT	Co-Directeur de Thèse

Thèse dirigée par Mohamed BOUTOUIL (ESITC Caen) et Daniel CHATEIGNER (CRISMAT-Unicaen) et co-encadrée par Fouzia KHADRAOUI (ESITC CAEN)

UNIVERSITÉ CAEN NORMANDIE

ESITC CAEN
Ecole Supérieure d'Ingénieurs des Travaux de la Construction

ED 591 PSIME

RISMA

Acknowledgments

My first thanks are addressed to my thesis supervisor Mr. Mohamed BOUTOUIL, director of research at ESITC Caen, and to my co-thesis supervisor Mr. Daniel CHATEIGNER, professor at the CRISMAT laboratory. I would like to thank them first of all for the quality of their scientific supervision, their availability, but also for their human qualities which allowed me to greatly appreciate these three years spent in the laboratory of ESITC Caen.

I would like to express my gratitude to my supervisor Mrs. Fouzia KHADRAOUI, who has been my daily supervisor, very present throughout the thesis to train me, guide me, boost me, etc. Thank you for teaching me and supporting me to progress not only in the field of research but also on a personal level. Thank you for your kindness and availability, as well as for your support in the difficult moments of the thesis.

I would also like to thank the members of the jury, Mr. Gilles ESCADEILLAS, Mrs. Siham KAMALI-BERNARD and Mr. Frédéric BECQUART, for having accepted and taken the time to evaluate this manuscript and this thesis work. Their remarks and the discussion during the defense really allow to consider many follow-ups to this thesis.

Also, I would like to thank Mr. Nassim SEBAIBI, Scientific Manager at ESITC Caen. He always knew how to listen to me, and his permanent support was really precious.

Also, thanks to all the teachers, staff members in ESITC Caen who shared their experiences with me, Hamze KARAKY, Amal BOURGUIBA, Mohammed-Hicham BENZAAMA, Aurélie FABIEN, Karim TOUATI, Malo LEGUERN and the Head of Materials Axis, Professor Yassine EL-MENDILI.

Finally, a huge thought for my friends, the PhD students, Farjallah ALASSAAD, Marine GEORGES, Manal BOUASRIA, Bechara HADDAD, Houssam AFFAN, Manon ARRETEAU, Athmane AZIL, Mohamed-Ali HAMDAOUI and Benjamin DELESTRE with whom I exchanged a lot, laughed, debated, the coffee breaks will remain memorable. It was a real pleasure to work with you daily.

A special thanks to my family and friends for their support and for having been present on the day of the defense, it was a real motivation to have them with me.

A mes chers parents Fatmé et Chahir, et mes chères sœurs
Racha, Amani, Nour et Farah pour être incessamment présents
à mes côtés avec la seule intention de me voir content de mon
parcours…

إلى أعز الناس وأقربهم إلى قلبي...
إلى والدتي ووالدي واخواتي...
الذين كانوا دائماً عوناً وسنداً لي...

شكراً جزيلاً

Summary

Abbreviations

Symbol	Unit	Indication
LC	-	Lightweight concrete
P_{int}	Pa	Bubble internal pressure
P_{ext}	Pa	Bubble surrounding liquid pressure
γ	(J/m^2 or N/m)	Surface tension
R_1	m	Radius of curvature no. 1
R_2	m	Radius of curvature no. 2
ρ_d	Kg/m^3	Dry density
ρ	Kg/m^3	Bulk density
ρ_{abs}	Kg/m^3	Absolute density
λ	W/(m.K)	Thermal conductivity
R	(m^2.K/W)	Thermal resistance
R_c	MPa	Compressive strength
Rc_{28}	MPa	Compressive strength at 28-days
Rc_7	MPa	Compressive strength at 7-days
Rf	MPa	Flexural strength
φ	%	Porosity
w(t)	%	Water content
Δw	%	Retained water content
ε	%	Porosity accessible to water
C_a	kg/(m^2.$\sqrt{h}$)	Capillary absorption coefficient
Q	J/g	Hydration heat
Q_{acc}	J/g	Sum of the heat accumulated in the calorimeter
Q_{dis}	J/g	Heat dissipated to the outside
Wh	kg	Hemp shiv consumed water
Wt	kg	Total water
B	kg	Binder amount
r_{10}	mm	Radius at 10% passing
r_{50}	mm	Radius at 50% passing
r_{90}	mm	Radius at 90% passing
R_m	mm	Mean radius = r_{50}
UC	-	Uniformity coefficient = r_{10}/r_{90}
C_p	(J/kg.K)	Heat capacity
E_c	kWh	Cooling energy consumption
E_h	kWh	Heating energy consumption
Wt/B	-	Total water/Binder mass ratio
Wb/B	-	Water consumed by binder/Binder mass ratio
W/B	-	Water/Binder(s) mass ratio
CEM I	-	Ordinary portlandite cement – type 1
GGBFS	-	Ground granulated blast furnace slag
MK	-	Métakaolin
HS	-	Hemp shiv
SP	-	Superplasticizer
PZ	-	Pozzolanic additions
FA	-	Foaming agent
Acc	-	Hardening accelerator

C70-BFCs	-	The bio-based foamed concrete of the C70P30H0 by-product
C100-BFCs	-	The bio-based foamed concrete of the C100P0H0 by-product
BFCs	-	Bio-based foamed concretes
LWA	-	Lightweight aggregates
ILUC	-	Indirect Land Use Change
IUPAC	-	International Union of Pure and Applied Chemistry
AFt	-	Abbreviation for "alumina, ferric oxide, tri-sulfate" or (Al_2O_3 – Fe_2O_3 – tri)
AFm	-	Abbreviation for "alumina, ferric oxide, mono-sulfate" or (Al_2O_3 – Fe_2O_3 – mono).
MW	-	Mass water repellent
SW	-	Surface water repellent
BBISE	-	**(B**éton **B**iosourcé **I**solant **S**tructurel et **E**tanche à l'eau) which means Biobased Concrete Structural Insulation and Waterproof
CRW	-	Concrete and Rock Wool
STD	-	Dynamic thermal simulation
CZ	-	Comfort zone
D-samples	-	Foamed concretes produced by direct method
P-samples	-	Foamed concretes produced by preformed method

Introduction

A. BACKGROUND

According to the Ministry of Ecological Transition, the building sector accounts for 44% of the energy consumed in France in 2020, ahead of the transport sector (31.3%). In addition, the sector generates 38% of all energy-related CO_2 emissions in 2019 when emissions from the building construction sector are included [1]. Therefore, to prevent this and reduce the French buildings energy consumption, the Environment Forum (Grenelle de l'Environnement) has set up a program to combat climate change and control energy consumption. Thermal regulation (RT2012) and environmental regulation (RE2020) are two of the measures adopted.

The RT 2012 aims to limit the new buildings primary energy consumption to a maximum of 50 kWh/(m^2. yr) on average. In addition, RT2012 aims to encourage all building and equipment sectors to make technological and industrial changes and to oblige designers to move towards bioclimatic architecture.

The planned environmental regulation (RE2020), which will apply from July 2021, is based on the circular economy and low-carbon design, and on the principle of positive energy buildings (BEPOS). These buildings provide minimum energy consumption which will then be balanced using renewable resources. Briefly, this RE2020 targets zero energy waste and energy production.

Furthermore, the National Low-Carbon Strategy (SNBC) has set an ambitious path for reducing emissions from this sector with a target of -49% in 2030 compared to 2015 and the

achievement of complete decarbonation of energy consumed in buildings by 2050. Thus, to reduce the CO_2 emissions in the building sector, SNBC advises of using the most suitable carbon-free energy sources for each type of building, improving the buildings energy efficiency (shell and equipment), promoting construction and renovation products and equipment with a lower carbon footprint (from the circular economy or bio-based) and high energy and environmental performance throughout their life cycle.

According to the RT2012 and RE2020 regulations, the creation of a semi-structural insulating and waterproof bio-based concrete has become necessary and warrants to be studied and developed. In this context, the light concretes knew an important development thanks to their thermal insulation which decreases the energy consumed for the heating and cooling. These materials are obtained by replacing part of the concrete components by lighter and less energy-intensive constituents such as plant materials or voids. Depending on their formulation and production method, lightweight concretes offer the possibility of reducing the building sector energy footprint through three major levers: improvement of the building shells thermal insulation, reduction of the embodied energy and CO_2 emissions during production and conservation of mineral resources.

B. OBJECTIVES

The PhD thesis objective is to create, develop and study non-autoclaved insulating (with thermal conductivity $\lambda < 0.2$ W/(m.K)), structural (with compressive strength > 17 MPa) or semi-structural (with compressive strength > 2 MPa) and waterproof (with capillary absorption coefficient < 0.01 $g/cm^2.\sqrt{h}$) bio-based foamed concrete. Pozzolanic additives and biomass materials will be used to partially replace cement to limit potentially harmful production energy in terms of environmental impact. Furthermore, two foam production mechanical methods carried out at ambient temperature are used, the direct mixing method and the preformed foam method, to further reduce the energy footprint of the material.

Several parameters are being investigated. First, the hemp shiv, pozzolanic addition and the foam production method effects are studied. Secondly, to improve the foamed concretes efficiency, a pore structure and the cementitious matrix analysis are investigated. Then the mechanical, thermal, and hydric properties are conducted. After that, the waterproofing development is investigated, followed by a study of physical, mechanical and thermal properties of these biobased foamed concretes. Finally, a thermal simulation on the new final material is realized.

C. MANUSCRIPT CONTENT

This thesis is structured in 5 chapters presenting the main results of the research.

Chapter 1 is dedicated to a literature review. It focuses first on the study of foamed concrete, especially on its constituents, production methods, properties, and applications. Then the properties of bio-based cementitious composites are also examined, particularly their composition and the types of plant materials used. Finally, an evolution of the bibliographical data is presented to determine the next steps in this study.

Chapter 2 presents the materials used and describes the methods used to carry out the various experimental tests. Moreover, a study of the mechanical and thermal performances, the CO_2 emission and the cost of two different foamed concretes incorporating three different hemp shiv contents is also investigated.

Chapter 3 focuses on the precise characterization of the porous structures and cementitious matrix of foamed concrete. First, the porous structure is investigated using two distinct analysis methods, one focusing on the type of porosity, opened or closed, and the other one on the air bubbles distribution, studying the effects of pozzolanic additions, the hemp shiv amount and the production method on the porous structure. Then a study of the cementitious matrix is realized, first on hydration reactions and then on mineralogy.

Chapter 4 focuses on the mechanical, thermal and hydric performances of the foamed concretes in order to identify the best characteristics achieved and operate selection for further study.

Chapter 5 targets the study of the mechanical performances, thermal conductivity and thermal absorption of the selected concretes using different water repellents type. Then a characterization of new sandwich materials, named BBISE, based on the selected concretes treated by water repellents is launched. This latter study includes a thermal simulation for the application of the BBISE sandwich in a house, to study its insulating capacity, its hygrothermal comfort and its effects on the heating and cooling energy consumptions.

Chapter 1 Literature review

1. Literature review

1.1 INTRODUCTION

This literature review starts with a reference of the main characteristics, production methods and aerated concrete components obtained by inserting voids in the form of gas or air bubbles in a mineral matrix. These construction materials have a wide range of mechanical, thermal, and hydric performances, making it possible to envisage the realization of potentially self-supporting insulation.

On another hand, the information concerning the bio-based part of this study is collected. Then, the plant materials specificities used in concrete are presented. After that, the focus will be on the hemp shiv which is the one used in this work to treat in more detail the hemp shiv characteristics. Afterward, the properties of mineral matrix composites incorporating plant materials will be discussed and finally, the durability of these materials will be reviewed.

1.2 FOAMED CONCRETE

1.2.1 Overview

Lightweight concrete included foamed concrete, aerated concrete and lightweight aggregates concrete have been widely used in construction due to their many advantages, lightweight concrete has a very low thermal conductivity compared to normal concrete and a compressive strength ranging between 1-10 MPa [1].

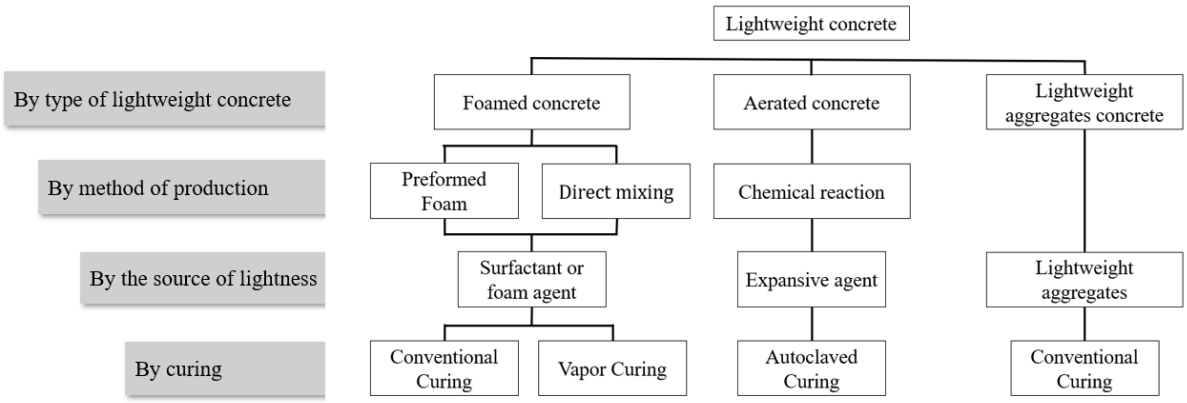

Figure 1 : *Flowchart of the different types of lightweight concretes.*

Lightweight concrete (LC) is a mineral matrix containing air or gas bubbles, or lightweight aggregates. In general, LC is designed to achieve a low density ranging from 400 to 1850 kg/m^3 compared to normal concrete with a density of 2000 to 2600 kg/m^3 and heavy concrete with a density larger than 2600 kg/m^3. In addition, the LC offers other advantages. It has high mechanical strength relative to its density, reduces construction costs, offers lightweight and environmentally friendly structures, improves fire resistance and sound insulation [2–5].

Lightweight concrete (LC) is subdivided into three groups (Figure 1): Foamed concrete (Figure 2 (a)) is obtained by using a foaming agent called surfactant which mechanically incorporates air bubbles into the concrete structure. Such a material is called non-autoclaved foamed concrete since it is cured in the open space. Aerated concrete (Figure 2 (b)), with a cellular structure obtained by integrating micro and macroscopic gas bubbles using an expanding agent with the support of an autoclave that stimulates chemical reactions by creating gas bubbles in the concrete. This latter material is called autoclaved aerated concrete. Lightweight aggregate concrete (Figure 2 (c)), which includes natural lightweight aggregates such as expanded clay, perlite, expanded schist, … or artificial lightweight aggregates as expanded polystyrene, sintered fly ash ...

(a)[1]

(b)[2]

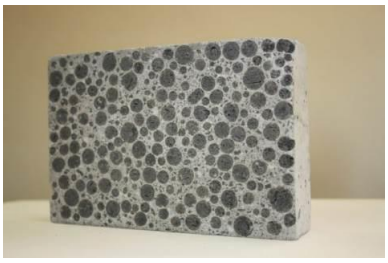

(c)

Figure 2 : *Foamed non-autoclaved concrete (a), aerated autoclaved concrete (b) and (c) lightweight aggregates concrete.*

The air and gas bubbles, or lightweight aggregates presence in such concrete, reduces the base mix density, which increases thermal resistivity. Therefore, lightweight concrete is considered as an excellent insulator [6].

Lightweight concrete is characterized by a low cement content, which reduces CO_2 emissions. It also exhibits several advantages, such as reducing structural loads, saving energy consumption,

[1] « PMS NV | Béton mousse - PMS NV », http://www.pms.be/isoler-du-sol/beton-mousse/?lang=fr.

[2] « Bloc Beton Cellulaire Avec Poignee 20x25x62, 5 », Bricoman, https://www.bricoman.fr/bloc-beton-cellulaire-avec-poignee-20x25x62-5.html.

reducing labour costs during construction, and minimizing production and transportation costs compared to traditional concrete [7].

Autoclaved aerated concrete cured in an autoclave to activate chemical reactions at a temperature of 180°C and a pressure of 10 bar for a period of 10 to 12 hours. This type of aerated concrete is the most popular, but it consumes a lot of energy during the manufacturing process: almost 340 kWh/m^3, which corresponds to an emission of 868 kg of CO_2/m^3. This energy is closely like that of ordinary concrete [8].

Furthermore, non-autoclaved aerated concrete does not require an autoclave [9]. Short et al [10] also ascribes the advantages of non-autoclaved aerated concrete to the low manufacturing costs, simplicity and accessibility of the technology. Thus, this type is the most economical and environmentally friendly.

1.2.2 Constituents

The constituents involved in the foamed concrete formation can be either mineral binders such as Portland or prompt cement, anhydrous calcium sulphate or gypsum... with pozzolanic additives such as blast furnace slag, fly ash, silica fume, metakaolin, ... or/and admixtures such as superplasticizers, retarders, accelerators... for saving costs and improving characteristics, with surfactants and a specific w/b ratio.

1.2.2.1 Binders

The binder is the most important constituent in foamed concrete since it provides a high adhesion and cohesion between the raw materials. Cement is the most dominant binder in most studies on foamed concrete. In general, the most used cements are ordinary portlandite cement, Portland cement, fast setting Portland cement, sulfo-aluminous cement, high alumina cement, etc.

Binders are divided into two parts depending on its environmental impact:

- The first type is the low environmental impact binders which emit a low amounts of CO_2 during the manufacturing process, such as (Calcium sulfate, gypsum, Anhydrit, Phosphogypsum, Cement over-sulfated [11], Lime...).
- The second type is the high environmental impact binders which are less ecological than the low environmental impact binders and it emits a large amount of CO_2 during the manufacturing process such as (Ordinary portlandite cement, Rapid hardening Portland cement, sulfo-alumina cement, high-alumina cement...).

Generally, binders with low environmental impact are more expensive and less mechanically efficient than those with high environmental impact. Some studies have used environmentally friendly binders in foamed concrete, as Samson et al. [12] have used prompt cement and calcium sulphate, they found that calcium sulphate gives better results than prompt cement. In another study, Yang et al. [13] have replaced 55 wt% of cement by phosphogypsum obtained from phosphate fertilizer with lime (7 wt%) to prepare non-autoclaved aerated concrete, phosphogypsum is composed mainly of calcium sulfate dihydrate ($CaSO_4$,$2H_2O$) and partially of phosphate, fluorides, sulfate ions and organic matter and they found that phosphogypsum acts as a filler and admixture with low environmental impact, but it is also dangerous. Baux et al. [11] studied the supersulfated cement which is composed of treated synthetic gypsum and slag. Supersulphated cement has a low environmental impact with a low amount of portlandite (<5%).

1.2.2.2 Foam

A bubble has a closed interface with the surrounding liquid. Figure 3 shows the ellipsoidal bubble geometry with half major axis (a) and half minor axis (b). In a Newtonian liquid whose wall has a local curvature such that the radii of curvature are R_1 and R_2, the local pressure difference between the internal pressure of the gas P_{int} and that of the surrounding liquid P_{ext} is given by Laplace's law:

$$P_{int} - P_{ext} = \gamma(\frac{1}{R_1} + \frac{1}{R_2}) \qquad \textbf{Eq. 1}$$

With:

γ = Surface tension (J/m^2 or N/m)

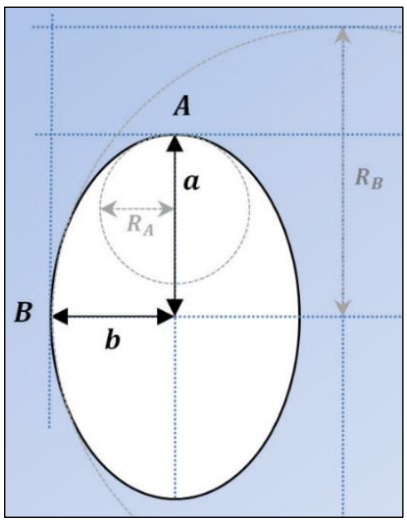

Figure 3 : *Geometry of an ellipsoidal bubble [12].*

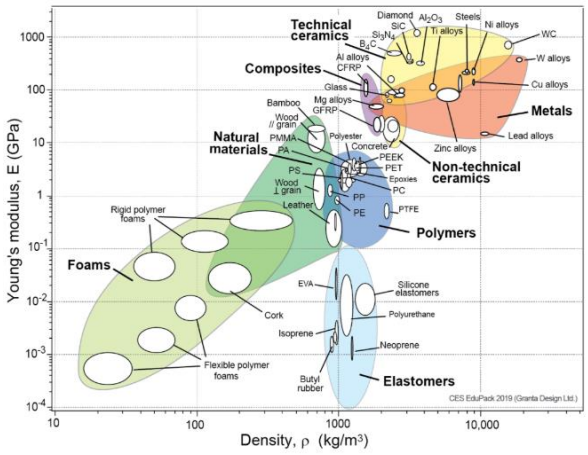

Figure 4 : *Young's modulus versus density [14].*

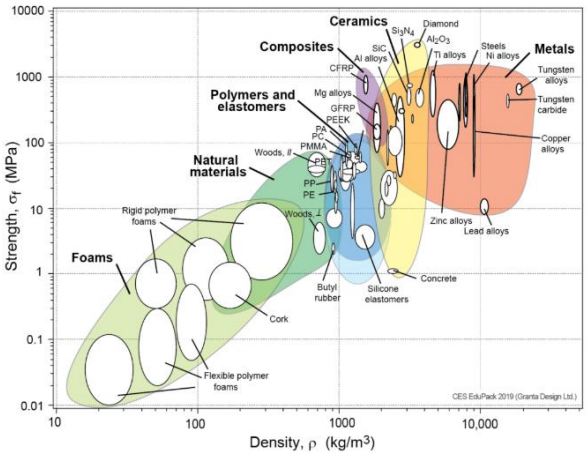

Figure 5 : *Strength versus density [14].*

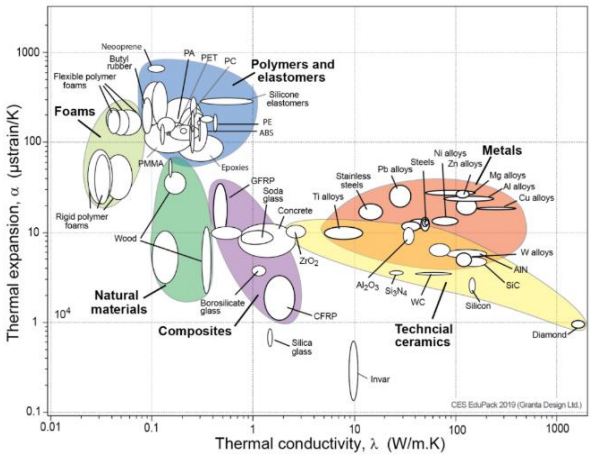

Figure 6 : *Thermal expansion versus thermal conductivity [14]*

Figure 4 represents the Young's modulus of the materials versus density, foams are the lighter weight materials, therefore it is the most insulating but at the same time the least rigid. Natural materials are stiffer than foams but also heavier. Globally, the materials stiffness depends on the density, the stiffness increases linearly with the increase in density of the material.

Furthermore, (Figure 5) it is remarkable that the strength decreases linearly with decreasing density. Additionally, foam is the most fragile material but the lightest.

Moreover (Figure 6), looking at the thermal conductivity of the materials, it is found that foam has a very small thermal conductivity between 0.02 and 0.09 (W/m.K), and natural materials between 0.1 and 0.14 (W/m.K). Therefore, it is thermally interesting to study a mixture of these two components.

The foam and its rigidity depend on the foaming agent used, as foam is a very sensitive material that can deflate easily due to external conditions or over time. Therefore, it is very important to choose a foaming agent that offers stable and rigid foam.

1.2.2.2.1 Foaming agents

Foaming agents are direct regulators of the foamed concrete density, having the ability to create air bubbles in the mineral suspension and affect both the fresh and hardened properties of the foamed concrete. The foam quality is a very important factor in the foamed concrete production due to the improvement of the foam stability, mechanical behaviour, and foamed concrete strength. The foam quality depends on the nature, the foaming agent dilution and the foam preparation process used [15]. For example, during the foam preparation, if the mixing time is prolonged, the foam quality decreases, i.e., the foam stability and, the voids and air bubbles contents decreases.

1.2.2.2.1.1 Surfactants

Surfactants are agents used to reduce the surface tension of the solution, which facilitates the air bubbles formation. There are 3 types of surfactants: synthetic, protein-based animal and vegetal-based.

Synthetic surfactants are highly hydrophilic chemicals that dissolve easily in water and form air bubbles in complex chemical reactions [16]. Protein-based surfactants form air bubbles due to protein degradation. The bonds between large protein molecules are broken down to form small hydrophilic molecules. This phenomenon reduces the surface tension of the solution, creates interfaces between the air bubbles and forms hydrogen bonds between the molecular groups which develop the air bubbles stability. The foaming efficiency of protein-based surfactant depends on pH and temperature [16].

The foam volume formed by a synthetic surfactant is higher than that formed by a protein-based surfactant, but the latter provides a more rigid, closed, stable and well-distributed air bubbles network [17]. Sun et al. [18] worked on the surfactant origin effect on the mechanical and hygroscopic performance and durability of a cellular concrete made by Portland cement CEM I and found that animal-origin surfactants gave the best results, followed by synthetic surfactants and then plant-based surfactants. Panesar et al. [16] have compared the effect of 1 protein-based surfactant and 2 synthetic surfactants, they found that the protein-based surfactant gives smaller, more spherical, and more isolated air bubbles than the synthetic surfactants.

Moreover, the surfactant effect on gypsum foam is studied by Samson et al. [12], they used 6 types of surfactants (Hostapur OSB, CTAB, Sitren, AER SIKA, Micro Air, Cetrimide) and it turns out that Hostapur OSB and Cetrimide surfactants give important results (for ρ=745 and 819 Kg/m^3, Rc= 3. 2 and 4.89 MPa, λ = 0.22 and 0.26 W/(m.K), respectively) with calcium sulphate using the preformed foam method.

Additionally, Zhao et al. [19] indicated that the foaming agent performance depends on the following three parameters:

- The foaming capacity is the ratio between the final foam volume and the solution volume before the incorporation of the voids.
- The drainage rate, which is the water infiltrated amount through the foam generated for one hour.
- The slump rate, which is measured in one hour at the slumped length of the foam in the specimen.

1.2.2.2.1.2 Expensive agent

Expansion agents are mainly used to incorporate gas bubbles (hydrogen, oxygen...) into the cement matrix structure by chemical reactions. Aluminium powder, zinc powder, hydrogen peroxide, sodium dodecyl sulphate (SDS) is the most used foaming agents.

Aluminium metal powder is widely used in the aerated concrete industry as an expansion agent, and it is a highly reactive metal that can easily generate H_2 gas and form aluminium hydroxide when placed in water. Corrosion of metallic aluminium in aqueous alkaline solutions is known as a useful process for generating hydrogen gas in various applications such as clean fuel production [20,21], the hydrogen gas produced by this corrosion reaction of aluminium metal introduces voids in the paste mixture and helps to develop a porous concrete structure [22].

1.2.2.3 Water

The amount of water required to produce a foamed concrete depends on the cementitious matrix formulation and the nature of the surfactants used.

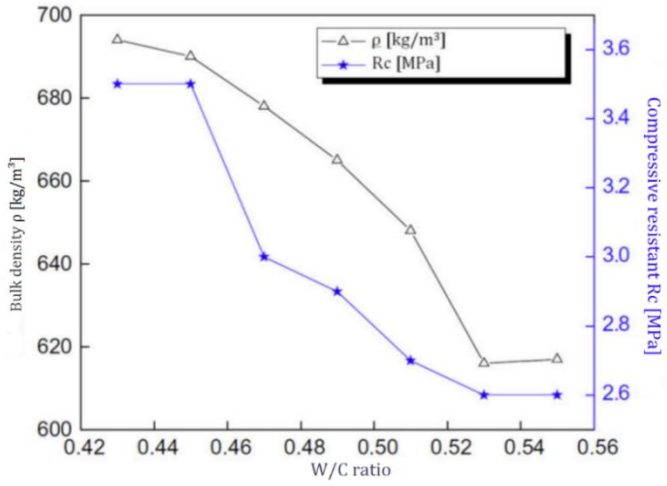

Figure 7 : *Effect of the water/cement mass ratio on density and mechanical strength by Yan [13].*

Generally, the water-to-binder mass ratio should be low to ensure good mechanical performance. Therefore, superplasticizers are used that can reduce the water/binder ratio while maintaining the same fluidity, thus improving mechanical performance. Indeed, Yan et al. [12] studied the effect of the w/c ratio on density and compressive strength (Figure 7) and found that with increasing w/c ratio, the bulk density and compressive strength decrease.

Moreover, Kearsley et al. [23] have found that the w/c ratio should be between 0.4 and 1.25 or between 6.5% and 14% of the target density. According to the British Cement Association [24], the optimum water/cement ratio should be between 0.5 and 0.6.

The water content affects the uniformity, consistency and stability of the foam formed. Furthermore, the low water content causes the destruction of air bubbles, which increases the density. Also, the high-water content makes it possible to tighten the films between air bubbles, which also destroys the air bubbles and increases the density [15].

According to ACI 523.3R-93, the water must be fresh, clean, and drinkable, since organic infections can damage the protein-based foaming agents, reducing the quality of the foams produced [24].

1.2.2.4 Additions and admixtures

Additions and admixtures are generally used to improve design consistency, long-term hygro-thermo-mechanical behaviour and to reduce mixing costs. The additions proportion ranging from 10 to 75% of the mass, the additions are divided into 3 groups [25,26]:

- Mineral additions such as silica fume, fly ash, ground slag, Lytag, metakaolin...
- Synthetic or vegetable fibres
- Additives such as superplasticizers, accelerators, retarders, water repellents...

Ameer et al. [27] have tested the mechanical behaviour of portlandite cement-based foamed concrete with/without additions. They used 2 additives (fly ash and silica fume) and one admixture (superplasticizer) with a w/b ratio between 0.3 and 0.5 (depending on the formulation and especially the amount of superplasticizer). They found that by using all 3 additives together, the compressive strength exhibited are the largest, then respectively with superplasticizers only, with fly ash only and with silica fume only.

Generally, pozzolanic additions increase the hydration heat amount and the hydration speed, then accelerate the setting and ensure the air bubbles stability in the concrete thereby improving mechanical resistance. For example, fly ash improves the air bubbles distribution in foamed concrete and silica fume improves the mechanical behaviour in the short term [28]. Moreover, the

ground granulated blast furnace slag (GGBFS) addition improves the mechanical strength. A study on the air-vacuum system of a foamed concrete consisting of a cement and ground granulated blast furnace slag mixture resulted in a high strength-to-weight ratio [29]. Additionally, several studies have considered granulated blast furnace slag, fly ash, metakaolin and others as sustainable materials in the development of environmentally friendly and sustainable concrete [30–33] .

Some studies explain the results of incorporating fibres into foamed concrete. The most used fibres are alkali-resistant glass, kenaf, steel, oil palm fibre, polypropylene fibre. According to Awang et al. [34], the fibres proportion should be between 0.25 and 0.4% of the total mass. In addition, Zollo et al. [35] used polypropylene fibres and found that polypropylene fibres improve the flexural strength and change the typical behaviour of foamed concrete from fragile to elastic plastic.

1.2.3 Foaming methods

The foam production methods are divided into 3 main methods, the chemical method preferred to produce autoclaved aerated concrete and mechanical methods such as the preformed foam method and the direct mixing method which are generally used to trap air in the mineral suspension with the surfactants addition that produce air bubbles by mechanical vibration and are preferred to produce non-autoclaved aerated concrete. Additionally, they are the most economical and controllable foamed concrete production [36], as no chemical reactions are involved.

1.2.3.1 Chemical method

The chemical method is a method of foaming by chemical reactions, the gas-generating chemicals or the expansion agent are mixed with the mineral suspension during the liquid phase, which reacts with water and hydroxides in an alkaline medium at high temperature up to 60°C to form hydrogen bubbles, thus increase the volume of the mass and, when the gas escapes, leaves a porous structure.

However, to optimise the performances of aerated concrete produced by the chemical method, the samples must be cured in an autoclave at high temperature and pressure, this process significantly increases the production energy consumption. The associated embodied carbon is 375 kg CO_2/m^3 [37] which is more than that of conventional concrete ($\simeq$ 324.18 kg CO_2/m^3) [38].

Wu et al. [39] have produced an ultra-light foam concrete with a density less than 300 Kg/m^3 and 2.23 MPa as a compressive strength. This aerated concrete is produced by using H_2O_2 as expansion agent, fly ash, metakaolin as binder with a ratio w/b = 0.17 - 0.19 using the chemical method.

Yang et al. [13] also used the chemical method to produce an aerated concrete with a density of 686 Kg/m^3 and a compressive strength around 6.3 MPa using aluminium powder as an expansion agent as well as cement, ground granulated blast furnace slag, phosphogypsum and lime. In addition, the water/binder mass ratio was 0.45 with a hardening temperature of 90°C.

1.2.3.2 Mechanical methods

The preformed foam method is based on the separate production of a light and stable aqueous foam which is gradually inserted into a mineral suspension. In other words, the foam is produced by mixing the diluted foaming agent with water. Then, the mineral suspension is added to the foam gradually and stirred until the mixture becomes homogeneous.

Several studies are dedicated to the several parameters influence on the physical and mechanical performance of foam concrete manufactured by the preformed method. Three main parameters are studied: the preformed foam volume, the mixing ratio, and the foamed concrete bulk density. These studies find that the average bubble size decreases with the w/b mixing ratio and increases with the volume of foam introduced. In addition, the optimum mechanical strength of high-strength foamed concrete is obtained when the water/cement or binder ratios are 0.19 and 0.17 [40,41]. Tian et al. [42] studied phosphogypsum with a protein-based surfactant to produce a non-autoclaved aerated concrete with a density = 758 Kg/m^3 and Rc= 2.8 MPa using the following formulation: phosphogypsum between 45-55%, cement/GGBFS ratio = 1, lime 4%, sulpho-aluminous cement 2%.

The direct mixing method is based on the surfactant addition directly to the mineral suspension to create a stable mineral foam when all components are mixed. The foam obtained gives a void structure in the foamed concrete [10]. It is strongly recommended that the foam be stable and stabilised to be able to support the pressure of the mortar until the initial setting of the cement to build a solid concrete skeleton in air-filled voids [43].

Both methods require the foam concrete structure to be maintained until its hardening [40]. This stability depends on several parameters such as the shear stress of the suspension, the nature and concentration of the surfactant, the surfactant molecular structure. According to Byun et al. [44], the preformed foam method is generally preferred to the rapid mixing method because it requires less surfactant and is easier to install on site during construction.

1.2.4 Properties

1.2.4.1 Fresh state

1.2.4.1.1 Rheology, consistency, and workability

Rheology and consistency represent the study of the concrete flow and deformation (plasticity, elasticity, viscosity, fluidity). According to Kunhanandan Nambiar et al. [45], the rheology and consistency of foamed concrete is acceptable if the flow time of the Abrams cone is between 8 and 12 s. In addition, the foam amount increases the fluidity and decreases the foamed concrete rheology and consistency [45]. Furthermore, the superplasticizer addition more than normal reduces the consistency of fresh foamed concrete.

The spreading of normal foamed concrete should be between 85 and 125 mm and between 115 and 140 mm for fly ash. For good workability, the plasticizer should be 0.2% of the cement if the water/cement ratio is low [46]. The superplasticizer and the ground granulated blast furnace slag increases workability.

1.2.4.1.2 Stability

The foam stability is an important factor that greatly affects the foamed concrete strength. The production of a stable foamed concrete has many influencing parameters such as the foam preparation method, the foaming agent type, the type of surfactants and additives used, the mix formulation, etc.

Foam stability is the ability to resist disturbances. Moreover, stability is determined by measuring the lifetime of the inter-bubble films, which leads to the destruction of the foam over time and the air volume reduction in the concrete [47]. Samson et al. [12] have studied the instability of foam and they found three different phenomena of instability: drainage (a), ripening (b) and coalescence (c). These phenomena lead to the foam aging.

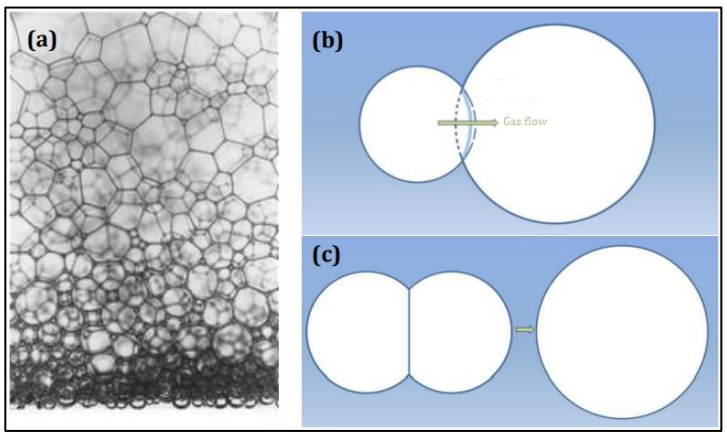

Figure 8 : *Sources of instability: (a) Drainage [48]; (b) Ripening; (c) Coalescence [12].*

First, Water at the edge of the tray is affected by gravity. What causes separation is drainage (Figure 8 (a)). There will be a vertical gradient in foam density, with the upper foam becoming dry and the lower foam thickening. The liquid loss at higher levels weakens the bubbles, and the surfactant molecules concentration in the film between the bubbles decreases.

When two different radii bubbles are in contact, the interface will curl due to the pressure difference. As the membranes are not completely impermeable to air, air diffusion from the smallest bubble to the largest will occur, this is called ripening (Figure 8 (b)). This phenomenon leads to the gradual disappearance of the smallest bubbles.

Finally, a much more aggressive phenomena can affect the foam durability, coalescence (Figure 8 (c)). Under the gravity effect, the concentration of surface-active molecules can decrease, which weakens the film. The film can then break, leading to the fusion of the two neighbouring bubbles. The coalescence phenomenon, like that of ripening, leads to a decrease in the bubbles total number, although the phenomena are quite different. The coalescence phenomenon leads to enhance the porous network, so the open porosity.

Moreover, The use of superplasticizer with a w/c < 0.3 increases stability by 43%. Stability is also affected in case of incompatibility between the superplasticizer and protein-based surfactants [49].

1.2.4.2 Mechanical

1.2.4.2.1 Compressive strength

Density and mechanical behaviour are highly dependent, the compressive strength gradually increases with density (Figure 9). Firstly, it is remarkable that for a density range between 300 and 900 Kg/m^3, the compressive strength ranges between 0.6 and 11 MPa.

All values shown in Figure 9 are 28-day compressive strength values, the average trend of 28-day maximum compressive strength as a function of density is:

$$Rc_{28} = 0.018\rho - 5.27, \qquad \textbf{Eq. 2}$$

While according to Samson [12] the trend is:

$$Rc_{28} = 0.01\rho - 2 \qquad \textbf{Eq. 3}$$

And the relationship between flexural strength and compressive strength is described by this equation [7]:

$$Rf = 0.23 \times Rc^{0.67} \qquad \textbf{Eq. 4}$$

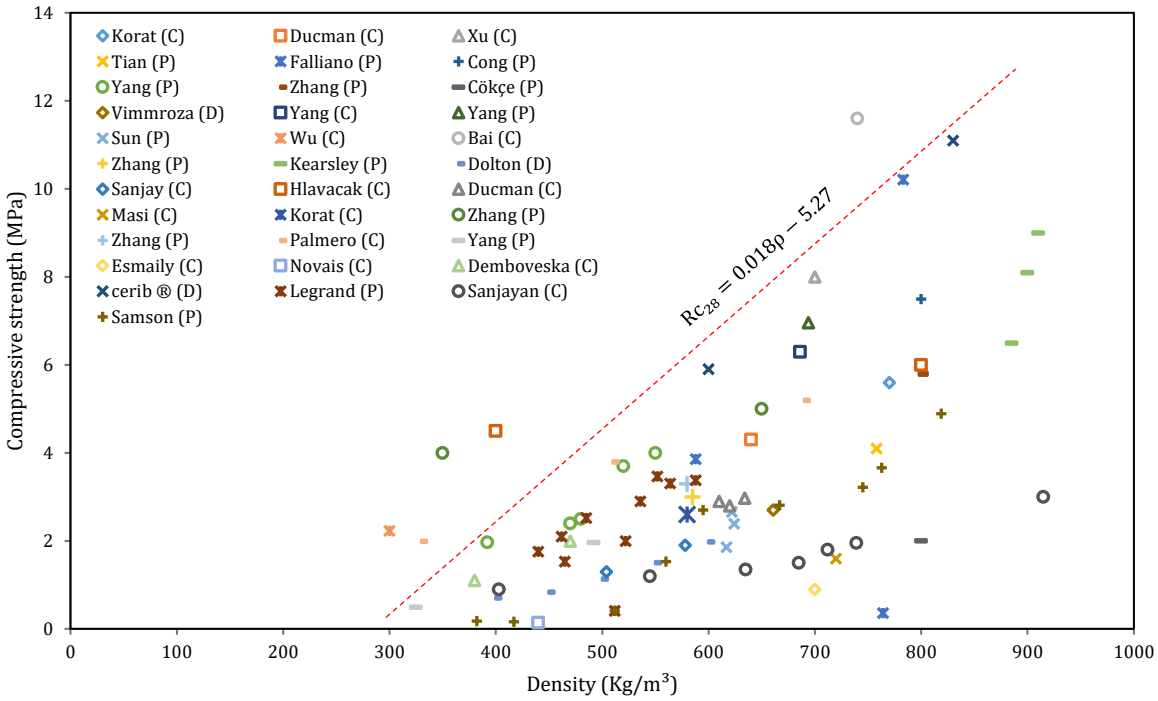

P: Preformed method, C: Chemical method, D: Direct method.

Figure 9 : *Compressive strength versus density of foamed concrete in several studies in the literature.*

The water optimal amount improves stability and reduces the air bubbles size, which improves compression strength. The silica fume and fly ash combination increases compressive strength by 25% [29]. Nambiar et al. [27] analysed the air voids structure in foamed concrete by identifying parameters such as the air bubbles size distribution and shape and studied the void size distribution influence on strength and density and found that foamed concrete with uniformly distributed spherical air voids had a higher compressive strength, while irregularly shaped or irregularly perimeter bubbles with a large uneven opening had a lower compressive strength.

The mechanical performances of all the lightweight concretes analysed in this literature review are referenced in Figure 9. Generally, the compressive strength tends to decrease when the density decreases [3,50]. However, as the constituents and their amounts may differ, density is not necessarily a very relevant indicator of compressive strength. Thus, the cement/sand, water/cement mass ratios, the type of cement used, its composition, the pores size, their distribution, the surfactants type as well as any treatments, especially during the curing process, will also modify the mechanical performance.

1.2.4.2.2 Flexural strength

The flexural strength of foamed concrete is lower than that of ordinary concrete, but its Rf/Rc ratio ranging between 0.2 and 0.4 is higher than that of ordinary concrete ranging between 0.08

and 0.11 [44]. Moreover, the tensile strength is ranging between 15 and 35 % of the compressive strength and it also improves with fibrous materials additions [51].

According to Zollo et al. [52], the fibres increase flexural/tensile strength, improve tenacity characteristics, and enrich the capacity and post-cracking behaviour. For example, polypropylene fibres improve flexural/ tensile strength by 31.5%, Nambiar et al. [53] also found that polypropylene fibres increase fire resistance and reduce crack propagation at temperatures above 600°C. Byun et al. [44] found a relationship between 7-day and 28-day compressive strengths:

$$Rc_{28} = 1.27 \times Rc_7 + 2.57 \qquad \textbf{\textit{Eq. 5}}$$

1.2.4.2.3 Elasticity modulus

The elasticity modulus of foamed concrete E is directly dependent on the density. It is four times smaller than that of ordinary concrete, ranging from 1 to 12 kN/m^2 [54].

Some researchers have studied the raw materials effects on the modulus of elasticity. For example, Jones et al. [55] studied the polypropylene fibres effects and they found that 0.5 vol% of fibres improved the elasticity modulus E without any effect on the air bubbles uniformity. They also found that the elasticity modulus E depends on the type and amount of aggregate used.

1.2.4.3 Physical characteristics

1.2.4.3.1 Density

Foamed concrete is characterised by its very low density compared to ordinary concrete. Its density is limited to 100-120 kg/m^3 and does not exceed 1800 kg/m^3 [56]. There are two types of densities: fresh and dry. The fresh density is the density of fresh foamed concrete, and the dry density is the density after the concrete has hardened.

To measure the actual fresh mix density, it is usually necessary to fill and weigh a pre-weighed standard container of known volume with the foam concrete produced. After that, the variation between the theoretical densities and the actual densities should be evaluated. For dry density, the most acceptable tolerance is limited to ±50 kg/m^3, up to ±100 kg/m^3 for high density foam concrete mixtures more than 1500 kg/m^3 [57].

Generally, density is affected by the foam volume, it decreases with increasing foam volume. Moreover, the additions also influence the density, for example, Nambiar et al. [15] found that the fly ash addition increases the foamed concrete dry density by 10%. Furthermore, the types of aggregates and their gradations have effects on the density. Indeed, McCormick et al. [58] indicated that the density increases with the aggregates proportion.

1.2.4.3.2 Porous structure

Several studies indicated that the higher foam volume had a significant effect on porosity [59]. The air-voids in the foam concrete can be characterized by a few parameters like volume, size, distribution, shape and spacing between air bubbles [7]. Like conventional cementitious materials, foamed concrete consists of nano-pores (also called gel pores) (dpore < 0.01 µm), capillary or micropores (0.01 µm < dpore < 10 µm) and macro-pores (10 µm < dpore; entrained and/or trapped air).

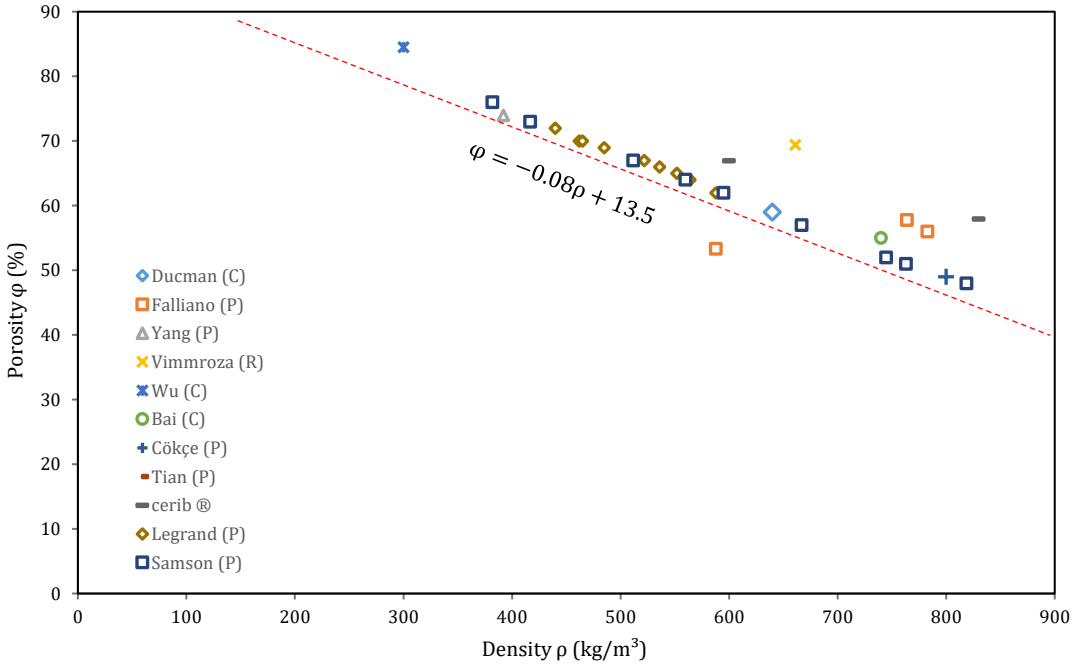

***Figure 10** : Porosity versus density of foamed concrete in several studies in the literature.*

As shown in figure 10, the dependency between density and porosity is significant. The density decreases with the increase of porosity due to the increase of the foamed concrete air content.

Foamed concrete is manufactured by entraining relatively large air volumes into the cement paste using a foaming agent. Porosity is influenced by formulation, foaming agents, and production method, is related to absorption rate, sorption and permeability and affects compressive behaviour, tensile strength, thermal resistance and durability [60]. Indeed, Kearsley et al. [61] proved that the air-void distribution is one of the most important micro properties influencing the foamed concrete strength. According to Visagie et al. [62], a high total porosity ϕ will significantly reduce compressive strength, especially if the pores are large. Moreover, it is noted that a high w/c ratio significantly impacts foamed concrete and provides porosity.

Furthermore, using image processing software, Samson et al. [60] carried out a 2D surface analysis of foam concrete to study the foaming agent, formulation, production methods impacts on the porosity and air bubbles distribution in the foamed concrete. They also studied the effects of air bubble distribution on mechanical performance. Finally, he found that mechanical performance is improved with fine (average radius less than 0.3mm) and homogeneous pore structures.

1.2.4.3.3 Shrinkage

Drying shrinkage represents the most recurrent problem in the foamed concrete production that occurs during the first 20 days of casting. It is 4 times greater in foamed concrete than in ordinary concrete.

Shrinkage should be limited to between 0.1% and 0.35% of the hardened concrete total volume. The hydration heat is the main reason for shrinkage, therefore there are 2 solutions to reduce the shrinkage [63]:

- Addition of fly ash, silica fume or lime which reduces the hydration heat and consequently reduces shrinkage.
- Using superplasticizers or reducing the w/b ratio.

1.2.4.4 Sustainability

1.2.4.4.1 Permeability

Permeability is defined as a measure of the water flow under pressure in a saturated porous material and is fundamentally dependent on water absorption measurements as well as vapour permeability. Generally, the foamed concrete water absorption is almost double that of normal concrete with a similar w/b ratio [64].

Permeability increases with increasing volume of aggregates used and with increasing CV/C ratio and decreases with decreasing porosity. Kearlsey et al. [29] have found that permeability does not depend only on the porosity amount, but also on the porosity structure. If pores are interconnected, permeability increases and vice versa. Additionally, permeability depends on the age and size of the sample.

1.2.4.4.2 Long-term resistance against aggressive environments

Long-term resistance to aggressive environments depends mainly on the formulation, the air bubbles distribution, the pores size and volume, and the ratio of the number of connected pores

to the pores total number [65]. As the connected pores number increases, the impurities level increases.

According to Jones et al. [55] the absorption rate, the depth of primary penetration describes the degree of foamed concrete freeze-thaw resistance. Kamada et al. [66] explained the influences of these parameters and they found that the water contained in foamed concrete is mainly absorbed water, compared to capillary water. Since voids are much greater than in normal concrete, the saturation depth and water volume can be much greater in foamed concrete than in normal concrete for the same duration of exposure to moisture. As a result, a larger surface area, with a higher water content and subsequent greater volume change in freezing temperatures, than a relatively drier interior area result. To measure the freeze-thraw cycles damage, a mass, dimensional and mechanical monitoring of the foamed concrete must be carried out [67].

Concerning foam concrete, as a high-porosity material, it is sensitive to environmental moisture and water penetration, which severely limit the wide application of the foam concrete product [68–70]. Sun et al [18] found that the foam concrete water absorption with a dry density ρ_d of 600 kg/m^3 was reduced by 15%-30% after 40 freeze-thaw cycles after immersion in water. Further, Nambiar and Ramamurthy [53] found that the foam concrete dry shrinkage was related to the foam concrete moisture content, moisture loss can contribute to dry shrinkage. In addition, Chen et al. [71] found that the foamed concrete total weight with a ρ_d of 550 kg/m^3 would increase about two times after water absorption, which significantly reduces the tensile strength. Furthermore, Del Coz Diaz et al. [72] found that the foamed concrete thermal insulation performance decreased with the increase of moisture content or decreased with the increase of the relative environment humidity. Therefore, water-repellent treatment of foamed concrete before application is essential for its long-term behaviour.

Falliano et al. [73] found that the mass water absorption rate decreased with increasing foamed concrete dry density ρ_d. Sang et al. [74] also found that ρ_d, water absorption kinetics, and volume increased with increasing porosity. Kearsley and Wainwright [3] examined the foam concrete permeability and porosity and found that water vapor permeability increased with increasing porosity and ash content.

Moreover, foamed concrete has a very high resistance to sulphate and carbonation. Sulphate penetration depends on the type of cement used, the additions, and the type of cation with sulphate anion, permeability, sulphate concentration, exposure time and duration. The fly ash addition improves carbonation resistance, and a very large foam volume reduces carbonation resistance. The alkali-silicate reaction is not remarkable, the chlorine resistance of aerated concrete is equivalent to that of normal concrete [7].

1.2.4.5 Waterproofing

According to Zhang et al. [75], waterproofing of foamed concrete reduces the carbonation and the corrosion. In addition, reducing the foamed concrete water absorption is an effective way to improve its overall performance.

Moreover, many additions can improve the waterproofing of foamed concrete, for example Wang et al. [76] found that 3% rubber crumb content can improve the waterproofing performance of foamed concrete by reducing water absorption by 10%. Furthermore, water repellent improves mechanical behaviour, does not affect foam stability, and hygroscopic humidity decreases the increasing water repellent amount. The optimum water repellent dosage (siloxane-based polymer) is 1%, it reduces the water absorption rate by 10% up to 2.5% [71]. Also, waterproofing can be improved by using surface coatings such as GO/silane composite which reduces water absorptivity by 97.3%.

1.2.4.6 Functional

1.2.4.6.1 Acoustic

Foamed concrete is a good sound insulator because of its structure, air bubble distribution and windy surface. Foamed concrete absorbs 10 times more sound waves than normal ordinary concrete. Sound insulation is affected by the foam amount and the air bubbles size, distribution, and uniformity [7].

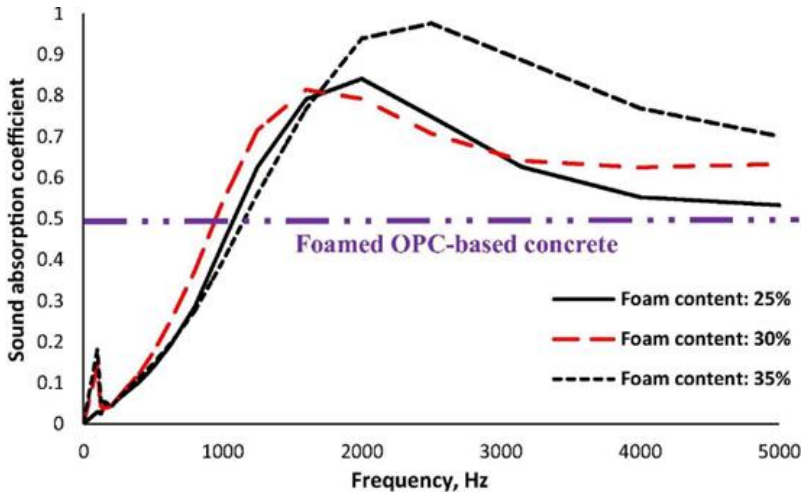

Figure 11 : *Sound absorption spectrum of concrete samples of 25%, 30% and 35% alkali activated slag foam concrete [77].*

As shown figure 11, Mastali et al. [77] studied the acoustic performance of an alkali activated slag fibre-reinforced foamed concrete and found that the acoustic insulation is improved with an

increase in the foam amount. Moreover, the closed and disconnected pore network blocks the sound propagation, which reduces absorption, even though the porosity is relatively high [78].

1.2.4.6.2 Fire resistance

Foamed concrete has the capacity to resist fire with a span close to that of normal concrete. Concrete with densities of 950 kg/m^3 and 1250 kg/m^3 can resist fire for 3.5 h and 2 h, respectively. Vilches et al. [79] reported that foamed concrete with a density of 400 kg/m^3 exhibited a fire resistance rate three times lower than that of a dry density of 150 kg/m^3.

In addition, the raw materials may affect the foamed concrete fire resistance. For example, coarse aggregates in normal concrete lead to various expansion and cracking rates. The coarse aggregates lack in foamed concrete provides excellent fire resistance [80]. Kearsly et al. [81] reported that foamed concrete comprising hydraulic cement with an Al_2O_3/CaO ratio over two has withstood temperatures up to 1450°C without exhibiting any signs of damage.

1.2.4.6.3 Thermal conductivity

Foamed concretes are mainly appreciated for their good thermal insulation properties, which means that buildings can save energy for cooling and heating, which are the main channels of energy consumption throughout the life cycle of a building. Thermal conductivity, specific heat, thermal diffusivity and thermal resistance are considered as foamed concrete thermo-physical properties. As known, a material thermal resistivity increases with decreasing thermal conductivity.

The cement-based materials thermal conductivity, such as cellular concrete, is an important factor when considering the conduction heat transfer degree. The heat dissipated amount through walls and roofs has a direct effect on the building energy consumptions.

Figure 12 shows the relationship between thermal conductivity and density. Thermal conductivity (λ) increases with increasing density (ρ). In other words, thermal resistance decreases with increasing density. Furthermore, this maximum thermal conductivity is related to the density by the relation following:

$$\lambda = 2.5 \times 10^{-4} \times \rho - 0.05 \qquad \textbf{Eq. 6}$$

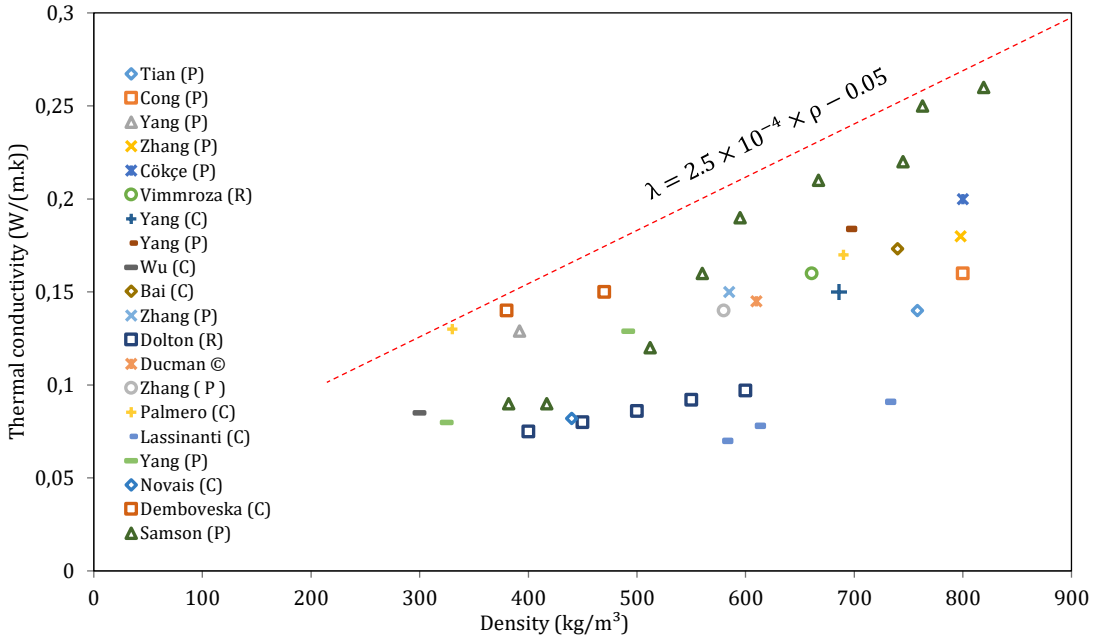

Figure 12 : *Thermal conductivity versus density of foamed concrete in several study*

Furthermore, moisture content, temperature, aggregate type, binder type and concrete density are important factors that influence the concrete thermal conductivity. Porosity plays an important role on the material thermal conductivity. Thermal conductivity decreases when using LWA and/or foam due to the increased the concrete porosity. Also, thermal conductivity decreases by about 0.6% when the concrete porosity increases by 1% [82]. In addition, the foamed concrete thermal conductivity increases by 54% when the density increases by 2/3 [83]. Moreover, it varies from 0.118 to 0.199 W/(m.K) for densities between 400 and 600 kg/m^3 and from 0.1 and 0.7 W/(m.K) for densities ranging from 600 to 1850 kg/m^3 [84]. Thermal conductivity of foamed concrete (1000 kg/m^3) is six times lower than that of conventional concrete [50]. It also increases by 15-20% with air humidity ranging from dry to 90% [85]. Briefly, it increases by about 6% with the addition of 1% humidity [82].

Moreover, Batool et al. [86] studied the air voids size distribution in cement-based foam. They found that mixtures with a smaller range of air void size distribution had higher conductivity and lower density, while a wider void size distribution resulted in lower conductivity.

1.3 BIO-BASED CONCRETE

1.3.1 Overview

Since the beginning of the 21st century, the world has been seeking to limit the pollution emitted by the construction sector and reduce its effects by seeking new construction and

consumption solutions that are more respectful of the environment. In this context, the use of materials of natural origin such as plants (wood, straw, flax, earth, hemp, etc.) is becoming increasingly important. Indeed, the plant material incorporation in the construction products formulation contributes to limiting CO_2 emissions in a significant way, thus reducing the global warming effect, provided plant growing does not give rise to larger emissions, considering the total life cycle of the process.

According to the French Ministry of Ecology, sustainable development and energy, "Bio-based materials are materials derived from biomass of plant or animal origin. Today these materials represent a wide range of products and offer many applications in the building and construction sector, as insulation (plant or animal fibre wool, recycled textiles, cellulose wadding, goats wool, shiv, straw bales, etc.), mortars and concretes (concrete made of hemp, wood, flax, etc.), panels (vegetable particles or fibres, compressed straw, etc.), plastic composite materials (matrices, reinforcements, fillers) or in building chemistry (adhesives, additives, paints, etc)".

Bio-based concrete is considered as a lightweight concrete. Seng et al. [86] studied the prefabricated hemp concrete physical properties and they found that its average density is 466 kg/m^3 and its high porosity (78%) is fully interconnected (76%).

In recent years, various works have been carried out for acoustic, mechanical, thermal and hydric characterisation [87–90]. These studies are essential for the certification implementation. However, it turns out that the results presented in the literature can vary significantly and are not necessarily representative of the material in use [91].

1.3.2 Constituents

1.3.2.1 Plant raw materials

Vegetable raw materials can be in the form of fibres, aggregates, powders or flours and each of these raw materials is manufactured by a specific process, characterised by a different shape and different properties.

Natural materials Composites are proposed to replace synthetic materials composites because of several advantages such as biodegradability, renewability, recyclability, abundance, permeability, corrosion resistance, high flexibility, hygroscopicity, non-toxicity, the ability to give up moisture, no release of substances hazardous to health, non-irritation of the skin, no allergic effects, competitive mechanical properties, reduced energy consumption, less treatment equipment abrasiveness and reduced waste disposal problems. Flax, hemp, jute, sisal and cotton

are the most used plant materials for reinforcing cement-based, geopolymer and polymer composite materials due to their relatively high strength and elasticity modulus.

The main chemical compositions of the above-mentioned ligno-cellulose plant materials are cellulose, hemicellulose, lignin, wax and pectin with small sugars amounts and starch proteins in varying amounts. Cellulose, hemicellulose and lignin are the basic components that determine the bio-based materials physical properties.

Cellulose is the most rigid and strongest organic component that gives plant materials strength, rigidity and stability. However, cellulose is a semi-crystalline polysaccharide with a hydroxyl group, giving the natural material a hydrophilic character when used to reinforce hydrophobic matrices [92].

Hemicellulose is strongly bound to cellulose fibrils, probably by hydrogen bonds. Hemi-celluloses are branched, totally amorphous and have a significantly lower molecular weight than cellulose. Due to its open structure containing many hydroxyl and acetyl groups, hemicellulose is partially soluble in water and hygroscopic [92].

Lignin and pectin serve as the chemical adhesive in the material [93]. Lignin is amorphous, highly complex, mainly aromatic polymers that absorb the least water amount of any natural fibre components [94].

Most plant materials contain 65-70% cellulose, which is crystalline and consists of three elements, C, H and O, with the general formula $C_6H_{10}O_5$ [95]. Lignin and other non-cellulosic substances are associated with the cells walls and their presence changes the final material properties. An important characteristic of plant materials is their ability to absorb moisture from the atmosphere in relatively large quantities, because cellulose is hygroscopic.

The plant materials ecological properties allow them to be applied more and more in various innovative industrial sectors, which are generally obliged to take sustainable development into account in their production methods. In addition, the plant fibres mechanical properties ensure the performance and competitiveness of the new used materials. Companies' R&D departments specialised technical institutes and universities now consider natural plant materials as an alternative solution to synthetic materials in the production of composite materials.

1.3.2.2 Hemp

Figure 13 : *The different types of hemp extracts [96].*

Figure 14 : *the hemp stalk attached by the hemp fibres [97].*

Hemp has been cultivated by humans since Neolithic times for its resistant fibres, oleaginous seeds and medicinal virtues. Its cultivation has lasted for several centuries mainly due to the use of its fibre to make boat sails, rope or clothing. It has long occupied a prominent place in the European agricultural landscape. Covering nearly 200,000 ha in France in the 19th century, it saw its activity decline due to competition from exotic or artificial fibres. This competition became increasingly fierce and led to the disappearance of hemp cultivation in Europe at the beginning of the 1960s. From the 1940s until the end of the 1990s, the paper industry was the only real industrial outlet for hemp. The current development of new markets (construction, plastics) offers new perspectives for hemp today.

As shown in Figure 13, Hemp provides three co-products: the powder, the fibres and the hemp shiv (for a long time considered as a waste product used mainly for straw). The seed is not used in building materials, the fibres can be used to produce wool (Figure 14) and the hemp shiv can be used to produce hemp concrete and plaster.

1.3.2.2.1 Hemp fibres

Hemp fibre has a lower density than other plant fibres and similar characteristics to other fibres regarding Young's modulus but also elongation. On the other hand, the breaking stress of hemp fibre is generally lower than that of other plant fibres [98].

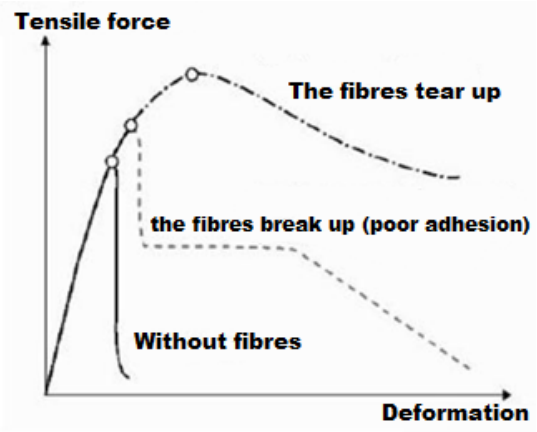

Figure 15 : *Comparison between concretes with/without incorporated fibres [93].*

Generally, the bio-based fibres are used to [93]:

- Improve the concrete mechanical performance, its tensile and flexural strength.
- Avoid the sudden cracks propagation in the cementitious material due to the opposition of the fibres at the crack opening.
- Transforming the fragile behaviour of the cementitious material into a practically elastic behaviour which improves safety during final charging (Figure 15).

1.3.2.2.2 Hemp shiv

Hemp shiv are aggregates made from the hemp stalk wood (Figure 16). Depending on the manufacturing process, different types of hemp shiv can be obtained: defibrated or fibrous, short or long. The used tool type in the process as well as the cultivation climatic conditions affect the hemp shiv morphological characteristics.

Figure 16 : *Hemp shiv particles.*

Hemp shivs have a porous tubular structure with a diameter varying between 10 and 50µm made up of parallel vessels in which circulates the plant's sap. Table 1 shows the hemp shiv chemical composition [99].

Table 1 : *Hemp shiv chemical composition.*

Water	10 to 15%
Total amount of organic content	97.9% from dry material
Cellulose	45 to 60%
Hemi-cellulose	15 to 20%
Lignin	15 to 30%
Ash	2 to 5%
Nitrogen	0.4 to 1%
K_2O	0.96 to 1.5%
CaO	0.89 to 1.4%
MgO	0.02 to 0.06%
Na	0.09%
S	0.16%

Like all cellulosic products, the hemp shiv is sensitive to water. The hemp shiv aggregate geometry can change according to water conditions. Additionally, the channel structure is favourable to water trapping by capillary action.

Hemp shiv is light in weight, which gives them a good insulating capacity. Moreover, air represents 92% of the total volume occupied with one-third to two-third distribution between intra-particle and inter-particle air, respectively. In addition, it has a water absorption capacity around three times its own weight, and the hemp shiv has a thermal conductivity between 0.05 and 0.06 W/(m.K) for densities between 88 and 155 kg/m^3 [100–102].

1.3.2.3 Binder

The main role of the mineral binder associated with hemp in the hemp concrete composition is to ensure a minimum of cohesion between the components. This mineral matrix provides the whole with sufficient rigidity and strength in the hardened state. The binders are almost systematically powdered minerals with a high fineness. The initial mixture of binder, hemp and water allows to obtain a soft paste, consistency necessary for the implementation (moulding, projection...) then the stiffening and the hardening of the mixture are obtained during the setting, the hardening and the drying of the whole.

A low hemp/ binder ratio increases the hemp concrete compressive strength and decreases the ductility of the material. Conversely, a high hemp/binder ratio makes the binder strength in the matrix low. Further, the bonding points between the binder and the hemp shiv are weak. Consequently, the deformation before material failure is important and the mechanical behaviour of the hemp shiv is dominant.

1.3.3 Properties of hemp concrete

This part presents the hemp concrete properties, and the hemp shiv effects in the fresh state, as well as the mechanical, thermal and hydric properties. Furthermore, solutions to improve the impermeability of hemp concrete are presented. Finally, durability studies in the bibliography will also be discussed.

1.3.3.1 Fresh state

Cerezo et al. [87] and Couedel et al. [103] show that the hemp shivs absorption capacities is around 250%, which changes the concrete rheological properties. In addition, Alvarez et al. [104] found that the high content of hydroxyl groups in cellulose increases the moisture absorption properties of plant materials. Moisture absorption by the natural hydrophilic materials leads to a decrease in workability.

Some studies have shown that natural materials of plant origin have a negative effect on the hydration of cement composites [105–107]. For example, hemp shiv affects thermal hydration due to the incompatibility of the binder-plant aggregate mixture, resulting in a loss of binder hydration, which reduces the mechanical strength [108]. Different studies have shown similar results [106,109], explained by the disruption of cement hydration reactions in the hemp shiv molecules presence. The exothermic hydration heat amount decreases as the hemp shiv amount increases. This difference in hydration heat is due to the change in the cement matrix structure. The delay in setting is due to the inability to develop aluminates (C_3A and C_4AF) [110].

Moreover, Bilba et al. [111] observed a delayed setting time and a reduction in the hydration heat in cement composites reinforced with sugarcane bagasse fibers. Also, Page et al. [110] found similar results using flax fibers.

Diquélo et al. [106] found that hemp shiv has damaging effects on the cement setting and hardening, as it delays and reduces the C-S-H and portlandite formation. This considerable modification of the setting and hardening process is further illustrated by the loss of mechanical properties. It was further demonstrated that a total absence of fixation occurs in the area around the shiv particle. Another major observation is that this lack of setting is related to both the aqueous extracts and the by-products of shiv degradation by the alkaline cementitious environment.

1.3.3.2 Mechanical

Hemp concrete is a material exhibiting an elasto-plastic behavior that is not fragile [87,98,112–114]. It has modest strength and rigidity compared to other construction materials of the same type (wood concrete). However, it can withstand high levels of deformation, which allows it to adapt to external stresses.

Furthermore, the results obtained by Cerezo et al. [87] show that the hemp concrete mechanical properties depend on the binder amount. Indeed, the mechanical strength varies between 0.25 and 1.25 MPa and the elasticity modulus between 4 and 160 MPa. As the binder content decreases, the mechanical resistance, elastic and Poisson's ratio decrease.

With a low binder content, hemp concrete acts as a stack of compressible particles connected by rigid binder bridges. For intermediate amounts, the hemp shiv particles are surrounded by thicker layers of hydrates, which improves the mechanical characteristics. For high binder contents, it behaves like a continuous binder matrix in which plant particles are embedded. Furthermore, the increase of the W/B ratio leads to a decrease in density which reduces the mechanical properties but improves the thermal and hygroscopic properties. Moreover, the tensile and flexural strength of composites is correlated with the compressive strength [99].

1.3.3.3 Thermal

Nguyen's experiments [113] also show that thermal conductivity is affected by the hemp shiv amount. Seng et al. [115] measured the thermal conductivity of precast hemp concrete using 2 measuring methods and found that the thermal conductivity of this material is equal to 0.103 W/(m.K) (hot plate) and 0.112 W/(m.K) (hot wire). Also, they found that the thermal conductivity increases with the increase of ambient humidity.

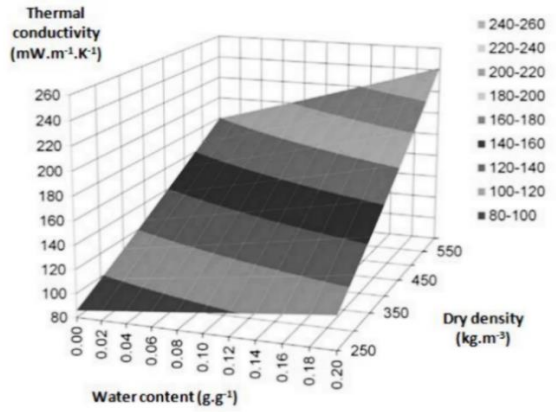

Figure 17 : *Simulated influence of density and relative humidity on the thermal conductivity of hemp concrete [165]*

According to Mazhoud et al. [99], the hemp concretes thermal conductivities at the dry point are between 0.089 and 0.128 W/(m.K), allowing them to be used in distributed insulation. The study points out that the thermal conductivity depends mainly on the the composite density and little on the type of binder and matrix used.

Furthermore, Figure 17 shows that the dry hemp concrete thermal conductivity varies between 0.08 and 0.18 W/(m.K) for densities between 250 kg/m^3 and 600 kg/m^3.

1.3.3.4 Hydric properties

The amount of water adsorbed or condensed in a porous material in equilibrium with an environment will influence its conductivity. The evolution plot of this water content as a function of the relative humidity for a given temperature is called the vapour sorption/desorption isotherm.

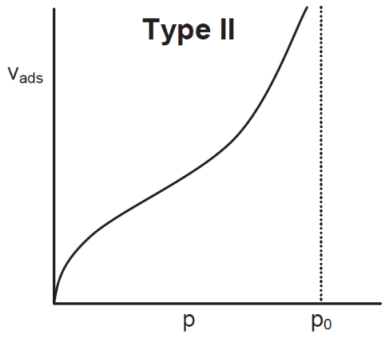

Figure 18 : *Type II classified by IUPAC, 1985.*

In the case of hemp shiv or hemp shiv concrete, the behaviour of the isotherms is of type II according to the IUPAC classification [89,116] (Figure 18).

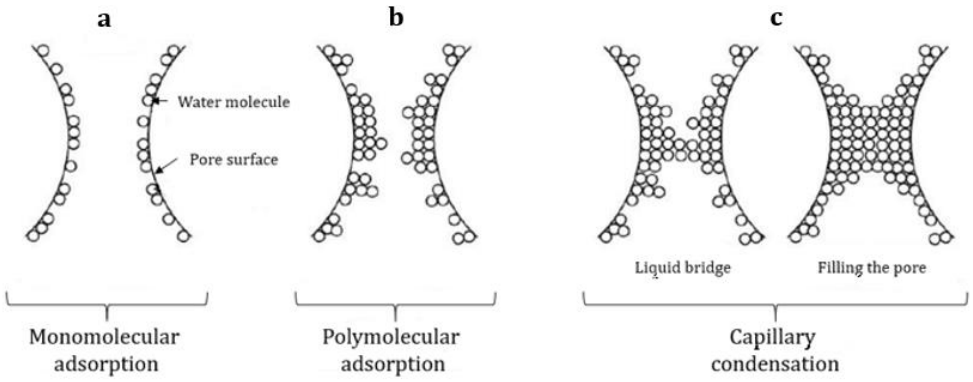

Figure 19 : *Moisture fixing mechanisms.*

Three phases can be identified for these isotherms. First, the vapor molecules adsorb on the surface of the solid phase and form a monomolecular layer (Figure 19 (a)). The first change of slope (Figure 18) corresponds to the beginning of adsorption of new gas molecules on the layer of molecules already adsorbed without the latter necessarily being complete (Figure 19 (b)). It is then called polymolecular adsorption. Finally, depending on the size of the pores, the water layers will condense the water vapor into liquid water and form a liquid bridge, then fill the pores (Figure 19 (c)).

Mazhoud et al. [99] studied the sorption desorption isotherms of hemp concrete and found that at low and medium hemp hygrometry, the mass waters contents are comparable regardless of the hemp/binder ratio. At the highest moisture content, the formulation with the highest hemp amount has the highest water content.

The binder type influences the hemp concrete capillary absorption. Increasing the hydraulic character of the binder and adding a water retainer reduces capillary absorption. The large interparticle spaces between the hemp particles (macropores) increase the permeability, while the micropores of the concrete (influenced by the hydraulicity of the binder) contribute to the permeability to a lesser extent [112].

1.3.3.5 Waterproofing

Several researchers have reported that the use of a water repellent can improve the interfacial adhesion of cellulosic plant materials and concrete, improving their mechanical properties and durability [117,118]. For instance, the water repellent addition in bamboo fibers absorbs only 4% of the water. Coated cellulosic materials can be water-resistant and without alkalinity and improve the cement-based composites durability. Bilba and Arsene [119] also recommend the use of a silane coating to improve the durability of cellulosic reinforced concrete, such as bagasse. Toledo et al. [120] recommends immersing the fibre in a silica fume suspension before adding it to the mix, resulting in more durable composites. Savastano et al. [121] reported that the use of pulp fibres can improve durability. Similarly, Juarez et al. [122] stated that the fibre extraction process may prevent a reduction in durability. Motta et al. [123] used high temperature heat treatment (120, 160 and 200°C) to increase fibre stiffness and reduce moisture absorption. The combination of pyrolysis and silane treatment improves the water resistance of the fibres, which become more hydrophobic [124]. Other studies have been carried out to study eucalyptus kraft cellulose fibres subjected to a chemical treatment to reduce their hydrophilicity and thus increase their durability [125].

1.3.4 Durability

1.3.4.1 Impact of the cementitious environment on plant materials

Durability is a very important factor in the design of cement-based materials, as it has a significant impact on the long-term strength of the materials. Cement is a highly alkaline material with a pH above 12,5. It contains metallic hydroxyl groups that are formed because of the calcium silicates hydration and hydroxylation, aluminates and ferrites present in the cement matrix. However, studies have shown that cement composites reinforced with natural plant fibres are susceptible to deterioration in cement matrices due to the weakening of the absorbed water and alkaline solution in these fibre pores. The composites deterioration is also weather-dependent. One of the main reasons for the deterioration of natural plant fibres in cement-based composites is the dissolution of the lignin and hemicellulose that bind the individual fibre cells with an alkaline pore solution [126]. In other words, the fibres durability in alkaline media is low due to the cellulose, hemicellulose and lignin dissolution. The fibres degradation in the cementitious-based matrix is one of the main causes of the mechanical properties decrease in the long term [92].

The degradation rate depends on the crystallinity and fibrillar morphology of the cellulose contained in these fibres [127]. Govin et al. [128] found that fibres containing more lignin are more sensitive to alkaline media. This is explained by the fact that lignin and hemicelluloses are more reactive than cellulose to alkaline attack. Therefore, the higher the cellulose crystallinity, the slower the degradation rate. Moreover, the cellulose crystallinity is higher than that of hemicellulose or lignin.

Yan et al. [92] explained the plant materials degradation mechanism in more details. Indeed, the cellulosic tissues degradation mechanisms in cement-based composites consist mainly of two components: (a) alkaline degradation (hydrolysis) and (b) plant matter mineralization. The alkaline degradation of cellulosic materials is due to the strong alkalinity of the cement solid phase and the porous solution. Advances in degradation include: (i) Lignin and part of hemicellulose degradation; (ii) hemicellulose degradation; (iii) cellulose degradation; and (iv) cellulose microfibrils failure, followed by complete degradation of cellulosic materials. Mineralization or self-mineralization of the plant particle cell wall is also an important degradation mechanism that attacks fibres in plant materials. Plant mineralization is sensitive to the CH content of the matrix. Precipitation of hydration products, probably calcium hydroxide, into the fibres cell wall structure is the main reason for cell wall mineralization [92].

1.3.4.2 Long-term properties

To observe changes in functional properties or microstructures, accelerated ageing is applied using relative humidity variations [129,130], immersion in water [131] or freeze-thaw cycles [132,133]. The water presence is indeed a risk factor for the hemp concrete durability. Moreover, the hemp shiv hydrophilic character leads to swelling of the particles, and thus leads to stresses at the interface between the aggregate and the binder [134]. Furthermore, in the presence of water and mineral binders, a high pH-value can be reached within the material, which leads to alkaline degradation, as well as plant mineralization [135]. The applied relative humidity value also has an influence on the carbonation kinetics [136].

1.3.4.3 ILUC effect as a drawback

As for all developments, at least one drawback can be foreseen as a risk in the bio-based materials development in civil engineering. Agriculture nowadays suffers deficiencies in Soil Organic Carbons (SOC), specifically in large farming and intensive cropping areas. Using agricultural spares in civil engineering applications in order to decrease latter's CO_2 emissions should not induce more CO_2 emissions in producing more biomass dedicated to civil engineering. Spares should remain real spares from agriculture. Unfortunately, such a drawback has already been observed previously, called ILUC effect (Indirect Land Use Change) in the biodiesel and bioethanol development, impeding soil-returned biomass and further decreasing SOC [137–140]. The bio-based concretes development must be strictly restricted to spare bio-sources.

1.4 CONCLUSION

The first part of this bibliographic study was focused on aerated concretes globally and then on non-autoclaved foamed concrete in particular. The latter is a construction material that consists of a cementitious matrix and voids, while most of this void is in the form of air bubbles. To manufacture non-autoclaved foam concrete, 2 production methods are considered the most popular and the most environmentally friendly, the preformed method and the direct method. Furthermore, it has been reported that foamed concrete is considered to be a good insulator, lightweight and makes construction easier.

Then, we proceeded to a review on the bio-based concretes and in particular the hemp concrete, which consists of binder and hemp particles mixture, this material presents excellent thermal performances and insulation capabilities, while being lightweight. Moreover, Hemp concrete reduces the environmental impact thanks to its bio-based character.

Much research discusses the properties of these two types of concrete but few of them discuss the combination of foamed concrete and hemp shiv. Mineral aggregates are already used in foam concrete. This can give important thermal performances, reducing the environmental impact, but the main challenges are to create a production method to produce this material without too much influence on mechanical performances and waterproofing of the material.

At the light of this literature review, hemp shiv (HS) is widely used in hemp concrete studies as an alternative to mineral aggregates. The valuable characteristics of hemp concretes are its lightweight, low carbon emission, excellent moisture buffering, low thermal conductivity and acoustic insulation, which can reduce energy consumption and gas emissions from buildings. At the same time, incentives are being offered for bio-based materials to play an increasingly important role in the building materials composition.

However, bibliography highlights that the foamed concrete is a very sensitive material at young age. It needs specific techniques during production to avoid deflation of foam, like avoiding vibration, ensuring the fluidity of the foamed concrete by increasing the water amount or by using superplasticizer, accelerating the concrete setting. Furthermore, it is found that both concretes (foamed and bio-based) present rather modest mechanical performances and an important permeability to water in the structure, because of the high porosity and the high connectivity of the porous network. Therefore, to improve the hemp concrete mechanical strength, it is necessary to add pozzolans, since it is more compatible with plant materials, and we can use water repellents to improve the waterproof character of the concrete.

Consequently, it remains necessary to create and optimize formulations for such new materials, based on the mechanical and thermal performances, and the environmental impact. This involves the study of the solid phase (the cementitious matrix) and porous structures in foamed concrete to understand the effects of incorporating hemp chips and how these incorporations affect the concrete structures.

Chapter 2

Methods, materials and production of bio-based foam concrete

2. Methods, materials and production of bio-based foam concrete

2.1 INTRODUCTION

The bibliographic study provided in the previous chapter highlighted the components effects on the bio-based foamed concretes formulations and properties. In this chapter, the different constituents used for the realization of the various cementitious formulations are presented, as well as the applied characterization techniques. This chapter is divided into three main parts. First part presents the raw materials used in this study (cement, additives, admixtures and hemp shiv) to formulate the bio-based foamed concretes. Second part, all the experimental methods and processes used to study the bio-based foamed concrete essential properties (physical, mechanical, thermal, hydric) are defined. Third, non-autoclaved bio-based foamed concrete formulations are investigated by studying thermal, mechanical, CO_2 emissions and production cost performances.

2.2 RAW MATERIALS

2.2.1 Water

The water used to make concrete is the water used for the distribution of the municipality of Epron. Its total chlorine content is equal to 0.07 mg/L, lower than the limit value given by the NF EN 1008 standard (0.27 mg/L). Its pH is equal to 7.4 [141].

2.2.2 Binders

2.2.2.1 Cement

The cement used comes from Calcia's Ranville plant. It is certified [NF EN 197-1] and referenced CEM I 52.5 N. The physical, mechanical and chemical properties of the cement delivered by the supplier. The ordinary Portland cement (CEM I) used is a cement composed of 97% clinker. Portland clinker is obtained by calcining a precisely fixed mixture of raw materials, containing elements commonly expressed as oxides CaO, SiO_2, Al_2O_3, MgO and small amounts of other materials.

The clinker contains at least two thirds of calcium silicates ($3CaO.SiO_2$ and $2CaO.SiO_2$), the remaining part consisting of phases containing aluminium, iron and other components. Cement hydration is a complex phenomenon that takes place in several main stages:

- Adsorption: Water fixation on the grains surface.
- Hydrolysis: Solid parts decomposition.
- Rapid dissolution of the clinker anhydrous phases.
- Obtaining a supersaturated solution in relation to hydrated phases. With the dissolution of anhydrous compounds, the mixing water becomes rich in calcium, silicon, sulphates, aluminium and alkalis. The saturation level of the hydrated phases is reached.
- Progressive crystallization of the minerals.

The next two mineral binders cannot be used as a total substitute for cement, but only as a partial mineral addition. They have been chosen for their pozzolanic character.

2.2.2.2 Ground Granulated Blast Furnace Slag

Ground Granulated Blast Furnace Slag (GGBFS) which is a by-product from iron production, fulfilling EN 206-1 has been widely used in concrete for a long time. The first norm for Portland blast-furnace cement was realized in 1923. A large amount of study carried out on GGBS-based concrete has shown that it offers advantages for fresh and engineering properties, as well as for some aspects of durability. Moreover, it can offer environmental and economic benefits to construction. However, its application in Portland cement concrete has been limited due to concerns about a slower rate of strength gain at early ages. The characteristics of these alternative binder are provided respectively in Appendix 1. Figure 20 shows XRD diagram of GGBFS used in this study, it is totally amorphous.

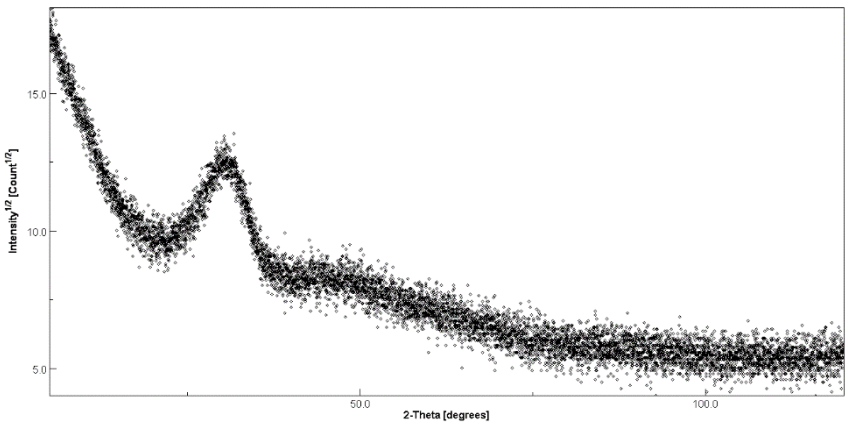

Figure 20 : *XRD diagram of GGBFS.*

2.2.2.3 Metakaolin

To solve the problem of slow strength gain at early ages when using GGBFS, it is necessary to add metakaolin (MK), which is obtained by flash calcining kaolinite at about 700°C. The presence of MK enhances the strength at early ages [142]. Thus, it reduces the negative effect of GGBFS at the early age of strength development. Although, it was also noted that the MK-slag mixes exhibited the most strength at 28 days.

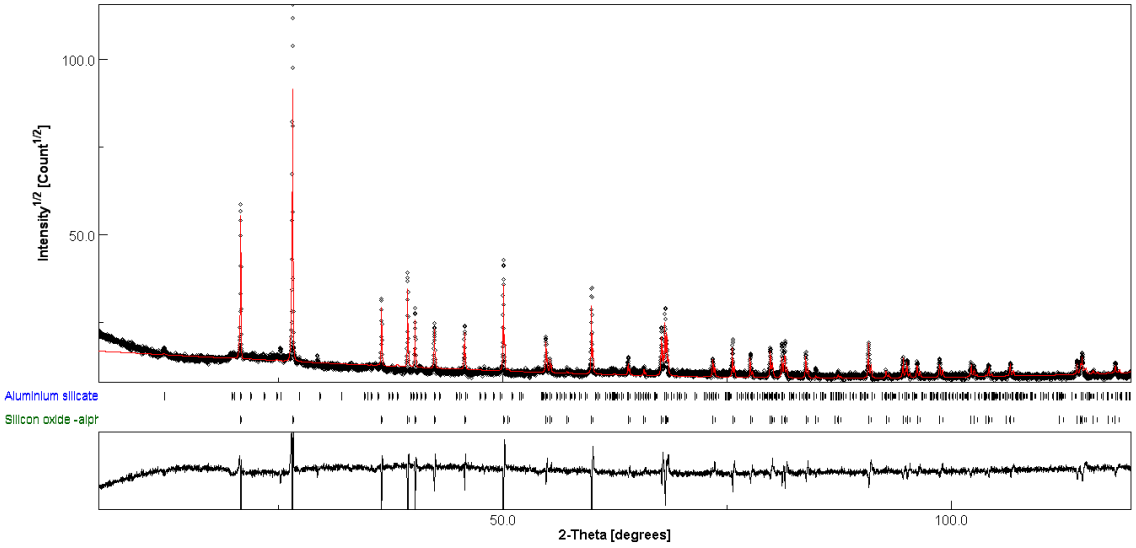

Figure 21 : *XRD diagram of MK.*

As shown in Figure 21, metakaolin is crystallized with a mineralogical composition of 77 wt% quartz and 23 wt% kaolinite. But we cannot also exclude some amorphous contents in MK, since the diagram exhibits small, modulated background around 30° in 2-theta. The chemical and physical characteristics is given by the supplier in Appendix 2.

2.2.2.4 Physico-chemical characteristics of the binders

The chemical composition of Portland cement, GGBFS and MK given in Table 2 is obtained from the supplier of each binder, together with their absolute density. The absolute density of CEM I and GGBFS is almost identical, but GGBFS requires more water for hydration. MK has the lower absolute density and the most pozzolan raw material with Al_2O_3 + SiO_2 more than 90%.

Table 2 : *Physico-chemical characteristics of the binders*

The chemical compound	Chemical composition (%)		
	CEM I	GGBFS	MK
Calcium oxide (CaO)	66.2	43	0.322
Aluminium oxide (Al_2O_3)	4.44	10.7	$Al_2O_3 + SiO_2$ = 92.5
Silicon dioxide (SiO_2)	20.6	37.3	
Ferric oxide (Fe_2O_3)	4	0.2	3.7
Sulfur trioxide (SO_3)	2.6	0.1	0.2
Sodium oxide (Na_2O)	0.07	0.7	0.252
Magnesium oxide (M_gO)	1.25	6.5	0.19
Potassium oxide (K_2O)	0.84	0.4	0.4
Others		1.1	2.436
Absolute density (kg/m^3)	3.1	2.9	2.5

The most common oxides for cementitious materials are silica (SiO_2), alumina (Al_2O_3) and lime (CaO). The Keil triangular diagram represents the ternary lime-silica-alumina system. It allows to locate and compare the compositions of the different binders. The Keil diagram of the binders used in this study is shown in Figure 22.

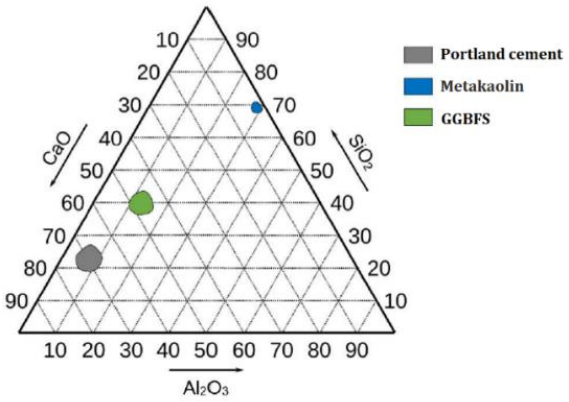

Figure 22 : *Keil ternary diagram for the different binders*

2.2.3 Admixtures

To control the setting time and workability of the studied concrete, additional additives are used in the mineral suspensions. According to standard NF EN 934-2 [143], an admixture is a "product incorporated at the time of mixing of concrete or mortar at a dose less than or equal to 5% by mass of the cement content of the concrete or mortar, in order to modify the properties of the mixture in the fresh and/or hardened state".

The water content of the mixtures should preferably be low to improve the mechanical behaviour, while avoiding vibrating the concrete to protect air bubbles, so that the foamed concrete paste should be fluid [144]. In this context, it is necessary to use superplasticizer (SP) to achieve a good fluidity of the fresh paste. Therefore, a superplasticizer with a high water-reducing capacity named MasterGlenium ACE 456 from BASF, based on polycarboxylates, is used.

A commercial foaming agent named BETOMOUSS® from SIKA is used to generate a stable bubble network and to maintain the foam structures until setting. This foaming agent (FA) is a liquid additive which produces a foam density of approximately 70 kg/m^3.

The foaming agent, GGBFS and hemp shiv have a retarding side effect that delays the hardening of the concrete [27,145]. Therefore, an accelerator (Acc) named CHRYSO®Xel 650 from CHRYSO is used to promote the cement initial hydration reactions, which accelerates the setting, improves the air bubbles stability in the cementitious matrix and develops the mechanical strength early. In addition, a CHRYSO®Dem Ekla 12 - DEV demoulding agent, which does not contain solvents in its composition, is used to create a non-stick film on the formwork surface. It is used to easily separate the foamed concrete after curing. The characteristics of the accelerator, superplasticizer and foaming agent are shown in Table 3.

Table 3 : *Characteristics of admixtures used to elaborate the cementing materials.*

	Acc	SP	FA
Consistence	liquid	liquid	liquid
Color	Yellow	brown	bright yellow
Density (g/cm^3)	1.45 ± 0.01	1.06 ± 0.01	1.04 ± 0.02
Recommended weight	1-1.5 %	1-3 %	-
Chlorides content	≤ 0.1 %	≤ 0.1 %	0.001 %
pH	6 ± 1	6 ± 1	9
Solids Content (%)	61.5 % ± 2.7 %	30.5 % ± 1.5 %	30 %

2.2.4 Hemp shiv

Hemp shiv (HS) used in this study is a commercial type of product supplied by Technichanvre® (Appendix 3). This product is composed of 95% hemp shiv and 5% of hemp fibers. All the characteristics presented in the following sections are studied according to the recommendations of the Rilem TC 236 BBM Technical Committee [146].

2.2.4.1 Absolute and Bulk density

Only bulk density and thermal conductivity is given by the supplier (Appendix 3). Therefore, according to ASTM B923, the measurement of absolute density is investigated by AccuPyc II 1340 helium pycnometer. It allows accurate measurement of the volume of the solid phase of a sample of known weight. The test should be repeated 3 times at least (with 3 hemp shiv different samples). In addition, Table 4 presents the bulk and absolute density, and thermal conductivity of the hemp shiv.

Table 4 : *Hemp shiv bulk and absolute density, and thermal conductivity.*

	Bulk density	Absolute density	Thermal conductivity
Hemp shiv	140 kg/m^3	1413±23 kg/m^3	0.048 W/(m.K)

2.2.4.2 Water absorption

According to the Recommendation of the RILEM TC 236-BBM [146], before testing, hemp shiv is dried in an oven at 60°C until the variation in mass is less than 0.1% between three successive weighing at 24 h intervals. To determine the water absorption capacity of the aggregates, measurements are realized on four samples of 25 g of aggregate. Water content is measured after 1, 15, 60 and 240 (4 hours) and 2880 minutes (48 hours) of immersion.

The sample mass at time t allows us to determine the water content w(t) which is expressed as the ratio between the sample mass gain at time t and its initial dry mass (Eq. 7).

$$w(t) = \frac{m(t)-m(0)}{m(0)} \times 100 \qquad \textbf{\textit{Eq. 7}}$$

$w(t)$: Water content at time t (%).

$m(t)$: Sample Mass at time t (g).

$m(0)$: Hemp shiv initial mass before immersion in water (g).

The variation of hemp shiv moisture content with time is modelled by the following equation:

$$w(t) = IRA + K1 \times log\ (t) \qquad \textbf{\textit{Eq. 8}}$$

IRA : Corresponds to the particles surface water content, thus to the absorbed water content during the first minute.

$K1$: The parameter reflecting the water absorption rate within the particle (varies with the particles porosity).

t : The immersion time of the hemp shiv.

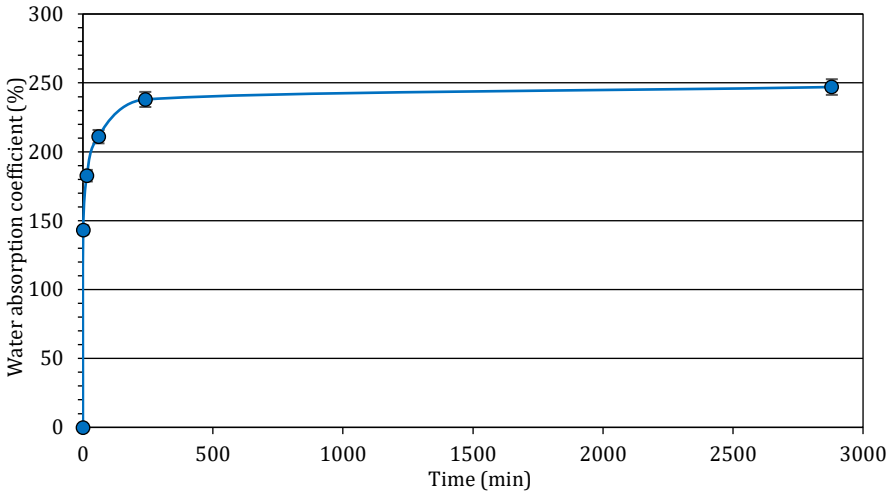

Figure 23 : *Water absorption kinetics of hemp shiv versus immersion time*

Hemp shiv used in this study has a high-water absorption capacity. Indeed, Figure 23 showed that the water absorbed by hemp shiv increases about 143% after one minute of immersion to become around 247% after 48 hours. These results confirm the high-water absorption and retention capacity of hemp shiv, attributed to their high porosity and capillary structure [114,134,147].

2.2.4.3 Particle size distribution

To study the size distribution of hemp shiv particles, two methods are used: mechanical sieving and image analysis.

Mechanical sieving is carried out on 3 samples of 100 g of aggregates. The sieve columns used are: 0.1, 0.25, 0.5, 1, 2, 4, 8 and 16 mm. Each of the sieves is weighed to form a cumulative mass curve of the sieve size. For elongated or flattened particles, such as hemp shiv particles, this method may not be the most appropriate. In fact, the particles can either pass through the sieve in the direction of their width or be retained if positioned across the opening [148].

Figure 24 : *Protocol of granulometric analysis by image treatment (Scan, conversion of the gray scale and adjustment in the form of ellipses).*

For image analysis, the images obtained by the Keyence microscope allow a first observation of the pore structure and the ImageJ software is used to analyze the scanned images. To obtain the best image contrast, a black background is deployed. This method is performed on a sample weighing about 6 g. The image analysis process consists of 5 steps. The first step consists of preparing hemp samples without drying. Then, the color images of the hemp particles are acquired by the scanner with a resolution of 600 DPI and a black background. Before scanning, the particles must be arranged in such a way that they do not touch or overlap. The third step is performed by the ImageJ software, as shown in Figure 24. The treatments consist in correcting the brightness and to binarize the image. The fourth step is to calculate the particles characteristics. The last step is to use the Excel software to exploit the results and generate the granulometric curves (Figure 25).

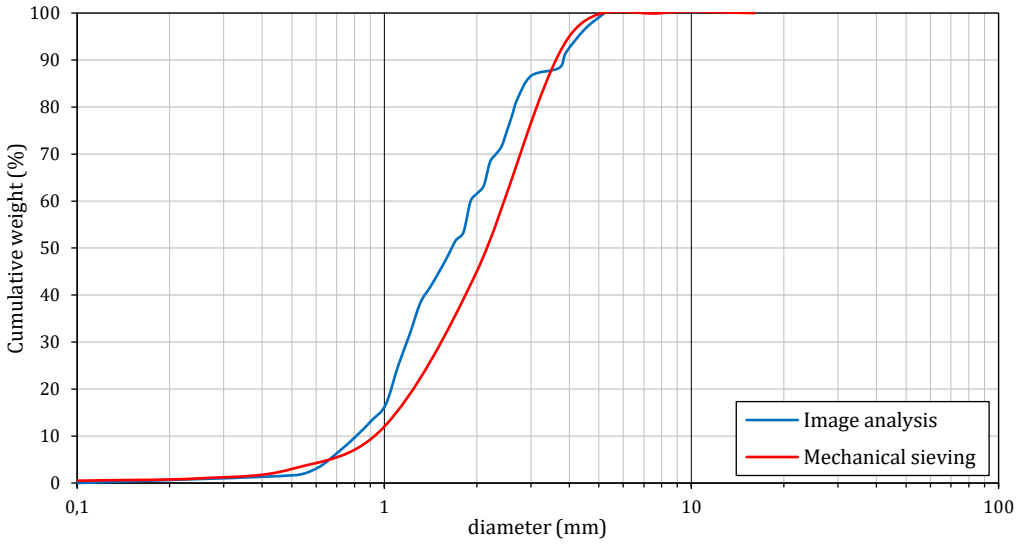

Figure 25 : *Aggregate size distribution determined by mechanical sieving and image hemp shiv analysis methods.*

Figure 25 shows the granulometry of hemp shiv used in this study obtained from mechanical sieving experiment and from image analysis. Both types of determination give very close distribution curves with particle sizes ranging between 0.6 and 5 mm.

2.3 METHODS

2.3.1 Production methods

Several parameters intervene in the elaboration of a foamed concrete and can influence its behaviour in the fresh and hardened states. Among these parameters, the mixing protocol is

important because it must be adapted to the mixture function to obtain a good homogeneity since the homogeneity of the cellular structure is one of the essential parameters to control. Air bubbles must remain stable in the concrete in a fresh state, without coalescence. Thus, it is preferable [144] to:

- Use a fast-setting binder and/or acceleration agent.
- Obtain a high viscosity cement matrix.
- Obey total absence of vibration.

With respect to the previous advice, two production methods are applied in this study, the preformed foam method and the direct mixing method.

2.3.1.1 Preformed foam method

Preformed foam method is based on the separate production of a light and stable aqueous foam which is gradually inserted into a mineral suspension. Figure 26 illustrates the protocol of the preformed foaming method which is divided into two stages. On the one hand, the foam is produced by mixing the diluted foaming agent with water in a ratio of 1:30 (by weight). On the other hand, the powdered constituents and hemp shiv are first mixed dry in the IGM mortar mixer with a capacity of about 20L complying with the EN 196-1 standard (Figure 27), then water is added with the accelerator and superplasticizer, the mixture is stirred until obtaining a homogeneous paste. Finally, the mineral suspension is added to the foam gradually and stirred (at high speed) until the mixture becomes homogeneous.

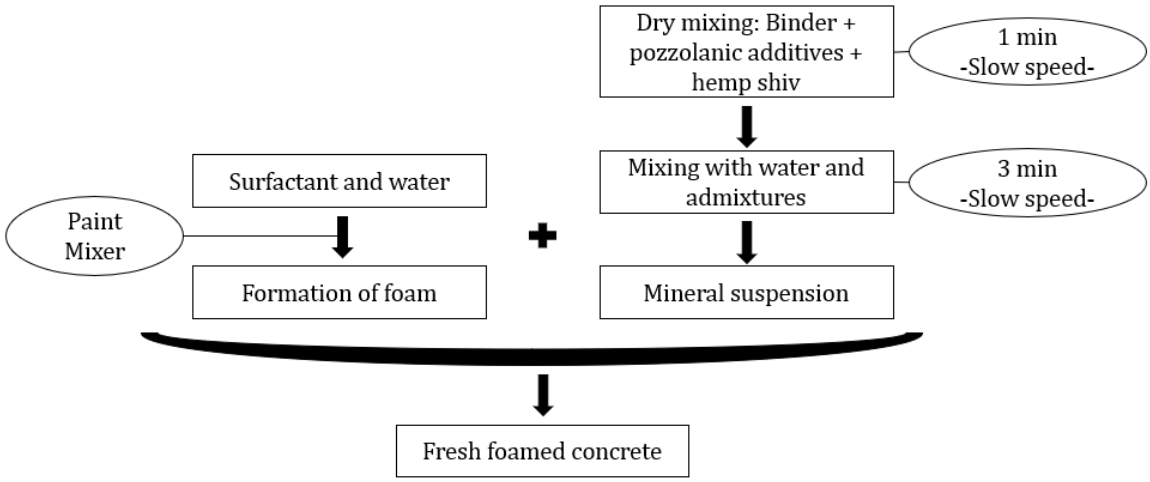

Figure 26 : *Protocol of the preformed foaming method.*

Figure 27 : *IGM mixer used to produce mineral suspensions.*

2.3.1.2 Direct mixing method

Foam concretes are also manufactured using the direct mixing method. Figure 28 illustrates the protocol of this method which is based on the addition of a foaming agent directly into the mineral mixture after its formation, the preparation of the mineral mixture is the same in both methods.

In the IGM mixer showed in Figure 27, all the solid elements (CEM I, GGBFS, MK and HS) are mixed for 1 minute to obtain a homogeneous paste. All the water, superplasticizer and accelerator are introduced in 30 seconds. Mixing at slow speed continues for 3 minutes. Then the surfactant is added, and the mixture is mixed by a paint mixer at high-speed for 3 minutes. This mixing allows air to be introduced into the suspension.

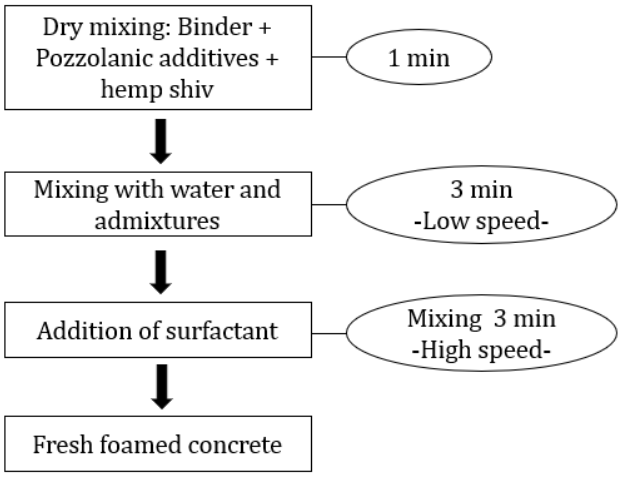

Figure 28 : *Protocol of the direct method.*

2.3.1.3 Specimen elaboration

With both methods, the concrete obtained is fluid and foamy, then placed without any vibration in the moulds. After 48 hours curing in the room air, the samples are demoulded and stored in a damp room (20 °C, RH > 95 %). Depending on the required measurements, several sizes of specimens were used:

- Rectangular prism specimens of 4 x 4 x 16 cm^3 for compressive strength and flexural strength.
- Rectangular prism specimens of 30 x 30 x 5.5 cm^3 for thermal conductivity.
- Ø11x22 cm^3 cylinders for porosity accessible to water.
- Cubic specimens of 15 x 15 x 15 cm^3 for capillary absorption.

2.3.2 Physical properties

2.3.2.1 Density

2.3.2.1.1 Bulk density

Fresh paste density is measured according to standard NF EN 12350-6, immediately after the end of the process by gravimetric measurements of the filled moulds. The maximum relative uncertainty on this measurement is estimated to 3%.

The bulk density ρ of the hardened foamed concrete samples is determined according to standard NF EN 12350-6 by the ratio between the mass and the volume of three samples of 4×4×16 cm^3, these samples is drying at the temperature of 60 °C until constant weight. An error on the mass, but especially on the volume of the samples is possible. The maximum error on bulk density measurement is estimated at 4%.

2.3.2.1.2 Absolute density

According to ASTM B923, the absolute density ρ_{abs} measurement is investigated by AccuPyc II 1340 helium pycnometer (Figure 29). It allows to accurately measure the solid phase volume of a known weight sample. Indeed, the measurement principle is to introduce helium into a reference enclosure with a known pressure and then extend this gas into the enclosure containing the sample by measuring the sample new pressure. This measurement method is adapted to porous solids with open porosity because helium has a small atomic diameter and penetrates easily into the pores.

Figure 29 : *Absolute density measuring device.*

The measurement is made on three samples whose masses are determined at room temperature using a 0.001 g precision balance; the volumes are then measured with a pycnometer at the same temperature. The density is taken equal to the average of the three values obtained.

2.3.2.2 Porosity

2.3.2.2.1 Total porosity

According to the NF EN 1097 standard, total porosity Φ is obtained from the absolute density and the bulk density using the following equation:

$$\Phi = (1 - \frac{\rho}{\rho_{abs}}) \times 100 \qquad \textbf{Eq. 9}$$

ρ : Bulk density (kg/m^3).

ρ_{abs} : Absolute density (kg/m^3).

2.3.2.2.2 Porosity accessible to water

The porosity accessible to water and the bulk density measurement was carried out by hydrostatic weighing according to the NF P18-459 standard (Figure 30 and 31).

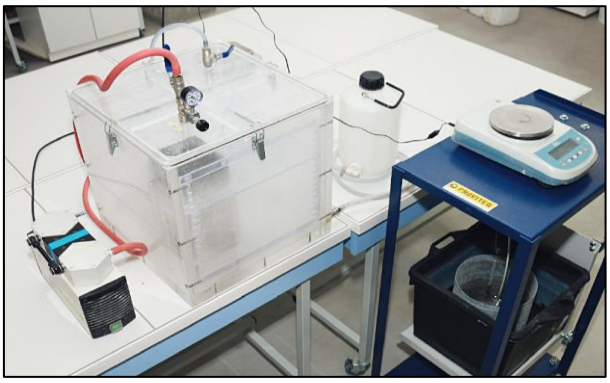

Figure 30 : *Water-accessible porosity device.*

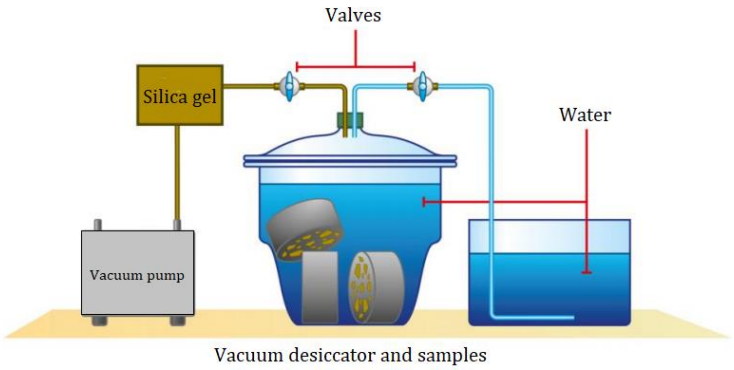

Figure 31 : *Scheme illustrating the process of water-accessible porosity.*

The foam concrete samples were introduced into a void space in the presence of silica gel at a relative pressure of 998±1 mbar. This pressure is maintained for 4 hours to reduce the contact angle of the water in the pores and thus facilitate their saturation. As soon as the water is introduced, the pressure is maintained for at least 44 hours. Then, the dry bulk density ρ_d, and the porosity accessible to water ε are deduced by the following equations:

$$\rho_d = \frac{m_{dry}}{m_{air} - m_{water}} \times \rho_{water} \qquad \textbf{Eq. 10}$$

$$\varepsilon = \frac{m_{air} - m_{dry}}{m_{air} - m_{water}} \times 100 \qquad \textbf{Eq. 11}$$

m_{dry} = The foamed concrete dried weight at 105±5 °C (g).

m_{air} = The foamed concrete weight in saturated conditions dry surface (g).

m_{water} = The saturated foam concrete weight in the suspension system of the hydrostatic balance after immersion for 48 hours (g).

2.3.3 Mechanical properties

There is no specific standard for foamed concrete. However, Cerib [144] has evaluated the mechanical performance of several foam concrete formulations according to the NF EN 196 standard.

2.3.3.1 Flexural strength

The three-point bending test was carried out on 4×4×16 cm^3 prismatic mortar specimens in accordance with NF EN 196-1. The device used is an electromechanical press from the IGM company with a capacity of 250 kN, equipped with a load cell with a capacity of 50 kN to improve the accuracy of the results (Figure 32). Three samples were tested per formulation. The NF EN 196-1 standard requires a loading speed of 50 N/s.

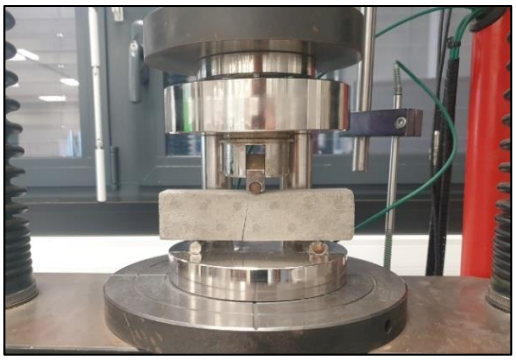

Figure 32 : *Flexural test device*

To observe this behaviour better, it is preferable to drive the test on the move instead of under load. Thus, the 3-point bending tests carried out on the mortars were conducted with a loading speed of 0.20 mm/min. The displacement is measured using a digital LVDT sensor. The specimen is placed on the press frame with 100 mm between the two supports and is then loaded until it ruptures. The flexural strength is calculated using the following equation:

$$R_f = \frac{3.F_{f,max}.L}{2.b.h^2} \qquad \textbf{Eq. 12}$$

R_f = The flexural strength of foam concrete (MPa).

$F_{f,max}$ = The maximum flexural load at rupture (N).

L = distance between supports (mm).

b, h = respectively the width and height of the specimen (b = h = 40 mm).

2.3.3.2 Compressive strength

The compression test was carried out following the flexural test, on one of the two halves of the broken specimen (Figure 33). The same press as for the flexural test was used, but the 50 kN load cell was replaced by another one with a higher capacity (250 kN).

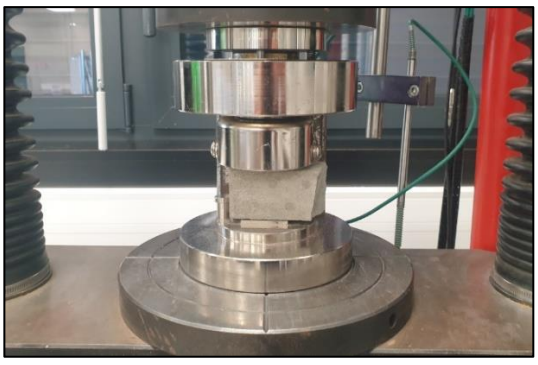

Figure 33 : *Compressive test device*

The loading speed is 2.4 kN/s, according to NF EN 196-1. The half-prisms to be tested are placed laterally in the center of the machine platform. The compressive strength is calculated according to the following equation:

$$R_c = \frac{F_{c,max}}{b.h} \qquad \textbf{Eq. 13}$$

R_c = The compressive strength of foam concrete (MPa).

$F_{f,max}$ = The maximum compressive load at rupture (N).

b, h = respectively the width and height of the specimen (b = h = 40 mm).

2.3.4 Thermal properties

2.3.4.1 Thermal conductivity

Throughout this study, thermal conductivity measurements are performed using the fluxmeter method. As mentioned in the first chapter (Section 1.3.1), this technique has good repeatability for large specimens as well as acceptable execution time cost and measurement uncertainties.

Figure 34 : *Thermal conductivity test device.*

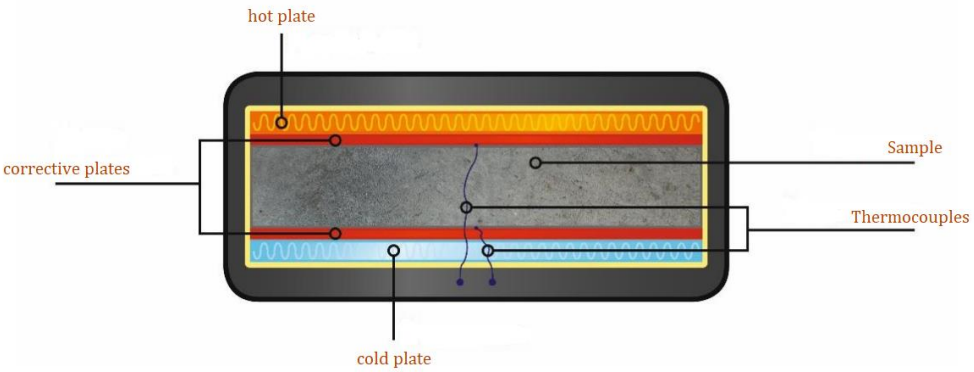

Figure 35 : *Scheme illustrating the process of thermal conductivity test.*

The device used is HFM 436 Lambda flowmeter (NETZSCH) (figure 34) following the EN 12667 standard. It allows the measurement of the thermal conductivity of materials with a surface area of 300x300 mm^2 and thicknesses ranging from 5 to 100 mm, at temperatures ranging from -30 to 90 °C and for conductivities ranging from 0.002 to 2 W/(m.K). Figure 35 explains the thermal conductivity operating process. The principle of this method is based on the circulation of a thermal flow through the sample. Indeed, the sample to be measured is inserted between the two hot and cold plates of the device, in contact. The temperature gradient between these two plates generates a heat flow that crosses the sample in steady state. The flow is quantified on both sides of the sample by flow sensors. Fourier's law of heat conduction allows us to derive the sample thermal conductivity (λ) and thermal resistance values (R=e/λ with e the thickness of the sample measured).

2.3.5 Hydration

2.3.5.1 Semi-adiabatic calorimetry

Hydration heat of foamed concrete during the first few hours is measured by semi-adiabatic calorimetry (Langavant method), according to the NF EN 196-9 standard (Figure 36).

Figure 36 : *Semi-adiabatic calorimeter (NF EN 196-9)*

This test allows the determination of the heat amount released by the cement during its hydration from the temperature evolution. At a given time, the cement hydration heat Q, expressed by Eq. 14, is equal to the sum of the heat accumulated Q_{acc} in the calorimeter and the heat dissipated to the outside Q_{dis}. The foamed concrete temperature under test is compared with that of an inert sample in the reference calorimeter.

$$Q = Q_{acc} + Q_{dis} \qquad \textbf{Eq. 14}$$

The heat accumulated in the calorimeter and the heat dissipated to the outside are calculated from Eq. 15 and Eq. 16 respectively:

$$Q_{acc} = \frac{c}{m_c}.\Delta T \qquad \textbf{Eq. 15}$$

With:

c = Total heat capacity of the calorimeter (J/K).

m_c = Cement Weight in the test sample (g).

ΔT = Temperature difference between the test calorimeter and the reference calorimeter at time t (K).

$$Q_{dis} = \frac{1}{m_c}\int_0^t \alpha.\Delta T.dt \qquad \textbf{Eq. 16}$$

With:

α = Total heat loss coefficient of the calorimeter (J/(h.K)).

t = Time elapsed since the beginning of hydration (h).

2.3.5.2 Thermo-gravimetric analyses

Cement hydration degree is obtained from the hydrated cementitious compounds bound water content. Furthermore, as temperature increases, cement hydration products decompose, releasing water and carbon dioxide [146]. Therefore, thermogravimetric analyses (TGA) were carried out.

Figure 37 : *Thermogravimetric analyses (TGA) device*

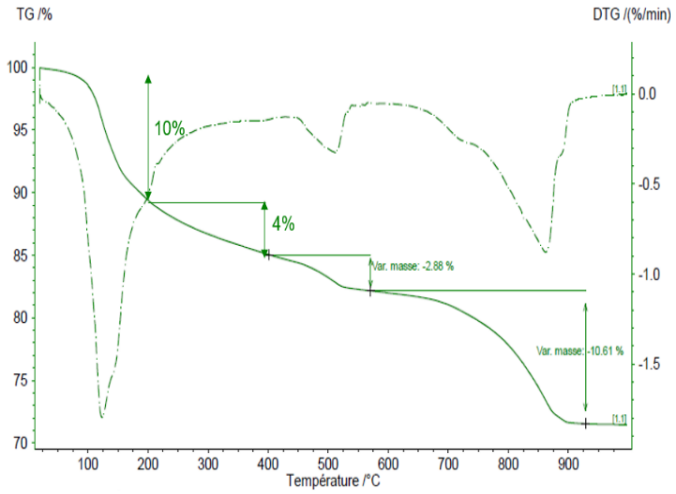

Figure 38 : *ATG chart.*

Thermogravimetric analyses (TGA) (Figure 37 and 38) were realized at a heating rate of 10°C/min in an inert environment (nitrogen) at a pressure of 1 bar in a Netzsch STA449 F3

Jupiter® furnace. To get representative samples of the processed materials, pieces of about 1 cm^3 were taken from the core of the test specimens. Each of these samples was then crushed (< 4 mm) and dried at 20 °C in a vacuum desiccator for 72 hours. They were then finely crushed (< 125 µm) and dried again in an oven at 70°C. TGA measurements were made on samples of 1000 ± 50 mg concrete powder.

2.3.5.3 X-ray diffraction

The hemp shiv impact on the foamed concrete mineralogical structure is studied through the determination of crystalline phases. X-ray diffraction measurements were carried out on polycrystalline samples with different proportions of hemp shiv.

The diffractometer used is a PANalytical model X'PERT Pro with a filtered copper radiation. The diffraction angles 2θ are recorded between 10 and 80° with a step of 0.013° and a total acquisition time of 2h. The foam concrete samples are previously crushed with a cryo-grinder.

The diffraction diagrams analysis is carried out using the Rietveld approach as implemented in the MAUD software (D. Chateigner Ed.: "Combined analysis", 2010, Wiley-ISTE, 496p. ISBN: 978-1-84821-198-8). We used this technique to identify and quantify crystalline phases.

2.3.6 Hydric properties

2.3.6.1 Capillary absorption

Dry concrete water absorption is influenced by two major parameters, the effective porosity of the concrete and the absorption rate by capillary ascent [149].

According to the NF EN 13057 standard, Capillary water absorption consists of following the weight of the material exposed to water along its bottom face (immersion depth of 2 mm) during the following immersion times: 5, 15, 30, 60, 120, 240, 1440, 2880, 5700 and 6600 minutes, then dried until reaching a constant mass in a ventilated oven at 80±2°C. Capillary absorption coefficient C_a (kg/(m^2.√h)) is defined by the slope of the mean linear capillary absorption line.

2.3.6.2 Sorption-desorption

The water sorption/desorption isotherms were obtained using the dynamic vapour sorption method (DVS) (Figure 39). This is a gravimetric technique for measuring the interactions of vapours with solids using the sorption/desorption instrument SPS11-10µ from ProUmid.

The measurements were performed at constant pressure with fixed total flow rate to minimize the weight variations associated with the Archimedean and trailing forces. The use of a fixed temperature allowed the isothermal sorption curve to be obtained by equilibrating the sample under a series of vapour concentrations. The measurement is often quite sensitive to temperature since this latter influences the sorption behaviour of materials.

Figure 39 : *Device used for DVS testing (ProUmid)*

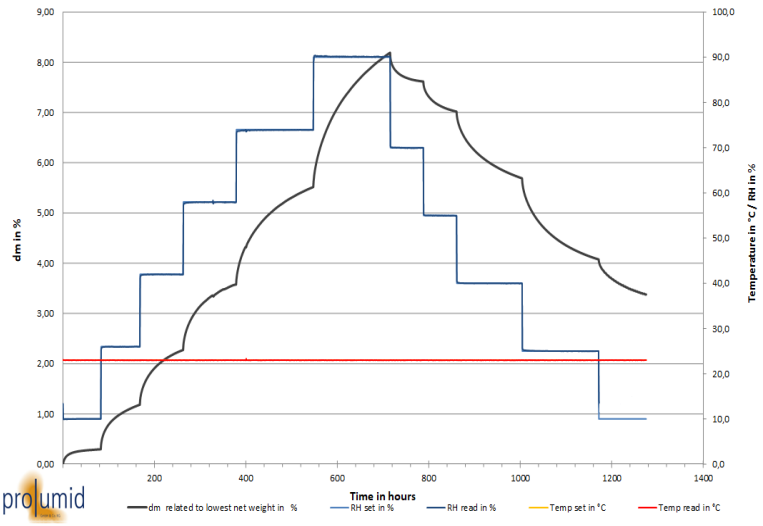

Figure 40 : *Relative humidity levels and the weight of a sample*

The isothermal sorption curves are determined discontinuously in successive steps of increasing and then decreasing relative humidity (or vice versa) (Figure 40), according to a method described in the NF EN ISO 12571 standard. The tests were carried out with representative samples of 10000 ± 100 mg. The samples were automatically weighed every 20 minutes throughout the test. The relative humidity (RH) in the chamber varies between 5 and 90% RH in 5% RH intervals. For each moisture content, equilibrium is considered to be reached when the variation in sample mass is less than 0.01% after 120 minutes.

2.3.7 Visualisation method

The images obtained by the Keyence microscope (Figure 41) provide a first observation of the pore structure (Figure 42). To investigate the air bubbles and hemp shiv distribution, an image analysis software is necessary.

Figure 41 : Keyence microscope

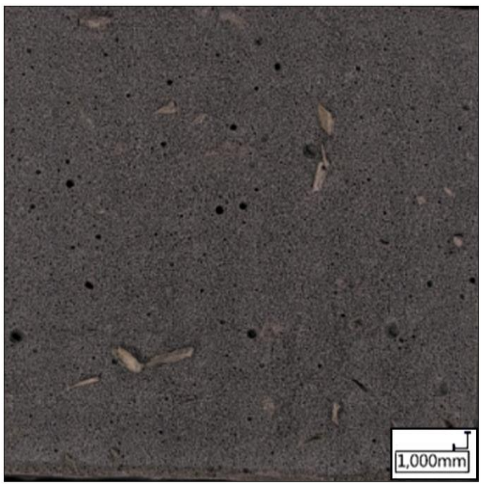

Figure 42 : *The raw image of the bio-based foamed concrete with size 10000x10000 (pixels).*

For this purpose, the ImageJ software is used firstly to determine the hemp shiv surface amount and to eliminate it (Figure 43). Then to characterise the air bubbles in the concrete structure according to the position (x;y), perimeter, surface, small and large radii of the ellipse and sphericity (Figure 44). However, it is sometimes difficult to identify two porous structures or to extract quantitative features for comparison; for this purpose, it is necessary to use charcoal powder to fill the air bubbles. All figures (Figure 42, 43 and 44) correspond to 10000x10000 pixels.

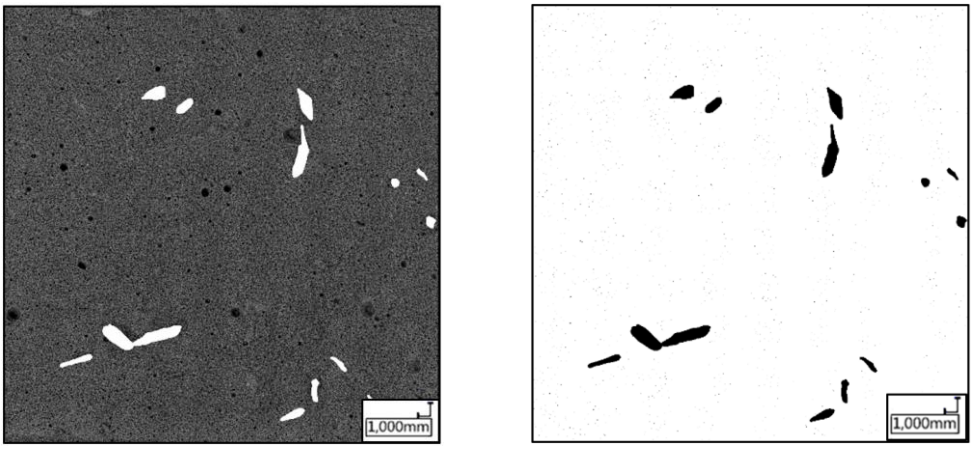

(a) *(b)*

Figure 43 : *Calculation and elimination of the amount of hemp shiv.*

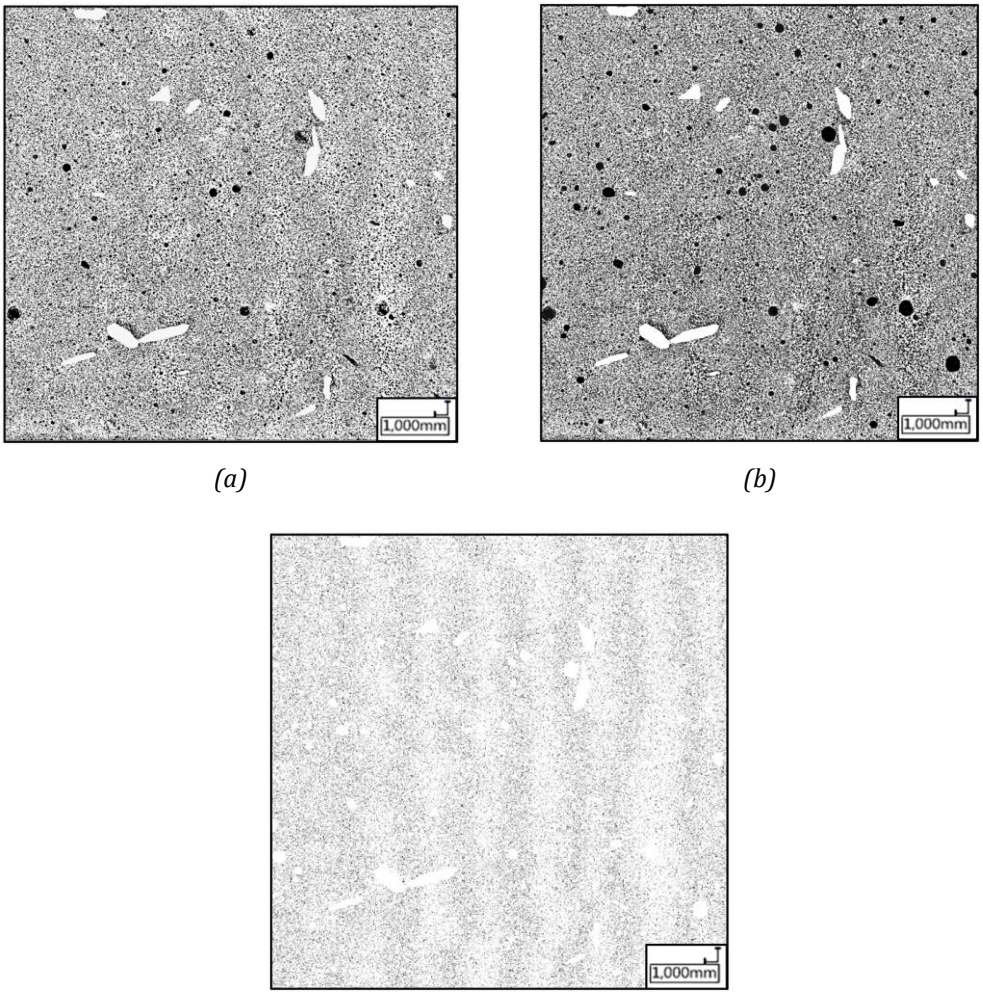

(a) *(b)*

(c)

Figure 44 : *The steps of image treatment by the Image J software: (a) Delimitation of the individual cells; (b) Removal of reflections present on the surface of the cells so that the bubble is coloured all black; (c) Edge detection analysis assuming ellipsoidal contours.*

2.4 CHARACTERIZATION OF BIO-BASED FOAM CONCRETE FORMULATIONS

A first study of bio-based foam concrete is performed. This first step allows to choose the formulations for the next stages. Fixed objectives are highlighted by the choice of formulations, the concretes must be light with a density lower than 800 kg/m^3, self-supporting with a compressive strength larger than 2 MPa and insulating with a thermal conductivity lower than 0.2 W/(m.K).

2.4.1 Formulations

Twenty of foamed concretes are manufactured according to the preformed method using eight different formulations. The control formulation is as follows in Table 5.

Table 5 : *Formulation of control foamed concrete.*

Mixes Names	Fresh density (kg/m^3)	Composition of mixture (kg/m^3)									Wt/B
		CEM I	GGBFS	MK	HS	SP	Acc	FAG	Wh	Wt	
C100P0H0	890	700	-	-	-	14	7	2.1	0,00	168,00	0,24

Wh: Water consumed by the used hemp shiv.
Wt: Total water used.
B: Binders.

Afterwards, all the formulations are based on this previous formulation. The modification of the control formulation is achieved in 2 phases, presented in Figure 45:

- The first phase consists of replacing the cement by pozzolanic additions (20% GGBFS and 10% MK) without adding hemp shiv.
- The second phase operates the replacement of 5, 10 and 15 wt% of cement by hemp shiv by fixing the pozzolanic additions content.

All the formulations are calculated based on constant total volume of the sample (Figure 46).

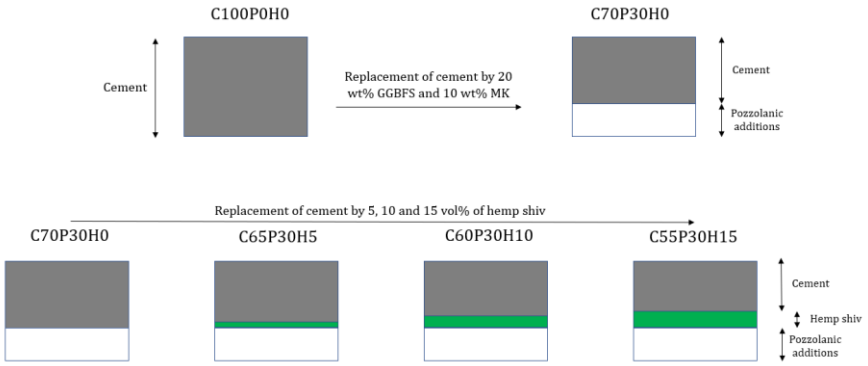

Figure 45 : *Composition of Bio-based foamed concrete.*

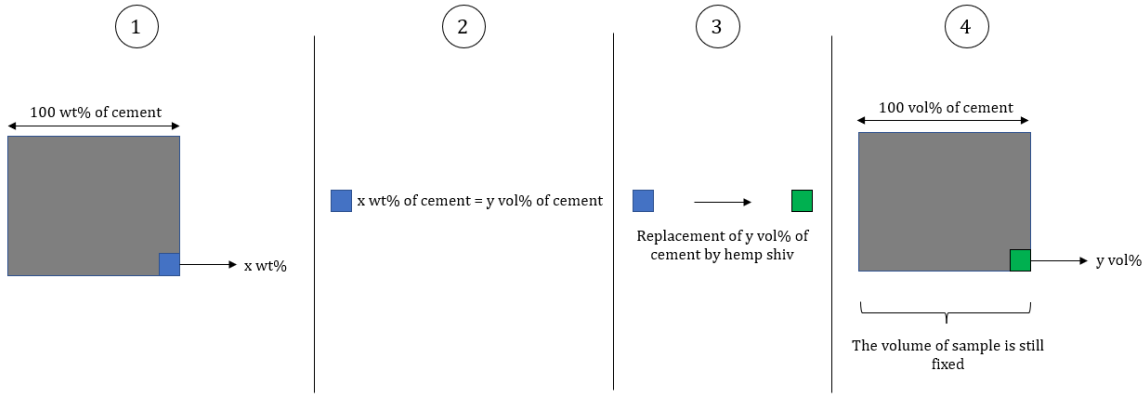

Figure 46 : *Protocol of cement replacement by the hemp shiv.*

The protocol to replace cement by hemp shiv (Figure 46) is the following (The idea is to replace the cement with hemp shiv and maintain the same volume):

1- Based on the control foamed concrete formulation with 100% cement, x wt% of the total content of cement is substituted.

2- Calculation of the volume occupied by this x wt% V_c using the following equation:

$$V_c = \frac{M_c}{\rho_c} \qquad \textbf{Eq. 17}$$

With,

ρ_c = Cement bulk density = 1500 kg/m^3.

M_c = Set cement weight.

V_c = Set cement Volume.

- Calculate the mass of hemp shiv M_H based on the volume of cement calculated in equation 1 using the following equation:

$$M_H = V_c \times \rho_H \qquad \textbf{Eq. 18}$$

V_c = Set cement volume = Hemp shiv volume.

ρ_H = Hemp shiv bulk density = 140 kg/m^3.

M_H = Hemp shiv weight.

In Table 6, Wt is the total amount of water, Wb is the amount of water for binder hydration, and Wh is the amount of water absorbed by the hemp particles, where Wt = Wb + Wh. We then used nearly constant Wb/B ratio, whatever the binder amount and variable Wt/B ratio in order to keep the same workability, relative to the added hemp shiv amount and removed cement amount.

Table 6 : *Formulations of all the samples studied in chapter 2.*

Mixes Names	Fresh density (kg/m^3)	Composition of mixture (kg/m^3)									Wt/B	Wb/B
		CEM I	GGBFS	MK	HS	SP	Acc	FAG	Wh	Wt		
C100P0H0	890	700	-	-	-	14	7	2.1	0,00	168,00	0,24	0.24
C70P30H0	933	490	140	70	-	7	7	2.1	0,00	217,00	0,31	0.31
C95P0H5	858	665	-	-	3.3	14	7	2.1	8.15	167.75	0,25	0.24
C65P30H5	900	455	140	70	3.3	7	7	2.1	8.15	214.3	0,32	0.31
C90P0H10	825	630	-	-	6.5	14	7	2.1	16.05	167.25	0,26	0.24
C60P30H10	867	420	140	70	6.5	7	7	2.1	16.05	211.35	0,33	0.31
C85P0H15	792	595	-	-	9.8	14	7	2.1	24.2	167	0,28	0.24
C55P30H15	834	385	140	70	9.8	7	7	2.1	24.2	208.65	0,35	0.31

Furthermore, Table 6 shows the composition of all the foamed concretes studied in this chapter for 1 m^3. The samples are identified by the following codes: CxPyHz where C, P and H represent Cement, Pozzolanic Additions and Hemp shiv respectively, followed by their respective quantities where x represents the weight percentages (wt%) of cement, y represents the weight percentage of cement replaced by Pozzolanic Additions, and z represents the weight percentage of cement replaced by hemp shiv. Note that it is required to maintain the same sample volume for each formulation.

As a result of the high-water absorption capacity of the hemp shiv particles, a competition for water between the hemp shiv particles and the mineral binder occurred during the hemp concrete setting: the hemp particles absorb the water necessary for the binder hydration [87,91,113]. This leads to chalking of the hydraulic binders at the interface between the binder and the hemp particle [87]. Therefore, the water quantities in the different formulations are adjusted in relation to the hemp shiv volume.

2.4.2 Density

The main factors affecting the concrete density are air content, binder, aggregate density and water content [150]. As shown in Figure 47, the density at 28-days varies between 675 kg/m^3 (C100P0H0) and 562 kg/m^3 (C85P0H15), which means that all samples are lighter than 800 kg/m^3, which fulfils the first objective. The density decreases regularly by about 7% when the hemp shiv content increases by 5% for both specimen C70-BFCs and C100-BFCs (Figure 47) since the cement bulk density (ρ = 1500 kg/m3) is higher ten times than that of the hemp shiv (ρ = 140 kg/m3) Briefly, the bulk density decreases with the increase of hemp shiv amount.

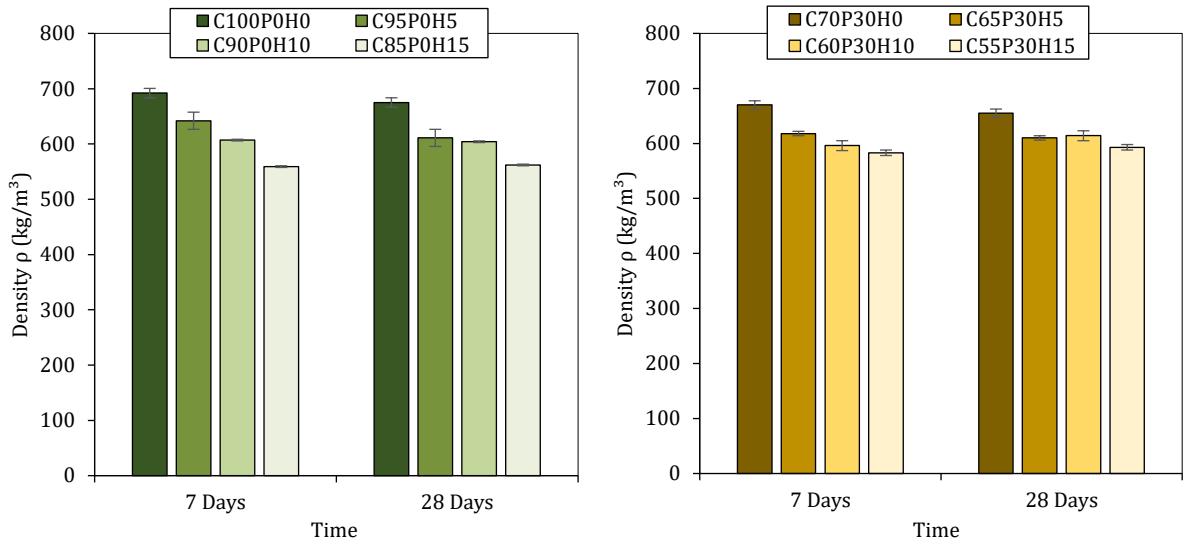

(a) (b)

Figure 47 : *Density of all samples versus time for (a) the C100-BFCs and (b) the C70-BFCs.*

Furthermore, by comparison of C70P30H0 (included pozzolanic additions) with C100P0H0 (without pozzolanic additions), it's found that the density slightly decreases with the addition of pozzolanic additions since that GGBFS and MK absolute density (respectively 2900 kg/m^3 and 2500 kg/m^3) is lower than that of the cement (3100 kg/m^3).

2.4.3 Mechanical strength

Usually, the foamed concrete compressive strength depends largely on age, raw materials, porosity and dry density [61,151]. As shown in Figure 48, the compressive strength increases with time with a ratio Rc7/Rc28 = 0.8, i.e. more than for ordinary concrete in which such a ratio is usually observed around 0.65. This effect is mainly due to the hardening accelerator used.

Page [152] noted that the contribution of a superplasticizer enhances the interface between the hemp aggregates and the pozzolanic binder, thereby improving the material stiffness. Nevertheless, with the addition of pozzolanic materials, the hydration process begins earlier, and it takes longer to stabilize over time [153]. This means that the curing process will take longer, which explains why the increase in the strength of foamed concretes with pozzolanic materials is greater than that of concretes without pozzolanic materials (Figure 48). For example, at 28 days, the C70P30H0 compressive strength is higher than that of C100P0H0, although it is lower at 7 days.

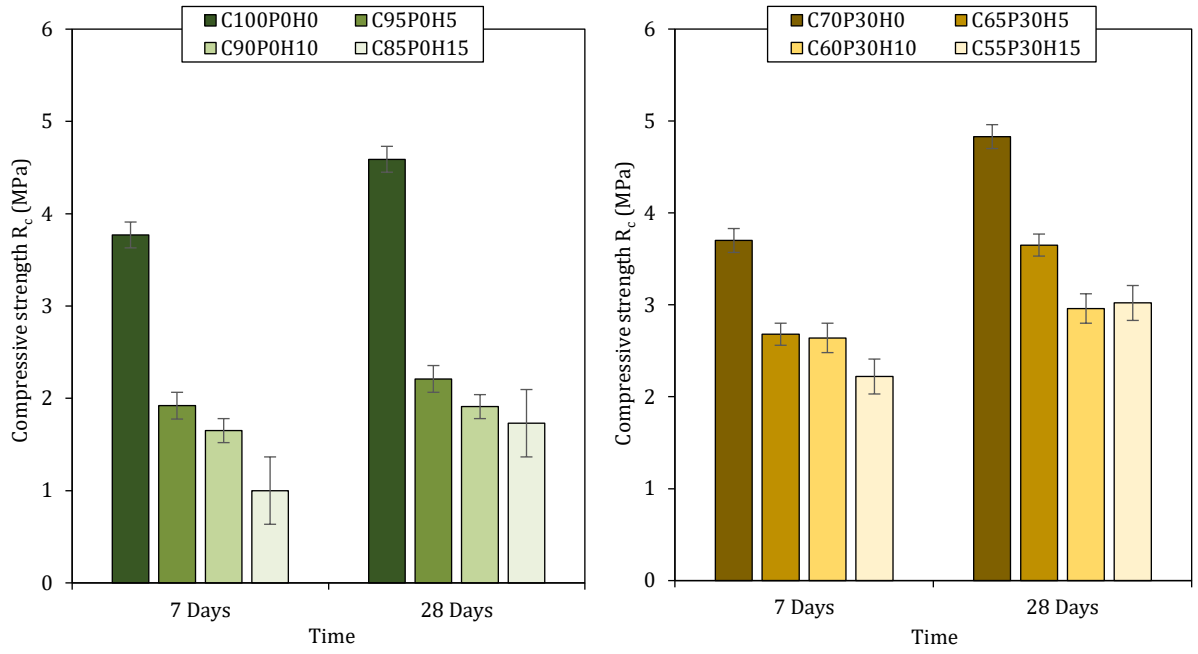

(a) (b)

Figure 48 : *Compressive strength versus time for (a) the C100-BFCs and (b) the C70-BFCs.*

The density decreases with increasing hemp shiv content [98,152]. Similarly, looking at Figure 48, the C100P0H0 compressive strength drops significantly after the hemp shiv addition, which does not occur with C70P30H0. This is due to the low cohesion between the cementitious matrix and the hemp particles, which alters the concretes stiffness, producing new gaps in the materials and increasing air entrapment [110]. As a result, the hemp shiv incorporation in FC results in a decrease in 28-day compressive strength ranging from 52% to 63% for C100-BFCs and from 24% to 37% for C70-BFCs. The material thus becomes more brittle and, as a result, the foam concrete specimens without HS have a higher strength than those containing 5%, 10% and 15% HS. These decreases in compressive strength have been demonstrated by other authors on bio-fibre concretes [154,155]. Furthermore, Chamoin et al. [98] also found that the hemp concrete compressive strength depends on the binder dosage in the mix design and can be improved by optimising the dosage.

Biobased foamed concrete (BFC) with the same amount of hemp shiv as C55P30H15 and C85P0H15 shows a remarkable difference in compressive strength. This is also due to the mixture of pozzolanic additives (GGBFS and MK) that improve the cohesion in the mineral matrix [156]. Similarly, in conventional bio-based concretes, hemp shiv is always mixed with lime or cement with additives, due to their ability to reduce the aqueous extracts of the hemp shiv and their impact on the final amount of hydrates and to increase the adhesion between the hemp shiv and the binder [145].

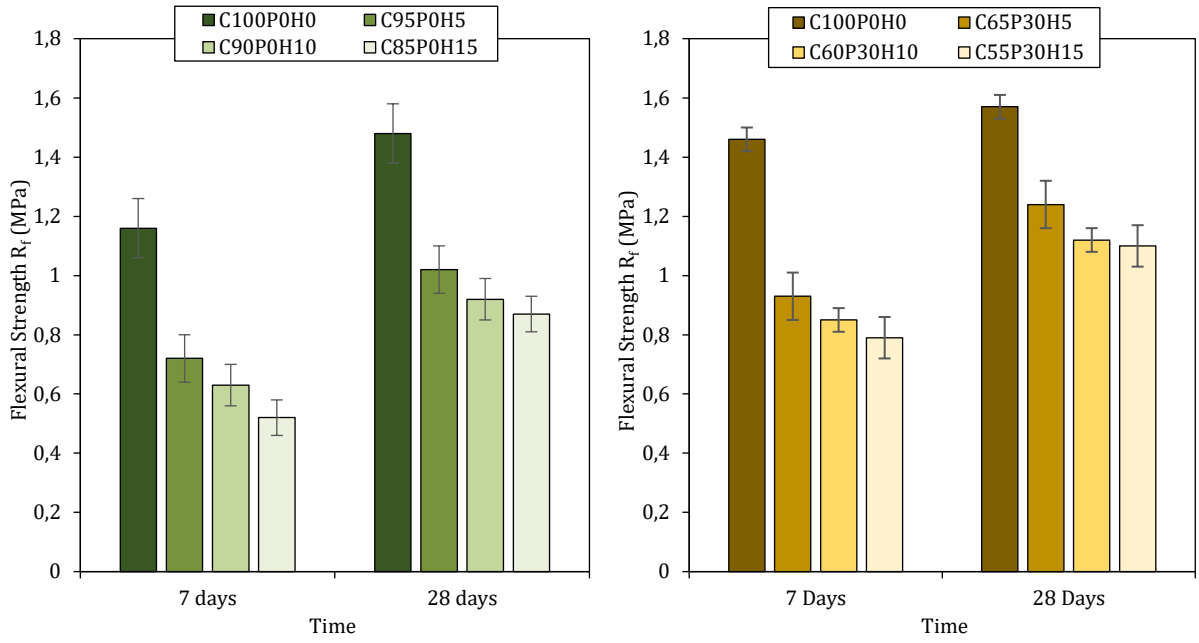

(a) (b)

Figure 49 : *Flexure strength versus time for (a) the C100-BFCs and (b) the C70-BFCs.*

The flexural strength R_f follows a similar behaviour to that of the compressive strength R_c (See Figure 48 and 49). The flexural strength of BFCs also shows a decrease from 31% to 44% for C100-BFCs and from 21% to 30% for C70-BFCs. According to Williams et al. [157], it was found that increasing the binder ratio increases the flexural strength in both perpendicular and parallel directions. Consequently, the flexural strength almost decreases.

The R_f/R_c ratio of BFC samples ranging from 0.28 to 0.45 is larger than that of foamed concrete in the literature with a ratio ranging from 0.2 to 0.4 and ordinary concrete with a ratio ranging from 0.1 to 0,2 [158]. Compared to ordinary and foamed concretes, the hemp shiv addition affects the compressive strength more than the flexural strength, so the hemp shiv reduces the compressive strength more than the flexural strength resulting in an increased R_f/R_c ratio.

2.4.4 Thermal resistance

Thermal conductivity represents the materials ability to transmit heat by conduction. It corresponds to the heat flow which passes in 1 second through a material with a surface of $1m^2$ and 1m thickness for a temperature difference of 1°K between the 2 faces. It is designated by the coefficient λ, expressed in W/(m.K).

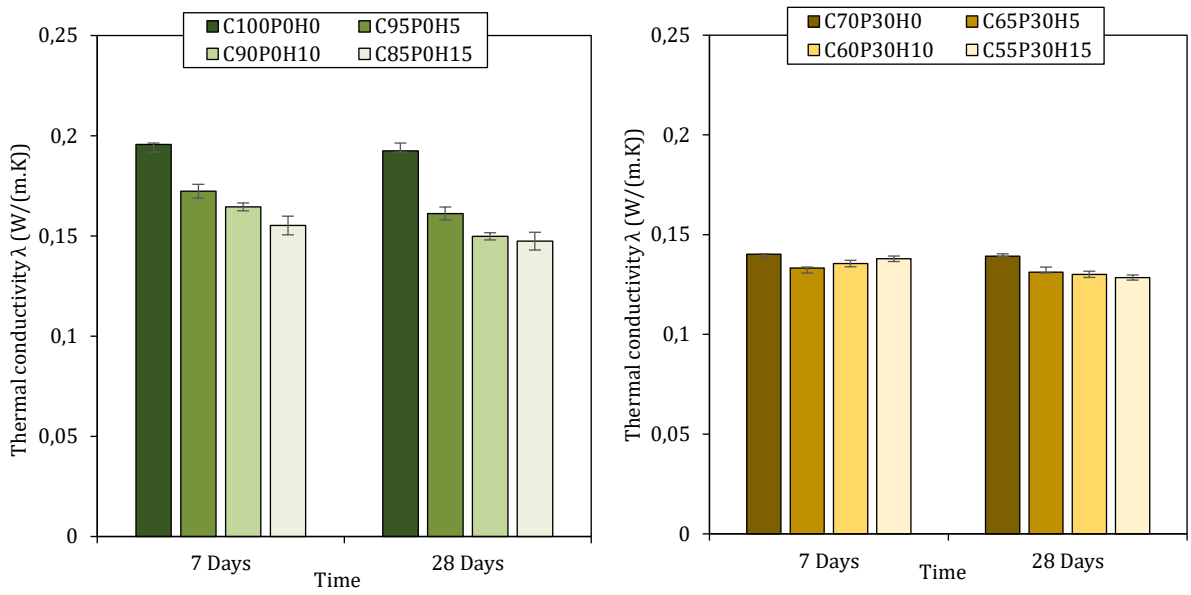

Figure 50 : *Thermal conductivity of all samples versus time for (a) the C100-BFCs and (b) the C70-BFCs.*

Figure 50 shows that there is no significant difference in thermal conductivity λ between 7 and 28 days. In general, the thermal conductivity is inversely proportional to the foamed concrete density [5,159]. Moreover, the thermal conductivity of each raw materials influences the overall thermal conductivity of the material [160].

According to Ramamurthy [2], pozzolanic additives in foamed concrete decrease slightly the thermal conductivity. Therefore, under low cement content and high pozzolanic additives content in the matrix, the thermal conductivity is lower. This is explain the difference of 25% in the thermal conductivity at 28-days between C100P0H0 (λ = 0.1925 W/(m.K)) and C70P30H0 (λ = 0.1392 W/(m.K)) before the hemp shiv addition is significant.

The C100-BFC samples thermal conductivity was affected by the hemp shiv incorporation, whereas this behaviour is slightly observed for C70-BFC samples. When 5% of the hemp shiv is added, the thermal conductivity of C95P0H5 decreases 16% while for C65P30H5 decreases only 6%. This decrease was normal since HS exhibit small thermal conductivities compared to cement, around 0.04 W/(m.K) [160]. In general, the hemp shiv incorporation creates gaps between the particles and the cement matrix, and increase the air entrapment, which decreases the thermal conductivity. But in the case of C65P30H5, the pozzolanic additions improve the cohesion of the hemp shiv particles and the cementitious matrix, which reduces the gaps created by the hemp shiv addition. Thus, by adding hemp shiv the thermal conductivities of C100-BFCs are decreased more than those of C70-BFCs.

2.4.5 Cost and CO_2 emissions

The most important factors for the feasibility of any material are its environmental and economic impacts. Thus, the cost and CO_2 emissions for the manufacturing of BFCs were evaluated. The classification of each foam concrete according to its performance is based on 5 levels between the maximum and minimum values of each performance in this analysis (Table 7). Thermal behaviour is considered here as the most important factor and in decreasing order of importance compressive strength, CO_2 emissions and cost, to which a weight of 4, 3, 2 and 1 respectively is assigned for a multi-criteria analysis (Table 8). The CO_2 emission and cost calculation methods for concretes are presented in Appendix 4, the cost values are based on supplier data and the CO_2 emission values are based on literature references [161–164].

The score is the sum of multiplication of each performance weight with the rating which presents as the score of the performance advantage. For example, for the thermal conductivity presented in Table 8, C70P30H0 (Rating =3) has a higher rating than C100P0H0 (Rating =1), so C70P30H0 is the most insulating. The score gives a global evaluation of the concrete according to these four performances.

Table 7 : *Rating based on performance.*

Rating	Thermal conductivity (W/(m.K))	Compressive strength (MPa)	Cost (€/m^3)	CO_2 emission (kg CO_2/m^3)
0	> 0.2	0 --> 1	> 400	> 600
1	0.175 --> 0.2	1 --> 2	300 --> 400	500 --> 600
2	0.15 --> 0.175	2 --> 3	200 --> 300	400 --> 500
3	0.125 --> 0.15	3 --> 4	100 --> 200	300 --> 400
4	0.1 --> 0.125	> 4	0 --> 100	0 --> 300

The materials cost per m^3 of BFC product is expensive (Table 8). Over 60% of the cost relates to high dose additives (superplasticizer, accelerator, foaming agent). Optimisation of formulations and their production process would be necessary to reduce their additives and their cost.

Noticeably, foamed concrete with 100% cement presents high thermal conductivity with high CO_2 emission value, while C70P30H0 exhibits low thermal insulation and high compressive strength with moderate CO_2 emission.

Table 8 : *Multicriteria ranking of the BFCs.*

Mixs	Cost (€/m³)	CO_2 Emission (kg CO_2/m³)	Ranking					
			Thermal conductivity	Compressive strength	CO_2	Cost	Score[b]	Global Rank[c]
			Weight[a] = 4	3	2	1		
C100P0H0	225	611	1	4	0	2	18	8
C70P30H0	206	458	3	4	2	2	30	1
C95P0H5	223	582	2	2	1	2	24	5
C65P30H5	203	429	3	3	2	2	27	3
C90P0H10	220	552	3	1	1	2	19	6
C60P30H10	201	399	3	2	3	2	26	4
C85P0H15	217	523	3	1	1	2	19	6
C55P30H15	198	370	3	3	3	3	30	1

[a] Weights are coefficients to give priority to a given characteristic.

[b] Score = sum (Weight x Rating)

[c] Global Rank is the classification of formulations from best (1) to worst (8).

As shown in table 8, among the biobased foamed concretes, C55P30H15 can be considered as a good compromise with a relatively low thermal conductivity (λ= 0.1285 W/(m.K)), a high compressive strength (Rc = 3.22 MPa) and CO_2 emissions half of those of C100P0H0. As a conclusion, the hemp shiv incorporation in foamed concrete reduces the mechanical strength but in terms of thermal resistance, CO_2 emission and lightness, the first results obtained are encouraging and they allowed to validate our experimental protocol.

2.5 CONCLUSION

This chapter has presented the characteristics of the different raw materials that enter the composition of composite materials developed in this study and more particularly the hemp shiv. Indeed, the introduction of these plant aggregates in the foamed concrete composition can imply modifications in the cohesion of the matrix, the hydration heat and the air bubbles distribution. Consequently, the physical, mechanical, thermal and hydric properties of the material can be changed.

The second part of this chapter was devoted to the presentation of the cementitious composites characterization methods. These methods are, in the vast majority, either derived from current standards, or adapted from preliminary tests.

The third part of this chapter discussed the preliminary results obtained on bio-based foamed concrete (BFC). A high amount of cement has been found to increase thermal conductivity and CO_2 emissions, so substitutions of cement with pozzolanic additives and/or hemp shiv can improve insulating thermal performances. Moreover, hemp shiv decreases density, compressive strength, and thermal conductivity. But the pozzolanic addition mix improves the cohesion of cementitious matrix in absence and presence of hemp shiv, and in addition reduces CO_2 emissions.

Moreover, all bio-based foam concretes are considered as bio-based lightweight concretes (density lighter than 700 kg/m^3), good thermal insulators with a thermal conductivity less than 0.2 W/(m.K), but only C100P0H0, C70P30H0, C95P0H5, C65P30H5, C60P30H10 and C55P30H15 have a reasonably compressive strength (Rc > 2 MPa).

Thus, it is necessary to complete the study and to analyze more precisely how the pore structures and the cementitious matrices evolve, according to the production method, the pozzolanic addition and the hemp shiv contents. A quantitative approach based on a pore structure characterization method, and a hydration and mineralogy analysis, is the objective of chapter 3.

Chapter 3

Porous structure and cementitious matrix analysis

3. Porous structure and cementitious matrix analysis

3.1 INTRODUCTION

Based on the results of Chapter 2, in this chapter, the BFC materials pore structure and cementitious matrix are investigated. First, the choice of BFC concrete formulations for analysis is conducted. Then a study of the physical properties such as density and porosities, is investigated. Air bubble surface distribution analysis provides insight into the effects of pozzolanic additions, hemp shiv contents, and production method on the porous structures. After that, the hydration heat and the mineralogy of the cementitious matrix are studied.

3.2 FORMULATIONS

Following the characterisation of the elaborated samples, four formulations are selected to characterise the pore structures and cementitious matrices, the mechanical, thermal and hydric behaviours.

Table 9 : *Formulations of all concretes studied in chapters 3 and 4.*

Mixes Names	Fresh density (kg/m^3)	Composition of mixture (kg/m^3)									Wt/B	Wb/B
		CEM I	GGBFS	MK	HS	SP	Acc	FAG	Wh	Wt*		
C100P0H0P	891	700	-	-	-	14	7	2.1	0,00	168	0,24	0.24
C100P0H0D	1600	1200	-	-	-	24	12	2.1	0,00	288	0,24	0.24
C70P30H0P	933	490	140	70	-	7	7	2.1	0.00	217	0,31	0.31
C70P30H0D	1589	840	240	120	-	12	12	2.1	0.00	372	0,31	0.31
C65P30H5P	900	455	140	70	3.3	6.7	6.7	2.1	8.07	214	0,32	0.31
C65P30H5D	1542	780	240	120	5.6	11.4	11.4	2.1	13.8	367	0,32	0.31
C55P30H5P	834	385	140	70	9.8	6.1	6.1	2.1	24.2	209	0,35	0.31
C55P30H5D	1227	660	240	120	16.8	10.3	10.31	2.1	41.5	358	0,35	0.31

* Wt = Wb + Wh

The total amount of water (Wt) shows the water amount absorbed by the hemp shiv particles (Wh) and the water amount required for binder hydration (Wb), always respecting the ratio Wb/B = 0.31.

Four formulations were chosen: C100P0H0, the main control formulation, C70P30H0 once the 30 wt% cement was replaced by 20 wt% GGBFS and 10 wt% MK. Thus, the first parameter was the addition of pozzolanic additives (GGBFS and MK).

Then, C65P30H5 was chosen to study the influence of the hemp shiv incorporation, and C55P30H15 to see the effects of increasing the hemp shiv amount, so the second parameter to be studied is the cement amount replaced by the hemp shiv (0, 5 and 15 wt%).

The third parameter is the production method. In the following, each sample elaborated by the preformed method is denoted by "P" and by “D” when using the direct method. For example, in Table 9 which represents the concretes compositions, "C55P30H15P consists of 55 wt% of cement, 30 wt% of cement replaced by pozzolans, 15% of cement replaced by hemp shiv and the production method is the preformed method".

3.3 PHYSICAL PROPERTIES

Porosity is the most influential factor in the foamed concretes performances. It directly impacts density, strength, thermal conductivity, water performance and durability, and is related to the amount of foam, water, admixtures, and hemp shiv in the formulation. According to the NF EN 1097 standard, total porosity is obtained from the absolute density and the bulk density using the following equation:

$$\varphi = \left(1 - \frac{\rho}{\rho_{abs}}\right) \times 100 \qquad \textbf{Eq. 19}$$

With,

ρ : Bulk density (kg/m^3).

ρ_{abs} : Absolute density (kg/m^3).

As shown in Table 10, the absolute densities of C100P0H0, C70P30H0, C65P30H5 and C5P305H15 mixtures are respectively 2444, 2386, 2380 and 2361 kg/m^3. As the absolute density of cement and pozzolanic additives is higher than that of hemp shiv, the absolute density decreases progressively with the increase of hemp shiv, but this decrease is not remarkable as the amount of hemp that has been modified is extremely low in weight.

Table 10 : *Absolute density of all samples*

Mix	Absolute density ρ_{abs} (kg/m^3)
C100P0H0	2444
C70P30H0	2386
C65P30H5	2380
C55P30H15	2361

As shown in Table 11, the bulk densities of the foamed concretes produced by the preformed method range from 579 kg/m^3 to 710 kg/m^3 with a high porosity in the range of 70.7% to 74.5%. Meanwhile, for the foamed concretes obtained by the direct method, the apparent densities range from 1092 kg/m^3 to 1617 kg/m^3 and a porosity between 33.3% and 54.6 %. Hence, the foamed concretes porosity obtained by the direct method is lower than that produced by the preformed method.

Table 11 : *Physical properties of the biobased foamed concrete*

Mix	Days	Bulk density ρ (kg/m^3)	Porosity φ (%)
C100P0H0P	7	710	71,4
	28	699	
C100P0H0D	7	1460	34.5
	28	1454	
C55P30H15P	7	579	74.5
	28	608	
C55P30H15D	7	1092	54,6
	28	1083	
C65P30H5P	7	597	72.2
	28	662	
C65P30H5D	7	1567	38.9
	28	1574	
C70P30H0P	7	690	70,7
	28	691	
C70P30H0D	7	1617	33.3
	28	1601	

The air bubbles creation in the direct method is more difficult since the air bubbles are formed directly in the mineral suspension which exerts a high pressure on their walls [60]. Thus, the air penetration into the concrete structure is more difficult than in the preformed method. Using the preformed method, air penetrates the water to generate foam and then the mineral suspension is added to the foam. By mixing at very high speed, the mineral slurry is incorporated into the foam and most of the air trapped in the foam remains in the cementitious matrix to form the foamed concrete. Moreover, many factors affect the air bubble production control such as speed, time, and mixing directions. Additionally, the pozzolanic admixtures absolute density is slightly lower than that of cement, but the density of C100P0H0D is lower than that of C70P30H0D. The explanation for this unexpected behaviour is that the direct method is hard to control, depending on several factors such as mixing time, mixing speed, surfactants amounts, water content and constituents of formulation [7].

Density is straightly and inversely influenced by porosity. However, the constituents used in the formulation are as many influencing factors as possible since the bulk density is affected by the absolute density of each constituent. Since the hemp shiv density is very low (ρ = 140 kg/m^3), the hemp shiv addition decreases the concrete density, therefore the densities of C70-based foamed concretes with both methods decreases as the hemp shiv amount increases.

Looking at Table 11, the porosity of C100P0H0P is equal to 71.4 %, and on adding pozzolans, the porosity of C70H30P0 becomes 70.7 %, hence pozzolanic additions reduce the foamed concrete porosity. This is in accordance with Gowripalan et al. [165], who proved that mineral admixtures can be used to reduce the porosity due to their finer particles.

As a conclusion of the density and porosity comparison of C55P30H15P, C65P30H5P and C70P30H0P (Table 11), the porosity increases with the increase of hemp shiv, since hemp shiv is a porous material with an absolute density of 1413 kg/m^3. This difference is more remarkable in the biobased foamed concrete produced by the direct method. This latter exhibits a bulk porosity between 30% and 55%, much less than the hemp shiv porosity around 77% [158]. Thus, the hemp shiv incorporation affects the porosity of a low-porosity foamed concrete (made by direct method) more than a high-porosity foam concrete (made by preformed method).

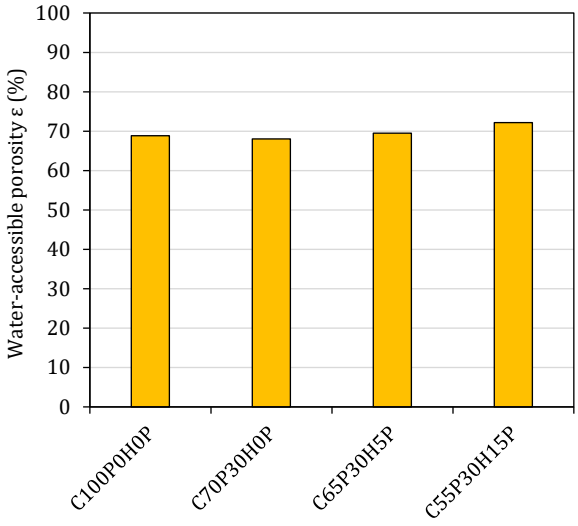

Figure 51 : *Water-accessible porosity of foamed concretes produced by the preformed method*

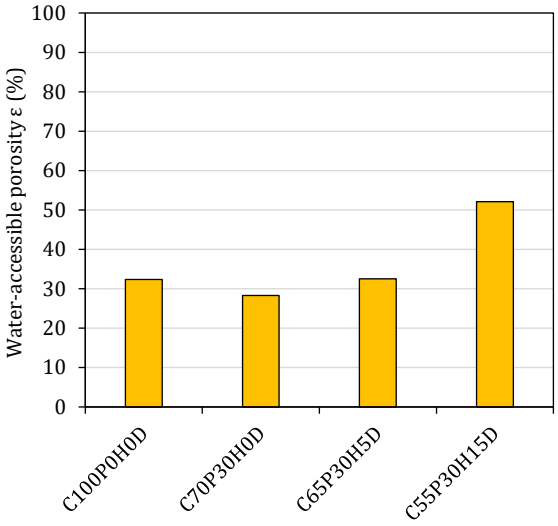

Figure 52 : *Water-accessible porosity of foamed concretes produced by the direct method*

The combination of Table 11, Figures 51 and 52 show that the water-accessible porosity increases with an increasing porosity, due to an increasing hemp shiv volume. In addition, the closed or ineffective porosity is very low, ranging from 1 to 2.5% of the total porosity for foamed concretes produced by the preformed method, and from 4.64 to 7.77% of the total porosity for foamed concretes produced by the direct method, This difference is due to the total porosity being

too high for the preformed method foamed concrete, which is considered to be a very porous concrete (70 - 75%) and has a network of open connected pores more than those produced by the direct methods.

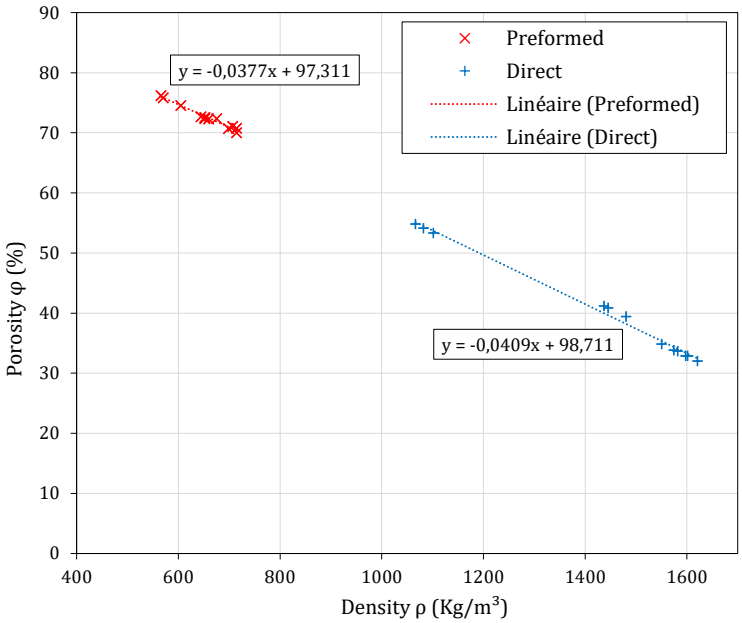

Figure 53 : *Porosity of all samples against density.*

As shown in figure 53, for all the foams produced with the two methods, it appears that the porosity evolves linearly with the density. Thus, the tendency lines of porosity as a function of density show the similar slopes for the preformed and directly produced samples, with respectively the following equations:

$$\emptyset = -0.0377\rho + 97.311, \qquad \textbf{Eq. 20}$$

$$\emptyset = -0.0409\rho + 98.713, \qquad \textbf{Eq. 21}$$

As a conclusion, the main parameter affecting bulk density is the porosity and absolute density of each raw material. The production method and the hemp shiv amount affect the porosity of the materials, and consequently the density of foamed concrete.

3.4 DISTRIBUTION OF AIR BUBBLES

3.4.1 2D characterisation methods

To better understand how the production method, hemp shiv and pozzolanic additions influence the mechanical resistance and the pore structure of the foamed concrete, we used image analysis. A 4x4x16 cm^3 sample is divided into 4 parts as shown in figure 54, the air bubble distribution for each side is studied, then the average of the curves is taken for the following analysis.

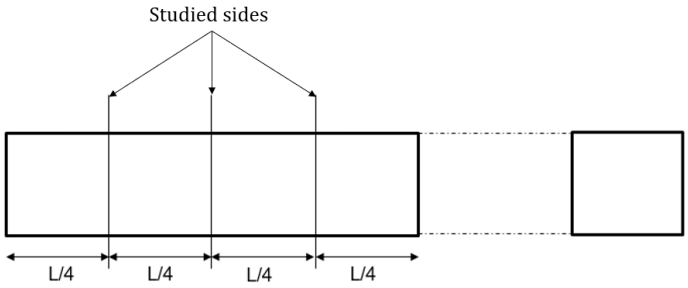

Figure 54 : *Air bubble distribution for the three sections of C65P30H5D.*

This approach allows to obtain the air bubble size distribution ("granulometry") of the different foam concretes considered. All the curves studied can be found in the Appendix 4. For clarification, C65P30H5D is chosen as an example to show the three sections air bubble distribution of samples.

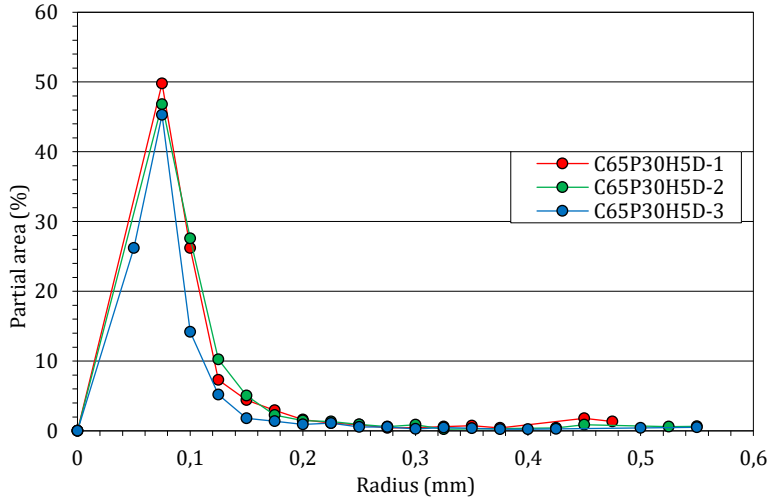

Figure 55 : *Air bubble distribution for the three sections of C65P30H5D.*

As shown in figure 55, the "% partial area", i.e. the sum of air bubble areas for each air bubble radius, only a slight difference between the distributions is shown between different sample sections, which means that the distribution of air bubbles is rather homogeneous laterally. Generally, most of the air bubbles in the foamed concrete of this research consists of small air bubbles smaller than 0.5 mm.

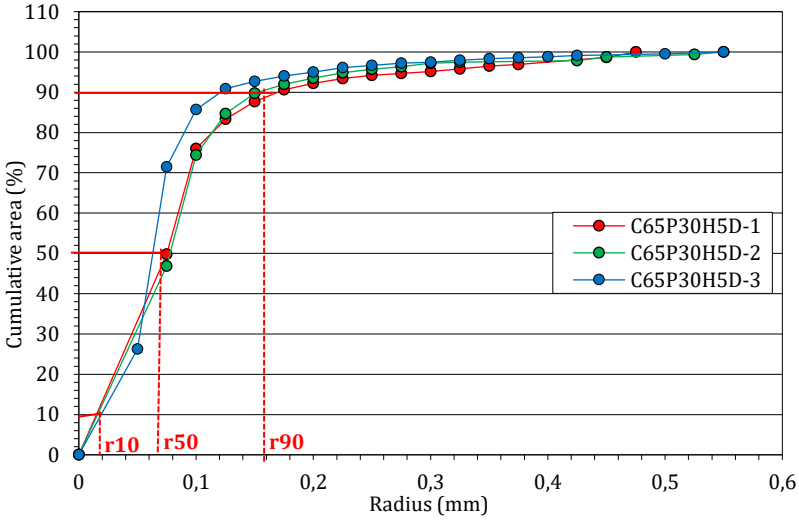

Figure 56 : *Cumulative air bubble distribution for the three sections of C65P30H5D.*

Figure 56 shows the "% cumulative area" which is the sum of "% partial area" for increasing void diameters. The parameters used to characterize the air bubble distributions are r_{90}, r_{50} and r_{10} corresponding to a cumulative area % of 90, 50 and 10% respectively. These radii are used in several studies [27,60,167–169] to determine the air bubbles distribution and to calculate the air bubbles uniformity.

3.4.2 Influences of the parameters on the air bubbles distribution

In this part, the influence of pozzolanic additions, the hemp shiv amount and the production methods on the air bubbles distribution are investigated.

3.4.2.1 Pozzolanic additions

To study the effects of cement replacement by pozzolanic additions on the BFC air bubbles distribution, two mixes are tested in this part. The first mix is C100P0H0 with 0 wt% of PZ and the second one is C70P30H0 with 30wt% of PZ (20 wt% GGBFS and 10 wt% MK). Each mix is produced with two methods, direct and preformed. For better analysis, the hemp shiv was

eliminated (HS = 0%) and the production method are tested to prevent the influence of these parameters on the results.

Table 12 : *Uniformity Coefficient UC and the mean radii Rm as a function of the pozzolanic additions amount (PZ).*

		Preformed		Direct	
Mix	%PZ	UC	R_m (mm)	UC	R_m (mm)
C100P0H0	0	8,41	0,242	9,73	0,153
C70P30H0	30	5,1	0,188	8,1	0,088

Table 12 shows the mean radius (R_m) and the uniformity coefficient (UC) of the foamed concretes. The air bubbles distribution is considered totally uniform if UC = r_{10}/r_{90} = 1, as the UC ratio increases the uniformity decreases.

Looking at Table 12 and figure 57, one can see a larger voids uniformity (UC closer to 1) for the mixes with pozzolanic additions (PZ=30%). This largest homogeneity is associated to smaller air bubble mean radius and is observed in the sample elaborated by the direct method. The difference in the curves between the two production methods is due to the foaming capacity, the preformed method has a greater capacity to generate air bubbles than the direct method.

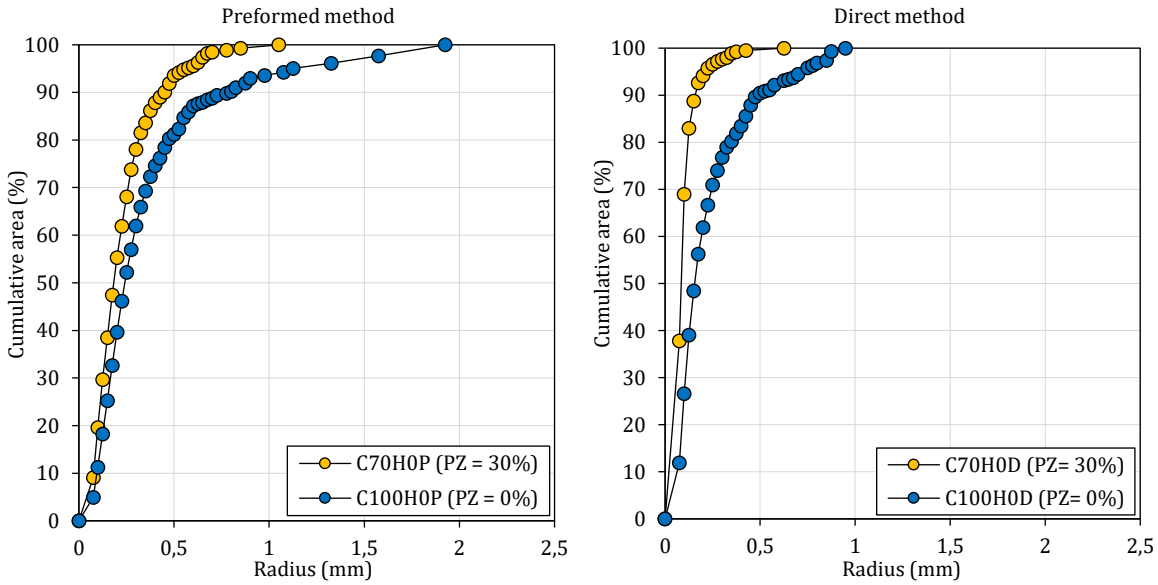

(a) *(b)*

Figure 57 : *Cumulative air bubbles distribution versus radius for 0 and 30% of pozzolanic additives (PZ) using: (a) preformed method, (b) direct method.*

Additionally, looking at the cross-section views of C100P0H0P and C70P0H0P preformed foamed concretes (Figure 58), we observe a very similar air bubble density. The pore structure of these two foams shows very connected bubbles which allows the formation of a very aerated structure with a very large open porosity amount.

Figure 59 shows the structure of the two foam concretes elaborated by the direct method (C70P30H0D and C100P0H0D). The pore structure appears remarkably with smaller and more uniformly distributed air bubbles, a good point for an improvement of the mechanical strength. Pozzolan additions ensure more cohesion between particles and have the capacity to fill micro-voids with C-S-H more than in Portland cements [162], by increasing air bubble interfaces thickness and blocking the air bubbles coalescence, resulting in smaller void sizes and more uniform distributions.

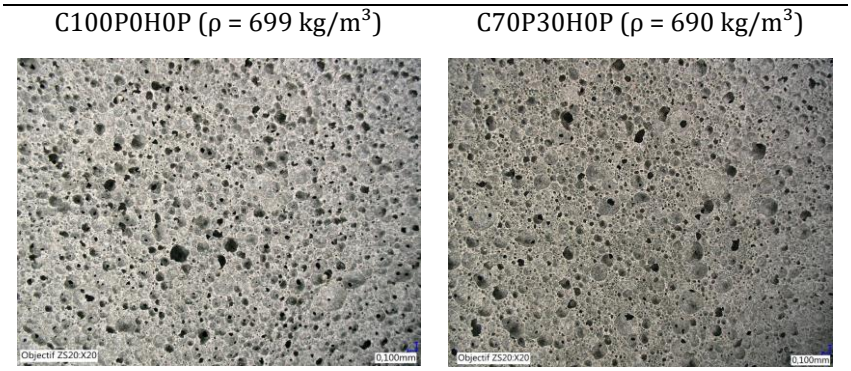

Figure 58 : *Pore structure evolution with and without pozzolanic additions using preformed method.*

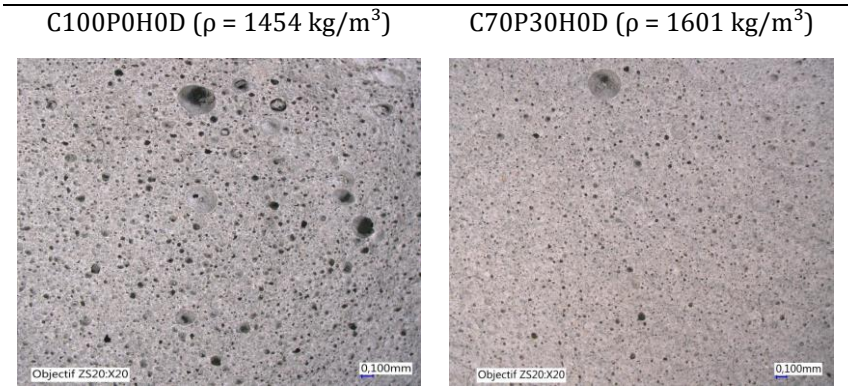

Figure 59 : *Pore structure evolution with and without pozzolanic additions using direct method.*

Consequently, pozzolanic additions affect both mean void sizes and their distribution in the porous structure, but this effect is more prominent when using the direct method. This void refinement effect accompanies the larger void uniformity obtained using the direct method.

3.4.2.2 Hemp shiv

Our previous results show that hemp shiv incorporation affects BFCs density and porosity, but we have not considered so far, their effect on the distribution and sizes of air bubbles.

Table 13 : *Uniformity Coefficient UC and mean radii Rm as a function of the amount of hemp shiv (HS).*

		Preformed		Direct	
Mix	%HS	UC	R_m (mm)	UC	R_m (mm)
C70P30H0	0	5.1	0,182	8.1	0.088
C65P30H5	5	5.79	0,219	11.33	0.063
C55P30H15	15	6.48	0.2	13.52	0.151

Note that UC cannot be smaller than 1, since r_{90} cannot be smaller than r_{10}. As shown in table 13, figure 60 (a) and 61, hemp shiv does not affect the air bubbles distribution in concretes using the preformed method. Uniformity coefficient (UC) and mean radius (R_m) increase very slightly with the increase of hemp shiv. In addition, figure 60 (a) shows that the shapes of all air distribution curves are very close to each other, pointing for a similar air bubble distribution in this hemp shiv incorporation range.

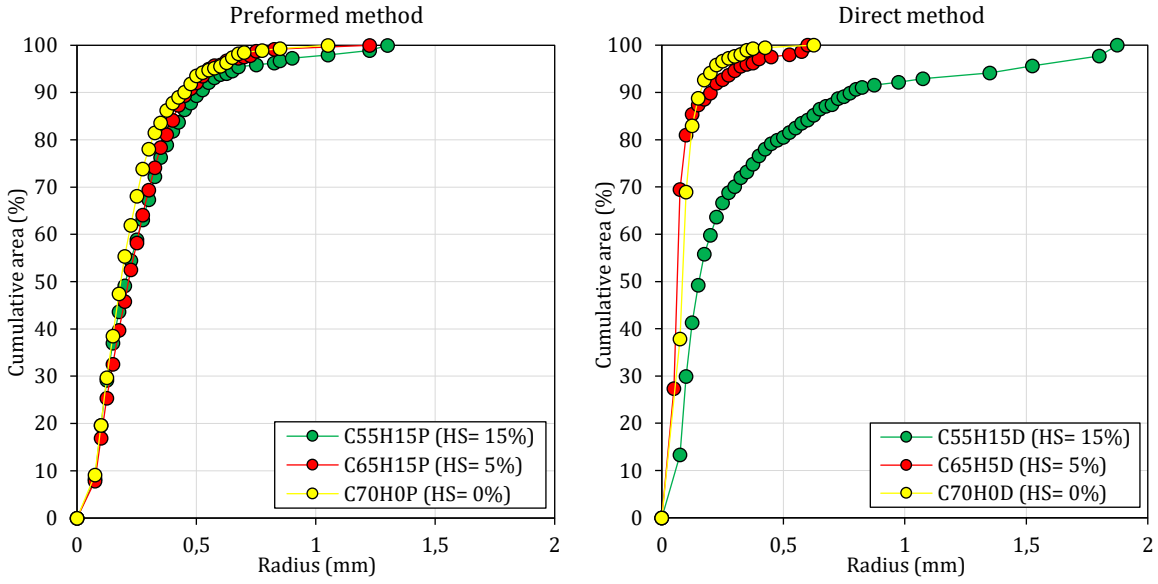

(a) *(b)*

Figure 60 : *Cumulative air bubbles distribution versus radius for various hemp shiv amounts (HS) using: (a) preformed method, (b) direct method.*

C70P30H0P (ρ = 690 kg/m^3)	C65P30H5P (ρ = 690 kg/m^3)	C55P30H15P (ρ = 690 kg/m^3)

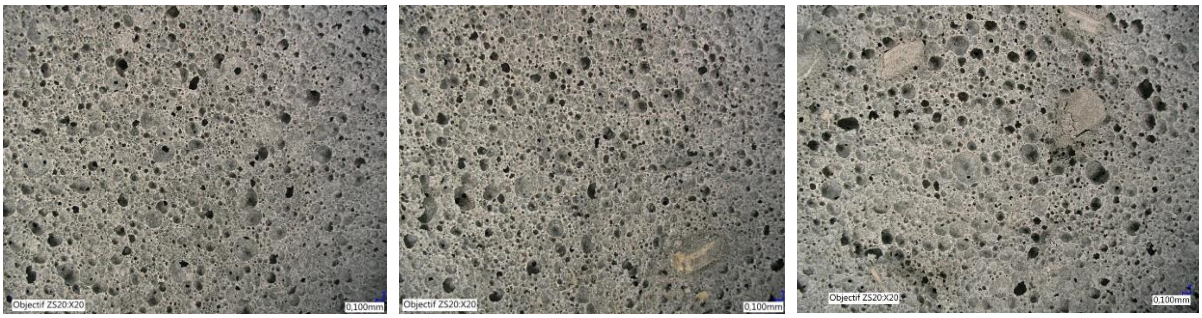

Figure 61 : *Pore structure evolution with increasing amount of hemp shiv using the preformed method.*

C70P30H0D (ρ = 690 kg/m^3)	C65P30H5D (ρ = 690 kg/m^3)	C55P30H15D (ρ = 690 kg/m^3)

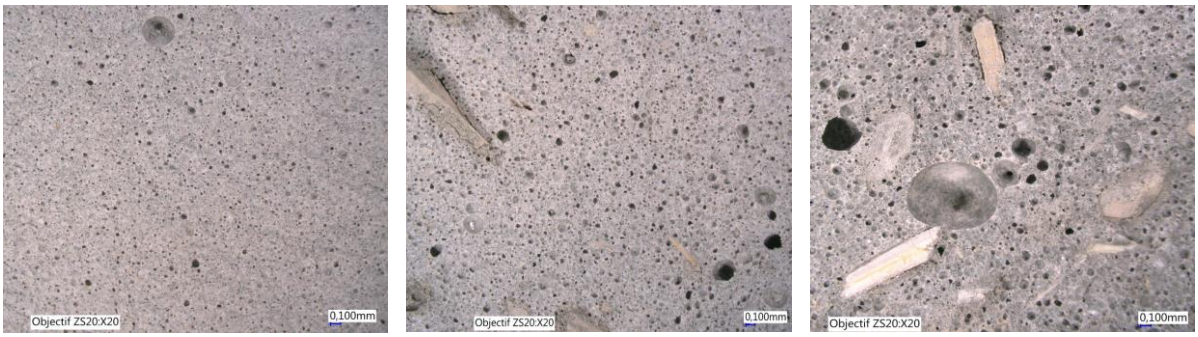

Figure 62 : *Pore structure evolution with increasing amount of hemp shiv using the direct method.*

Using the direct method (Figure 60 (b) and 62), BFCs air distribution curves point out that with a small hemp shiv amount (HS = 5%) the void distribution is not affected. However, increasing the hemp shiv amount to 15%, this distribution is significantly modified, and a significant shift takes place, also the air bubbles radius increases significantly. Similarly, regarding the table, the UC and the mean radius Rm increase significantly, so bubbles uniformity decreases since UC increased. Figure 62 shows the difference between the BFCs surface with 5% and 15% hemp shiv using the direct method. Looking at the surface of C55P30H15, the difference in the air bubbles diameters is remarkable due to coalescence, which is an air bubbles instability phenomenon. Therefore, the UC and R_m are increased.

The low cohesion between hemp shiv and the cement matrix has been pointed out, resulting in a non-homogeneous voids distribution [106,112], then decreasing the mechanical resistance. Therefore, larger incorporations of hemp shiv are aimed to result in a decrease of the compressive strength.

3.4.2.3 Production methods

The air bubble production process also affects the physical properties and air bubbles distribution; therefore, the production method choice is very important to achieve the required BFCs functionalities.

Table 14 : *Uniformity Coefficient UC and the mean radii R_m as a function of production methods.*

Mix	R_m (mm)	UC
C100P0H0P	0,181	8
C100P0H0D	0,09	4,58
C55P30H15P	0,172	12,84
C55P30H15D	0,165	15
C65P30H5P	0,137	6,3
C65P30H5D	0,075	10,26
C70P30H0P	0,15	5.8
C70P30H0D	0,08	4,54

As shown in table 14, all foams produced by the direct method represent much finer air bubble distributions than those produced by the preformed method, e.g., C65P30H5D (R_m = 0.075 mm) and C65P30H5P (R_m = 0.137 mm) have the same formulation with different production methods. C65P30H5D is produced using the direct mixing method while C65P30H5P is produced using the preformed method. The direct method requires a large surfactant amount to generate the same foam volume produced by the preformed method [60]. The air bubbles distributions of these two BFCs are shown in figure 60. The air bubbles size of C65P30H5D is much finer than that of C65P30H5P. C65P30H5D presents a very small radius R_m (mean radius), R_m = 0.075 mm, much smaller than that of the C65P30H5P foam, R_m = 0.137 mm. Except for the C55P30H15P/D foamed concretes, the radii are close due to the low uniformity caused by the low cohesion between the hemp shiv and the cement matrix.

3.5 CEMENTITIOUS MATRIX

3.5.1 Hydration heat

Several studies report that hemp shiv affects the hydration heat and the hydration rates, as the extractive molecules diffuse in the mixing water and delay the binder hydration kinetics [108,150,171]. This can alter the materials properties, particularly by reducing their mechanical strength [29,151].

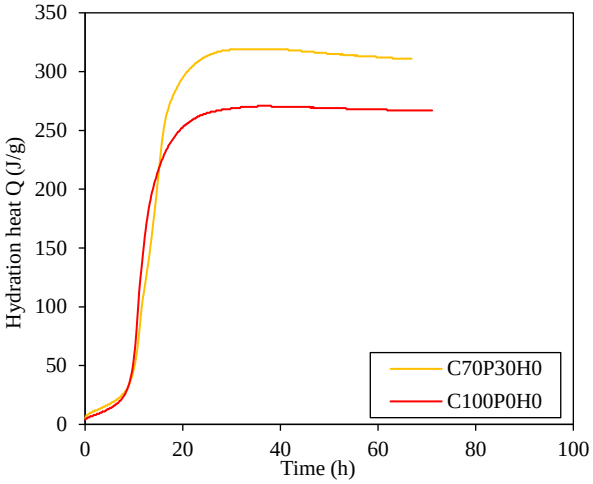

Figure 63 : *Hydration heat variation versus time.*

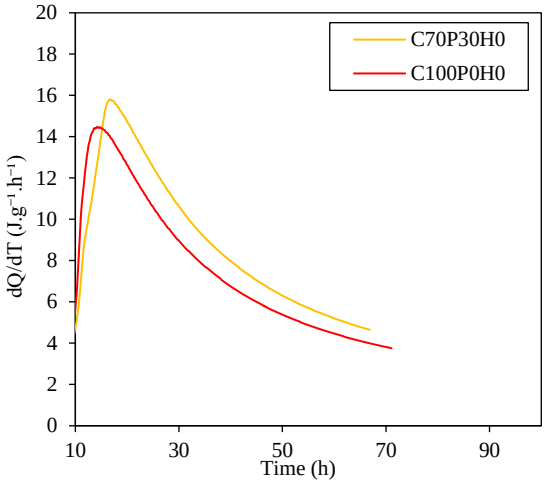

Figure 64 : *Hydration heat kinetics.*

As shown in figure 63, pozzolanic additions increase the hydration heat since the metakaolin activates the reactions of GGBFS with the cement, creating new exothermic chemical reactions [152]. MK appearing to have excellent potential as an active additive for concrete production [172]. However, this material appears somehow particular. The hydrated phases (C_2ASH_8 and C_4AH_{13}), formed during the pozzolanic reaction at early periods of curing, tend to be metastable phases. With longer curing times, the conversion of these hydrates to hydrogarnet (stable phase) can be envisaged [173], increasing the hydration heat, despite the fact that GGBFS slow down the hydration kinetics [60,174]. Figure 64 shows that the C100P0H0 hydration reaction kinetics is faster than that of C70P30H0, which is normal due to the delayed effect of GGBFS on hydration, as it does not react directly with water.

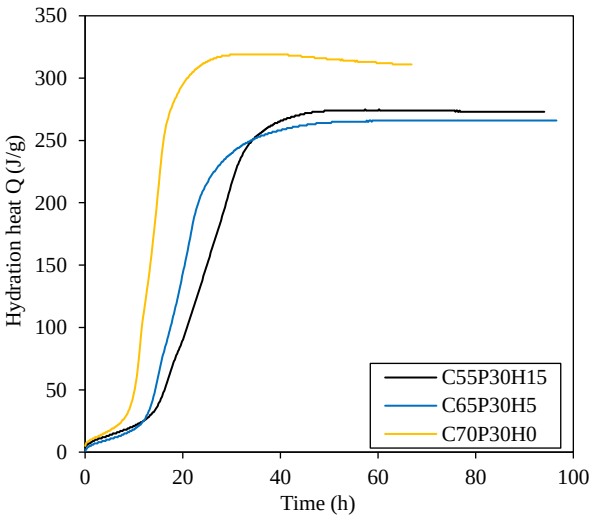

Figure 65 : *Hydration heat variation versus time.*

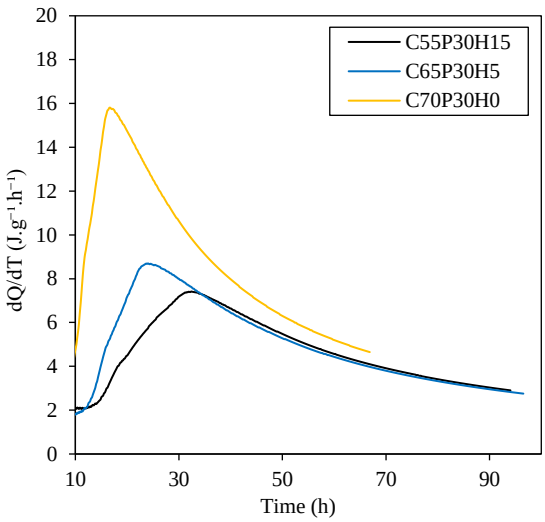

Figure 66 : *Hydration heat kinetics.*

Looking at figure 65 and comparing the foamed concrete without hemp shiv C70P30H0 with the biobased foam concretes C65P30H5 and C55P30H15, it is found that the hydration reaction of the first one is the faster. On the other hand, the reaction speeds decrease with the hemp shiv amount. Moreover, curing is almost completed after 30h for C70P30H0, while nearly 50h is needed for the other mixtures. The hydration heat also decreases with hemp shiv incorporation, due to cementitious matrix structure modifications. The delay in setting observed in figure 66 could consequently be explained by an impediment in the aluminates development (C_3A and C_4AF) due to the high alkalinity of the cement, leading to the degradation of the lignocellulosic compounds and generating by-products that prevent the setting and hardening process of hemp shiv [145]. Consequently, hemp shiv delay the concrete hardening [175]. In addition, the pozzolanic materials present in the hemp shiv composition delay the hydration process and prolong stabilisation over time [145].

3.5.2 Study of the minerology

Hydration heat and kinetics affect the anhydrous formation in the cement matrix and influence the material properties. Therefore, it is interesting to study the elemental composition and mineralogy (crystallographic phases). In this paragraph, the hemp shiv and pozzolanic additions effects on the foamed concrete mineralogical composition are studied using XRD and TGA.

3.5.2.1 XRD

Before discussing XRD results, it is necessary to describe the hydration reactions in action in portlandite cements. Based on Table 15, Portland cement hydration involves the reaction of the four mineral phases of which it is composed. Since cement is composed mainly of C_3S, it is the hydration of C_3S that controls the overall hydration kinetics.

Table 15 : *Mineralogical composition of ordinary portlandite cement [176].*

Compound	Weight percentage (%)
C_3S	40 to 75
C_2S	6 to 30
C_3A	0.1 to 12
C_4AF	2 to 16

The terms C_3S, C_2S, C_3A and C_4AF are the abbreviations used in cement chemistry, with the following correspondence:

- C = CaO: Lime
- S = SiO_2: Silica
- H = H_2O: Water
- A = Al_2O_3: Alumina
- F = Fe_2O_3: Hematite

Moreover, the hydration reactions equations of silicates (C_3S and C_2S) can be written [177]:

For C_3S: $2C_3S + 6H \rightarrow C_3S_2H_3 + 3CH$

For C_2S: $2C_2S + 4H \rightarrow C_3S_2H_3 + CH$

With:
$C_3S_2H_3$: C-S-H,
CH: Portlandite,

Furthermore, aluminates C_3A reacts with gypsum to form ettringite [177]:

$$C_3A + 3C\bar{S}H + 26H \rightarrow C_3A.3C\bar{S}H_{32}$$

With: $\bar{S} = SO_3$ (Sulfuric Anhydride)

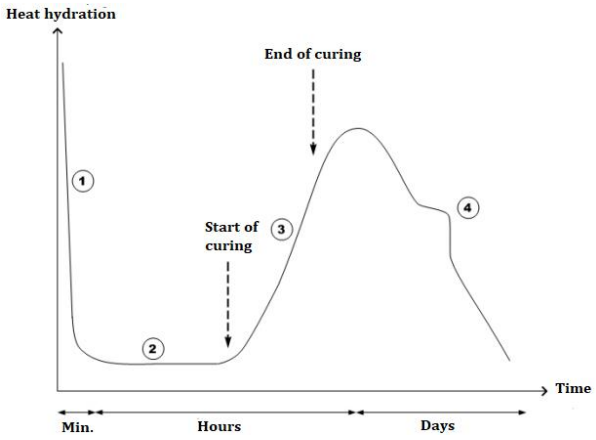

Figure 67 : *Typical isothermal calorimetry curve of a cement.*

Figure 67 shows a cement isothermal calorimetry characteristic which can be divided into four distinct ranges, according to Boivin [178].

Period 1, named initial reactions. This period starts as soon as the water comes into contact with the cement and lasts a few minutes. The C_3S and C_3A of the cement grains react immediately with the water, forming ettringite and C-S-H (metastable): the ions enter into solution.

Period 2, named sleeping period. Heat release is low. No evolution of the paste seems to occur. However, chemical reactions have started: ions go into solution in the water during this phase (calcium ions, silicates, hydroxides and sulfates). When the mixing water is saturated with ions, the start of setting occurs. pH of the solution increases, which slows down the dissolution of the constituents.

Period 3, named acceleration period. This period begins when the concentration of Ca_2^+ and OH^- ions in the solution becomes critical, the electrical conductivity of the solution being then at its maximum. This supersaturation induces the precipitation of the portlandite. It follows then the mechanisms of dissolution, nucleation and precipitation of the various phases, allowing the formation of hydrates (ettringite, portlandite, C-S-H). This chemical activity releases a lot of heat. The formed hydrates begin to entangle and thus create a solid.

Period 4, named period of slowing down. The anhydrous grains are covered by a layer of hydrates which thickens more and more. For the hydration to continue, water must diffuse through the gel pores. The heat released decreases. If the pore network is closed, part of the cement is never reached and therefore will never be hydrated. It is during this period that the ettringite of type AFt dissolves in order to be transformed into type AFm. The complex mechanisms at the origin of the creation of the various hydration products that are silicates and aluminates are adsorption, hydrolysis, dissolution, solvation and crystallization.

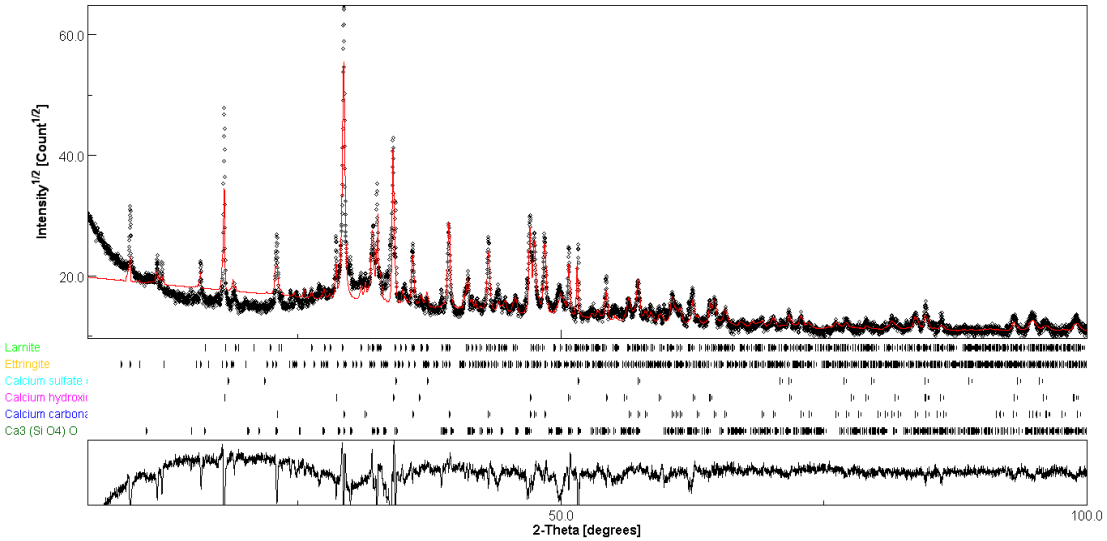

Figure 68 : *XRD diagram of C100P0H0.*

XRD allows to analyze the pozzolanic addition and hemp shiv influence on the cement matrix. Moreover, it is found that the main anhydres in concrete are calcite, ettringite, portlandite, belite and alite.

Figure 68 shows the mineralogical composition of C100P0H0 obtained by XRD. It is useful to remember that this foam concrete is produced by 100% cement. The results obtained show that C100P0H0 presents mainly calcite ($CaCO_3$), alite (C_3S), belite (C_2S), portlandite (CH), ettringite ($C_3A.3C\bar{S}H_{32}$) and gypsum ($C\bar{S}H$). This is similar to the results obtained in previous works [176,179,180].

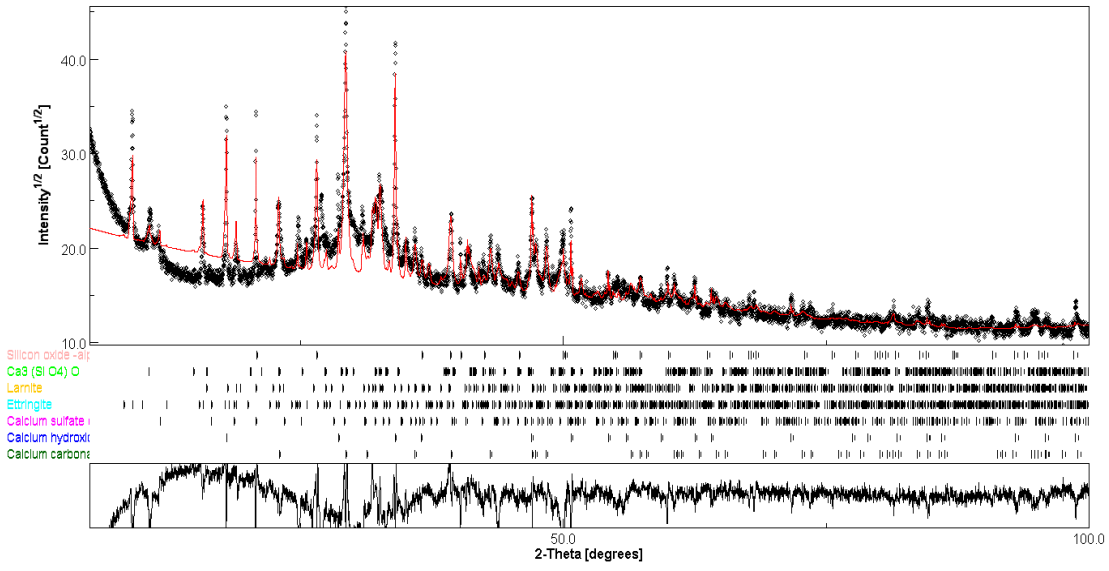

(a)

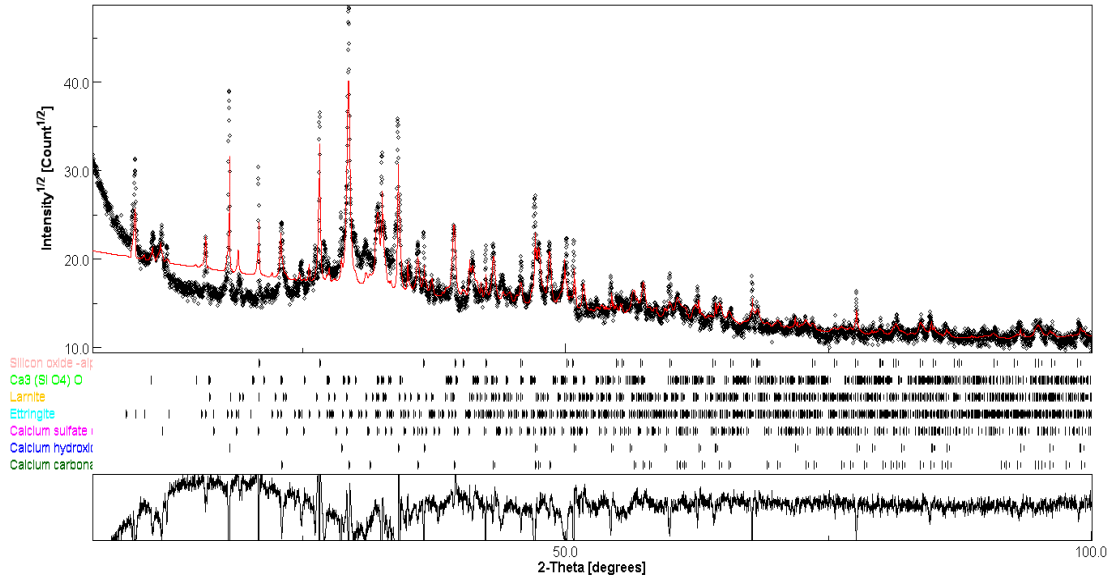

(b)

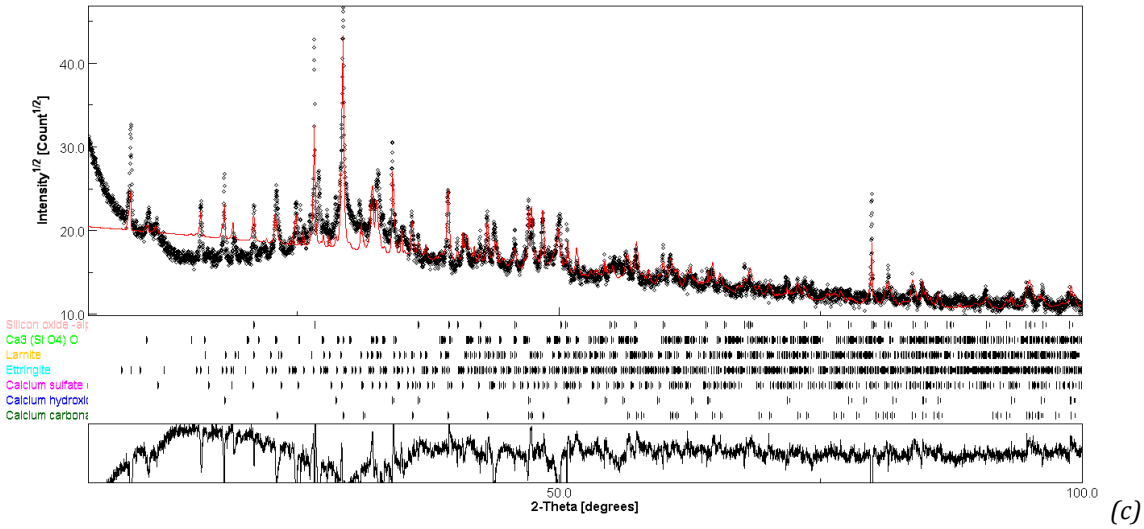

Figure 69 : *XRD diagram of: (a) C70P30H0, (b)C65P30H5 and (c) C55P30H15.*

Figure 69 shows XRD diagrams measured on the different types of concrete incorporating pozzolanic and hemp shiv. Comparing the XRD diagrams of C100P0H0 without pozzolanic additions (Figure 68) and of C70P30H0 with pozzolanic additions (Figure 69 (a)) the peaks from quartz originating from MK appear in the latter sample (see 2.2.2.1.3). Also, the diagram exhibits a more pronounced amorphous signature (the background oscillations are more visible, particularly around 2theta values below 50 degrees), due to slags (see 2.2.2.1.2). There are no differences in the peaks detected in the different concretes (Figure 69), so the hemp shiv does not modify the resulting phases of the concrete, only again a small amorphous signal increase is observed, due to the poorly crystalline hemps shiv structure. We did not attempt to add cellulose alpha or beta structures in the analysis of the concretes containing hemp shiv. Such an addition could provide a better fit of the diagrams but would not significantly modify the phase contents, since x-ray scattering from cellulose remains weak compared to other, crystalline, phases.

Table 16 : *Mineralogical composition of all foamed concretes obtained after Rietveld analysis of the XRD diagrams.*

	Weight %			
Compounds	C100P0H0	C70P30H0	C65P30H5	C55P30H15
Calcite	44.6± 3	33 ± 2	35 ± 2	36.2 ± 1.8
Portlandite	12.5 ± 0.7	9.9± 0.6	9 ± 0.3	6.7 ± 0.3
Ettringite	8.4 ± 0.4	14.7 ± 0.8	14.3 ± 0.7	14.1 ± 0.8
Alite	10.8 ± 0.6	6.8 ± 0.3	10.2 ± 0.4	9.6 ± 0.4
Belite	15.2 ± 0.8	23 ± 1.1	19.5 ± 1	17.4 ± 0.8
Gypsum	7.9 ± 0.1	2.3 ± 0.3	2.5 ± 0.2	1.7 ± 0.2
Quartz	0	8.7 ± 0.4	9.2 ± 0.6	11.9 ± 0.8

Pozzolanic additions, composed mainly of silica and aluminate as well as metakaolin, react with portlandite to form C-S-H and AFm [181]. According to Badogiannis et al. [182], the cement replacement by 10% to 20% of metakaolin improves mechanical performances. The following reactions between silicates and aluminates contained in the metakaolin and portlandite occur in portlandite cement and water:

$$2S + 3CH \rightarrow C_3S_2H_3$$

$$A + 4CH + 9H \rightarrow C_4AH_{13}$$

Moreover, the aluminates presence favors the ettringite formation. For this reason, looking at Table 16, it is found that the portlandite and calcite amounts decrease and the ettringite amount increases with the addition of pozzolanic additives.

The large amount of C_2S and C_3S means that the hydration reactions of the silicates are not totally complete. This may be due to the water small amount and the setting accelerators addition to reduce the setting time and ensure the stability of the foam incorporated into the cement paste.

As opposed to portlandite cement which is soluble in water, and hydrates by simple water addition, GGBFS needs an activator to hydrate. In this study these activators are gypsum, already present in the cement. Therefore, the gypsum amount is reduced in the presence of pozzolanic additions.

The presence of quartz in C70P30H0, C65P30H5 and C55P30H15 is due to unreacted quartz caused by the presence of metakaolin which consists of 77% quartz (see 2.2.2.1.3).

Comparing the mineralogical compositions of C70P30H0, C65P30H5 and C55P30H15, it is found that portlandite and gypsum amounts decrease, while calcite and quartz amounts increase with the increase of hemp shiv. Since cement is replaced by hemp shiv in this sample series, the (GGBFS + MK)/cement ratio increases, mineralogical compositions [183].

3.5.2.2 TGA

Figure 70 shows the TGA curves of all the foamed concretes studied in this part of the work, The parameters to be studied are the inclusion of pozzolanic additives and the hemp shiv content (5% and 15%). It should be noted that all samples are aged for 28-days. Generally, the first peak in the 80 - 250°C range is related to the dehydration of the pozzolanic reaction products. The first peak between 80 and 200°C is attributed to water release from ettringite and C-S-H [184,185]. Furthermore, the peak between 400 and 550°C is related to the consumption of portlandite, and the one between 600°C and 1000°C is attributed to calcium carbonates decompositions [186].

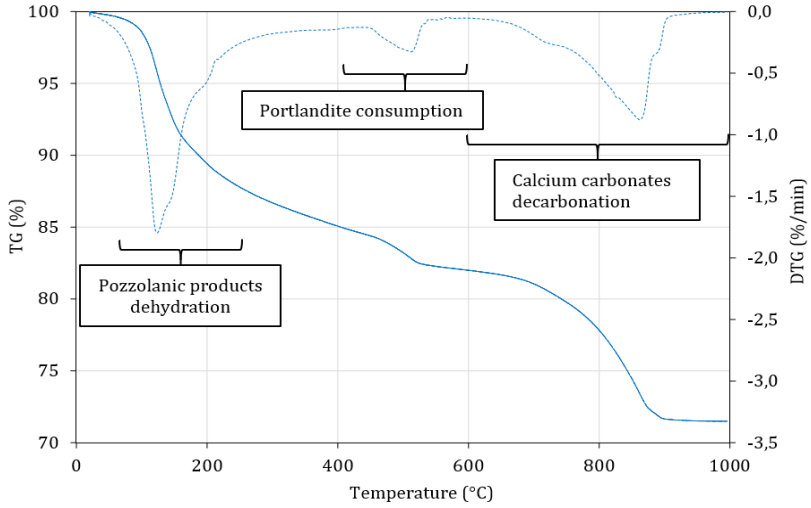
Portlandite consumption
Calcium carbonates decarbonation
Pozzolanic products dehydration
TG (%)
DTG (%/min)
Temperature (°C)
100
95
90
85
80
75
70
0,0
-0,5
-1,0
-1,5
-2,0
-2,5
-3,0
-3,5
0
200
400
600
800
1000

(a)

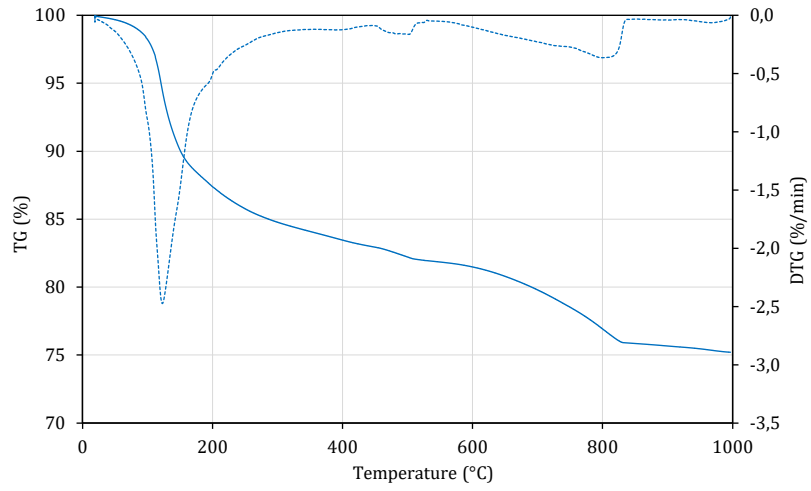
TG (%)
DTG (%/min)
Temperature (°C)
100
95
90
85
80
75
70
0,0
-0,5
-1,0
-1,5
-2,0
-2,5
-3,0
-3,5
0
200
400
600
800
1000

(b)

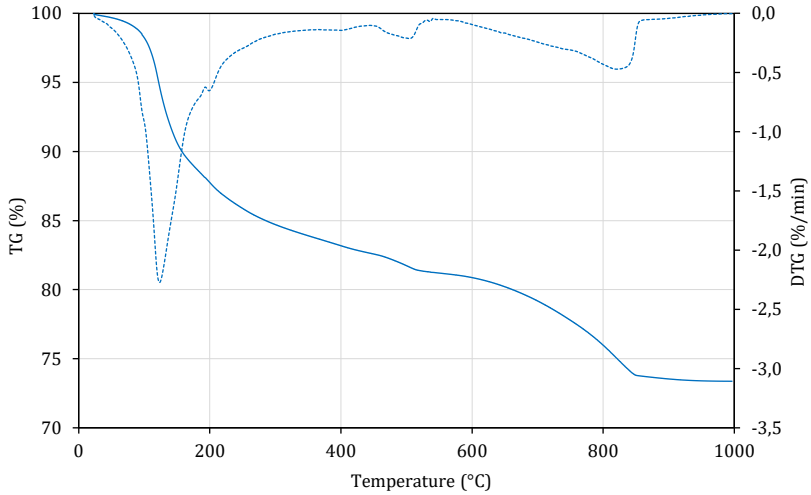
TG (%)
DTG (%/min)
Temperature (°C)
100
95
90
85
80
75
70
0,0
-0,5
-1,0
-1,5
-2,0
-2,5
-3,0
-3,5
0
200
400
600
800
1000

(c)

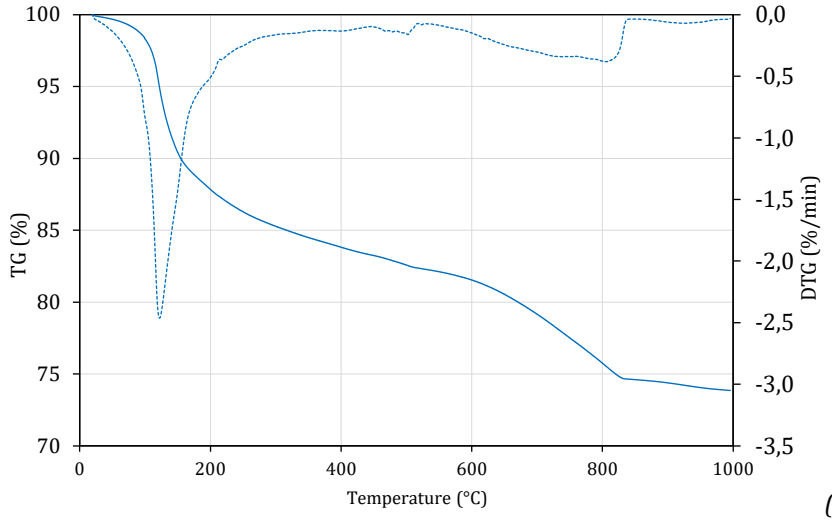

(d)

Figure 70 : *TGA curves for the different foam concretes: (a) C100P0H0, (b) C70P30H0, (c) C65P30H5 and (d) C55P30H15.*

Table 17 : *Mass variations of all foamed concretes for the different phases.*

		Mass variation (%)			
Temperature (°C)	Phases	C100P0H0	C70P30H0	C65P30H5	C55P30H15
80 - 250	Evaporation of water + Dehydration of ettringite + Decomposition of C-S-H (and aluminates)	13.3 ± 0.6	17.3 ± 0.8	16.5 ± 0.8	16.2 ± 0.8
400 - 600	Portlandite dehydration	2.9 ± 0.1	1.6 ± 0.1	1.4 ± 0.1	1.3 ± 0.1
600 – 1000	Calcium carbonate decomposition	10.6 ± 0.5	6.1 ± 0.3	7.6 ± 0.4	7.8 ± 0.4

Thermogravimetric analyses (Table 17) allow to estimate the portlandite amount present in the cementitious materials. With increasing temperatures, portlandite decomposes into water and lime (CaO) according to the reaction:

$$Ca(OH)_2 \rightarrow CaO + H_2O \qquad \textbf{Eq. 22}$$

And according to equation (22):

$$m_{portlandite} = \frac{M_{portlandite} \times m_{eau}}{M_{eau}} \qquad \textbf{Eq. 23}$$

With:

$m_{portlandite}$: Weight of portlandite (g).

$M_{portlandite}$: Molar mass of portlandite (73 g/mol).

m_{eau} : Weight of water (g) lost during the specific temperature rise in the decomposition of the portlandite.

M_{eau} : Molar mass of water (18 g/mol).

To calculate the mass percentage of $Ca(OH)_2$, the following equation must be followed:

$$\text{Weight (\%)} = \frac{m_{portlandite}}{m_{total}} \times 100 \qquad \textbf{Eq. 24}$$

At larger temperatures, calcium carbonates decompose into carbon dioxide and lime:

$$CaCO_3 \rightarrow CaO + CO_2 \qquad \textbf{Eq. 25}$$

Similarly, to portlandite, the amount of calcium carbonate present in the material is estimated from the mass loss corresponding to the departure of carbon dioxide:

$$m_{CaCO_3} = \frac{M_{CaCO_3} \times m_{CO_2}}{M_{CO_2}} \qquad \textbf{Eq. 26}$$

With:

m_{CaCO_3} : Weight of $CaCO_3$ (g).

M_{CaCO_3} : Molar mass of $CaCO_3$ (100 g/mol),

m_{co_2} : Weight of CO_2 (g) lost during the specific temperature rise in the decomposition of $CaCO_3$.

M_{CO_2} : Molar mass of CO_2 (44 g/mol).

Which consequently gives the mass percentage of $CaCO_3$:

$$\text{Weight (\%)} = \frac{m_{CaCO_3}}{m_{total}} \times 100 \qquad \textbf{Eq. 27}$$

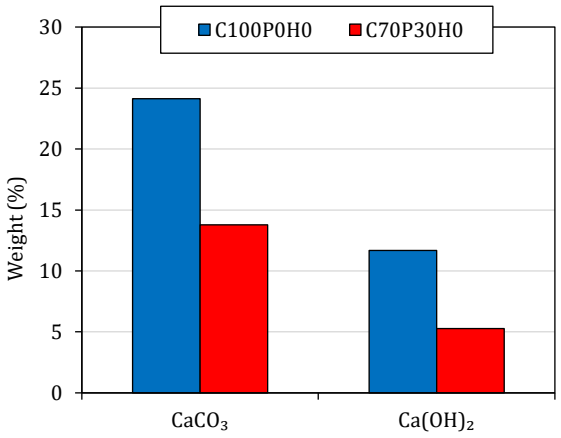

Figure 71 : *Percentage of $CaCO_3$ and $Ca(OH)_2$ in the cement matrix according to the pozzolanic additions presence.*

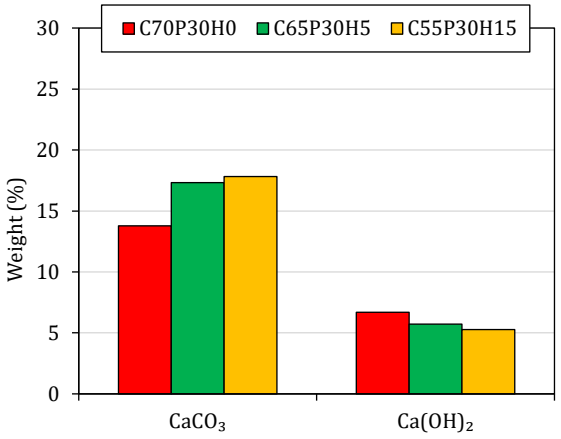

Figure 72: *Percentage of $CaCO_3$ and $Ca(OH)_2$ in the cement matrix according to the hemp shiv amount.*

Table 17 shows the mass variation of all foamed concretes for the different phases obtained from the TGA curves in Figure 70. Pozzolanic additions lead portlandite to react with silica (SiO_2) to form CSH [187], and it promotes the pozzolanic products formation (Figure 70(a)) such as ettringite [189]. Therefore, for temperatures between 80 and 250°C, the amount of material released to the atmosphere (within CSH and ettringite) is larger in C70P30H0 than in C100P0H0. In addition, the amount of material released into the atmosphere for a temperature between 400 and 600°C (Within Portlandite) is larger in C100P0H0 than in C100P30H0. Consequently, the portlandite weight percentage decreases by almost half (Figure 71).

Furthermore (Figure 72), the portlandite amount decreases after the hemp shiv incorporation, which is normal since the hemp shiv inhibits pozzolanic reactions and favours carbonation [188] on the one hand and the MK/cement ratio still increases since the cement content is substituted, which reduces the portlandite content [189]. This explains the decrease in portlandite in the temperature range between 400 and 600°C and the TGA peak in the temperature between 600 and 1000°C. For Govin et al. [128], the carbonates formation is related to the release of carbon dioxide induced by the alkaline degradation of the hemp particles, which was responsible for the portlandite carbonation, favoured by the very high open porosity (looked at 3.3, $\varphi > 70\%$). Hemp shiv negatively influences the binder hydration and hardening. Hydration and indirect setting are delayed, this could reduce the compressive strength, and this could be related to the limited amount of pozzolanic reaction products found using TGA.

Finally, comparing the mineralogical compositions obtained by TGA and XRD a global coherence between the results is found, with differences in amounts of compounds and identifications of mineral phases. Several points should be mentioned at this stage which explain the difference observed. On one hand, TGA does not directly verify mineral species. For instance, between 0 and 250°C adsorbed water evaporates, and hydrates decompose and release gaseous water, without distinction of the hydrates in presence. Also, the "carbonates" TGA peak cannot identify which carbonate is present in the material, calcite, aragonite, magnesite… On the other hand, amorphous compounds which are hardly distinguishable using XRD can contribute to TGA curves. For instance, CSH is barely not visible using XRD while the corresponding signal in TGA clearly visible. Thus, the complementarity of the two approaches allows for a better characterization of the material.

3.6 CONCLUSION

The different types of concretes are porous materials which consist of a hollow part (pore structure) and a solid part (cement matrix), and we have studied these two parts according to the

method of production and the replacement of cement by pozzolanic additions and different amounts of hemp shiv.

Regarding the void part, porosity, water accessible porosity, density and air bubble distribution was studied. It has been proved that the hemp shiv increases the porosity and thus decreases the density. Moreover, it increases the air bubble radius, which decreases uniformity. Additionally, the amount of cement and pozzolanic materials improve slightly the uniformity of air bubbles, which increases the mechanical resistance especially at 28 days. Moreover, the production method plays an important role in the formation of air bubbles, the pre-formed method is more efficient in forming foam for lightweight concretes with a density lower than 700 kg/m^3, but the direct method gives finer bubbles and a more uniform distribution.

Regarding the solid part, it is found that the hydration heat increases with the addition of pozzolanic additives, and it decreases with increasing hemp shiv amounts. Studying the mineralogy of BFCs, it is found that the cement is not fully hydrated and by adding pozzolans, the portlandite amount decreases while the C-S-H and ettringite amount increases, which improves the mechanical strength. It is also found that the hemp shiv effect on mineralogy is only by its activation of carbonation in the cement paste, which negatively influences the binder hydration and hardening and reduces the compressive strength.

Chapter 4

Mechanical, thermal and hydric properties

4. Mechanical, thermal and hydric properties

4.1 INTRODUCTION

As studied in the chapter 3, pozzolanic addition, hemp shiv and the production methods affected the cementitious matrix and the porous structure of concretes which directly influence their properties.

In this part, we will study the mechanical properties, since it is considered to be the most important factors in measuring the foamed concrete applicability in the hardened state, then the thermal conductivity is investigated. Finally, sorption-desorption isotherms and capillary absorption are studied since is the are the most important hydric properties to study in order to improve the waterproofing of a material. This chapter opens the way to obtain an overview on the characteristics of each concrete in order to know their strengths and weaknesses.

4.2 MECHANICAL PROPERTIES

4.2.1 Compressive strength

Generally, the foamed concretes compressive strength is largely dependent on dry density, porosity, age and raw materials [29,151].

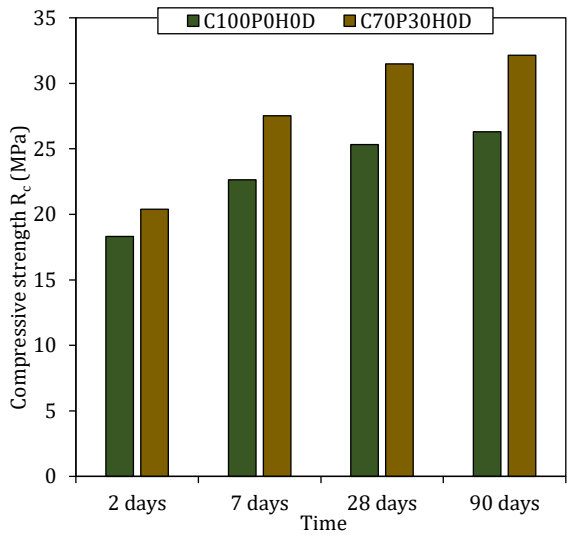

Figure 73 : *Compressive strength versus density for concrete with/without pozzolanic additions using the direct method.*

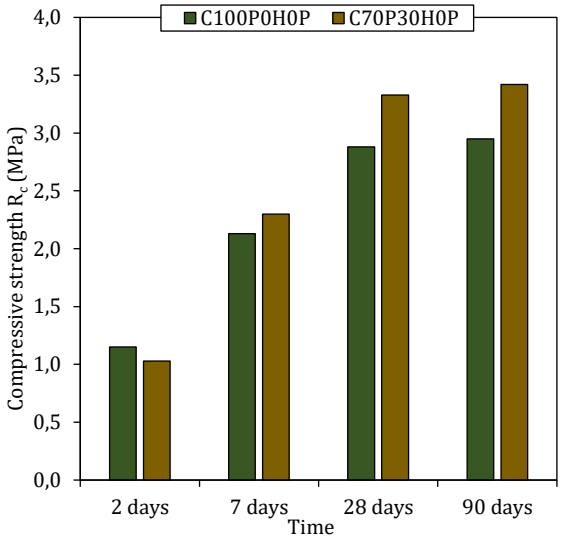

Figure 74 : *Compressive strength versus density for concrete with/without pozzolanic additions using the preformed method.*

At first sight (Figures 73 and 74), the foamed concretes produced by the direct method reach 72% of Rc_{max} (compressive strength maximal at 90 days) for C100P0H0D and 63.5% for C70P30H0D after 2 days while the concretes produced by the preformed method reach 53% of Rc_{max} for C100P0H0P and 44% for C70P30H0P. In the literature, an ordinary concrete reaches 30% of Rc_{max} at 2 days, in this case the rate is higher because accelerators were used.

Moreover, the rate of reaching maximum compressive strength of C70P30H0P/D concretes is smaller than those of C100P0H0P/D. This is explained by the slower hydration reactions occuring in C70P30H0P/D (see 3.5.1) which makes curing slower. However, at day 2, the C70P30H0P compressive strength was smaller than these of C100P0H0P, but it become larger at 7, 28 and 90 days. Similar results were obtained by Al-Jumaily [170]. Using the direct method, the difference in compressive strengths between C100P0H0P and C70P30H0P becomes larger. Moreover, pozzolanic additions improve the BFCs compressive strength in both method, due to their ability to fill pores with C-S-H more than in portlandite cements (see 3.5.1).

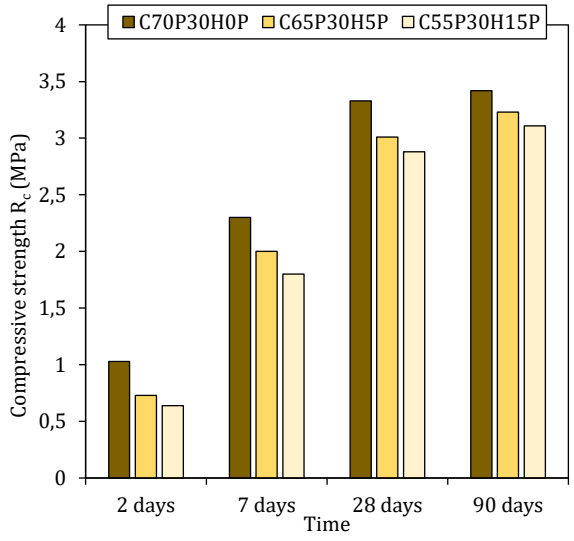

Figure 75 : *Compressive strength versus time of various hemp shiv amounts using preformed method.*

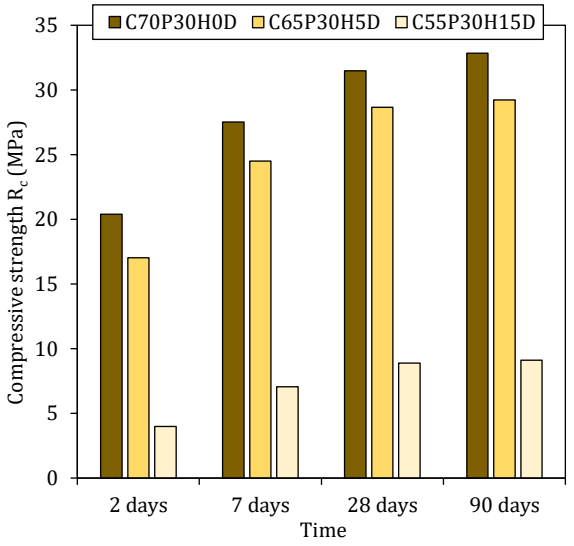

Figure 76 : *Compressive strength versus time of various hemp shiv amounts using direct method.*

In figures 75 and 76, the Rc_7/Rc_{28} ratio for C55P30H15, C65P30H5 and C70P30H0 is respectively 0.53, 0.59 and 0.61 for the foamed concrete produced by the preformed method and 0.79, 0.85 and 0.88 for the foamed concrete produced by the direct method. It also increases with the hemp shiv amount, which is coherent since these latter have an influence on the hydration heat and on the porosity of the material (see chapter 3). Furthermore, a study of the hemp shiv effects on cement hardening [145] shows that the high alkalinity of cement can degrade

lignocellulosic compounds and produce by-products which prevent the setting and hardening process. Consequently, hemp shiv delays the concrete hardening [175].

Figure 76 shows a significant drop of mechanical resistance between C70P30H0D and C55P30H15D. Compressive strength at 28-days decreases from 31.48 MPa to 8.88 MPa with 15% hemp shiv (C55P30H15D). Corresponding with the results obtained in section 3.2., the instability of the air bubbles due to the large hemp shiv amount resulted in low uniformity. In addition, the low cohesion between the hemp shiv and the cementitious matrix resulted in the formation of new porosity channels in the cementitious matrix. As a result, the material becomes more fragile and therefore the foam concrete samples without or with 5% HS have a higher strength compared to those with 15% HS.

Moreover, the mechanical strength is mainly dependent on the air bubbles uniformity, distribution and the mean radius. Indeed, the hemp shiv effect on the mechanical resistance is limited with the preformed method, the mechanical resistances at 28-days range between 2.88 and 3.33 MPa as the air bubbles distribution and their radius are closely similar.

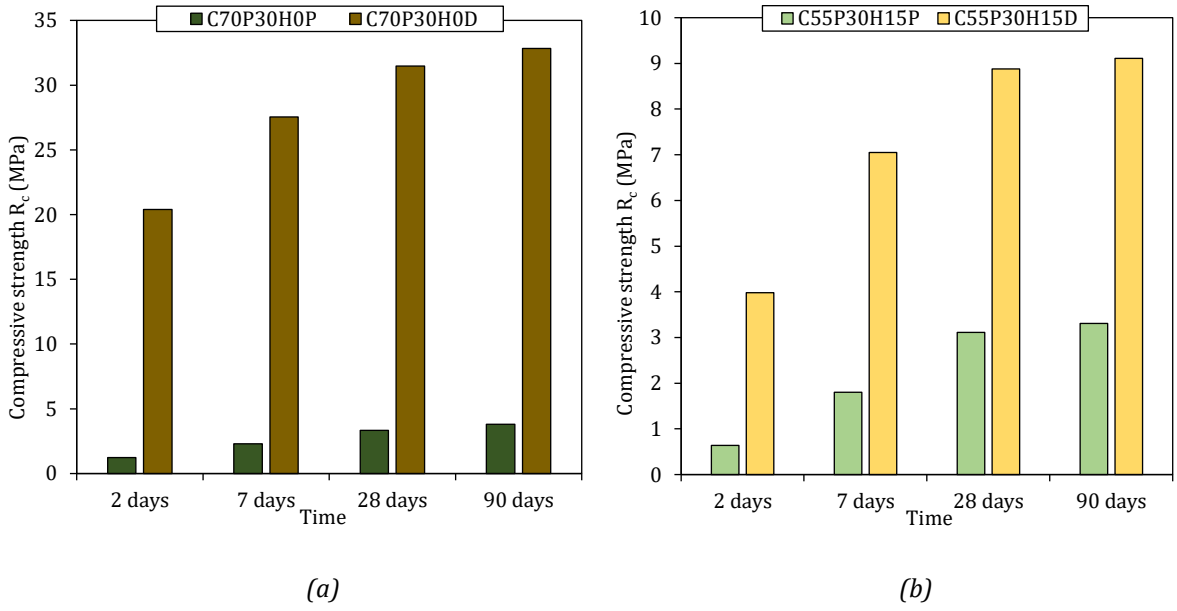

(a) *(b)*

Figure 77 : *Compressive strength of all samples in function of production method versus time.*

As shown in the figures 77, there is a significant difference in mechanical strength between the direct method and the preformed method. This difference is due to the variation in the air entrained amount into the concrete by these two methods. The air incorporated into the concrete by the preformed method is produced by a foam made from mixing the surfactant and water and then combining with the mineral suspension. With the direct method, air bubbles are formed

directly in the mineral suspension, so its formation is more difficult than with the preformed method.

In addition, as already shown in 3.1, the radius size affects the porosity. Moreover, at a higher foam volume, bubble collapse affects negatively on the air bubbles uniformity which leads to lower strengths [27,190]. In addition to the air voids size and their distribution, the compressive strength is also influenced by the void-to-paste ratio, the air voids spacing and the number (frequency). Therefore, the preformed method achieves higher porosity, then lower mechanical strength.

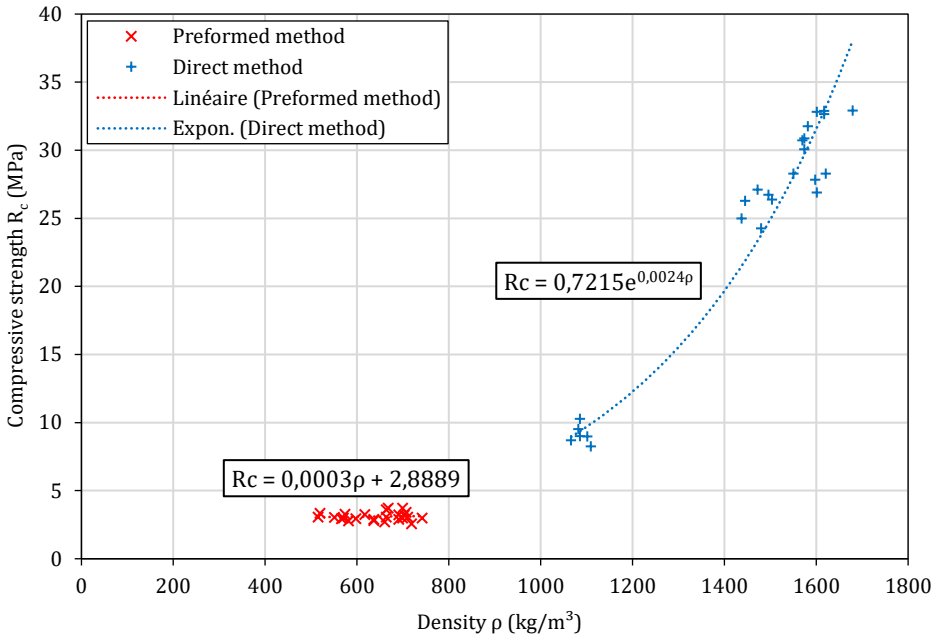

Figure 78 : *Compressive strength of all samples in function of production method against density at 28-days.*

As shown in the figure 78, the important difference in the compressive strength of concretes produced by the two methods is due to density differences as explained in part 3.1. Two studies proposed that the compressive strength increases exponentially with density [7,8], the compressive strength curve as a function of foamed concrete density produced by the direct method follows the equation: $\varphi = 0.7215e^{0.0024\rho}$. The compressive strengths tendency of foamed concretes produced by the preformed method is linear, slightly positively sloped and followed the equation: $R_c = 0.0003\rho + 2.8889$.

Compressive strengths of the concretes C100P0H0D, C70P30H0D and C65P30H5D are larger than 25 MPa, then C65P30H5D can be considered as a structural bio-based concrete. On the other hand, the others BFCs are semi-structural bio-based concretes as they all have a compressive strength larger than 2 MPa. Therefore, the direct method can be used to produce structural

foamed concretes and the preformed method can be used to create semi-structural foamed concretes.

4.2.2 Flexural strength

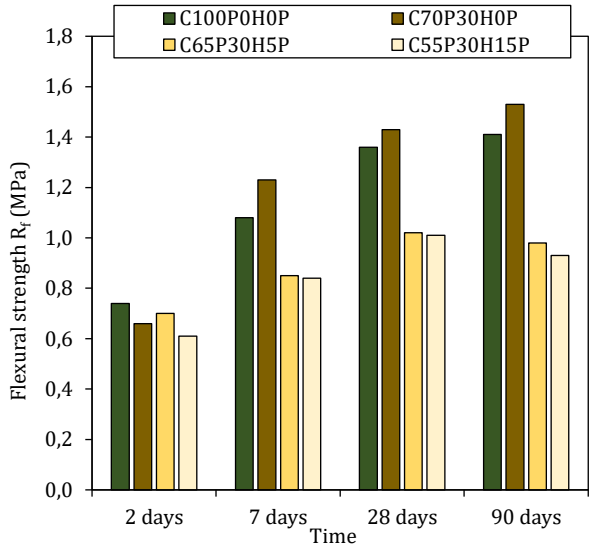

Figure 79 : *Flexural strength versus time of bio-based foamed concrete (BFC) using the preformed method.*

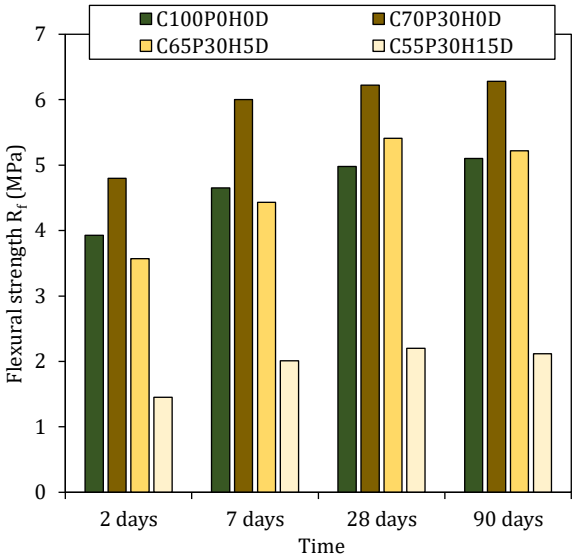

Figure 80 : *Flexural strength versus time of bio-based foamed concrete (BFC) using the direct method.*

For BFC elaborated by both the preformed (Figure 79) and direct (Figure 80) methods, flexural strength follows similar behaviors as the compressive strength. For the BFC elaborated by the preformed method, the flexural strengths at 2 days are almost the same for all concretes. A difference between flexural strengths of hemp shiv-free (C100P0H0P and C70P30H0P) concretes and concretes with hemp shiv (C65P30H5P and C55P30H15P) start to be significant at 7 days. This is due to the beginning of the hemp shiv lignocellulose degradation in the alkaline environment (in this case the cementitious matrix) which reduces the flexural strength [171]. This is also due to the formation of gaps between the hemp shiv particles and the cementitious matrix.

Moreover, at 90 days, the flexural strengths of concretes without hemp shiv continue to increase slightly while it decreases in concretes with hemp shiv, as the concrete hardening is almost over but the hemp shiv degradation continues. Similarly, for the BFC generated by the direct method (figure 80), the flexural strength of foamed concrete without hemp continues to develop with time, while that for foamed concrete with hemp shiv decreases between 28 days and 90 days.

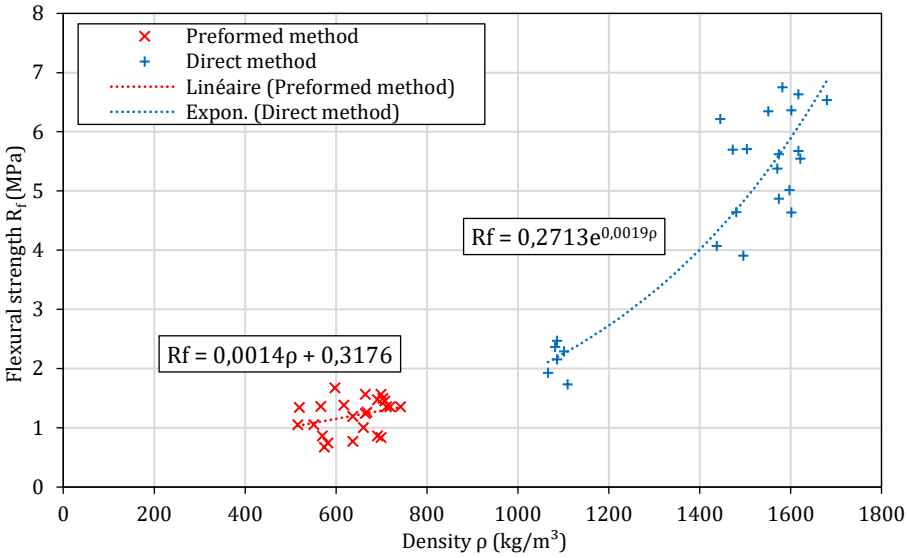

Figure 81 : *Flexural strength of all samples against density at 28-days.*

Similarly, to what was observed in the compressive strength curves, flexure strengths vs density curves (Figure 81) can be fitted for foamed concretes produced by the direct method using: $R_f = 0.2713e^{0.0019\rho}$. For samples produced by the preformed method, the equation is: $R_f = 0.0014\rho - 0.3176$, also the line slope is slightly positive for the same reasons of the compressive strength curve.

The R_f/R_c ratio for the samples prepared by the direct method is between 0.15 and 0.25, while using the preformed method a slightly larger ratio between 0.3 and 0.45 is obtained. This difference is due to the density as the R_f/R_c ratio decreases with increasing density. In the literature, this ratio in foamed concretes with densities lower than 1000 kg/m^3 is between 0.25 and 0.35 [36] and in ordinary concretes between 0.1 and 0.2 [158]. As a result, the hemp shiv incorporation decreases the compressive strength more than the flexural strength resulting in an increased R_f/R_c ratio.

4.3 THERMAL PROPERTIES

Usually, foamed concretes exhibit excellent thermal insulation properties due to their cellular microstructures, and hemp shiv is also a raw material with a low thermal conductivity (almost 0.048 W/(m.K)). Therefore, using a combination of hemp shiv in foamed concretes, one might expect concretes with good thermal insulation performances.

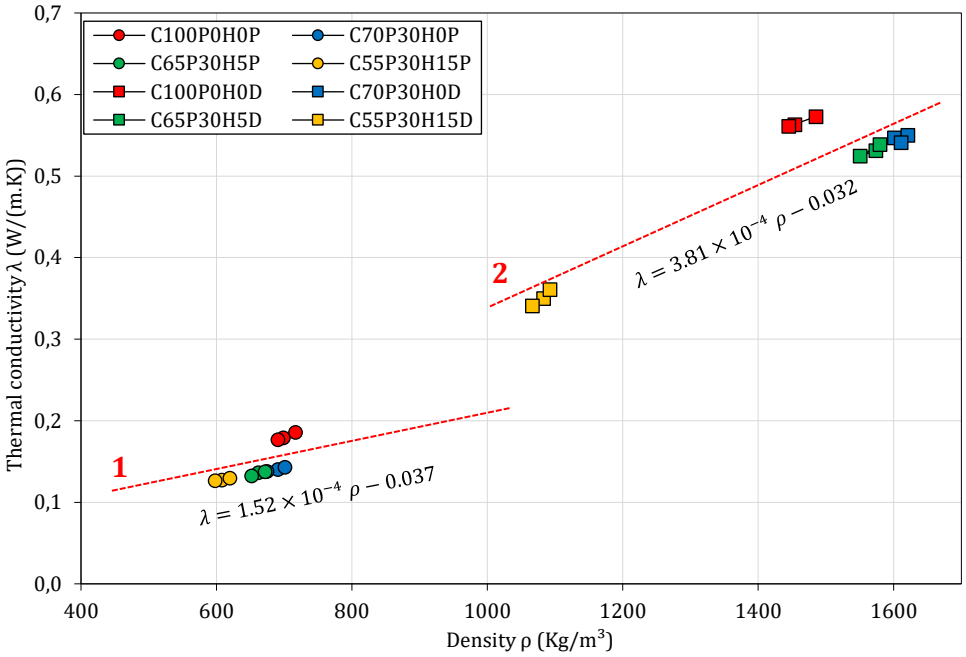

Figure 82 : *Thermal conductivity of all samples against density at 28-days.*

As shown in Figure 82, regarding C100P0H0P and C70P30H0P which represent almost the same density, pozzolans addition decreases the thermal conductivity by 21% in accordance with the results obtained by Ramamurthy [2]. Also, whatever the elaboration method, the thermal conductivity decreases with the decrease of density, this latter being further decreased with hemp shiv incorporation in the foamed concrete. Indeed, the replacement of cement by hemp shiv in foamed concretes increases the porosity due to the low cohesion between the hemp particles and the cement matrix which create gaps in the cement matrix, also the hemp shiv incorporation in the cementitious matrix can induce porosity from the mixing phase, leading to a reduction in density.

The BFCs obtained by the preformed method exhibit thermal conductivities between 0.1275 and 0.1377 W/(m.K) for densities between 598 and 672 kg/m^3, while in the literature for conventional foamed concretes it was observed from 0.118 to 0.199 W/(m.K) for densities between 300 and 500 kg/m^3 [83]. Using the direct method values are observed from 0.32 to 0.65 W/(m.K) for densities between 926 and 1632 kg/m^3 [60], while the thermal conductivity of a normal concrete is 1.5 W/(m.K). Such observations are coherent with our values between 0.35 and 0.55 W/(m.K) for hemp shiv containing samples.

Furthermore, the BFCs thermal conductivity values in function of hemp shiv amount (0, 5, 15%) produced by the preformed method show a linear maximum range (dashed line (1) in the Figure 82) described by the following equation:

$$\lambda = 1.52 \times 10^{-4}\ \rho - 0.037 \qquad \textit{Eq. 28}$$

Between 598 and 703 kg/m^3, a decrease in density of 100 kg/m^3 results in a decrease in thermal conductivity of 0.0152 W/(m.K). This value is lower than the value proposed by Morozov et al. [191], 0.04 W/(m.K) in the case of foam concrete with a higher density (between 600 and 1850 kg/m^3).

While the BFCs thermal conductivity values in function of hemp shiv amount (0, 5, 15%) produced by the direct method draws a linear maximum equation (dashed line (2) in the Figure 82):

$$\lambda = 3.81 \times 10^{-4}\ \rho - 0.032 \qquad \textit{Eq. 29}$$

A decrease in density of 100 kg/m^3 results in a decrease in thermal conductivity of 0.0381 W/(m.K). This value is close to 0.04 W/(m.K) found by Samson et al [12] .

Therefore, the hemp shiv influence has almost the same influence of the air on the thermal performance of foamed concrete with density above 1000 kg/m^3, while their influence decreases with the decrease of density. In addition, the production method affects the thermal conductivity slope. On the other hand, pozzolans decrease the thermal conductivity regardless of the method used, but with the preformed method, the slope is smaller than with the direct method, which makes this method preferable from the thermal conductivity point of view.

4.4 HYDRIC PROPERTIES

4.4.1 Sorption-desorption Isotherms

Figure 83 shows the isotherms obtained for the formulations in function of hemp shiv amount and in function of the production method. The obtained curves both sorption and desorption curves are sigmoids. According to the IUPAC classification, the sorption curves could be classified as type II, while the desorption curves are type III. The results are consistent since these types of curves (Type II for sorption curves and type III for the desorption curves) are usually obtained in macro-porous materials.

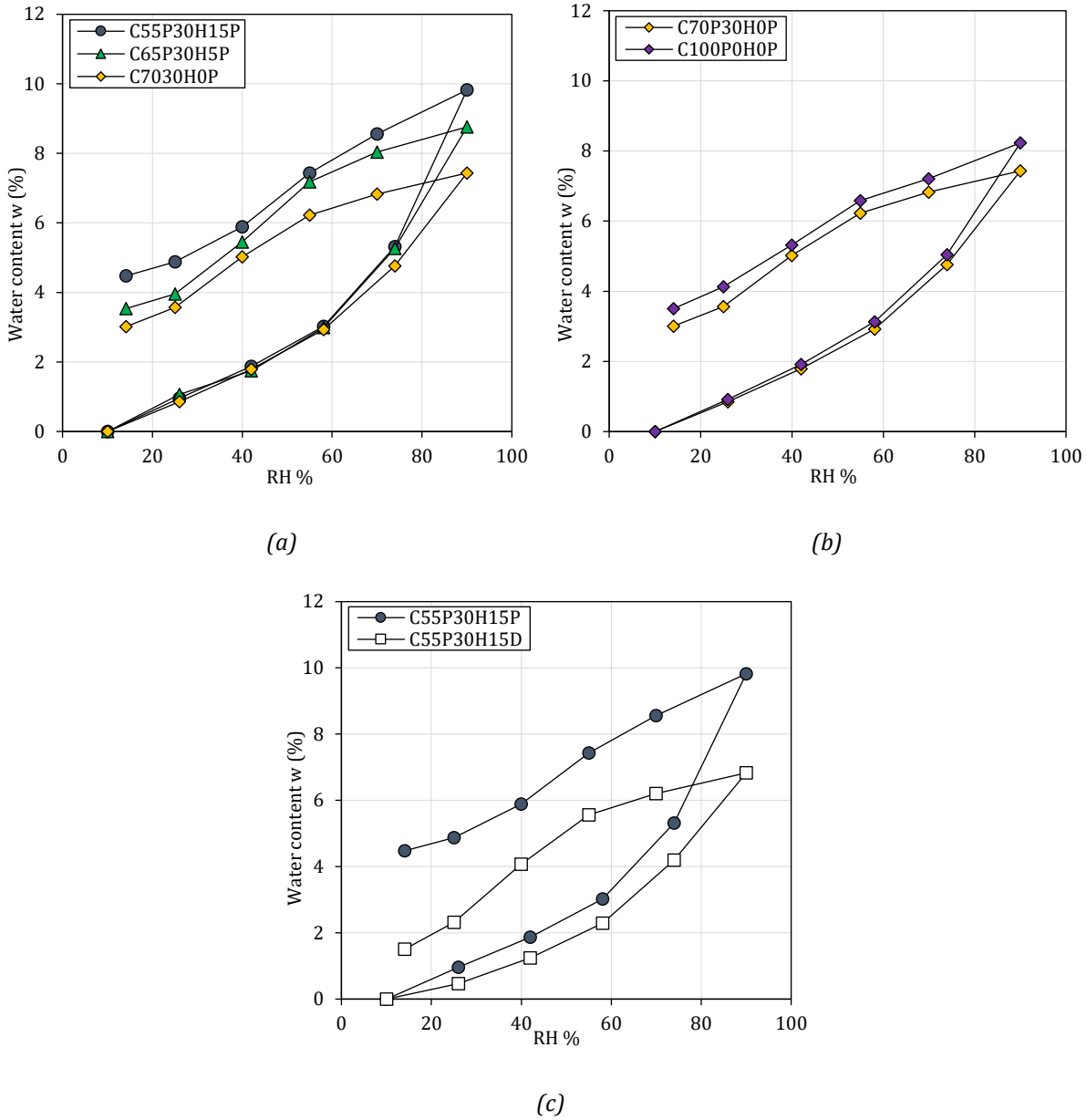

Figure 83 : *Isotherms of BFC in function of: (a) hemp shiv content, (b) presence of pozzolanic additions and (c) production method.*

As shown in Figure 83 (a), at low and medium relative humidity, the water content in the sorption phase increases at the same rate for all 3 concretes. Moreover, at RH ≤ 80 %, the sorption curve is nearly identical, so at low relative humidity, the hemp shiv does not affect BFC sorption. At the highest relative humidity levels, the C55P30H15P water content rises significantly with increasing humidity. At 95% RH, the water content is 9.82%. In this range of humidity, capillary condensation is intense for C55P30H15P while it appears progressively for the others. During desorption, the hemp shiv increases the water retention capacity of the material since the water content of the individual hemp shiv increases with the surrounding humidity due to the highly

hydrophilic character of all lignocellulosic materials, which brought about by their free hydroxyl bonds [192].

The sorption-desorption isotherms (Figure 83 (b)) depend on the open porosity of the material [193], and back to Table 11 (cf. 3.3) the C100P0H0P porosity is 71.4% while that of C70P30H0P is equal to 70.7%, slightly smaller. Therefore, in Figure 83 (b), the two curves are close together, the one of C70P30H0P pointing slightly lower water contents. In conclusion, pozzolanic additions present an indirect effect on the sorption-desorption isotherms through its influence on the porosity.

At low and medium humidity levels (Figure 83 (c)), the change in BFC water content with relative humidity is lower with the direct method than with the preformed method. At higher humidity levels, the difference in water content between the two concretes increases sharply with humidity. At 60% RH, regarding the sorption curve, the difference between the two methods is 0.7%, increasing to 3% up to 95% RH. This difference is due to the difference in porosity in the materials [98,194].

In Figure 83 ((a), (b) and (c)), the end of the desorption branch does not close the loop, there is still a retained water content. This difference in dry mass is explained by entrapped water as chemically bound water and other chemical reactions such as carbonation, and the capacity of the material to retain water in the pores [195], in this case the material is very porous and the presence of hemp shiv also improves the capacity to retain water.

Table 18 : *Sorption-desorption rates and weight difference values.*

	RH (%)	10 %	25 %	40 %	60 %	75 %	90 %
C100P0H0P	Sorption (%)	0	0.92 ±0,16	1.92 ±0,09	3.13 ±0,13	5.05 ±0,19	8.23 ±0,1
	Desorption (%)	3.5 ±0.17	4.13 ±0,12	5.33 ±0,21	6.58 ±0,15	7.12 ±0,18	
	Δw (%) *	3.5	3.21	3.41	3.45	2.07	
C70P30H0P	Sorption (%)	0	0.85 ±0.03	1.79 ±0.05	2.92 ±0.09	4.76 ±0.15	7.43 ±0,13
	Desorption (%)	3.01 ±0.1	3.56 ±0.12	5.01 ±0.17	6.22 ±0.21	6.82 ±0.24	
	Δw (%)	3.01	2.71	3.22	3.3	2.06	
C65P30H5P	Sorption (%)	0	1.06 ±0.05	2.16 ±0.07	3.49 ±0.11	5.66 ±0.31	8.23 ±0,19
	Desorption (%)	3.53 ±0.09	4.15 ±0.12	5.94 ±0.23	7.37 ±0.41	8.03 ±0.32	
	Δw (%)	3.53	3.09	3.78	3.88	2.37	
C55P30H15P	Sorption (%)	0	0.95 ±0.02	1.86 ±0.08	3.02 ±0.18	5.31 ±0.18	9.82 ±0,24
	Desorption (%)	4.4 ±0.22	4.87 ±0.19	5.88 ±0.28	7.43 ±0.36	8.55 ±0.43	
	Δw (%)	4.4	3.92	4.02	4.41	3.24	
C55P30H15D	Sorption (%)	0	0.47 ±0.01	1.24 ±0.07	2.29 ±0.04	4.19 ±0.1	6.83 ±0,03
	Desorption (%)	1.5 ±0.04	2.31 ±0.08	4.07 ±0.09	5.55 ±0.1	6.2 ±0.07	
	Δw (%)	1.5	1.84	2.83	3.26	2.01	

* Retained water content Δw (%) presents the difference of water content (%) between desorption and sorption at a specific RH (%).

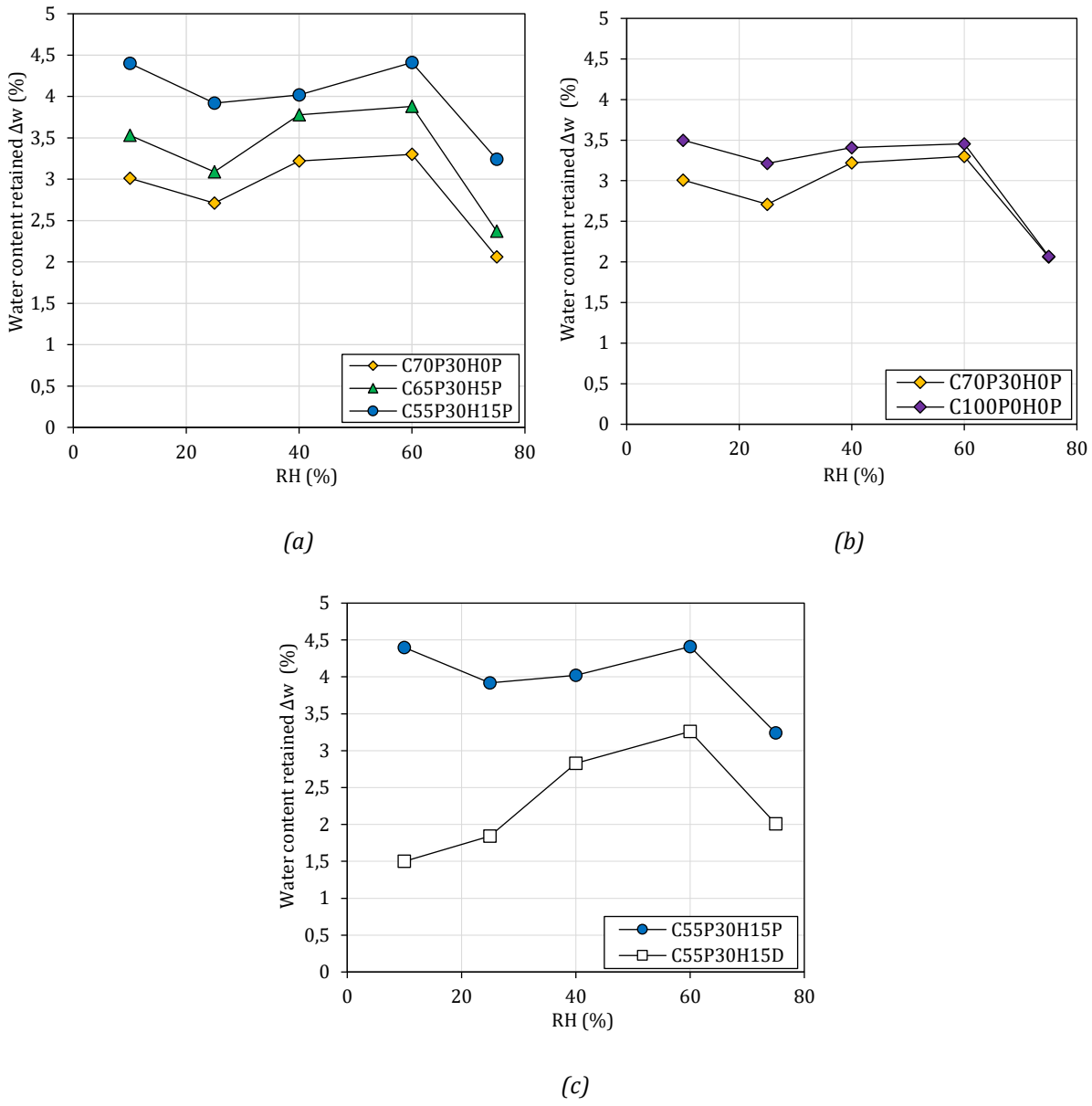

Figure 84 : *Retained water content of BFC in function of: (a) hemp shiv content, (b) presence of pozzolanic additions and (c) production method.*

The retained water content Δw is greater than 0% when a material containing more water during desorption than during sorption at low %RH. Table 18 and Figure 83 shows the evolution of retained water contents Δw over the relative humidity. For all formulations, retained water content presents its maximum value for a humidity of 60% in relation to the phenomenon of capillary condensation which tends to retain water in high quantities.

Figure 83 (a) shows that Δw increases with the hemp shiv amount showing that the hemp shiv is responsible for adsorption surfaces of the material. Figure 83 (b) discusses the difference of retained water content Δw between the foamed concrete C100P0H0P (without pozzolans) and

C70P30H0P (with pozzolans). It is noticed that the curves shape is the same, the difference between the values of these curves starts remarkably at 10% humidity to become almost similar at a humidity 75%, therefore at high humidity both foam concretes retain the same water amount. While in figure 83 (c), the direct method decreases the water retention due to the porosity and provides more hygroscopic comfort than the preformed method since for RH ranging between 20 and 80%, C55P30H15D retains almost two times less water than C55P30H15P.

4.4.2 Capillary absorption

Capillary water absorption or sorptivity test is a reliable way of measuring the ability of a material to absorb and transmit water by capillarity [196].

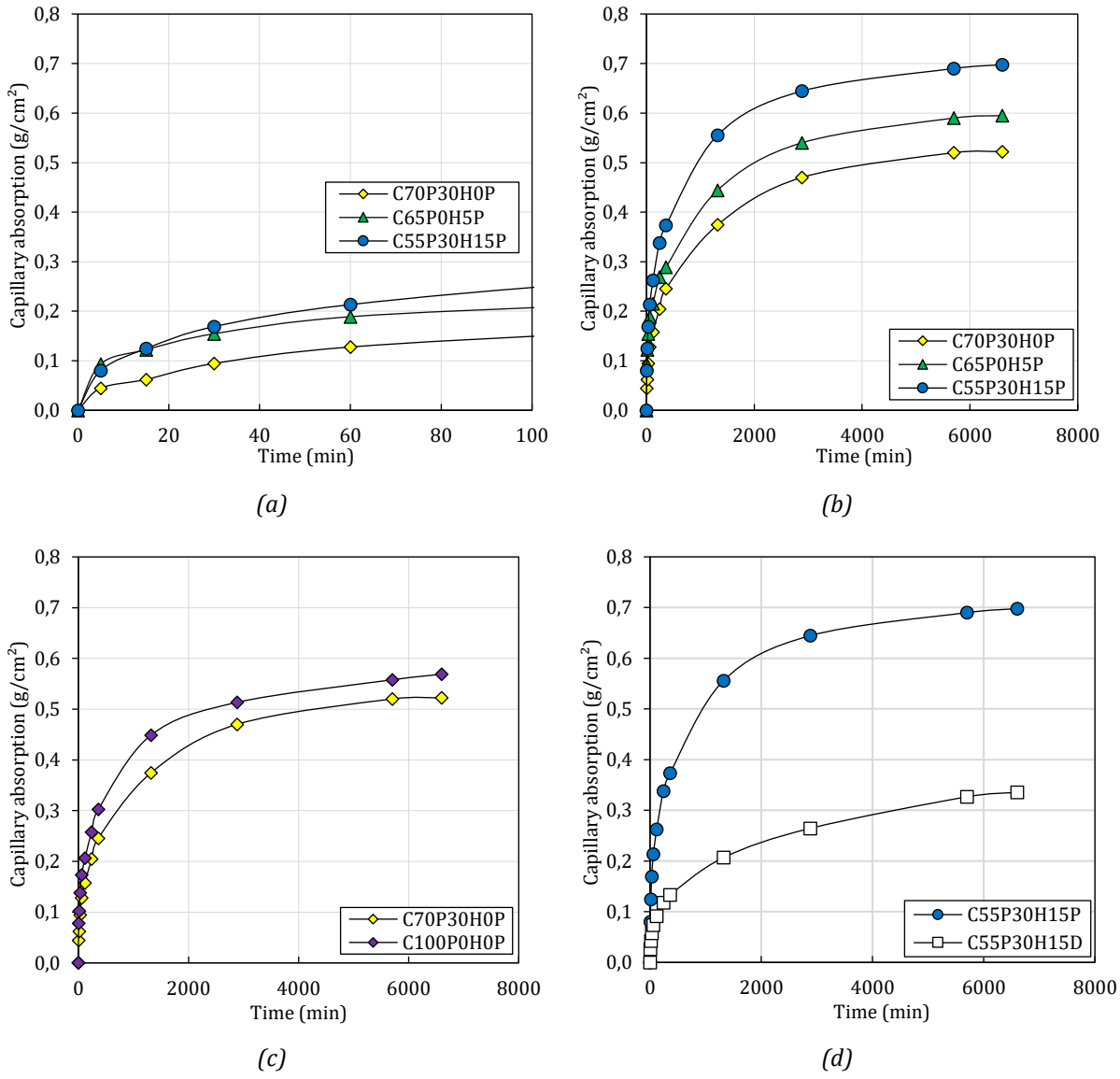

Figure 85 : *Capillary absorption of BFC in function of: (a) hemp shiv content at first 100 min, (b) hemp shiv content, (c) presence of pozzolans and (d) production method.*

The water absorption process observed in our samples can be divided into two stages: rapid and steady state absorption (Figure 85). In the period of rapid absorption stage (Figure 85 (a)), typically in the first hour, water absorption is nearly coincident for the foamed concretes included hemp shiv. This stage is mainly controlled by capillary pores [197]. At the end of this rapid absorption process, water continues to penetrate the samples, water transport reaching the gel pores which are the pores of the hydration product structure. This process is then mainly controlled by diffusion mechanisms [198]. It has been noted that the movement of water in foamed concretes is not just a function of porosity, but it depends on the distribution, diameter and continuity of the pores, as tortuosity. Therefore, the hydric behavior of foamed concretes is becoming more complex due to the larger volume of air voids [199].

Additionally, Figure 85 (b) shows the biobased foamed concretes capillary absorption with different hemp shiv amounts (0, 5, 15%). Capillary absorption of these concretes increases with increasing hemp shiv content. According to Yang et al. [200], there is a correlation between capillary absorption and sorption. Indeed, looking at Figure 83 (a) and Figure 85 (b), it is remarkable that sorption and capillary absorption increase with the hemp shiv content. This is due to porosity, hemp shiv increasing the porous network connectivity and increasing the porosity accessible to water (see 3.3). In addition, the high absorption capacity of hemp shiv (about 247% of its volume) possibly contributed to this increase in capillary absorption.

Figure 85 (c) represents the foamed concretes with and without pozzolanic additions, as well as without the hemp shiv addition. In this figure, it is found that both curves evolve with time in the same way, but C70P30H0P absorbs less water by capillarity than C100P0H0. Looking at the porosity and water accessible porosity of these two concretes (see 3.3) and their air bubble distributions (see 3.4), it appears that the ones of C70P30H0 are slightly smaller than that of C100P0H0, and the air bubbles distribution of C70P30H0 is more uniform than that of C100P0H0. Moreover, the average radius of C70P30H0 voids is smaller than that of C100P0H0, so the air bubble instability phenomenon (coalescence) (see 1.1) is more significant in C100P0H0. In addition, the coalescence lead to more connected and larger porosity which raises the capillary absorption [201]. Indeed, it was proven that the capillary absorption rate depends on the porosity [74] and it increases with decreasing density [202].

The direct method results in low water accessible porosity samples compared to the preformed method (see 3.3). It is then coherent to observe a lower capillary absorption in the former than in the latter (Figure 85 (d)). This is also in accordance with the isotherm sorption-desorption results.

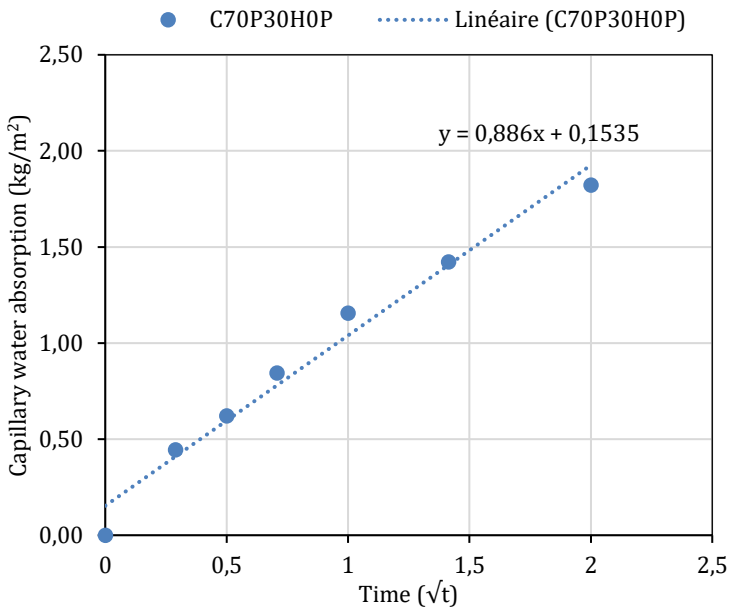

Figure 86 : *Capillary water absorption versus Time.*

The capillary water absorption coefficient C_a is usually used as the main parameter to estimate the liquid water transfer capacity in building materials. Figure 86 shows an example of the capillary absorption coefficient C_a calculation, the linear variation slope equation represents the capillary absorption coefficient which in this case is equal to 0.886. The lines slopes calculation of the other concretes is found in the Appendix 5.

Table 19 : *Capillary absorption coefficients for all samples.*

Samples	Capillary absorption coefficient C_a (kg/(m².√h))
C100P0H0P	1.21
C70P30H0P	0.88
C65P30H5P	1.19
C55P30H15P	1.62
C100P0H0D	0.83
C70P30H0D	0.63
C65P30H5D	0.72
C55P30H15D	0.976

Table 19 shows that the capillary absorption coefficients of the BFCs range between 0.63 and 1.62 kg/(m².√h)). According to the norm NF EN 1504-2, a concrete is considered waterproof if its capillary absorption coefficient is smaller than 0.1 kg/(m².√h). Clearly, according to our measured capillary absorption coefficients, the elaborated BFC's cannot be considered waterproof with

respect to this norm. However, the direct method provides samples two times more waterproof the ones elaborated using the preformed method. The use of pozzolans also slightly favors waterproofing, this latter property not being destroyed for low contents of hemp shiv (compare D-samples). Also, the hemp shiv incorporation in D-samples has less destructive effect concerning waterproof properties than in P-samples.

4.5 FOAMED CONCRETES GLOBAL EVALUATION

The objective of this thesis is to develop and investigate a bio-based, structural, insulating and waterproof foamed concrete. We selected consequently, five main performances in order to evaluate the concretes:

- Mechanical performances, based on the previous compressive and flexural strengths to identify the potential functionality of these concretes (self-supporting or structural).
- Thermal performances, based on the thermal conductivity, to identify insulating capacities.
- Lightness, based on the density values, to ease implementation and reduce construction costs, make the material more fire resistant and sound insulator.
- Ecology, using estimation of CO_2 emissions.
- Waterproofing, based on capillarity measurements

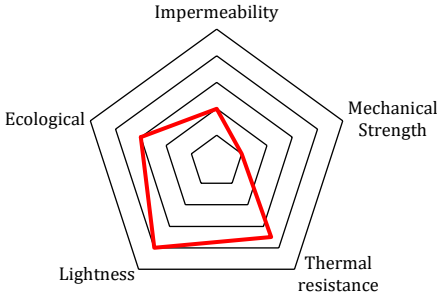

(a) C100P0H0P

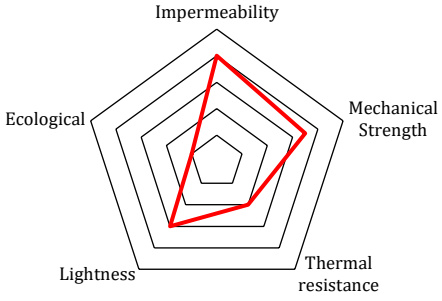

(b) C100P0H0D

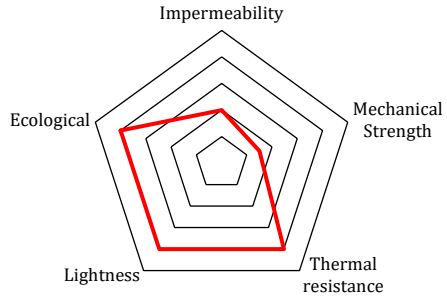

(c) C70P30H0P

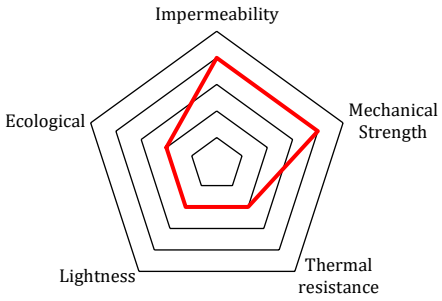

(d) C70P30H0D

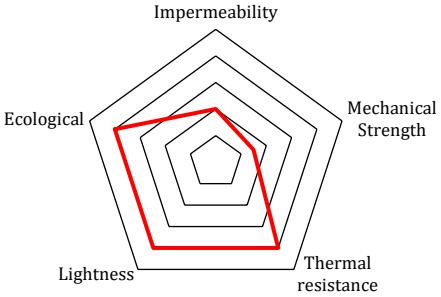

(e) C65P30H5P

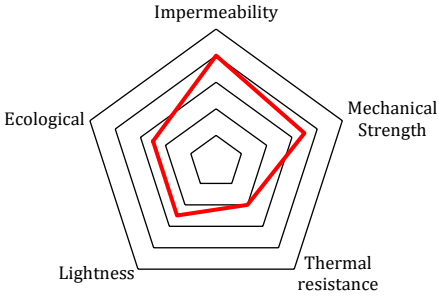

(f) C65P30H5D

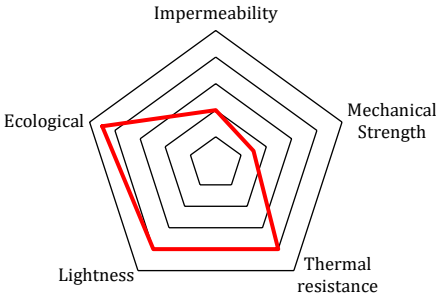

(g) C55P30H15P

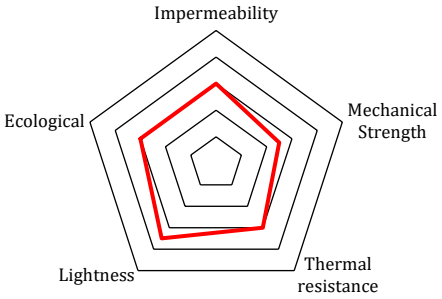

(h) C55P30H15D

Figure 87 : *performance radar of different foamed concrete.*

Looking at Figure 87 (a, c, e and g), we notice that the foamed concretes manufactured by the preformed method are characterized by their lightness, their thermal resistance and their ecological characteristics, but their levels of mechanical resistance and waterproofing are modest. While it is the opposite for the concretes made by the direct method (see Figure 87 (b, d, f and h)).

Looking at Figure 87 (c and d), the pozzolanic additions reduce the CO_2 emissions and slightly improve the mechanical performances. The remaining performances are almost negligibly affected and globally, the pozzolans addition goes the right way.

In this study, the cement was replaced by two different hemp shiv quantities, 5 wt% and 15 wt% of cement:

- With 5% (Figure 87 e and f), the ecological character is slightly improved, for the other performances the influence is almost negligible globally.
- With a higher amount of hemp shiv (Figure 87 g and h), using the preformed method, the performance is very close to that of C70P30H0 and C65P30H5 except that it is more ecological but using the direct method, the thermal performances and impermeability are reduced.

So, using the preformed method, we find that, comparing the different concretes, the bio-based foamed concrete C55P30H15P gives the best performances, a good insulation (λ = 0.12 W/(m.k)), lightweight (ρ < 600 kg/m^3) and ecological (CO_2 emission: 384 kg CO_2/m^3), but at the level of mechanical resistance, it is a non-structural self-supporting concrete. Concerning waterproofing, the results are modest, with a capillary absorption coefficient of 1.62 kg/(m^2.$\sqrt{h}$) while for a waterproof concrete, this rate must be equal to w = 0.1 kg/(m^2.$\sqrt{h}$).

On the other hand, the C65P30H5D exhibits the best mechanical performances among the concretes manufactured by the direct method, it is structural with a compressive strength almost of 32 MPa, a lightweight (ρ = 1600 kg/m^3) and an average thermal insulation character (λ = 0.53 W/(m.K)), almost 3 times less than a thermal conductivity of an ordinary concrete (λ = 1.75 W/(m.K)). In addition, the water absorption coefficient is equal to 0.72 kg/(m^2.$\sqrt{h}$), which is still far from a waterproofing capacities.

Therefore, to improve the waterproofing of the material, it is necessary to use water repellents.

4.6 CONCLUSION

This chapter shows an analysis on the effects of cement replacement by hemp shiv and pozzolanic additions, and foaming method on the mechanical strength, thermal and hydric properties.

Pozzolanic additives delay the hydration, therefore the mechanical strength increases slowly between 2 to 7 days compared to concretes without pozzolans. It is also found that the compressive strength is increased when using pozzolans thanks to their pore filling ability. Their effect on thermal resistivity is low. Also, it slightly decreases sorption and capillary absorption.

Hemp shiv also delays the hydration. Moreover, it has a negative effect on the mechanical strength, since the lignocellulose degradation in the cementitious matrix creates new pores in the cementitious matrix, which increases the porosity amount and decreases the density and mechanical strength. Additionally, at low and medium relative humidity, the hemp shiv has no effects on the BFC adsorption, but at the highest relative humidity levels the adsorption increases significantly with the increase of hemp shiv amount. Hemp shiv enhances the retained water amount in the concrete.

Furthermore, since the porosity changes significantly between the direct method (70%) and the preformed method (40%), the process method influences on all properties is evaluated. Using the direct method provides structural concretes with adequate mechanical strengths for all concretes except the concrete with a large amount of hemp shiv (15%). But their thermal resistance remains modest compared to the ones of concretes produced by the preformed method, which also are self-supporting or semi-structural foam concretes. The direct method decreases the adsorption more than the preformed method. Capillary water absorption increases with the increase of the hemp shiv amount and the direct method decreases this absorption compared to the preformed method.

A global evaluation of concrete foams is investigated. This evaluation is based on 5 main performances, mechanical and thermal performances, lightness, ecology and waterproofing. C55P30H15P is the best among the foamed concretes produced by the preformed method. This concrete is characterized by its lightness, low thermal conductivity and ecological character. On the other hand, C65P30H5D is chosen among the foamed concretes produced by direct method due to its mechanical and medium thermal performances. However, these two concretes have low water resistance.

Finally, among the concretes studied, we find non-autoclaved, bio-based, insulating and structural foamed concretes, but none of them exhibits a waterproof character, and cannot find applicability toward hygrothermal comfort. Therefore, in the following chapter we will discuss the waterproofing of the material and the ways to develop it, and then operate a thermal simulation using an optimized material.

Chapter 5

Waterproofing and thermal simulation of bio-based foamed concrete

5. Waterproofing and thermal simulation of bio-based foamed concrete

5.1 INTRODUCTION

The objective of this chapter is to study the surface and mass water repellents influence on the formation of foam, and on its physical, thermal, hydric and mechanical properties in order to improve the waterproof character of our material. Also, to analyze a thermal simulation of a house using the BBISE material as a wall.

The BFC concretes selected previously are chosen for studying their waterproofing character after the mass and surface water repellents addition. Studies on capillary absorption, physical and mechanical properties are investigated to determine the influence of the use of mass and surface water repellents on the concretes.

Furthermore, a thermal simulation using the software Pleiades is launched after the application of the new sandwich concrete which is based on the selected BFC in a house to study the hygrothermal comfort and the energy consumed for heating and cooling.

5.2 WATER REPELLENTS

The water absorption or moisture has a significant negative influence on the physical and mechanical properties, and durability of the foamed concretes. Moreover, it is reported that the water flow in foamed concretes depends on the pore distribution, diameter, continuity and tortuosity [76].

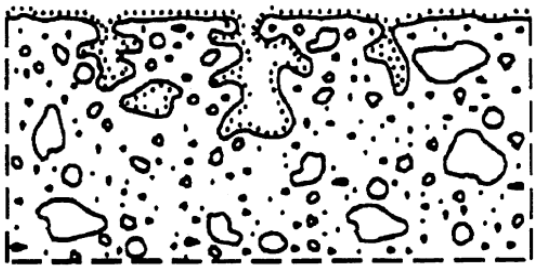

Figure 88 : *Schematic representation of mass water repellents on the pores [203].*

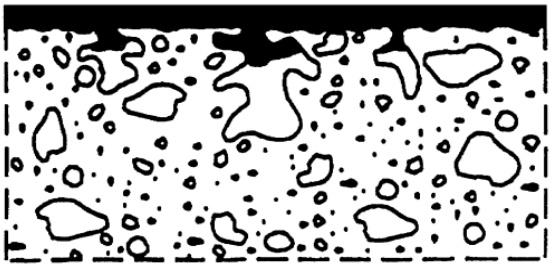

Figure 89 : *Schematic representation of surface water repellents on the pores [203].*

Figure 90 : *External waterproofing coating*

To improve the foamed concretes waterproofing, it is advisable to use water repellents, due to their ability to prevent water from penetrating the concrete. Medeiros et al. [68] studied the water repellents effects on a conventional concrete and found that the chloride diffusion coefficient is reduced by 80%, while the capillary absorption coefficient is reduced from 73% to 98%.

Waterproofing methods include mainly internal mixing (Figure 88) and external coating (Figure 89) [204,205]. External coating is achieved by spraying the water repellent on the surface (Figure 90). It is applied after the concrete has fully cured (at 28 days). It decreases water absorption by changing surface tensions to repel water. In fact, water repellents penetrate inside the concrete where they attach themselves to the inner walls of pores. These products do not block the pores, but rather coat them with a very thin film that leads to a reduction in surface tension. Thus, a water drop will remain in a spherical form on the surface and will not spread. Therefore, the water repellents only influence the water absorption but not the hydration property of concrete in the external coating method. Internal mixing method is performed by mixing the water repellent with the fresh mix. Compared with the external coating method, when water repellent is mixed with the raw materials, it not only reduces the BFC water absorption but also influences the paste mechanical properties. In other words, the mass water repellent is not only a water repellent for the internal mix of the cement paste that improves the concrete waterproofing, but it is also favorable for the compressive strength [71].

Two water repellents are applied in this study, to investigate the influence of two different types of water repellents on the physical and mechanical properties and on the capillary absorption.

MasterLife WP 760 concrete mass water repellent (MW) works by dispersing into the concrete. Its action consists in obstructing the capillary networks, thus preventing the water flow in these networks. This action has two effects: on the one hand, the capillary effect is strongly reduced, thus reducing the water penetration or external agents into the concrete; on the other hand, the free lime naturally resulting from the cement hydration is fixed in the interior of the concrete, thus reducing the risk of efflorescence.

MasterPel 300 concrete surface water repellent (SW) is a colorless product in aqueous phase for the concrete protection, to pulverize, guaranteeing the protection of the concretes surfaces without modifying their aspect. Non-film forming, it allows the substrate to breathe, protects against water, oil and dirt penetration. Table 20 represents characteristics of the used water repellents.

Table 20 : *Characteristics of water repellents used to elaborate the cementing materials.*

	MW	SW
Consistence	liquid	liquid
Color	White	Incolor
Density (g/cm^3)	1.03 ± 0.02	1.00 ± 0.02
pH	10.5 ± 1	6 ± 1

5.3 FORMULATIONS

In this chapter, there is only one parameter that changes for two basic formulations that are chosen in 5.2, C65P30H5D and C55P30H15P. These nomenclatures are followed by "S" which designates the concrete treated by the surface water repellent MasterPel 300 and "M" which designates the concrete in which the mass water repellent MasterLife WP 760 is incorporated.

Table 21 : *Formulations of all concretes studied in chapter 5.*

Mixes Names	Fresh density (kg/m^3)	Composition of mixture (kg/m^3)								Wt/L
		CEM I	GGBFS	MK	HS	SP	Acc	MW	FAG	
C65P30H5D	1542	780	240	120	5.6	11.4	11.4	-	2.1	0,32
C65P30H5DS	1542	780	240	120	5.6	11.4	11.4	-	2.1	0,32
C65P30H5DM	1542	780	240	120	5.6	11.4	11.4	11.4	2.1	0,32
C55P30H5P	834	385	140	70	9.8	6.1	6.1	-	2.1	0,35
C55P30H5PS	834	385	140	70	9.8	6.1	6.1	-	2.1	0,35
C55P30H5PM	834	385	140	70	9.8	6.1	6.1	11.4	2.1	0,35

For example, in Table 21 which represents the concretes compositions, "C55P30H5PM consists of 55 wt% of cement, 30 wt% of cement is replaced by pozzolans, 15% is replaced by hemp shiv, the production method is the preformed method " P " and mass water repellent applied is " M ".

The mass water repellents amount used is 1 wght%. This percentage is based on previous studies looking at the effect of different water repellents quantities on foamed concretes, 1% being the optimum amount between capillary absorption and compressive strength [70].

5.4 WATERPROOFING

5.4.1 Physical properties

Several studies have shown the influence of the water repellents addition on the conventional concrete physical properties, but these studies on foamed concretes are very rare. Most of these studies have found limited influence. Furthermore, the effects of adding water repellents vary between concrete types. With conventional concretes the density is found to decrease due to their ability to encapsulate air into the paste [206], while with foamed concretes it increases the density as it slightly affects the foam stability [71].

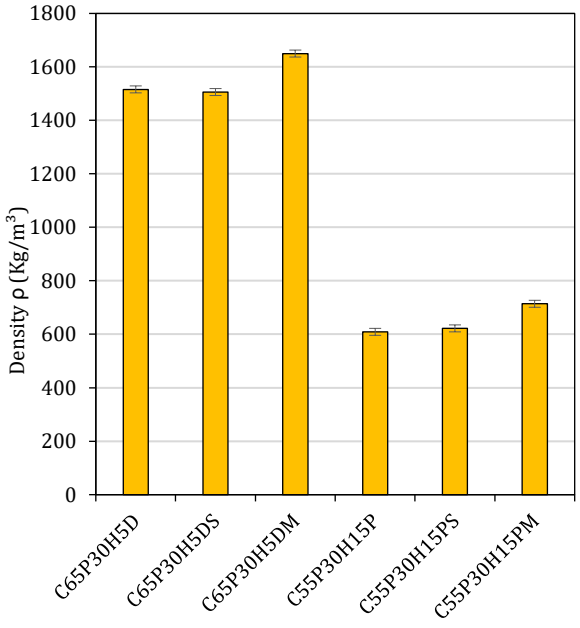

Figure 91 : *Density of all samples*

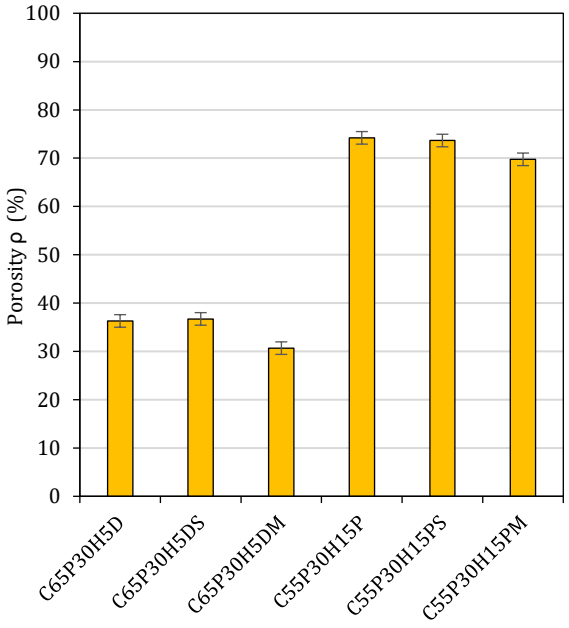

Figure 92 : *Porosity of all samples.*

In Figures 91 and 92, Comparing BFCs porosity and density without water repellent (C65P30H5D and C55P30H15P) and others with surface water repellent (respectively C65P30H5DS and

C55P30H15PS), it is found that they are almost equal. The surface water repellent is applied to the hardened concretes, and it does not change these physical properties.

But it is found that by incorporating water repellent in mass, porosity reduces by 15.5% and 5.3%, for C65P30H5DM and C55P30H15PM, while density increases by 8.8% and 12.9%, respectively. This difference shown by the addition of bulk water repellent is caused by the change in the material phases since the bulk water repellent included in the cement paste affects the foam stability. Indeed, Ma et al. [71] found that the water repellent added to the foam concrete has low influence on the foam stability, resulting in the dry density since the stability of the foam reduces the air bubbles deflation, then it keeps the air in the cementitious matrix which affects the dry density.

5.4.2 Capillary absorption

Foamed concrete structure is characterized by the formation of macropores and micropores in the cementitious matrix [207]. Macropores are pores with a diameter larger than 60 µm [208], and are formed due to the mass expansion during the aeration process, while micropores are formed between the macropores walls [209]. It is known that water tends to be absorbed easily into the foam concrete due to the large air voids amount available inside the concrete. Therefore, the water repellents are used to reduce the water absorption of foamed concrete.

Water repellents are used primarily to improve the material impermeability, i.e. to reduce water penetration into the cementitious structure. Capillary absorption or sorptivity tests are used in several studies to measure the water repellents feasibility on concretes [71,76,204,206] in accordance with NF EN 1504-2 .

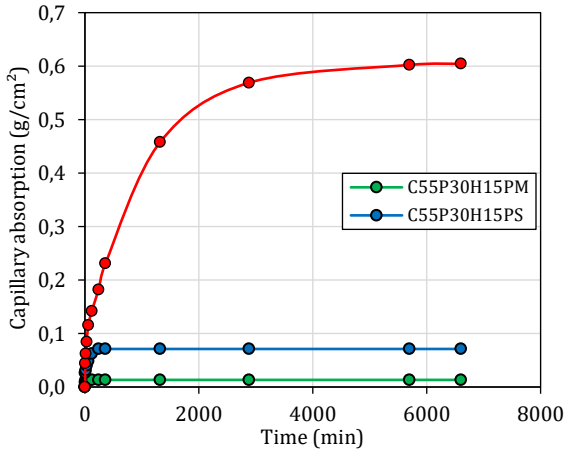

Figure 93 : *Capillary absorption of C55P30H15P using the two types of water repellents*

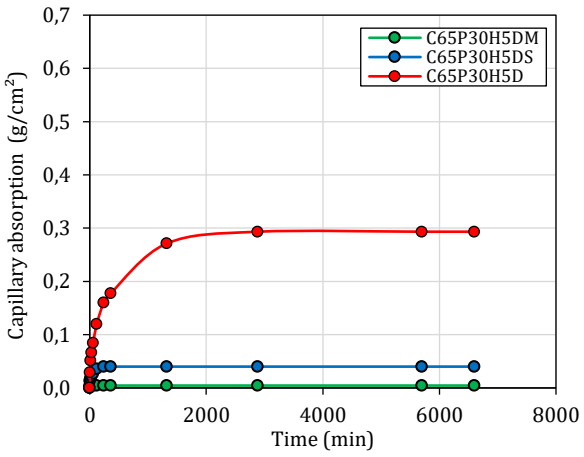

Figure 94 : *Capillary absorption of C65P30H5D using the two types of water repellents*

Figure 93 shows C55P30H15P capillary absorption with and without using water repellents. It can be seen that the capillary water absorption of C55P30H15P needed a long time to reach stability (almost 100h) due to its high porosity (> 74%), while for C55P30H15PS and C55P30H15PM it required only 8h and 30 min respectively. Capillary absorption is decreased by 89% (from 0.604 to 0.071 g/cm^2) using a surface water repellent, while it decreases by 99% (from 0.604 to 0.013 g/cm^2) for a bulk water repellent.

Similarly, Figure 94 shows capillary absorption of C65P30H15P with and without water repellent. The C65P30H15D initial capillary absorption needing 48h to reach its maximum value, while for C65P30H15DS and C65P30H15DM only 8h and 5 min are necessary respectively. For the latter sample, capillarity is filled completely quasi instantaneously. Capillary absorption is decreased by 99%, from 0.293 to 0.004 g/cm^2.

Table 22 gives the determined capillary absorption coefficients for all samples. The calculation of the capillary water absorption coefficient C_a is presented in the Appendix 6 by determining the linear variation slopes of the capillary water absorption.

Table 22 : *Capillary absorption coefficients using different water repellents.*

Samples	Capillary absorption coefficient C_a (kg/(m^2.√h))
C55P30H15P	1.52
C55P30H15PM	0,04
C55P30H15PS	0,33
C65P30H5D	0,78
C65P30H5DM	0,01
C65P30H5DS	0,19

It is found that for both BFCs, surface water repellency reduces capillary absorption coefficient between 75 and 78%, while mass water repellency reduces 99% of capillary absorption. Mass water repellency is therefore more effective than surface water repellency.

Figure 95 : *Waterproofing of C55P30H15PM*

Figure 96 : *Waterproofing of C65P30H5DM*

Moreover, C55P30H15PM (figure 93) and C65P30H15DM (figure 94) capillary absorption coefficients are equal to 0.04 and 0.01 kg/(m².√h), respectively. Both are considered as a waterproof concrete according to NF EN 1504-2 [203], since they exhibit capillary absorption coefficients lower than 0.1 kg/(m².√h). Moreover, the capillary absorption coefficients are significantly reduced by using the surface water repellent but the BFCs do not exhibit waterproof character since the capillary absorption coefficients show 0.19 and 0.33 kg/(m².√h), respectively for C55P30H15PS and C65P30H15DS .

5.4.3 Mechanical strength

Since the water repellent affects the porosity and especially the surface porosity, it is necessary to study the mechanical strength. Figures 95 and 96 show the compressive and flexural strengths of C55P30H15P and C65P30H5D, respectively, with and without water repellents.

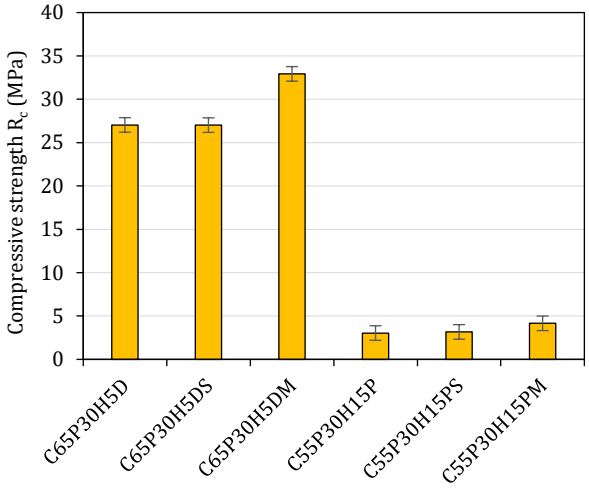

Figure 97 : *Compressive strength of all samples.*

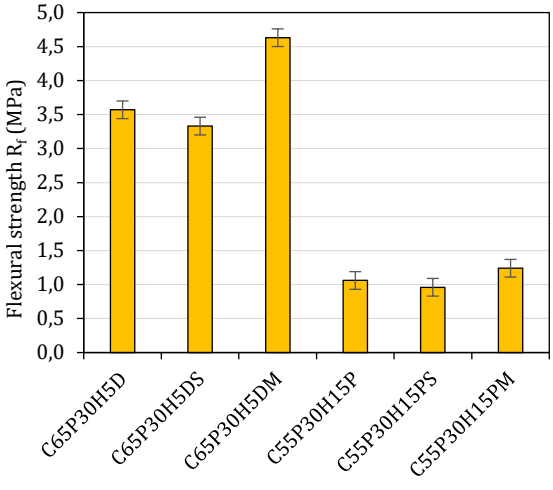

Figure 98 : *Flexural strength of all samples*

Figure 97 shows that the compressive strength is not affected when using surface water repellent for both BFCs C55P30H15P and C65P30H5D, but when using mass water repellent, the compressive strength increases significantly, by 23.8% from 3.17 to 4.16 MPa for C55P30H15P and by 17.9% from 27.02 to 32.93 MPa, same results were found in the literature [210,211]. This increase in compressive strength is related to the porosity amount which is decreased when using mass water repellent. Figure 92 shows that the porosity decreased by using mass water repellents from 74.1 to 69.7 % and from 36.3 to 30.6 %, for C55P30H15P and C65P30H5D respectively.

Figure 98 shows that the flexural strength follows a similar behaviour as the compressive strength. Comparing the Rf/Rc ratio of BFCs without and with mass water repellents, we find that

for C65P30H5D this ratio ranges between 0.13 and 0.14, and for C55P30H15P between 0.30 and 0.34. As a result, in general, we find that there is no significant difference when using water repellents, though they affect compressive and flexural strengths proportionally.

5.4.4 Thermal conductivity

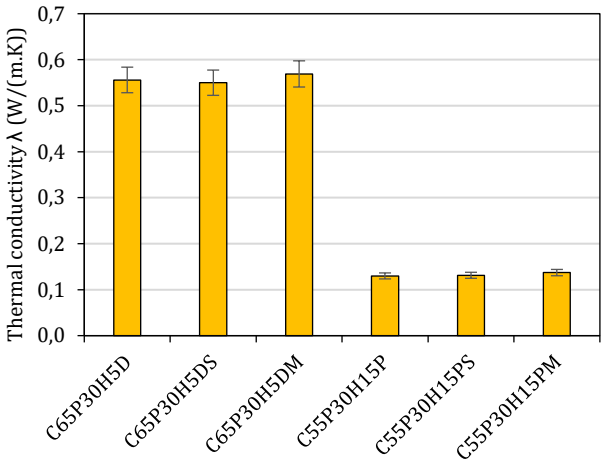

Figure 99 : *Thermal conductivity of all samples.*

The measurement of thermal conductivity is essential to identify the insulating character of the material. Surface water repellent does not affect thermal conductivity (Figure 99). However, a 2% and 5% increase occurred, from 0.556 to 0.5691 W/(m.K) and from 0.1299 to 0.1371 W/(m.K), adding mass water repellent to C65P30H5D and C55P30H15P, respectively. In conclusion, the water repellents addition has no significant effect on the biobased foamed concrete thermal conductivity.

5.5 THERMAL SIMULATION

The objective of this numerical analysis is to evaluate how the thermal simulation of a house using our bio-based foam concretes can be valorized to feed a calculation tool likely to numerically model the mechanical response of foam concretes. This feasibility study is mainly focused on thermal and hygrothermal comfort, and energy consumption during heating and cooling. RT2012 compliant materials used in real life low energy buildings are compared with the results using our sandwich materials.

5.5.1 Methods

Figure 100 : *3D house vision*

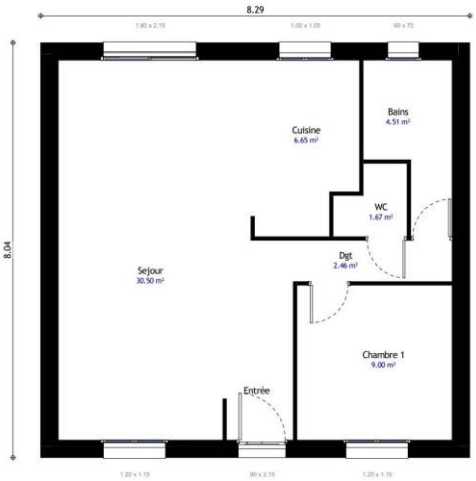

Figure 101 : *2D house plan*

To launch a thermal simulation using the Pleiades software, several steps must be identified. The first step consists in designing a house model. A free model from an internet site (figure 100 and 101) was chosen [212]. This house is small and simple, consisting of a living room and kitchen, bedroom, WC and a bathroom. In this study the thermal behavior and hygrothermal comfort of the living room and the heating and cooling total consumption are targeted.

Then the scenario must be identified, i.e., the number of inhabitants (2 persons), the electrical instruments (television, light...) and the time of functioning must be defined (see annex). It is very important to determine the living system since it affects the energy consumption in the building.

Next, the weather and the house location was identified, because for each environment the weather and the effective temperature and humidity are different. These parameters are the main criteria that define the functioning and the feasibility of the used materials.

5.5.1.1 Materials

In this study, all conditions are unchanged, only the exterior wall materials are modified. Two materials are used and compared in this part. On the one hand, the sandwich material **BBISE** coming from the French acronym: (**B**éton **B**iosourcé **I**solant **S**emi-structurel et **E**tanche à l'eau) which means Biobased Concrete Semi-structural Insulation and Waterproof. On the other hand, an assembly of heavy concrete and rock wool identified in the library of software Pleiades. Both materials are heterogeneous.

5.5.1.1.1 BBISE

5.5.1.1.1.1 Input

Since Pleiades can include heterogeneous materials, we need to know several values, such as density, thermal conductivity and specific heat of each compound of BBISE, C55P30H15PM and C65P30H15DM. As known, density and thermal conductivity are already measured in section 5.5.1 and 5.5.4 respectively.

The specific heat at constant pressure, C_p is the energy that necessary to increase by 1 degree 1 kg of the material or conversely the quantity of heat that 1 kg of material releases when its temperature decreases by 1 degree. The unit for Cp is J/(kg.K) in the international SI unit system. I wonder if this paragraph is necessary. These are definitions of 1st year thermodynamics at university ...

Heat capacity of a mixture can be calculated using the rule of mixtures. The new heat capacity depends on the proportion of each component, which can be calculated from the mass at a given temperature:

$$C_p mixture = \left(\frac{m_1}{m_{mixture}}\right).C_{p1} + \left(\frac{m_2}{m_{mixture}}\right).C_{p2} \qquad \textbf{Eq. 30}$$

With,

C_p = Heat capacity (J/kg.K).

mi = Mass of constituent i (kg).

$m_{mixture}$ = Total mass of the mixture, $m_1 + m_2$ (kg).

Table 23 : *Heat capacity of principal compounds of BFCs.*

Concrete type	Heat capacity C_p (J/kg.K)
Foamed Concrete (1400 kg/m^3) [213]	794
Foamed Concrete (700 kg/m^3) [213]	879
Hemp shiv	2100

To calculate the BFCs heat capacity, raw material values are extracted from the literature (Table 23), then a calculation based on eq. 30 and the values of Table 23 for the total heat capacity of C55P30H15PM and C65P30H15DM (see Table 24).

Table 24 : *Density, thermal conductivity and heat capacity of BFCs.*

Concrete type	Density ρ (kg/m^3)	Thermal conductivity λ (W/m.K)	Heat capacity C_p (J/kg.K)
C55P30H15PM	1650	0.1371	1062
C65P30H15DM	714	0.5691	859

After obtaining the BBISE components density, thermal conductivity and heat capacity, their dimensions must be identified.

5.5.1.1.1.2 Dimensions

As shown in figure 102, BBISE is a sandwiched concrete which made of 3 layers, 2 outer layers of structural insulation, waterproof concrete based on C65P30H5DM, and one inner layer of non-structural insulation based on C55P30H15PM. Figure 103 shows a real example of the BBISE20.

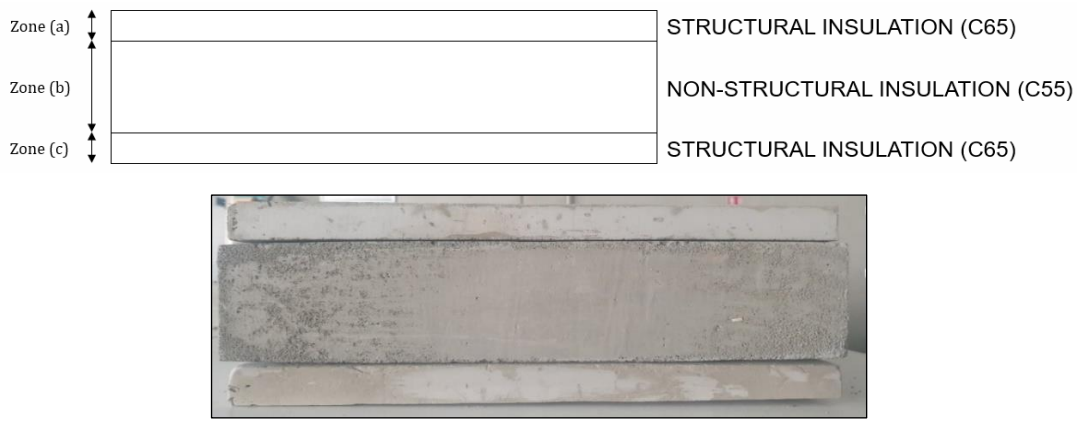

Figure 102 : *Composition of the different sandwiched concretes.*

Figure 103 : *Sandwiched concrete BBISE.*

As shown in Table 25, BBISE several dimensions are studied (20, 25, 30 and 40 cm). The thermal conductivity of this concrete is 0.1969 W/(m.K).

A material thermal resistance depends on the thickness of the material (e, in meters) and its thermal conductivity (λ):

$R = e/\lambda$ in m^2.K/W units. **Eq. 31**

The total thermal resistance of a wall is equal to the thermal resistances sum of each material layer that constitutes it: R*wall* = R*material1*+R*material2*+ ...

Table 25 : *Different types of BBISE used in this simulation.*

Concrete type	Zone (a) (cm)	Zone (b) (cm)	Zone (c) (cm)	Thermal resistance R (m^2.K/W)
BBISE20	4	12	4	1.02
BBISE25	5	15	5	1.27
BBISE30	6	18	6	1.52
BBISE40	8	24	8	2.03

The larger the thermal resistance, the more insulating the wall is. Thermal resistance increases with the thicknesses of the constituting concretes. Based on RT2012, thermal resistance of the material used in a new building must be greater than 2.8 m^2.K/W, so that the BBISE thickness would have to reach 55 cm to become eligible to RT2012.

5.5.1.1.2 Heavy Concrete and Rock Wool (CRW)

CRW presents a combination between conventional heavy concrete with a specific dimension (20 cm) and various thicknesses of an insulation used often in the market, the rock wool, with respect to the dimensions used with the BBISE. Note that CRW40 (Table 26) is given in the software library of Pleiades and this assembly is used in the low energy building which granted to RT2012.

Table 26 : *Different types of CRW used in this simulation.*

Concrete type	Heavy concrete (cm)	Rockwool (cm)	Thermal resistance R (m^2.K/W)
CRW20	20	0	0.11
CRW25	20	5	1.33
CRW30	20	10	2.55
CRW40	20	20	4.99

Table 26 presents the dimensions of CRW materials and their thermal resistance. CRW's exhibit clearly a larger thermal resistance than BBISEs.

5.5.1.2 Pleiades

We chose this software because it is certified and provides thermal simulation of a building in real conditions, including hygrothermal comfort and energy consumption at heating and cooling.

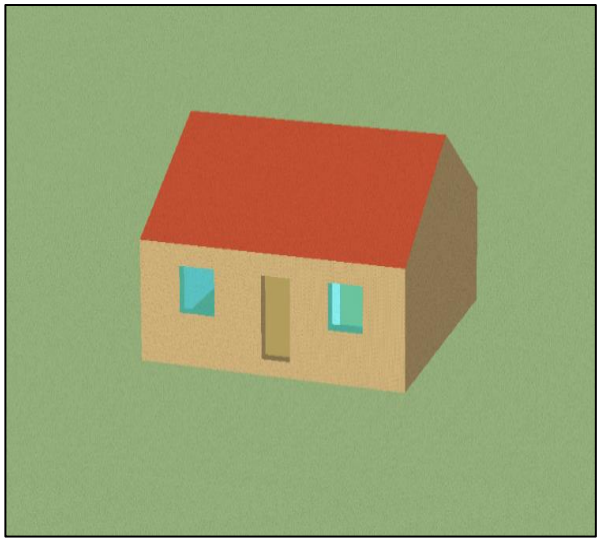

Figure 104 : *3D vision on Pleiades*

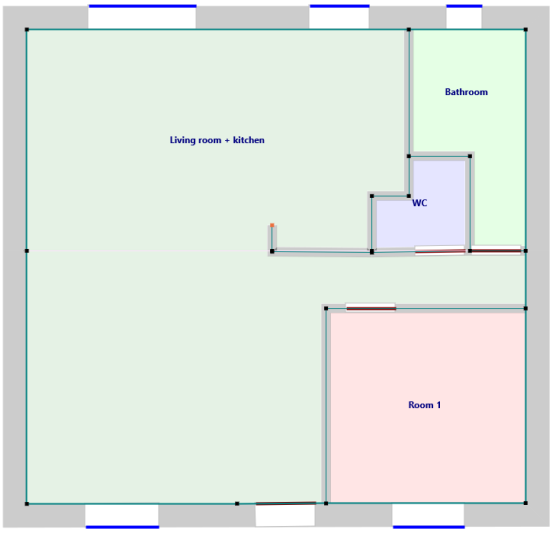

Figure 105 : *2D plan of the house on Pleiades*

Firstly, the software requires a definition and dimensioning of the house (Figures 104 and 105), then the materials used in the external and internal walls, ceiling and slab. After this stage, the heat transfer technique, the house location and the living scenario (Inhabitants number, occupancy hours, ideal temperature in the rooms) are described. All these scenarios are standardly included in Pleiades.

5.5.2 Results and discussion

5.5.2.1 Thermal comfort

BBISE and CRW concretes are compared by thickness, for example BBISE20 is compared to CRW20. This eases to check influences of thermal and hygrothermal performances.

5.5.2.1.1 Brager zone

In warm periods, the occupants accept a larger temperature than in cold periods. This is the hypothesis on which the Brager comfort diagram is based, and which is now used in the STD module.

This model is valid between -10 and 40°C of outside temperatures (x-axis of Figure 106). It assumes that the ideal inside temperature (y-axis of Figure 106) for 90% of the population is between 17 and 22°C in cold weather and between 26 and 31°C in warm weather. This assumption sets the "comfort zone" materialized by the two black lines on the diagram (low limit and high limit). A linear interpolation is assumed between the two regimes of cold and warm weathers.

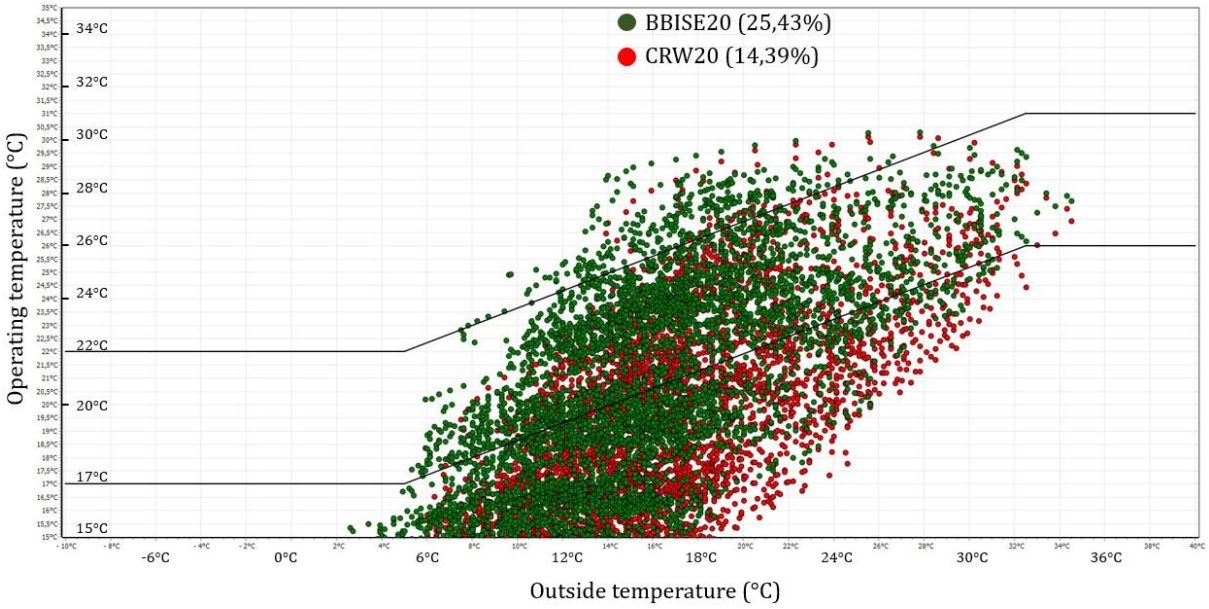

Figure 106 : *Brager zone of BBISE20 and CRW20.*

The Brager diagram gives an image of the evolution of the house operating (inside) temperature (weighted average between the temperatures of the ambient air and the room walls temperature) as a function of the outside temperature of the moment. The study is made for one year, 365 consecutive days, each point represents a day (red for using CRW and green using BBISE). When the point is located between the two black lines, the comfort is normally assured. It

should be noted that this simulation was launched without putting any heating or cooling application.

Figure 106 shows the Brager zone of BBISE20 and CRW20. For 25.4% of all days for one year, BBISE20 provides thermal comfort while for CRW20 it is only 14.4%. This difference is due to the variation in thermal resistance between the two materials, especially since CRW20 is made of heavy concrete only, which has a very low thermal resistance, almost 0.11 (m^2.K/W), while the thermal resistance of BBISE20 is 1.02 (m^2.K/W).

It is also found that for both materials most of the temperature points are below the Brager zone, the insulation capacity of both materials being poor.

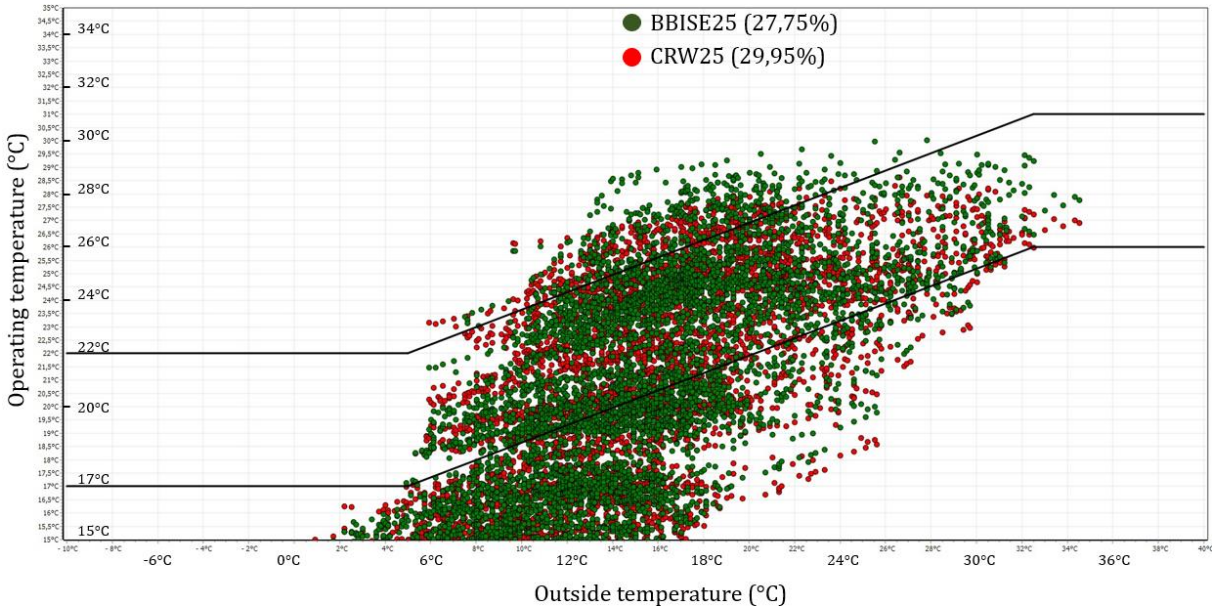

Figure 107 : *Brager zone of BBISE25 and CRW25.*

Looking at figure 107, it is found that the CRW thermal comfort percentage doubles with the 5 cm addition of rockwool to become 29.5% while for BBISE, it increases by 2% only to become 27.7% due to the increase of 5 cm in thickness. These results are expected, the CRW thermal resistance increases from 0.11 (m^2.K/W) without rockwool (CRW20) to 1.33 (m^2.K/W) by adding 5cm of rockwool (CRW25). For BBISE, the slight increase in thermal comfort percentage is due to the increase in thickness, keeping the same physical and thermal properties. In this case the thermal resistance is increased from 1.02 (m^2.K/W) with BBISE20 to 1.27 (m^2.K/W) with BBISE25.

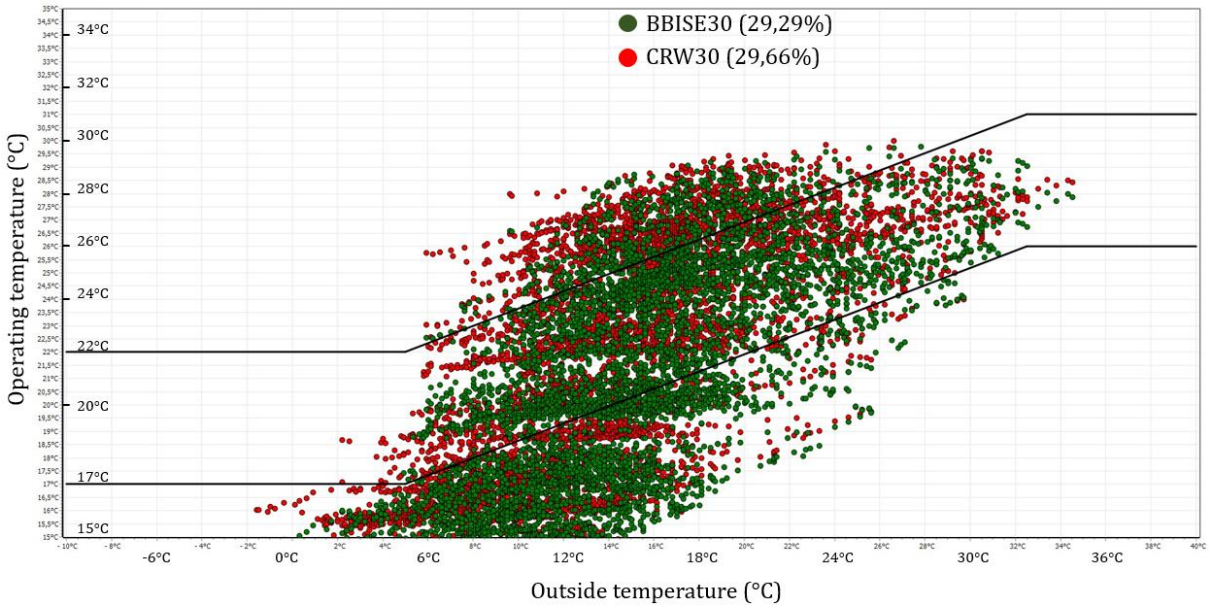

Figure 108 : *Brager zone of BBISE30 and CRW30.*

Comparing CRW25 and CRW30, it is found that the thermal comfort percentage did not increase by a large amount (0,16% only), compared to the increase observed between CRW20 and CRW25 when the first 5 cm of rockwool was added. In Figure 108, CRW30 makes the thermal comfort percentage reach 29.66%, while it was 29.5% in CRW25. On the contrary, for BBISE concretes thermal comfort increases almost linearly (2%), by adding 5 cm thickness to become 29.7%. The CRW30 thermal resistance is 2.55 (m^2.K/W) while this resistance is 1.52 (m^2.K/W) for BBISE. Despite the difference in thermal resistance between both materials, their thermal comfort percentage is similar, so is the distribution of temperature points.

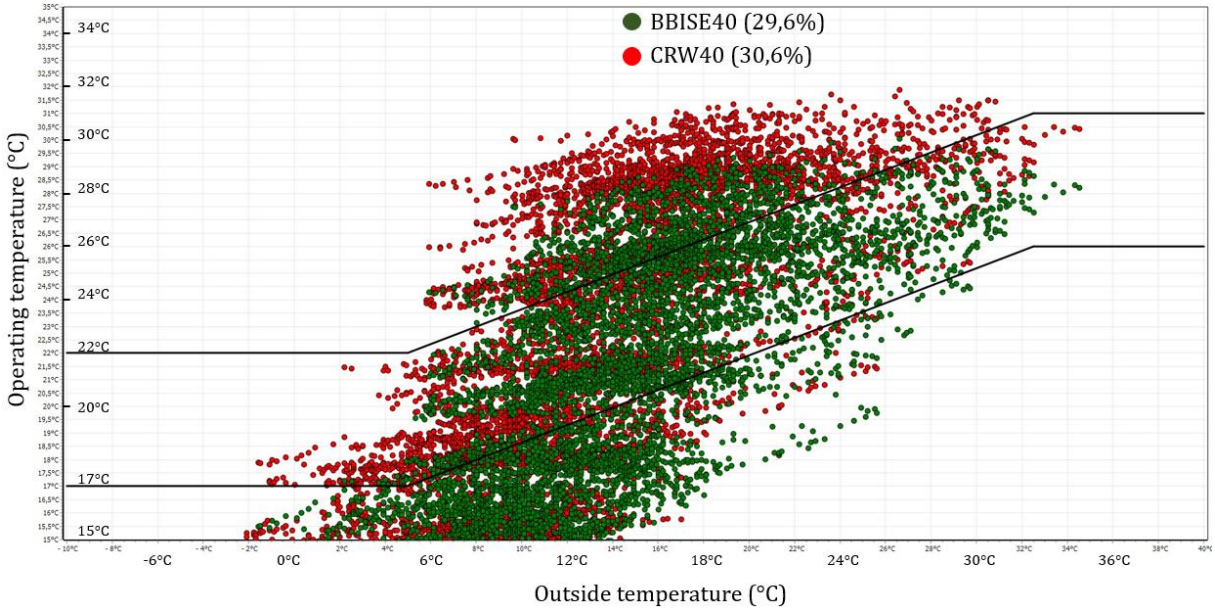

Figure 109 : *Brager zone of BBISE40 and CRW40.*

Further, with increasing the insulating material thickness (Figure 109), the CRW40 largest temperature points concentration is above the Brager zone (T > 22°C), while that of BBISE40 is concentrated below it. The CRW40 thermal resistance is 4.99 (m^2.K/W), 2.5 times larger than that of BBISE40 (2.03 (m^2.K/W)), so the ability to retain heat in the house using CRW40 is larger than using BBISE40. Despite this capacity, it is found that the thermal comfort percentage using CRW40 is 30% instead of 29.6% using BBISE40. These 2 percentages are almost similar, so using BBISE40 we will have the same thermal comfort without heating or cooling.

For a better comfort in the house, it is important to consider the hygrothermal comfort which is not only influenced by the thermal resistance and the outside temperature but also by the air humidity effect. Givoni has created a diagram from which we can study the comfort based on the temperature, the humidity and the air velocity.

5.5.2.1.2 Givoni diagram

Givoni's diagram makes it possible to plot comfort ranges on a psychrometric chart (Figure 110). In this diagram, the absolute humidity is the ordinate, the dry-air temperature on the abscissa and the relative humidity gives the functioning zone. This model for determining thermal comfort includes evapotranspiration and considers no gaz condensation. The Givoni diagram, established for a passive activity, defines, on the diagram of humid air, comfort zones corresponding to different ranges of air speed. In this study, the air speed is considered 0 m/s in all cases, this range corresponds to the classical comfort models (valid up to 0.20 m/s). So, the comfort zone is CZ presented in Figure 110.

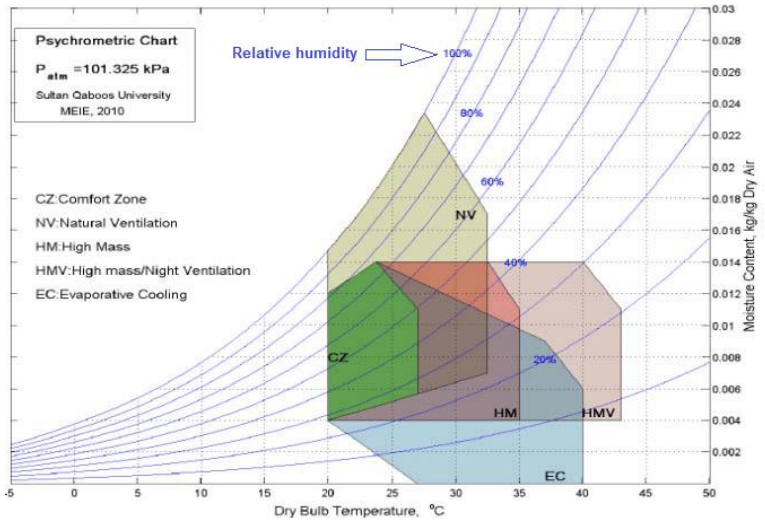

Figure 110 : *Givoni's diagram based on a psychrometric chart [214].*

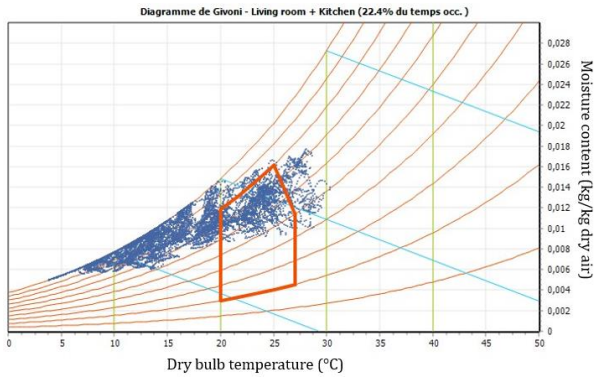

Figure 111 : *Givoni diagram using BBISE20.*

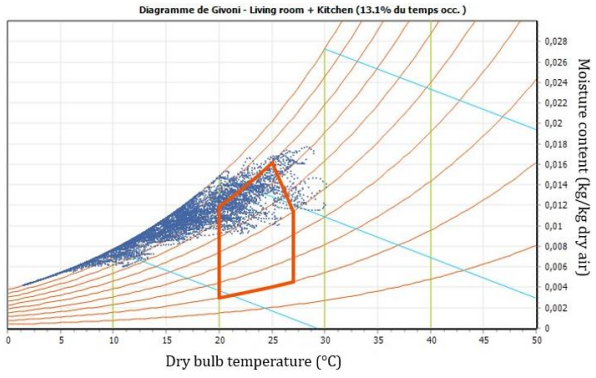

Figure 112 : *Givoni diagram using CRW20.*

Figures 111 and 112 show the BBISE20 and CRW20 Givoni diagram, respectively. At first sight, CRW20 and BBISE20 hygrothermal comfort percentages are close to the previous thermal comfort percentages obtained by the Brager zone, 22.4% and 13.1% for BBISE20 and CRW20 respectively. Also, using CRW20, it is found that there are points on the graph that represent temperatures reached 2°C with high relative humidity almost 100% (The orange curves in the figures 111 and 112 represents the relative humidity). Looking at the distribution of the points on the chart, the CRW20 relative humidity is larger than that of BBISE20, since foamed concrete and hemp concrete present a better water and vapor permeability than heavy concrete [98,215]. Having a high open porosity, BBISE has a particularity of being able to store and destock vapor within the material. Consequently, it contributes to stabilize the interior relative humidity of the space [215]. In addition, the vapor permeability (= diffusion openness) is an advantage of BBISE, since surface condensation can be avoided, which considerably increases the hygrothermal comfort.

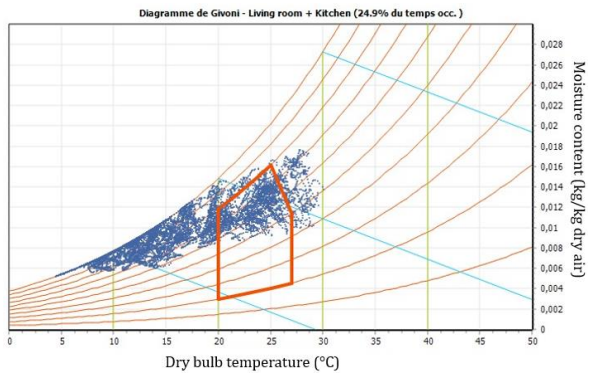

Figure 113 : *Givoni diagram using BBISE25.*

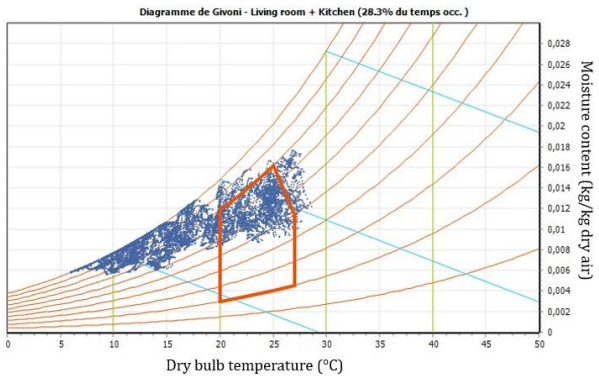

Figure 114 : *Givoni diagram using CRW25.*

Also looking at figures 113 and 114 it can be noticed that the comfort percentage doubles to become 28.3% by adding 5 cm of rockwool thickness, while by increasing the thickness of BBISE by 5 cm the thermal comfort percentage increases by 2.5% to become 24.9%. Looking at the

distribution of the points on the diagrams, we find that the relative humidity decreases on an average compared to Figures 111 and 112, and the inside temperature increases significantly for CRW25 and slightly for BBISE25, which is expected, especially since the thermal resistance is more increased for CRW25.

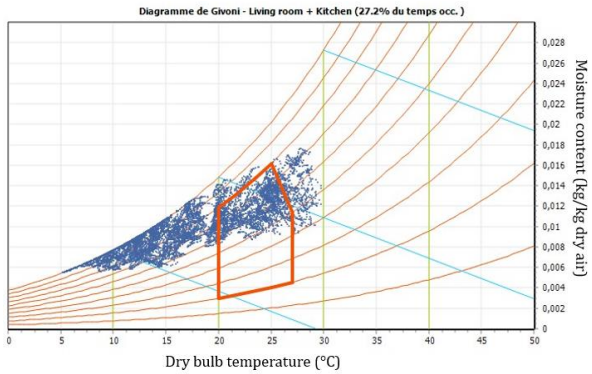

Figure 115 : *Givoni diagram using BBISE30.*

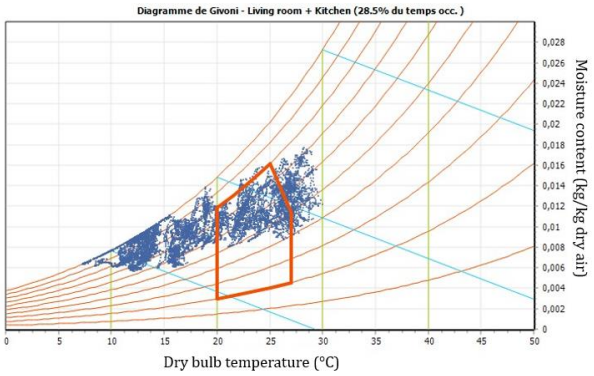

Figure 116 : *Givoni diagram using CRW30.*

Now, based on the diagram presented in Figure 115, the BBISE30 hygrothermal comfort percentage increases by 2.3% compared to the one obtained using BBISE25. With the addition of 5 cm thickness, the hygrothermal comfort increases linearly since this increase in thickness does not change neither the physical and hydric properties, nor the thermal conductivity. But comparing the CRW25 hygrothermal comfort percentage presented in Figure 114 and those of CRW30 presented in Figure 116, it is found that the hygrothermal comfort percentage increases only by 0.2%, despite the addition of 5 cm of rockwool.

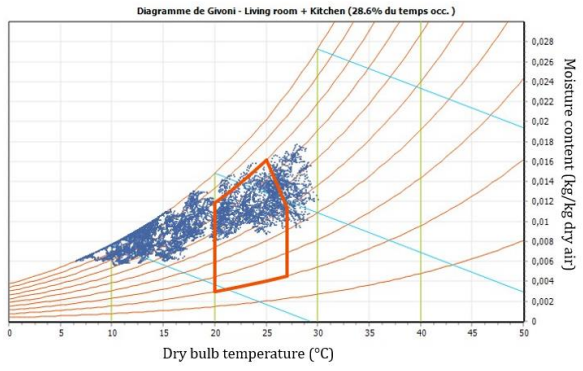

Figure 117 : *Givoni diagram using BBISE40.*

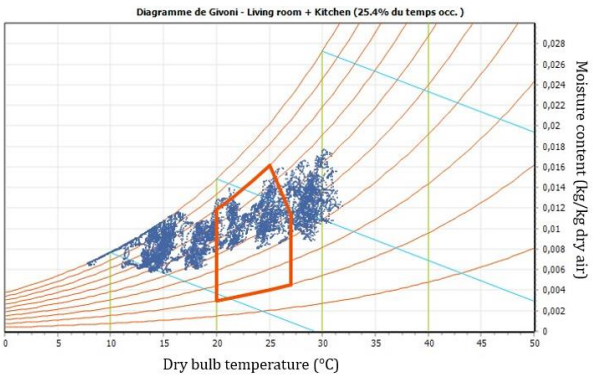

Figure 118 : *Givoni diagram using CRW40.*

In Figure 117, it is noted that the BBISE40 thermal comfort percentage is 28.6%. This percentage increases by 1.6% compared to CRW30, so the hygrothermal comfort increases by increasing the thickness almost linearly. Figure 118 shows Givoni diagram of CRW40 which presents a high thermal insulation with a thermal resistance of 4.99 (m^2.K/W). But the hygrothermal comfort

percentage decreases to 25.4% since the points distribution becomes more concentrated for higher temperatures at 27°C to reach in some cases 31°C. So, this thermal insulation could have a negative effect on the hygrothermal comfort, especially in summer.

Looking at the relative humidity, it is seen that it becomes more comfortable by increasing the BBISE thickness and by adding rock wool. Most of the points represent humidity between 40% and 80%, which is in the comfort zone (from 20% to 80%).

5.5.2.2 Heating and cooling.

To improve the thermal comfort in a building, it is important to apply heating and cooling. For this reason, it is interesting to simulate the energy consumption by heating and cooling in order to know the capacity of our material to reduce the energy consumption by comparison with the CRW which is already used in the market. For heating and cooling, 2 standard scenarios are used during this simulation.

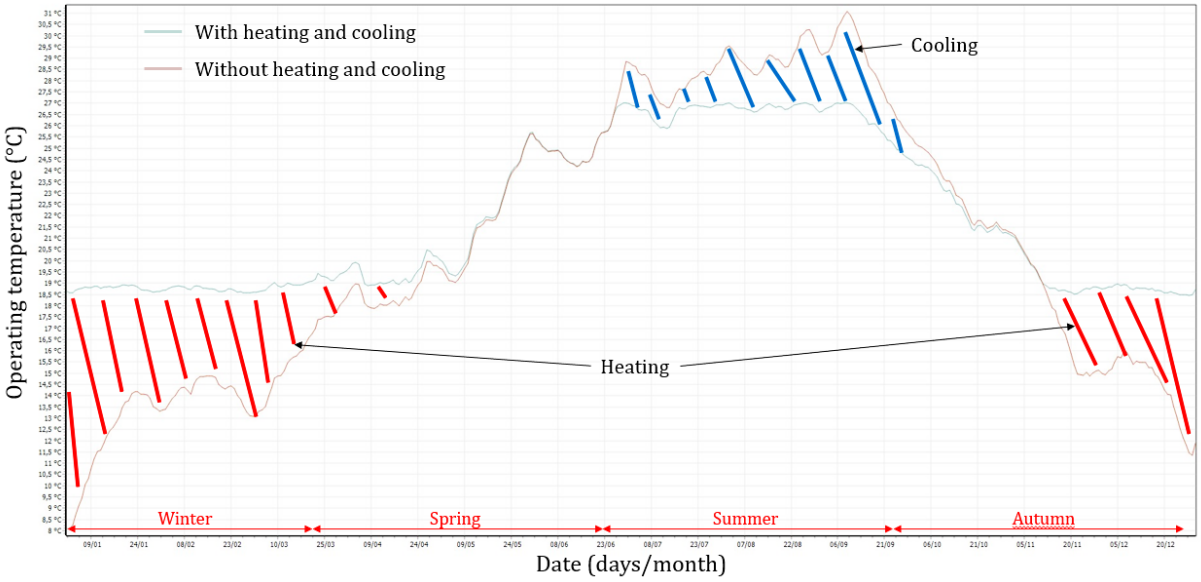

Figure 119 : *Operating temperature distribution in one year using CRW40, with and without heating and cooling.*

Based on standard scenarios given by the Pleiades, the cooling scenario consists of maintaining the inside temperature under 27°C during the 24 hours. While for heating, the scenario consists in keeping a constant temperature for a specific time. In this case, 2 initial time intervals are applied in 24h, one keeping the temperature above 15°C and the other above 19°C, these intervals are used in the standard scenario in a single day (24h):

- 15°C : from 21h to 6h.
- 19°C : from 6h to 21h.

Figures 119 and 120 show the operating temperatures distribution over a year with and without heating and cooling, using CRW20 and BBISE40 to observe the effect of material used on energy consumption for heating and cooling.

Figure 119 represents the temperatures of each day in one year inside the house using CRW40. The only parameter applied in this figure is the heating and cooling application. Moreover, there is a difference in temperature between the two graphs in most of the year except in the May-June months (In spring), and in the late October - early November period (In autumn). In these periods the two graphs are merging so there is no heating or cooling. In the other months, the difference hatched in red designates the heating period and in blue the cooling period. It can be noticed that the heating areas are larger than the cooling areas, which is normal behavior for the weather in Normandy, rather cold most of the year.

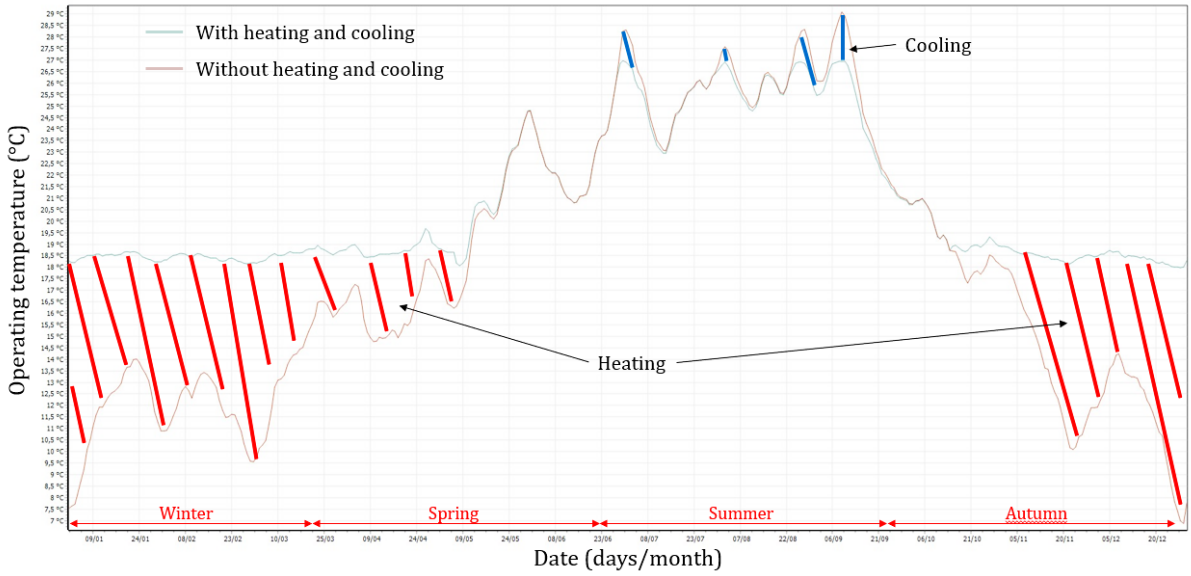

Figure 120 :*Distribution of temperature in one year using BBISE40, with and without heating and cooling.*

Looking at figure 120, using the BBISE, neither heating nor cooling is needed from mid-May to mid-October except for almost 3 non-consecutive weeks during the summer.

Moreover, it is noticed that the area hatched in red in figure 119 is smaller than the one hatched in figure 120. Consequently, using CRW40, the house needs less heating energy than using BBISE40. But for cooling, the opposite was found. BBISE40 in summer provides a thermal comfort

more than CRW40, because the area difference between the 2 graphs is smaller with BBISE40, so the need for cooling is more limited.

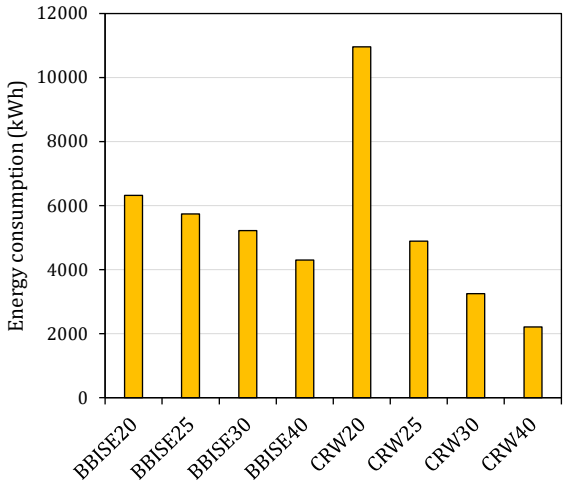

Figure 121 :*Heating energy consumption of all materials*

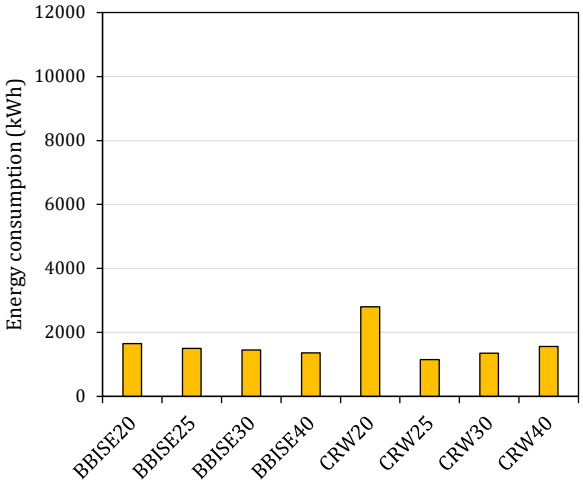

Figure 122 : *Cooling energy consumption of all materials*

Indeed, in figure 121, heating energy consumption in kWh for all materials (CRW and BBISE) are shown. CRW20, which is composed only of heavy concrete without the rockwool addition, consumes a huge energy for heating, almost 11000 kWh for one full year, this energy decreasing by one half by adding 5 cm of rockwool to become nearly 4900 kWh. By adding another 5 cm of rockwool, this energy is reduced by another third. Looking at the energy consumption of CRW25, CRW30 and CRW40, it is found that this energy decreases linearly by 33% with the 5cm rockwool addition each time.

In the case of BBISE the energy consumption decreases by 10% linearly with 5 cm of thickness increments.

By fixing the thickness, BBISE concretes consume more energy for heating than CRWs, the difference in energy consumption between BBISE concretes and CRW materials starts with a difference of 15% for CRW25 against BBISE25. This difference continues to increase to 36% for CRW30, where CRW40 consumes half of the energy compared to BBISE40. This is due to the thermal resistance of CRW which rises significantly by adding each time 5 cm of rockwool (which has a thermal conductivity λ = 0.025 W/(m.K)) compared to adding 5 cm of BBISE which has a thermal conductivity λ = 0.179 W/(m.K). Also, by looking at the Brager diagrams, it is seen that the temperature concentration of BBISE is below the Brager zone.

Cooling is concentrated to maintain the temperature below 27°C, this operation is mainly applied in summer. Figure 122 shows that as for heating CRW20 consumes the largest energy, around 2800 kWh. The addition of 5 cm of rockwool decreases the energy consumption for cooling by 3. But unlike heating, adding another 5 cm of rockwool increases the energy consumption, since heat is kept inside, which increases the operating temperature. For this reason, the temperatures in Figures 114, 116 and 118 using CRW, sometimes reach 31°C. While for BBISE, it decreases 10% linearly with the increase of the thickness, this decrease is the same of those for heating.

5.6 CONCLUSION

At the beginning, to improve waterproofing of the foamed concretes selected by the evaluation, two water repellents were used, one in mass and the other on surface. Surface water repellents reduce water absorption and make the BFCs waterproofness without effect on their other properties. Mass water repellents reduce water absorption of BFCs more than the surface water repellent and make them waterproof, but it changes the BFCs properties by decreasing porosity, increasing density, mechanical strength and decreasing thermal conductivity.

Finally, a thermal simulation using Pleiades is investigated. BBISE which is composed of C65P30H5DM and C55P30H15PM with all the thicknesses studied (20, 25, 30 and 40 cm) thermal and hygrothermal comfort percentages are very close to those of the heavy concretes and rockwool assembly (called CRW) which is often used in insulation. In terms of energy consumption, at 40 cm thickness BBISE40 reduces the cooling energy consumption but it has almost double the heating energy consumption compared to CRW40.

Overall conclusion and perspectives

In many European countries, including France, the building sector is the largest energy consumer and the second largest gases emitter, including CO_2. Therefore, energy and environmental regulations are applied to reduce the environmental impact of this sector, including RT2012 and RE2020. In our study, we are interested in the development of biobased, insulating, semi-structured and waterproof materials to reduce the environmental impact of the building sector. For this reason, we decided to work on this subject

In the first part of this thesis, the bibliographical study starts by the definition of the light concrete which is considered as excellent thermal insulators. Among the types of lightweight concretes studied, foamed concretes are considered the most economical and ecological because they cure without autoclave in the open air and the incorporating air bubbles process in the cement paste is low energy consuming. Foamed concrete is a very sensitive material at young age, and it needs specific technics during production to avoid deflation of foam, usually it is produced using two methods: by preformed foaming and by direct mixing. In addition, besides cement, pozzolanic additions are often used in foam concrete formulations. Moreover, it is also found that the hemp shiv incorporation makes the concrete lightweight, low carbon emission, excellent moisture buffering, low thermal conductivity and acoustic insulation, which can reduce energy consumption and gas emissions of buildings.

In this context, different performance objectives are chosen. Two types of foam concrete incorporating hemp shiv are sought. The first is used as a self-supporting material with a minimum compressive strength of 2 MPa. In order to be considered as an insulating material, a maximum thermal conductivity of 0.2 W/(m.K) is set. Moreover, in order to participate in the preservation of raw material resources and to facilitate the implementation on site, these mineral foams must be light, so a maximum density of 800 kg/m^3 is fixed. The second cellular concrete must be structural with a minimum compressive strength of 17 MPa. In addition, since moisture and high water absorption rate have a negative effect on the foamed concrete insulation, the capillary water absorption coefficient of both foam concretes must be less than 0.1 kg/(m^2.√h).

The study started with preliminary studies of bio-based foamed concrete using only the preformed method, replacing 30 wt% of cement by pozzolans (10% metakaolin and 20% Ground Granulated Blast Furnace Slags) and then replacing different cement amounts (5, 10 and 15 wt%) by hemp shiv. It is found that a high cement amount increases thermal conductivity and CO_2 emissions, so cement substitutions with pozzolanic additives and/or hemp shiv can improve thermal insulating performance. In addition, hemp shiv decreases density, compressive strength

and thermal conductivity. But the pozzolanic addition mixture improves the cementitious matrix cohesion in the hemp shiv absence and presence, in addition it reduces the CO_2 emissions.

Furthermore, the two phases of bio-based foam concrete are studied, the void part (porous structure) and the solid part (cementitious matrix). Moreover, two production methods are used, the preformed method and the direct method. The void part studies concern the pozzolanic additions, hemp shiv and the production method influence on the physical properties, absolute and apparent density, water accessible and total porosity, and air bubble distribution. Hemp shiv have been shown to increase the water-accessible and total porosity and thus decrease the bulk density. In addition, it increases the air bubble radius, which decreases uniformity. In addition, the cement amount and pozzolanic additions improves slightly the air bubbles uniformity, which increases the mechanical strength, especially at 28 days. In addition, the production method plays an important role in the air bubbles formation, the preformed method is more effective in the foam formation for lightweight concrete with density less than 700 kg/m^3, but the direct method gives finer bubbles and a more uniform distribution.

The pozzolanic additives, hemp shiv amount, and production method effects are investigated on the solid part, by studying the hydration heat and mineralogy of bio-based foamed concrete using XRD and TGA. It is found that the hydration heat increases with the pozzolans addition, since it promotes further reactions, and decreases with increasing the hemp shiv amount, since hemp shiv have retarding effects on hydration. For the mineralogical study, it is found that the cement is not completely hydrated and by adding pozzolans, the portlandite amount decreases while the C-S-H and ettringite amount increase, which will improve the mechanical strength. It has also been found that hemp shiv affects the mineralogy by activating carbonation in the cement paste.

After investigating the different parts of biobased foam concrete, mechanical properties including compressive and flexural strength, water properties such as sorption-desorption isotherm and capillary absorption, and thermal conductivity are studied. It is found that compressive strength is increased when pozzolanic additives are used due to their ability to fill pores, but hemp shiv has a negative effect on mechanical strength since the lignocellulose degradation creates new pores in the cementitious matrix, increasing the porosity amount, and decreasing density and mechanical strength. The pozzolanic additives effect on thermal resistivity is negligible, while hemp shiv slightly reduces thermal conductivity because they increase the porosity amount. Regarding adsorption and capillary absorption, pozzolanic additives decrease them slightly, while hemp shiv has no effect on BFC adsorption at low and medium relative humidity, but they increase adsorption at high humidity.

Production methods affect mechanical properties since they significantly affect porosity. The direct method can favor structural mechanical strength (Rc > 17MPa) but it presents modest thermal conductivity (0.341 < λ < 0.573 W/(m.K)) compared to concrete produced by the preformed method (0.127 < λ < 0.186 W/(m.K)) which also presents self-supporting or semi-structural foamed concrete. In addition, for BFC adsorption, the direct method decreases the adsorption and capillary absorption more than the preformed method because the difference in porosity is too large, on average 70% for the preformed method and 35% for the direct method.

To improve the waterproofing of the foamed concrete selected by the evaluation, two water repellents were used, one in mass and the other on surface. Surface water repellents reduce water absorption without effect on their other properties but does not make the BFCs waterproof since capillary absorption coefficient is 0.19 kg/(m^2.√h) higher than 0.1 kg/(m^2.√h). The mass water repellent reduces the BFCs water absorption more than the surface water repellent and makes them waterproof, but it modifies the properties of BFCs by decreasing the porosity, which increases the density, the mechanical strength and decreases the thermal conductivity.

Thermal simulation using Pleiades is studied. A new sandwich material (BBISE) is created, composed of C65P30H5DM and C55P30H15PM. The thermal and hygrothermal comfort percentages are very close to those of the heavy concrete and rock wool assembly (called CRW) which is often used for insulation in low-energy buildings in France. In terms of energy consumption, BBISE reduces cooling energy consumption but at 40 cm thickness BBISE40 has almost double the heating energy consumption compared to CRW40. But the BBISE will be consistent with RT2012 with a thickness of 50 cm.

So, focusing on the global objective of creating a bio-based insulating and waterproof, structural and non-structural concrete. We succeeded in creating a non-autoclaved foam concrete that is partially biobased, lightweight (ρ = 714 kg/m^3), insulating (λ = 0.1371 W/(m.K)), semi-structural (Rc = 4.16 MPa), waterproof (w = 0.04 kg/(m^2.√h)) and with a low environmental impact (15% of the cement is replaced by hemp shiv and 30% of the cement is replaced by pozzolanic additions). In addition, a non-autoclaved foam concrete was created that is partially bio-based, lightweight (ρ = 1506 kg/m^3), structural (Rc = 27 MPa), four times more insulating than conventional concrete (λ = 0.55 W/(m.K)), waterproof (w = 0.01 kg/(m^2.√h)). BBISE sandwich concrete which is composed of these two previous BFCs, presents an insulating (λ = 0.1969 W/(m.K)) and waterproof concrete.

The list below allows to highlight a series of ideas for future research that will serve as a complement and improvement to the contributions already made in this work:

- It would be interesting to study the hemp shiv effect on the Bio-based foamed concrete rheology and fresh state properties, which may improve the foam stability and the air bubbles uniformity in the structure, thus increasing the mechanical strength.

- It seems important to study the shrinkage in biobased foamed concrete, especially since it is known that the shrinkage is one of the most important difficulty that crosses the foam concrete generally.

- The durability of the material is extremely critical, especially for foamed concrete incorporating plant materials such as hemp shiv. Moreover, it is necessary to look for solutions to improve the BFC durability.

- It is necessary to work to increase the hemp shiv amount in the BFC to become greater than 15%, also to replace the cement by another more ecological binder as the gypsum or clay-based cement.

- Geopolymer is often used in recent research, so by using chemical foam method, it is possible to create aerated geopolymer concrete.

- The porous structures study of the hemp shiv incorporated foam concrete in 3D using tomography 3D, which gives more accurate results.

- It is interesting to study the BBISE sandwich concrete performance and mechanical behavior.

- It seems important to use or create bio-based surfactants.

References

[1] Énergie dans les bâtiments, Ministère de la Transition écologique. (2020). https://www.ecologie.gouv.fr/energie-dans-batiments..

[2] K. Ramamurthy, E.K. Kunhanandan Nambiar, G. Indu Siva Ranjani, A classification of studies on properties of foam concrete, Cement and Concrete Composites. 31 (2009) 388–396. https://doi.org/10.1016/j.cemconcomp.2009.04.006.

[3] E.P. Kearsley, P.J. Wainwright, Porosity and permeability of foamed concrete, Cement and Concrete Research. 31 (2001) 805–812. https://doi.org/10.1016/S0008-8846(01)00490-2.

[4] N. Mohamad, W. Omar, R. Abdullah, Precast Lightweight Foamed Concrete Sandwich Panel (PLFP) Tested under Axial Load: Preliminary Results, Advanced Materials Research. 250–253 (2011) 1153–1162.

[5] X. Zhang, Q. Yang, Y. Shi, G. Zheng, Q. Li, H. Chen, X. Cheng, Effects of different control methods on the mechanical and thermal properties of ultra-light foamed concrete, Construction and Building Materials. 262 (2020) 120082. https://doi.org/10.1016/j.conbuildmat.2020.120082.

[6] N. Mohamad Ibrahim, R. che amat, N.L. Rahim, S. Sallehuddin, Performance of Lightweight Foamed Concrete With Replacement Of Concrete Sludge Aggregate As Coarse Aggregate, Advanced Materials Research. 689 (2013) 265–268. https://doi.org/10.4028/www.scientific.net/AMR.689.265.

[7] Y.H.M. Amran, N. Farzadnia, A.A. Abang Ali, Properties and applications of foamed concrete; a review, Construction and Building Materials. 101 (2015) 990–1005. https://doi.org/10.1016/j.conbuildmat.2015.10.112.

[8] Y.H. Mugahed Amran, R. Alyousef, H. Alabduljabbar, M.H.R. Khudhair, F. Hejazi, A. Alaskar, F. Alrshoudi, A. Siddika, Performance properties of structural fibred-foamed concrete, Results in Engineering. 5 (2020) 100092. https://doi.org/10.1016/j.rineng.2019.100092.

[9] H.S. Gökçe, D. Hatungimana, K. Ramyar, Effect of fly ash and silica fume on hardened properties of foam concrete, Construction and Building Materials. 194 (2019) 1–11. https://doi.org/10.1016/j.conbuildmat.2018.11.036.

[10] A. Short, W. Kinniburgh, Lightweight concrete, 3rd ed, Applied Science Publishers, London, 1978.

[11] C. Baux, C. Lanos, A. Phelipot-Mardelé, E. Gutierrez, Béton cellulaire à base d'éco-liants, (n.d.) 10.

[12] G. Samson, Synthèse et propriétés des mousses minérales, phdthesis, INSA de Rennes, 2015. https://tel.archives-ouvertes.fr/tel-01275900 (accessed November 30, 2020).

[13] L. Yang, Y. Yan, Z. Hu, Utilization of phosphogypsum for the preparation of non-autoclaved aerated concrete, Construction and Building Materials. 44 (2013) 600–606. https://doi.org/10.1016/j.conbuildmat.2013.03.070.

[14] Chart created using CES EduPack 2019, ANSYS Granta © 2020 Granta Design, (n.d.).

[15] E.K.K. Nambiar, K. Ramamurthy, Influence of filler type on the properties of foam concrete, Cement and Concrete Composites. 28 (2006) 475–480. https://doi.org/10.1016/j.cemconcomp.2005.12.001.

[16] D.K. Panesar, Cellular concrete properties and the effect of synthetic and protein foaming agents, Construction and Building Materials. 44 (2013) 575–584. https://doi.org/10.1016/j.conbuildmat.2013.03.024.

[17] P.J. Tikalsky, J. Pospisil, W. MacDonald, A method for assessment of the freeze–thaw resistance of preformed foam cellular concrete, Cement and Concrete Research. 34 (2004) 889–893. https://doi.org/10.1016/j.cemconres.2003.11.005.

[18] C. Sun, Y. Zhu, J. Guo, Y. Zhang, G. Sun, Effects of foaming agent type on the workability, drying shrinkage, frost resistance and pore distribution of foamed concrete, Construction

and Building Materials. 186 (2018) 833–839. https://doi.org/10.1016/j.conbuildmat.2018.08.019.
[19] F. Zhao, J. Liu, Q. Li, H. Li, Study of Foamed Concrete from Activated Ash/Slag Blended Cement, Advanced Materials Research. 160–162 (2010) 821–826. https://doi.org/10.4028/www.scientific.net/AMR.160-162.821.
[20] X. Huang, T. Gao, X. Pan, D. Wei, C. Lv, L. Qin, Y. Huang, A Review: Feasibility of Hydrogen Generation from the Reaction Between Aluminum and Water for Fuel Cell Applications, Journal of Power Sources. 229 (2013) 133–140. https://doi.org/10.1016/j.jpowsour.2012.12.016.
[21] A.V. Ilyukhina, A.S. Ilyukhin, E.I. Shkolnikov, Hydrogen generation from water by means of activated aluminum, International Journal of Hydrogen Energy. 37 (2012) 16382–16387. https://doi.org/10.1016/j.ijhydene.2012.02.175.
[22] A. Laukaitis, B. Fiks, Acoustical properties of aerated autoclaved concrete, Applied Acoustics. 67 (2006) 284–296. https://doi.org/10.1016/j.apacoust.2005.07.003.
[23] E.P. Kearsley, M. Visagie, Micro-properties of Foamed Concrete, Specialist Techniques and Materials for Construction,. (1999) 173–184.
[24] British Cement Association, Foamed Concrete, Composition and Properties, (1994).
[25] T.-H. Wee, D.S. Babu, T. Tamilselvan, H.-S. Lim, Air-void system of foamed concrete and its effect on mechanical properties, ACI Materials Journal. 103 (2006) 45–52.
[26] K. RUIWEN, Properties of high-strength foam concrete, Thesis, 2004. https://scholarbank.nus.edu.sg/handle/10635/27683 (accessed April 27, 2021).
[27] E.K.K. Nambiar, K. Ramamurthy, Air-void characterisation of foam concrete, Cement and Concrete Research. 37 (2007) 221–230. https://doi.org/10.1016/j.cemconres.2006.10.009.
[28] Z. Zhang, J.L. Provis, A. Reid, H. Wang, Geopolymer foam concrete: An emerging material for sustainable construction, Construction and Building Materials. 56 (2014) 113–127. https://doi.org/10.1016/j.conbuildmat.2014.01.081.
[29] E.P. Kearsley, P.J. Wainwright, The effect of high fly ash content on the compressive strength of foamed concrete, Cement and Concrete Research. 31 (2001) 105–112. https://doi.org/10.1016/S0008-8846(00)00430-0.
[30] A. Fabien, N. Sebaibi, M. Boutouil, Effect of several parameters on non-autoclaved aerated concrete: use of recycling waste perlite, European Journal of Environmental and Civil Engineering. (2019) 1–18. https://doi.org/10.1080/19648189.2019.1647465.
[31] N. Sebaibi, F. Khadraoui-Mehir, S. Kourtaa, M. Boutouil, Optimization of non-autoclaved aerated insulating foam using bio-based materials, Construction and Building Materials. 262 (2020) 120822. https://doi.org/10.1016/j.conbuildmat.2020.120822.
[32] F. Alassaad, K. Touati, D. Levacher, N. Sebaibi, Impact of phase change materials on lightened earth hygroscopic, thermal and mechanical properties, Journal of Building Engineering. 41 (2021) 102417. https://doi.org/10.1016/j.jobe.2021.102417.
[33] A. Gholampour, T. Ozbakkaloglu, Performance of sustainable concretes containing very high volume Class-F fly ash and ground granulated blast furnace slag, Journal of Cleaner Production. 162 (2017) 1407–1417. https://doi.org/10.1016/j.jclepro.2017.06.087.
[34] M. Hafiz Ahmad, Durability Properties of Foamed Concrete with Fiber Inclusion, International Journal of Civil, Structural, Construction and Architectural Engineering. 8 (2014) 269–272.
[35] R.F. Zollo, C.D. Hays, Engineering material properties of a fiber reinforced cellular concrete (FRCC), ACI Materials Journal. 5 (1998).
[36] R.C. Valore, Jr, Cellular Concretes Part 1 Composition and Methods of Preparation, JP. 50 (1954) 773–796. https://doi.org/10.14359/11794.
[37] A. Klemm, D. Wiggins, 12 - Sustainability of natural stone as a construction material, in: J.M. Khatib (Ed.), Sustainability of Construction Materials (Second Edition), Woodhead Publishing, 2016: pp. 283–308. https://doi.org/10.1016/B978-0-08-100370-1.00012-3.

[38] T. McGrath, S. Nanukuttan, P.A.M. Basheer, A. Long, K. Owens, W. Doherty, Embodied energy and carbon footprinting of concrete production and use, Proceedings of the 3rd International Conference on the Durability of Concrete Structures, ICDCS 2012. (2012).
[39] J. Wu, Z. Zhang, Y. Zhang, D. Li, Preparation and characterization of ultra-lightweight foamed geopolymer (UFG) based on fly ash-metakaolin blends, Construction and Building Materials. 168 (2018) 771–779. https://doi.org/10.1016/j.conbuildmat.2018.02.097.
[40] H. Fujiwara, E. Sawada, Y. Ishikawa, Manufacture of High-Strength Aerated Concrete Containing Silica Fume, SP. 153 (1995) 779–794. https://doi.org/10.14359/1141.
[41] T. Kamaya, M. Uchida, M. Tsutsumi, Production of lightweight and high strength foamed concrete product, JP Patent No. 08-283080. (1996).
[42] T. Tian, Y. Yan, Z. Hu, Y. Xu, Y. Chen, J. Shi, Utilization of original phosphogypsum for the preparation of foam concrete, Construction and Building Materials. 115 (2016) 143–152. https://doi.org/10.1016/j.conbuildmat.2016.04.028.
[43] I.T. Koudriashoff, Manufacture of Reinforced Foam Concrete Roof Slabs, JP. 46 (1949) 37–48. https://doi.org/10.14359/12042.
[44] K.J. Byun, H.W. Song, Development of structural lightweight foamed concrete using polymer foam agent, Congres Polymer Concrete. 19 (1998).
[45] E. Nambiar, R. K, Fresh State Characteristics of Foam Concrete, Journal of Materials in Civil Engineering - J MATER CIVIL ENG. 20 (2008). https://doi.org/10.1061/(ASCE)0899-1561(2008)20:2(111).
[46] K. Ramamurthy, N. Narayanan, Influence of composition and curing on drying shrinkage of aerated concrete, Mat. Struct. 33 (2000) 243–250. https://doi.org/10.1007/BF02479334.
[47] T. Sanada, A. Sato, M. Shirota, M. Watanabe, Motion and coalescence of a pair of bubbles rising side by side, Chemical Engineering Science. 64 (2009) 2659–2671. https://doi.org/10.1016/j.ces.2009.02.042.
[48] A. Saint-Jalmes, Physical chemistry in foam drainage and coarsening, Soft Matter. 2 (2006) 836–849. https://doi.org/10.1039/B606780H.
[49] G. McGovern, Manufacture and supply of ready-mix foamed concrete, One Day Awareness Seminar on Foamed Concrete Properties, Applications and Potential. 294 (2000).
[50] D. Aldridge, Introduction to foamed concrete: what, why, how?, in: Use of Foamed Concrete in Construction, Thomas Telford Publishing, 2005: pp. 1–14. https://doi.org/10.1680/uofcic.34068.0001.
[51] N. Narayanan, K. Ramamurthy, Structure and properties of aerated concrete: a review, Cement and Concrete Composites. 22 (2000) 321–329. https://doi.org/10.1016/S0958-9465(00)00016-0.
[52] R.F. Zollo, C.D. Hays, Engineering Material Properties of a Fiber Reinforced Cellular Concrete (FRCC), MJ. 95 (1998) 631–635. https://doi.org/10.14359/405.
[53] E. Nambiar, R. K, Shrinkage Behavior of Foam Concrete, Journal of Materials in Civil Engineering - J MATER CIVIL ENG. 21 (2009). https://doi.org/10.1061/(ASCE)0899-1561(2009)21:11(631).
[54] K.C. Brady, G.R.A. Watts, I.R. Jones, K.C. Brady, G.R.A. Watts, M.R. Jones, Specification for Foamed Concrete, n.d.
[55] M.R. Jones, A. McCarthy, Behaviour and assessment of foamed concrete for construction applications, in: Use of Foamed Concrete in Construction, Thomas Telford Publishing, 2005: pp. 61–88. https://doi.org/10.1680/uofcic.34068.0008.
[56] W.A. Thanoon, M.S. Jaafar, M.R. Abdul Kadir, A.A. Abang Ali, D.N. Trikha, A.M.S. Najm, Development of an innovative interlocking load bearing hollow block system in Malaysia, Construction and Building Materials. 18 (2004) 445–454. https://doi.org/10.1016/j.conbuildmat.2004.03.013.
[57] W. Zhen, L. Ning, Experimental Research on Properties of High-Strength Foamed Concrete, Journal of Materials in Civil Engineering. 24 (2012) 113–118. https://doi.org/10.1061/(ASCE)MT.1943-5533.0000353.
[58] F.C. McCormick, Rational proportioning of preformed foam cellular concrete, American Concrete Institute. 2 (1967) 104–110.

[59] A. Hilal, N. Thom, A. Dawson, Pore Structure and Permeation Characteristics of Foamed Concrete, Journal of Advanced Concrete Technology. 12 (2014) 535–544. https://doi.org/10.3151/jact.12.535.

[60] G. Samson, A. Phelipot-Mardelé, C. Lanos, Structure porale de mousses minérales, in: 33ème Rencontres Universitaires de Génie Civil - Entre Terre et Mer, Université de Pau et des Pays de l'Adour, Bayonne, France, 2015: pp. 1057–1066. https://hal.archives-ouvertes.fr/hal-01167751 (accessed April 26, 2021).

[61] E.P. Kearsley, P.J. Wainwright, The effect of porosity on the strength of foamed concrete, Cement and Concrete Research. 32 (2002) 233–239. https://doi.org/10.1016/S0008-8846(01)00665-2.

[62] M. Visagie, The effect of microstructure on the properties of foamed concrete, Dissertation, University of Pretoria, 2007. https://repository.up.ac.za/handle/2263/23075 (accessed July 10, 2020).

[63] P. Chindaprasirt, S. Rukzon, V. Sirivivatnanon, Resistance to chloride penetration of blended Portland cement mortar containing palm oil fuel ash, rice husk ash and fly ash, Construction and Building Materials. 22 (2008) 932–938. https://doi.org/10.1016/j.conbuildmat.2006.12.001.

[64] B.B. Sabir, S. Wild, M. O'Farrell, A water sorptivity test for martar and concrete, Mat. Struct. 31 (1998) 568. https://doi.org/10.1007/BF02481540.

[65] Y.U. Hongfa, S.U.N. Wei, M.A. Haiyan, Analysis of damage degradation parameters of concrete subjected to freezing-thawing cycles and chemical attack, Journal of Architectural Engineering. 4 (2011) 1–8.

[66] E. Kamada, Y. Koh, M. Tapata, Frost deterioration of cellular concrete, Third International Conference on the Durability of Building Materials and Components. 3 (1984) 372–382.

[67] W. Yan, Z. Wu, F. Niu, T. Wan, H. Zheng, Study on the service life prediction of freeze–thaw damaged concrete with high permeability and inorganic crystal waterproof agent additions based on ultrasonic velocity, Construction and Building Materials. 259 (2020) 120405. https://doi.org/10.1016/j.conbuildmat.2020.120405.

[68] M. Medeiros, P. Helene, Efficacy of surface hydrophobic agents in reducing water and chloride ion penetration in concrete, Mater Struct. 41 (2008) 59–71. https://doi.org/10.1617/s11527-006-9218-5.

[69] Z. Liu, W. Hansen, Effect of hydrophobic surface treatment on freeze-thaw durability of concrete, Cement and Concrete Composites. 69 (2016) 49–60. https://doi.org/10.1016/j.cemconcomp.2016.03.001.

[70] F. Tittarelli, G. Moriconi, The effect of silane-based hydrophobic admixture on corrosion of galvanized reinforcing steel in concrete, Corrosion Science. 52 (2010) 2958–2963. https://doi.org/10.1016/j.corsci.2010.05.008.

[71] C. Ma, B. Chen, Properties of foamed concrete containing water repellents, Construction and Building Materials. 123 (2016) 106–114. https://doi.org/10.1016/j.conbuildmat.2016.06.148.

[72] J.J. del Coz Díaz, F.P. Álvarez Rabanal, P.J. García Nieto, J. Domínguez Hernández, B. Rodríguez Soria, J.M. Pérez-Bella, Hygrothermal properties of lightweight concrete: Experiments and numerical fitting study, Construction and Building Materials. 40 (2013) 543–555. https://doi.org/10.1016/j.conbuildmat.2012.11.045.

[73] D. Falliano, D. De Domenico, G. Ricciardi, E. Gugliandolo, Compressive and flexural strength of fiber-reinforced foamed concrete: Effect of fiber content, curing conditions and dry density, Construction and Building Materials. 198 (2019) 479–493. https://doi.org/10.1016/j.conbuildmat.2018.11.197.

[74] G. Sang, Y. Zhu, G. Yang, H. Zhang, Preparation and characterization of high porosity cement-based foam material, Construction and Building Materials. 91 (2015) 133–137. https://doi.org/10.1016/j.conbuildmat.2015.05.032.

[75] P. Zhang, H. Shang, D. Hou, S. Guo, T. Zhao, The Effect of Water Repellent Surface Impregnation on Durability of Cement-Based Materials, Advances in Materials Science and Engineering. 2017 (2017) 1–9. https://doi.org/10.1155/2017/8260103.

[76] R. Wang, P. Gao, M. Tian, Y. Dai, Experimental study on mechanical and waterproof performance of lightweight foamed concrete mixed with crumb rubber, Construction and Building Materials. 209 (2019) 655–664. https://doi.org/10.1016/j.conbuildmat.2019.03.157.
[77] M. Mastali, P. Kinnunen, H. Isomoisio, M. Karhu, M. Illikainen, Mechanical and acoustic properties of fiber-reinforced alkali-activated slag foam concretes containing lightweight structural aggregates, Construction and Building Materials. 187 (2018) 371–381. https://doi.org/10.1016/j.conbuildmat.2018.07.228.
[78] N. Neithalath, J. Weiss, J. Olek, Acoustically Efficient Concretes Through Engineered Pore Structure, SP. 226 (2005) 135–152. https://doi.org/10.14359/14395.
[79] J. Vilches, M. Ramezani, T. Neitzert, Experimental investigation of the fire resistance of ultra lightweight foam concrete, International Journal of Advanced Engineering Applications. 5 (2012) 15–22.
[80] F.N. Leitch, The properties of aerated concrete in service, Proceedings of the Second International Conference on Lightweight Concretes. (1980).
[81] E. Kearsley, D. Mostert, The use of foamed concrete in refractories, Proceedings of the International Conference on the Use of Foamed Concrete in Construction. (2005) 89–96.
[82] I. Asadi, P. Shafigh, Z.F.B. Abu Hassan, N.B. Mahyuddin, Thermal conductivity of concrete – A review, Journal of Building Engineering. 20 (2018) 81–93. https://doi.org/10.1016/j.jobe.2018.07.002.
[83] F. Collet, S. Pretot, Thermal conductivity of hemp concretes: Variation with formulation, density and water content, Construction and Building Materials. 65 (2014) 612–619. https://doi.org/10.1016/j.conbuildmat.2014.05.039.
[84] A.M. Neville, Properties of Concrete, 5e édition, Pearson, Harlow, England ; New York, 2011.
[85] M. Rahim, O. Douzane, A.D. Tran Le, G. Promis, B. Laidoudi, A. Crigny, B. Dupre, T. Langlet, Characterization of flax lime and hemp lime concretes: Hygric properties and moisture buffer capacity, Energy and Buildings. 88 (2015) 91–99. https://doi.org/10.1016/j.enbuild.2014.11.043.
[86] F. Batool, M.M. Rafi, V. Bindiganavile, Microstructure and thermal conductivity of cement-based foam:A review, Journal of Building Engineering. 20 (2018) 696–704. https://doi.org/10.1016/j.jobe.2018.09.008.
[87] V. Cerezo, Propriétés mécaniques, thermiques et acoustiques d'un matériau à base de particules végétales : approche expérimentale et modélisation théorique, 2005.
[88] A. Evrard, Sorption behaviour of Lime-Hemp Concrete and its relation to indoor comfort and energy demand, in: 2006.
[89] F. Collet, M. Bart, L. Serres, J. Miriel, Porous structure and water vapour sorption of hemp-based materials, Construction and Building Materials. 22 (2008) 1271–1280. https://doi.org/10.1016/j.conbuildmat.2007.01.018.
[90] S. Elfordy, F. Lucas, F. Tancret, Y. Scudeller, L. Goudet, Mechanical and thermal properties of lime and hemp concrete ("hempcrete") manufactured by a projection process, Construction and Building Materials. 22 (2008) 2116–2123. https://doi.org/10.1016/j.conbuildmat.2007.07.016.
[91] Y. HUSTACHE, L. ARNAUD, Synthèse des connaissances sur les bétons et mortiers de chanvre - PDF Téléchargement Gratuit, (2008). https://docplayer.fr/53129567-Synthese-des-connaissances-sur-les-betons-et-mortiers-de-chanvre.html (accessed April 26, 2021).
[92] L. Yan, B. Kasal, L. Huang, A review of recent research on the use of cellulosic fibres, their fibre fabric reinforced cementitious, geo-polymer and polymer composites in civil engineering, Composites Part B: Engineering. 92 (2016) 94–132. https://doi.org/10.1016/j.compositesb.2016.02.002.
[93] S. Chafei, F. Khadraoui, M. BOUTOUIL, G. Moussa, Influence de différents traitements des fibres de lin sur les propriétés rhéologiques d'un mortier cimentaire incorporant ce renfort, in: 2014.
[94] L.W.G. Zhenhai, Experimental Investigation of Strength and Deformation of Concrete at Elevated Temperature, Journal of Building Engineering. 1 (1993).

[95] G.C. Davies, D.M. Bruce, Effect of Environmental Relative Humidity and Damage on the Tensile Properties of Flax and Nettle Fibers, Textile Research Journal. 68 (1998) 623–629. https://doi.org/10.1177/004051759806800901.
[96] http://www.technichanvre.com/informations/le-chanvre-culture-ecologique-et-durable/tige-de-chanvre-fraiche/
[97] https://flores-amo.fr/materiau-chanvre-lyon-paris/
[98] J. Chamoin, Optimisation des propriétés (physiques, mécaniques et hydriques) de bétons de chanvre par la maîtrise de la formulation, thesis, Rennes, INSA, 2013. http://www.theses.fr/2013ISAR0016 (accessed October 11, 2018).
[99] B. Mazhoud, Elaboration et caractérisation mécanique, hygrique et thermique de composites bio-sourcés, phdthesis, INSA de Rennes, 2017. https://tel.archives-ouvertes.fr/tel-01801946 (accessed March 1, 2021).
[100] G. Balčiūnas, J. Žvironaitė, S. Vėjelis, A. Jagniatinskis, S. Gaidučis, Ecological, thermal and acoustical insulating composite from hemp shives and sapropel binder, Industrial Crops and Products. 91 (2016) 286–294. https://doi.org/10.1016/j.indcrop.2016.06.034.
[101] M. Rahim, O. Douzane, A.D. Tran Le, T. Langlet, Effect of moisture and temperature on thermal properties of three bio-based materials, Construction and Building Materials. 111 (2016) 119–127. https://doi.org/10.1016/j.conbuildmat.2016.02.061.
[102] M. Viel, F. Collet, C. Lanos, Chemical and multi-physical characterization of agro-resources' by-product as a possible raw building material, Industrial Crops and Products. 120 (2018) 214–237. https://doi.org/10.1016/j.indcrop.2018.04.025.
[103] I. Couedel, Le béton de chanvre comme matériau de construction, première approche mécanique du béton de chanvre, Rapport de DEA. (1998).
[104] V.A. Alvarez, R.A. Ruscekaite, A. Vazquez, Mechanical Properties and Water Absorption Behavior of Composites Made from a Biodegradable Matrix and Alkaline-Treated Sisal Fibers, Journal of Composite Materials. 37 (2003) 1575–1588. https://doi.org/10.1177/0021998303035180.
[105] G. Delannoy, S. Marceau, P. Glé, E. Gourlay, M. Guéguen-Minerbe, D. Diafi, S. Amziane, F. Farcas, Impact of hemp shiv extractives on hydration of Portland cement, Construction and Building Materials. 244 (2020) 118300. https://doi.org/10.1016/j.conbuildmat.2020.118300.
[106] Y. Diquélou, E. Gourlay, L. Arnaud, B. Kurek, Impact of hemp shiv on cement setting and hardening: Influence of the extracted components from the aggregates and study of the interfaces with the inorganic matrix, Cement and Concrete Composites. 55 (2015) 112–121. https://doi.org/10.1016/j.cemconcomp.2014.09.004.
[107] L. Wang, H. Lenormand, H. Zmamou, N. Leblanc, Effect of variability of hemp shiv on the setting of lime hemp concrete, Industrial Crops and Products. 171 (2021) 113915. https://doi.org/10.1016/j.indcrop.2021.113915.
[108] G. Delannoy, Durabilité d'isolants à base de granulats végétaux, phdthesis, Université Paris-Est, 2018. https://tel.archives-ouvertes.fr/tel-02141189.
[109] V. Sabathier, S. Louvel, G. Correa, C. Magniont, P. Evon, L. Labonne, Incidence of the water soluble compounds contained into lavender and sunflower bioaggregates on the hardening process of mineral binders, 2nd International Conference Bio-Based Building Material, Clermont-Ferrand. (2017) 62–68.
[110] J. Page, M. BOUTOUIL, F. Khadraoui, G. Moussa, Etude des propriétés mécaniques d'un béton renforcé par des fibres de lin, in: 2015.
[111] K. Bilba, M.-A. Arsène, A. Ouensanga, Sugar cane bagasse fibre reinforced cement composites, Cement and Concrete Composites. 25 (2003) 91–96. https://doi.org/10.1016/S0958-9465(02)00003-3.
[112] P. Strandberg-de Bruijn, P. Johansson, Moisture transport properties of lime–hemp concrete determined over the complete moisture range, Biosystems Engineering. 122 (2014) 31–41. https://doi.org/10.1016/j.biosystemseng.2014.03.001.

[113] T.T. Nguyen, Contribution à l'étude de la formulation et du procédé de fabrication d'éléments de construction en béton de chanvre, phdthesis, Université de Bretagne Sud, 2010. https://doi.org/10/document.
[114] L. Arnaud, E. Gourlay, Experimental study of parameters influencing mechanical properties of hemp concretes, Construction and Building Materials. 28 (2012) 50–56. https://doi.org/10.1016/j.conbuildmat.2011.07.052.
[115] B. Seng, C. Magniont, S. Lorente, Characterization of a precast hemp concrete. Part I: Physical and thermal properties, Journal of Building Engineering. 24 (2019) 100540. https://doi.org/10.1016/j.jobe.2018.07.016.
[116] IUPAC, Reporting physisorption dat for gas/solid systems with special reference to the determination of surface area and porosity, Pure and Applied Chemistry. (1985) 603–619.
[117] H. Assaedi, T. Alomayri, F. Shaikh, I. Low, Characterisation of mechanical and thermal properties in flax fabric reinforced geopolymer composites, Journal of Advanced Ceramics. 4 (2015) 1–10. https://doi.org/10.1007/s40145-015-0161-1.
[118] K. Ghavami, Ultimate load behaviour of bamboo-reinforced lightweight concrete beams, Cement and Concrete Composites. 17 (1995) 281–288. https://doi.org/10.1016/0958-9465(95)00018-8.
[119] K. Bilba, M.-A. Arsene, Silane treatment of bagasse fiber for reinforcement of cementitious composites, Composites Part A: Applied Science and Manufacturing. 39 (2008) 1488–1495. https://doi.org/10.1016/j.compositesa.2008.05.013.
[120] F. Silva, R. Toledo Filho, J. Melo Filho, E. Fairbairn, Physical and mechanical properties of durable sisal fiber cement composites, Construction and Building Materials. 24 (2010). https://doi.org/10.1016/j.conbuildmat.2009.10.030.
[121] H. Savastano, P.G. Warden, R.S.P. Coutts, Ground iron blast furnace slag as a matrix for cellulose-cement materials, Cement and Concrete Composites. 4–5 (2001) 389–397. https://doi.org/10.1016/S0958-9465(00)00083-4.
[122] C. Juarez, A. Durán, P. Valdez, G. Fajardo San Miguel, Performance of "Agave lecheguilla" natural fiber in portland cement composites exposed to severe environment conditions, Building and Environment. 42 (2007) 1151–1157. https://doi.org/10.1016/j.buildenv.2005.12.005.
[123] L. Motta, V. John, V. Agopyan, ThermoMechanical Treatment to Improve Properties of Sisal Fibres for Composites, Materials Science Forum - MATER SCI FORUM. 636–637 (2010) 253–259. https://doi.org/10.4028/www.scientific.net/MSF.636-637.253.
[124] B. Barra, B. Paulo, C. Alves Junior, H. Jr, K. Ghavami, Effects of Methane Cold Plasma in Sisal Fibers, Key Engineering Materials. 517 (2012) 458–468. https://doi.org/10.4028/www.scientific.net/KEM.517.458.
[125] G.H.D. Tonoli, M.N. Belgacem, G. Siqueira, J. Bras, H. Savastano, F.A. Rocco Lahr, Processing and dimensional changes of cement based composites reinforced with surface-treated cellulose fibres, Cement and Concrete Composites. 37 (2013) 68–75. https://doi.org/10.1016/j.cemconcomp.2012.12.004.
[126] R.D.T. Filho, K. Scrivener, G. England, K. Ghavami, Durability of alkali-sensitive sisal and coconut fibres in cement mortar composites, Undefined. (2000). /paper/Durability-of-alkali-sensitive-sisal-and-coconut-in-Filho-Scrivener/182263688487dd263f6b4e79414e2f6fd67bf1b0 (accessed May 20, 2021).
[127] C. Knill, J. Kennedy, Degradation of Cellulose under Alkaline Conditions, Carbohydrate Polymers. 51 (2003) 281–300. https://doi.org/10.1016/S0144-8617(02)00183-2.
[128] A. Govin, A. Peschard, R. Guyonnet, Modification of cement hydration at early ages by natural and heated wood, Cement and Concrete Composites. 28 (2006) 12–20. https://doi.org/10.1016/j.cemconcomp.2005.09.002.
[129] A. Arizzi, H.A. Viles, G. Cultrone, I. Sánchez, Predicting the long-term durability of hemp–lime renders in inland and coastal areas using Mediterranean, Tropical and Semi-arid climatic simulations, Science of The Total Environment. 542 (2015) 757–770. https://doi.org/10.1016/j.scitotenv.2015.10.141.

[130] S. Marceau, P. Glé, M. Guéguen-Minerbe, E. Gourlay, S. Moscardelli, I. Nour, S. Amziane, Influence of accelerated aging on the properties of hemp concretes, Construction and Building Materials. 139 (2017) 524–530. https://doi.org/10.1016/j.conbuildmat.2016.11.129.
[131] C. Sentenac, M. Sonebi, S. Amziane, INVESTIGATION ON THE PERFORMANCE AND DURABILITY OF TREATED HEMP CONCRETE WITH WATER REPELLENT, in: M.S. Eds. Sofiane AMZIANE (Ed.), ICBBM 2017, 2nd International Conference On Bio-Based Building Materials, RILEM, Clermont Ferrand, France, 2017. https://hal.archives-ouvertes.fr/hal-01576193 (accessed April 27, 2021).
[132] R. Walker, S. Pavia, R. Mitchell, Mechanical properties and durability of hemp-lime concretes, Construction and Building Materials. 61 (2014) 340–348. https://doi.org/10.1016/j.conbuildmat.2014.02.065.
[133] E. Sassoni, S. Manzi, A. Motori, M. Montecchi, M. Canti, Experimental study on the physical–mechanical durability of innovative hemp-based composites for the building industry, Energy and Buildings. 104 (2015) 316–322. https://doi.org/10.1016/j.enbuild.2015.07.022.
[134] V. Nozahic, S. Amziane, G. Torrent, K. Saïdi, H. De Baynast, Design of green concrete made of plant-derived aggregates and a pumice–lime binder, Cement and Concrete Composites. 34 (2012) 231–241. https://doi.org/10.1016/j.cemconcomp.2011.09.002.
[135] J. Wei, C. Meyer, Degradation mechanisms of natural fiber in the matrix of cement composites, Cement and Concrete Research. 73 (2015) 1–16. https://doi.org/10.1016/j.cemconres.2015.02.019.
[136] M. Chabannes, E. Garcia-Diaz, L. Clerc, J.-C. Benezet, Studying the hardening and mechanical performances of rice husk and hemp-based building materials cured under natural and accelerated carbonation, Construction and Building Materials. 94 (2015) 105–115. https://doi.org/10.1016/j.conbuildmat.2015.06.032.
[137] S.C. Bhatia, 26 - Issues relating to biofuels, in: S.C. Bhatia (Ed.), Advanced Renewable Energy Systems, Woodhead Publishing India, 2014: pp. 688–718. https://doi.org/10.1016/B978-1-78242-269-3.50026-7.
[138] N. Scarlat, J.-F. Dallemand, Chapter Ten - Future Role of Bioenergy, in: C. Lago, N. Caldés, Y. Lechón (Eds.), The Role of Bioenergy in the Bioeconomy, Academic Press, 2019: pp. 435–547. https://doi.org/10.1016/B978-0-12-813056-8.00010-8.
[139] N.A.Z. Abidin, A.H.A. Ghani, H. Mohammad, Identifying the Environmental Strategies in Construction Site for Malaysian Contractors in Johor, IOP Conf. Ser.: Earth Environ. Sci. 498 (2020) 012108. https://doi.org/10.1088/1755-1315/498/1/012108.
[140] C. De Lucia, Sustainability assessment of gasification processes for synthetic liquid fuel production, in: Gasification for Synthetic Fuel Production, Elsevier, 2015: pp. 73–100. https://doi.org/10.1016/B978-0-85709-802-3.00004-7.
[141] MCS, Résultats des analyses du contrôle sanitaire des eaux destinées à la consommation humaine, (2017).
[142] M.R. Jones, A. McCarthy, Preliminary views on the potential of foamed concrete as a structural material, Magazine of Concrete Research. 57 (2005) 21–31. https://doi.org/10.1680/macr.2005.57.1.21.
[143] AFNOR NF EN 934-5, Adjuvants pour bétons, mortier et coulis, (2012).
[144] F. Jacquemot, Développement d'une gamme de Béton Ultra Léger : THERMOLITYS®, (2015).
[145] Y. Diquélou, E. Gourlay, L. Arnaud, B. Kurek, Influence of binder characteristics on the setting and hardening of hemp lightweight concrete, Construction and Building Materials. 112 (2016) 506–517. https://doi.org/10.1016/j.conbuildmat.2016.02.138.
[146] S. Amziane, F. Collet, M. Lawrence, C. Magniont, V. Picandet, M. Sonebi, Recommendation of the RILEM TC 236-BBM: characterisation testing of hemp shiv to determine the initial water content, water absorption, dry density, particle size distribution and thermal conductivity, Materials and Structures. 50 (2017). https://doi.org/10.1617/s11527-017-1029-3.

[147] T.M. Dinh, Contribution au développement de béton de chanvre préfabriqué utilisant un liant pouzzolanique innovant, phd, Université de Toulouse, Université Toulouse III - Paul Sabatier, 2014. http://thesesups.ups-tlse.fr/2383/ (accessed November 25, 2020).
[148] V. Picandet, P. Tronet, C. Baley, Caractérisation granulométrique des chènevottes, in: 2012.
[149] S. Assié, Durabilité des bétons auto-plaçants, These de doctorat, Toulouse, INSA, 2004. http://www.theses.fr/2004ISAT0024.
[150] P.-C. Aïtcin, 4 - Supplementary cementitious materials and blended cements, in: P.-C. Aïtcin, R.J. Flatt (Eds.), Science and Technology of Concrete Admixtures, Woodhead Publishing, 2016: pp. 53–73. https://doi.org/10.1016/B978-0-08-100693-1.00004-7.
[151] E. Kearsley, D. Mostert, Designing mix composition of foamed concrete with high fly ash contents, Proceedings of the International Conference on the Use of Foamed Concrete in Construction. (2005) 29–36.
[152] J. Page, S. Amziane, M. Sonebi, Effet d'un adjuvant viscosant sur les propriétés du béton de chanvre, in: 2015.
[153] K. Ezziane, A. Bougara, A. Kadri, H. Khelafi, E. Kadri, Compressive strength of mortar containing natural pozzolan under various curing temperature, Cement and Concrete Composites. 29 (2007) 587–593. https://doi.org/10.1016/j.cemconcomp.2007.03.002.
[154] A. Kriker, G. Debicki, A. Bali, M.M. Khenfer, M. Chabannet, Mechanical properties of date palm fibres and concrete reinforced with date palm fibres in hot-dry climate, Cement and Concrete Composites. 27 (2005) 554–564. https://doi.org/10.1016/j.cemconcomp.2004.09.015.
[155] C. Sawsen, K. Fouzia, B. Mohamed, G. Moussa, Optimizing the formulation of flax fiber-reinforced cement composites, Construction and Building Materials. 54 (2014) 659–664. https://doi.org/10.1016/j.conbuildmat.2013.12.038.
[156] N.A. Mohd Nasir, M.J. McCarthy, Effect of Metakaolin on early Strength of GGBS Ternary Concrete, Applied Mechanics and Materials. 584–586 (2014) 1551–1557. https://doi.org/10.4028/www.scientific.net/AMM.584-586.1551.
[157] J. Williams, M. Lawrence, P. Walker, The influence of constituents on the properties of the bio-aggregate composite hemp-lime, Construction and Building Materials. 159 (2018) 9–17. https://doi.org/10.1016/j.conbuildmat.2017.10.109.
[158] E. Namsone, G. Šahmenko, A. Korjakins, Durability Properties of High Performance Foamed Concrete, Procedia Engineering. 172 (2017) 760–767. https://doi.org/10.1016/j.proeng.2017.02.120.
[159] A. Hamad, Materials, Production, Properties and Application of Aerated Lightweight Concrete: Review, International Journal of Materials Science and Engineering. 2 (2014). https://doi.org/10.12720/ijmse.2.2.152-157.
[160] T. Li, F. Huang, J. Zhu, J. Tang, J. Liu, Effect of foaming gas and cement type on the thermal conductivity of foamed concrete, Construction and Building Materials. 231 (2020) 117197. https://doi.org/10.1016/j.conbuildmat.2019.117197.
[161] A. Alsalman, L.N. Assi, R.S. Kareem, K. Carter, P. Ziehl, Energy and CO2 emission assessments of alkali-activated concrete and Ordinary Portland Cement concrete: A comparative analysis of different grades of concrete, Cleaner Environmental Systems. 3 (2021) 100047. https://doi.org/10.1016/j.cesys.2021.100047.
[162] A. Hasanbeigi, L. Price, E. Lin, Emerging energy-efficiency and CO2 emission-reduction technologies for cement and concrete production: A technical review, Renewable and Sustainable Energy Reviews. 16 (2012) 6220–6238. https://doi.org/10.1016/j.rser.2012.07.019.
[163] T. Hills, N. Florin, P.S. Fennell, Decarbonising the cement sector: A bottom-up model for optimising carbon capture application in the UK, Journal of Cleaner Production. 139 (2016) 1351–1361. https://doi.org/10.1016/j.jclepro.2016.08.129.
[164] A. Heath, K. Paine, M. McManus, Minimising the global warming potential of clay based geopolymers, Journal of Cleaner Production. 78 (2014) 75–83. https://doi.org/10.1016/j.jclepro.2014.04.046.

[165] N. Gowripalan, J.G. Cabrera, A.R. Cusens, P.J. Wainwright, Effect of curing on durability, Concrete International. 12 (1990) 47–54.
[166] Y. Jiang, M. Ansell, X. Jia, A. Hussain, M. Lawrence, Physical characterisation of hemp shiv: Cell wall structure and porosity, in: 2017.
[167] A.A. Hilal, N.H. Thom, A.R. Dawson, On void structure and strength of foamed concrete made without/with additives, Construction and Building Materials. 85 (2015) 157–164. https://doi.org/10.1016/j.conbuildmat.2015.03.093.
[168] F. Batool, V. Bindiganavile, Air-void size distribution of cement based foam and its effect on thermal conductivity, Construction and Building Materials. 149 (2017) 17–28. https://doi.org/10.1016/j.conbuildmat.2017.05.114.
[169] A.A. Hilal, N.H. Thom, A.R. Dawson, On entrained pore size distribution of foamed concrete, Construction and Building Materials. 75 (2015) 227–233. https://doi.org/10.1016/j.conbuildmat.2014.09.117.
[170] I. Al-Jumaily, Q. Kareem, N. Hilal, An overview on the Influence of Pozzolanic Materials on Properties of Concrete, 4 (2015) 81–92.
[171] J. Page, Formulation et caractérisation d'un composite cimentaire biofibré pour des procédés de construction préfabriquée, phdthesis, Normandie Université, 2017. https://tel.archives-ouvertes.fr/tel-01713160/document (accessed October 11, 2018).
[172] M.H. Zhang, V.M. Malhotra, Characteristics of a thermally activated alumino-silicate pozzolanic material and its use in concrete, Cement and Concrete Research. 25 (1995) 1713–1725. https://doi.org/10.1016/0008-8846(95)00167-0.
[173] P.S. de Silva, F.P. Glasser, Phase relations in the system CaO□Al2O3□SiO2□H2O relevant to metakaolin - calcium hydroxide hydration, Cement and Concrete Research. 23 (1993) 627–639. https://doi.org/10.1016/0008-8846(93)90014-Z.
[174] E. Gruyaert, Activation of Pozzolanic and Latent-Hydraulic Reactions by Alkalis in Order to Repair Concrete Cracks, J. Mater. Civ. Eng. (n.d.) 12.
[175] G. Balčiūnas, I. Pundienė, L. Lekūnaitė-Lukošiūnė, S. Vėjelis, A. Korjakins, Impact of hemp shives aggregate mineralization on physical–mechanical properties and structure of composite with cementitious binding material, Industrial Crops and Products. 77 (2015) 724–734. https://doi.org/10.1016/j.indcrop.2015.09.011.
[176] A. Bresson, Influence de la minéralogie sur le comportement des mortiers de ciment au jeune âge, (2006). https://corpus.ulaval.ca/jspui/handle/20.500.11794/19047 (accessed May 21, 2021).
[177] Proprietes des betons - Adam M. Neville - Librairie Eyrolles, n.d. https://www.eyrolles.com/BTP/Livre/proprietes-des-betons-9782212013207/ (accessed May 21, 2021).
[178] S. Garcia Boivin, Retrait au jeune age du beton : developpement d'une methode experimentale et contribution a l'analyse physique du retrait endogene, These de doctorat, Marne-la-vallée, ENPC, 1999. http://www.theses.fr/1999ENPC9912.
[179] B. Kolani, Comportement au jeune âge des structures en béton armé à base de liants composés aux laitiers, phd, Université de Toulouse, Université Toulouse III - Paul Sabatier, 2012. http://thesesups.ups-tlse.fr/1849/.
[180] E. Guillon, Durabilité des matériaux cimentaires - Modélisation de l'influence des équilibres physico-chimiques sur la microstructure et les propriétés mécaniques résiduelles, (n.d.) 176.
[181] V.G. PAPADAKIS, Experimental investigation and theoretical modeling of silica fume activity in concrete, Cement and Concrete Research. 29 (1999) 79–86.
[182] E. Badogiannis, S. Tsivilis, V.G. Papadakis, E. Chaniotakis, The effect of metakaolin on concrete properties, in: Innovations and Developments In Concrete Materials And Construction, Thomas Telford Publishing, 2002: pp. 81–89. https://doi.org/10.1680/iadicmac.31791.0008.
[183] C.S. Poon, L. Lam, S.C. Kou, Y. Wong, R. Wong, Rate of pozzolanic reaction of metakaolin in high-performance cement pastes, Cement and Concrete Research. 31 (2001) 1301–1306. https://doi.org/10.1016/S0008-8846(01)00581-6.

[184] M. Frías, J. Cabrera, Influence of MK on the reaction kinetics in MK/lime and MK-blended cement systems at 20°C, Cement and Concrete Research. 31 (2001) 519–527. https://doi.org/10.1016/S0008-8846(00)00465-8.
[185] C. Magniont, G. Escadeillas, C. Oms-Multon, P. De Caro, The benefits of incorporating glycerol carbonate into an innovative pozzolanic matrix, Cement and Concrete Research. 40 (2010) 1072–1080. https://doi.org/10.1016/j.cemconres.2010.03.009.
[186] A. Bourdot, C. MAGNIONT, M. Lagouin, C. NIYIGENA, P. Evon, S. Amziane, Impact of Bio-Aggregates Properties on the Chemical Interactions with Mineral Binder, Application to Vegetal Concrete, Journal of Advanced Concrete Technology. 17 (2019) 542–558. https://doi.org/10.3151/jact.17.542.
[187] A. Ahmed, J. Kamau, J. Pone, F. Hyndman, H. Fitriani, Chemical Reactions in Pozzolanic Concrete, MAMS. 1 (2019) 128–133. https://doi.org/10.32474/MAMS.2019.01.000120.
[188] A. Bourdot, T. Moussa, A. Gacoin, C. Maalouf, P. Vazquez, C. Thomachot-Schneider, C. Bliard, A. Merabtine, M. Lachi, O. Douzane, H. Karaky, G. Polidori, Characterization of a hemp-based agro-material: Influence of starch ratio and hemp shive size on physical, mechanical, and hygrothermal properties, Energy and Buildings. 153 (2017) 501–512. https://doi.org/10.1016/j.enbuild.2017.08.022.
[189] R.S. Nicolas, Approche performantielle des bétons avec métakaolins obtenus par calcination flash, phdthesis, Université Paul Sabatier - Toulouse III, 2011. https://tel.archives-ouvertes.fr/tel-00756481 (accessed May 22, 2021).
[190] M. Visagie, E. Kearsley, Properties of foamed concrete as influenced by air-void parameters, Concrete/Beton. 101 (2002) 8–14.
[191] M. Morozov, P. Strizhak, Investigation of energy efficiency of innovate thermal insulating materials and their influence on the building heat regime, MATEC Web of Conferences. 23 (2015) 01025. https://doi.org/10.1051/matecconf/20152301025.
[192] S. Alix, L. Lebrun, S. Marais, E. Philippe, A. Bourmaud, C. Baley, C. Morvan, Pectinase treatments on technical fibres of flax: Effects on water sorption and mechanical properties, Carbohydrate Polymers. 87 (2012) 177–185. https://doi.org/10.1016/j.carbpol.2011.07.035.
[193] A. Grosman, C. Ortega, Capillary Condensation in Porous Materials. Hysteresis and Interaction without Pore Blocking/Percolation Process, Langmuir. 24 (2008) 3977. https://doi.org/10.1021/la703978v.
[194] P. Glouannec, F. Collet, C. Lanos, P. Mounanga, T. Pierre, P. Poullain, S. Prétot, J. Chamoin, A. Zaknoune, Propriétés physiques de bétons de chanvre, Matériaux & Techniques. 99 (2011) 657–665. https://doi.org/10.1051/mattech/2011047.
[195] Z. Zhang, Modelling of sorption hysteresis and its effect on moisture transport within cementitious materials, (n.d.) 237.
[196] C. Hall, Water sorptivity of mortars and concretes: a review, Magazine of Concrete Research. 41 (1989) 51–61. https://doi.org/10.1680/macr.1989.41.147.51.
[197] D. Bentz, M. Ehlen, C. Ferraris, E.J. Garboczi, Sorptivity-Based Service Life Predictions For Concrete Pavements, 1 (2001).
[198] N.S. Martys, C.F. Ferraris, Capillary transport in mortars and concrete, Cement and Concrete Research. 27 (1997) 747–760. https://doi.org/10.1016/S0008-8846(97)00052-5.
[199] E.K.K. Nambiar, K. Ramamurthy, Sorption characteristics of foam concrete, Cement and Concrete Research. 37 (2007) 1341–1347. https://doi.org/10.1016/j.cemconres.2007.05.010.
[200] L. Yang, D. Gao, Y. Zhang, J. Tang, Y. Li, Relationship between sorptivity and capillary coefficient for water absorption of cement-based materials: theory analysis and experiment, Royal Society Open Science. 6 (2019) 190112. https://doi.org/10.1098/rsos.190112.
[201] G. Pia, L. Casnedi, U. Sanna, Pore Size Distribution Influence on Suction Properties of Calcareous Stones in Cultural Heritage: Experimental Data and Model Predictions, Advances in Materials Science and Engineering. 2016 (2016) e7853156. https://doi.org/10.1155/2016/7853156.

[202] D. Falliano, D. De Domenico, G. Ricciardi, E. Gugliandolo, Experimental investigation on the compressive strength of foamed concrete: Effect of curing conditions, cement type, foaming agent and dry density, Construction and Building Materials. 165 (2018) 735–749. https://doi.org/10.1016/j.conbuildmat.2017.12.241.
[203] Afnor, NF EN 1504-2, (2005).
[204] N.Z. Muhammad, A. Keyvanfar, M.Z. Abd. Majid, A. Shafaghat, J. Mirza, Waterproof performance of concrete: A critical review on implemented approaches, Construction and Building Materials. 101 (2015) 80–90. https://doi.org/10.1016/j.conbuildmat.2015.10.048.
[205] Q. Zhou, Q. Xu, Experimental study of waterproof membranes on concrete deck: Interface adhesion under influences of critical factors, Materials & Design. 30 (2009) 1161–1168. https://doi.org/10.1016/j.matdes.2008.06.023.
[206] B. Yan, F. Ren, M. Cai, C. Qiao, Influence of new hydrophobic agent on the mechanical properties of modified cemented paste backfill, Journal of Materials Research and Technology. 8 (2019) 5716–5727. https://doi.org/10.1016/j.jmrt.2019.09.039.
[207] N. Neithalath, R. K, Structure and properties of aerated concrete: A review, Cement and Concrete Composites. 22 (2000) 321–329. https://doi.org/10.1016/S0958-9465(00)00016-0.
[208] I. Petrov, E. Schlegel, Application of automatic image analysis for the investigation of autoclaved aerated concrete structure, Cement and Concrete Research. 5 (1994) 830–840.
[209] J. Alexanderson, Relations between structure and mechanical properties of autoclaved aerated concrete, Cement and Concrete Research. 9 (1979) 507–514. https://doi.org/10.1016/0008-8846(79)90049-8.
[210] P. Matar, J. Barhoun, Effects of waterproofing admixture on the compressive strength and permeability of recycled aggregate concrete, Journal of Building Engineering. 32 (2020) 101521. https://doi.org/10.1016/j.jobe.2020.101521.
[211] M. Cong, Properties of foamed concrete containing water repellents, Construction and Building Materials. 123 (2016) 106–114. https://doi.org/10.1016/j.conbuildmat.2016.06.148.
[212] https://www.lesmaisons.com/modeles-de-maisons/maison-individuelle-lesmaisonscom-96.
[213] S. Ganesan, M. Azree, M.A. Othuman Mydin, M. Yazid, M.Y. Mohd YUNOS, M. Nasrun, M.N. Mohd Nawi, Thermal Properties of Foamed Concrete with Various Densities and Additives at Ambient Temperature, Applied Mechanic and Material. 747 (2015) 230–233. https://doi.org/10.4028/www.scientific.net/AMM.747.230.
[214] N.A. Al-Azri, Y.H. Zurigat, N.Z. Al-Rawahi, Development of bioclimatic chart for passive building design, International Journal of Sustainable Energy. 32 (2013) 713–723. https://doi.org/10.1080/14786451.2013.813026.
[215] A.D. Tran Le, Etude des transferts hygrothermiques dans le béton de chanvre et leur application au bâtiment (sous titre: simulation numérique et approche expérimentale), (2010).

List of Figures

List of Tables

Appendices

Appendix 1: Technical sheet of GGBFS

ecocem FRANCE

FICHE TECHNIQUE

Laitier granulé de haut-fourneau moulu CE produit à Fos-sur-Mer

Répond à la norme européenne **NF EN 15167-1** Laitier granulé de haut-fourneau moulu pour utilisation dans le béton, mortier et coulis – Partie 1 : Définitions, exigences et critères de conformité.

Le certificat CE de constance des performances **1 164-CPR-LGM001**, a été renouvelé le 10 janvier 2017, par le CERIB, organisme notifié n° 1164. Ecocem est un laitier moulu de classe A, suivant les distinctions faites dans la norme **NF EN 206/CN**.

FABRICATION

Ecocem est produit par le séchage et le broyage du laitier granulé de haut-fourneau.

Le laitier granulé est obtenu par trempe à l'eau du laitier à la sortie des hauts-fourneaux de Fos sur-Mer, au moyen de granulateur de nouvelle génération (INBA®).

Le **taux de vitrification moyen obtenu est supérieur à 90 %** (mesure par diffraction de rayons X).

Ecocem est livré en vrac.

CE

COMPOSITION CHIMIQUE (centésimale moyenne)

SiO_2	Al_2O_3	Fe_2O_3	CaO	MgO	TiO_2	SO_3	Cl^-	S^{2-}	Na_2O	K_2O	$Na_2O_{eq.}$
37,3	10,7	0,2	43,0	6,5	0,7	0,1	0,01	0,8	0,23	0,35	0,45

Module chimique (CaO+MgO)/SiO2 : > 1,25 (≥1,2 : classe A selon NF EN 206-1/CN)

CARACTÉRISTIQUES CHIMIQUES (valeurs indicatives représentatives)

Formulation		Résistances en compression			INDICE D'ACTIVITÉ			Temps de prise initiale (min)
Ecocem	Ciment référence	7jrs	28jrs	90jrs	7jrs	28jrs	90jrs	
0%	100 %	43	55	64	--			170
50 %	50 %	31	55	66	72 %	100 %	103 %	210
Limites de la norme produit NF EN 15 167-1					≥ 45%	≥ 70%		< 2 x Tps ciment
Limites classe A selon norme NF EN 206/CN					≥ 65%	≥ 85%		

AUTRES CARACTÉRISTIQUES

Surface spécifique blaine	4 450 ± 250 cm²/g ≥ 2 750 cm²/g : NF EN 15167-1 ≥ 4 200 cm²/g : classe A selon NF EN 206/CN
Diamètre médian indicatif (d50)	11 µm
Passant à 32 µm	≥ 95 %
Masse volumique	2,90 ± 0,03 g/cm³
Densité apparente	0,8 ± 0,1 g/cm³
Indice [cie L*a*b*] avec CR410	L* = 89,5 ± 2
Perte au feu (950 °C)	< 1,5 %
Humidité (100 °C)	< 0,5 %

Révision : 11/03/2019
Les valeurs indiquées sont des valeurs moyennes, elles peuvent varier légèrement dans les limites autorisées par la norme de référence.

Appendix 2: Technical sheet of Metakaolin

argeco DEVELOPPEMENT

FICHE TECHNIQUE PRODUIT

argicem®

METAKAOLIN (NF P 18-513) A - F_M - W_M

CARACTERISTIQUES CHIMIQUES

Exigences chimiques	Norme appliquée	Valeur garantie	Valeur moyenne
Silice (SiO_2) + Alumine (Al_2O_3)	NF EN 196-2	> 90,0 %	92,45 %
Chlorures	NF EN 196-2	< 0,1 %	0,002 %
Sulfates	NF EN 196-2	< 1,0 %	0,20 %
Oxyde de calcium (CaO) libre	NF EN 451-1	< 1,0 %	0,322 %
Teneur en alcalins totaux (Na_2O équivalent)	NF EN 196-2	-	0,251 %
Oxyde de magnesium (MgO)	NF EN 196-2	< 4,0 %	0,19 %
Perte au feu	NF EN 196-2	< 4,0 %	1,30 %
Valeur au bleu MB_F	NF EN 933-9	< 10 g/kg	7,48 g/kg
Fixation de l'hydroxyde de calcium ($Ca(OH)_2$)	Essai Chapelle modifié	> 700 mg/g	773,9 mg/g

Les valeurs moyennes, données à titre indicatif, sont les valeurs des douze derniers mois

CARACTERISTIQUES PHYSIQUES

Exigences physiques	Norme appliquée	Valeur garantie	Valeur moyenne
Masse volumique des particules	NF EN 196-6 NF EN 197-7	2500 kg/m3 ± 200 kg/m3	2551 kg/m3
Finesse	NF EN 933-1	Passant à 0.063 mm ≥ 70 % (Catégorie F_M)	74,6 %
Indice d'activité à 28 jours	NF EN 196-1	> à 100 % (Type A)	i_{28} = 101,93 %
Demande en eau	NF EN 196-3	≤ 1,15 (Catégorie W_M)	1,08
Temps de début de prise	NF EN 196-3	< 25 %	3,40 %
Stabilité	NF P 18-513	Si (CaO) libre < 1%	N.A.
Surface spécifique BET	NF ISO 9277	-	15,65 m^2/g

Les valeurs moyennes, données à titre indicatif, sont les valeurs des douze derniers mois

Appendix 3: Technical sheet of Hemp shiv

Référence	C005
Composition	chènevotte 95%, fibres 5% (en volume)
Granulométrie	1 à 5 mm - granulométrie répartie
Conditionnement	**Sac de 100 litres** - 13.5 kg (=100 L de mortier soit 0.100 m^3)
Palettisation	30 sacs/ palettes
Densité du granulat sec	**130 à 140** kg/m^3
Conductivité thermique seul	λ =**0,048** W/m.K
Capacité de rétention d'eau (EN 13041)	370 ml/l
Ph en suspension à 10%	6,7 à 7,2
Stockage	au sec à l'abri des intempéries

Voie hum

Technichanvre - BP 3 - 29340 RIEC SUR BELON
Service technique et commercial :
Tél : +0033 (0)2 98 06 45 34 - Fax : +0033 (0)2 98 06 56 68
technichanvre@wanadoo.fr - www.technichanvre.com

Technichanvre®
les solutions chanvre pour le bâtiment

Appendix 4: Cost and CO_2 emissions calculation

Table 27 : *Cost and CO_2 emissions for each raw material.*

	Product	CO_2 emissions (t-CO_2/t)	Cost (€/kg)
	CEM I	0.84	0.12
	GGBFS	0.052	0.09
	MK	0.33	0.49
	HS	0	0.5
Admixtures	SP	1.88	5.85
	Acc		3.95
	FA		15

$$FC\ CO_2\ emission = \sum CO_2\ Raw\ material\ per\ kg \times Mass\ of\ raw\ material\ (kg\ in\ m^3)$$

$$FC\ cost = \sum Cost\ Raw\ material\ per\ kg\ \times Mass\ of\ raw\ material\ (kg\ in\ m^3)$$

Appendix 5 : Air bubbles distribution

C100P0H0P

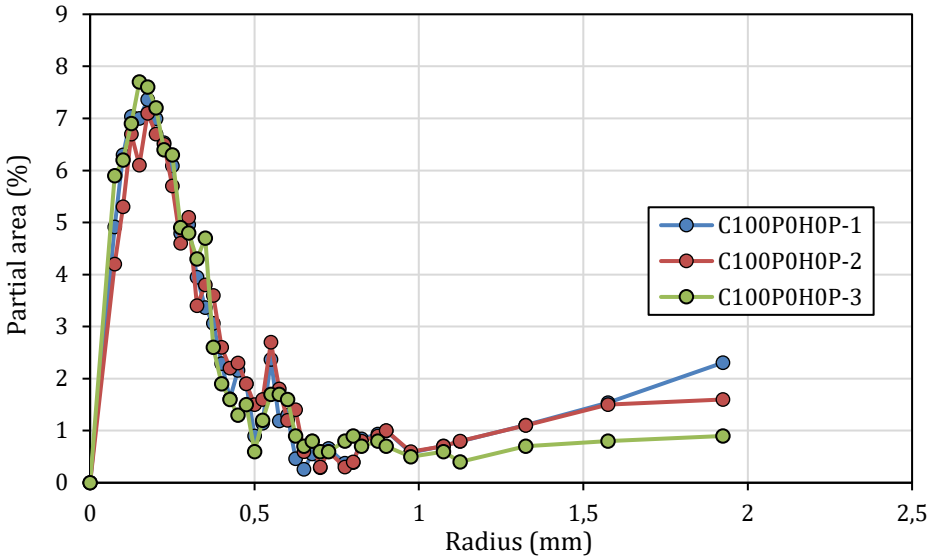

Figure 4.1: *Air bubble distribution for the three sections of C100P0H0P.*

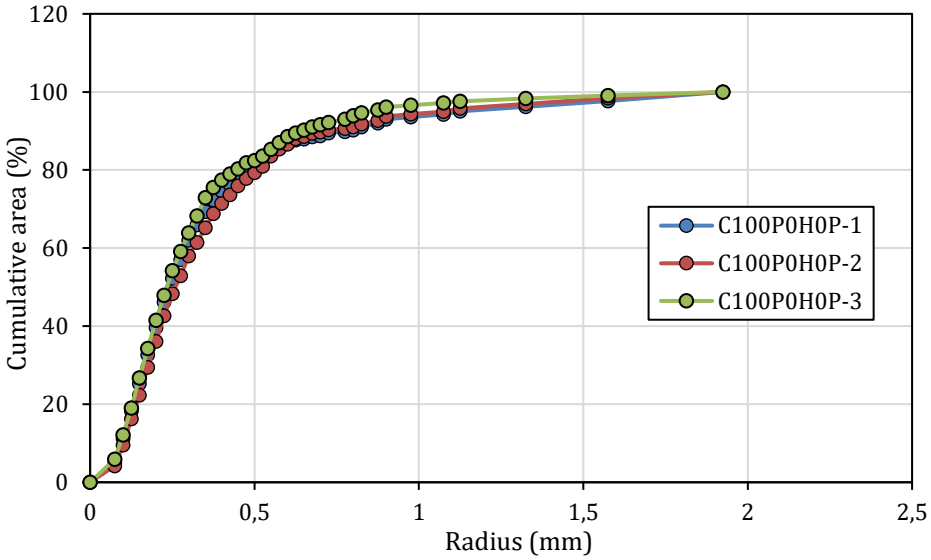

Figure 4.2: *Cumulative air bubble distribution for the three sections of C100P0H0P.*

C100P0H0D

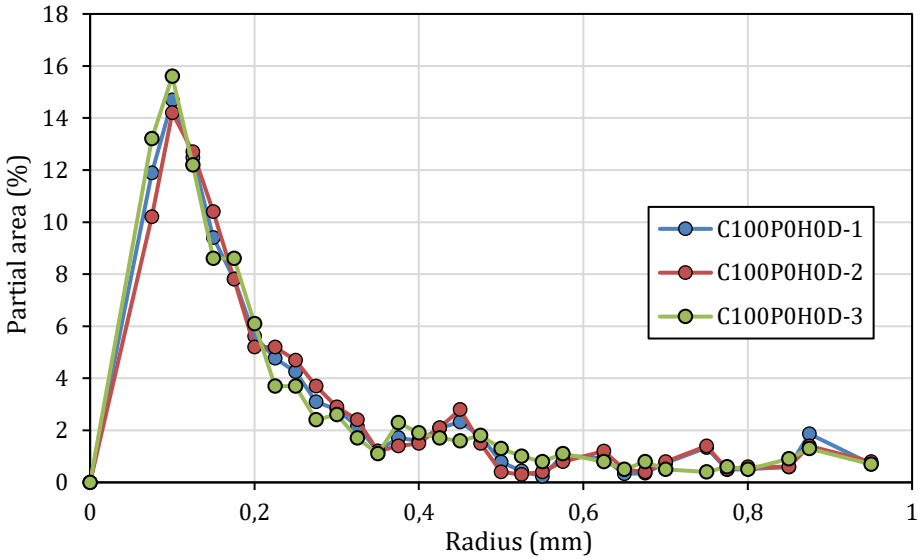

Figure 4.3: *Air bubble distribution for the three sections of C100P0H0D.*

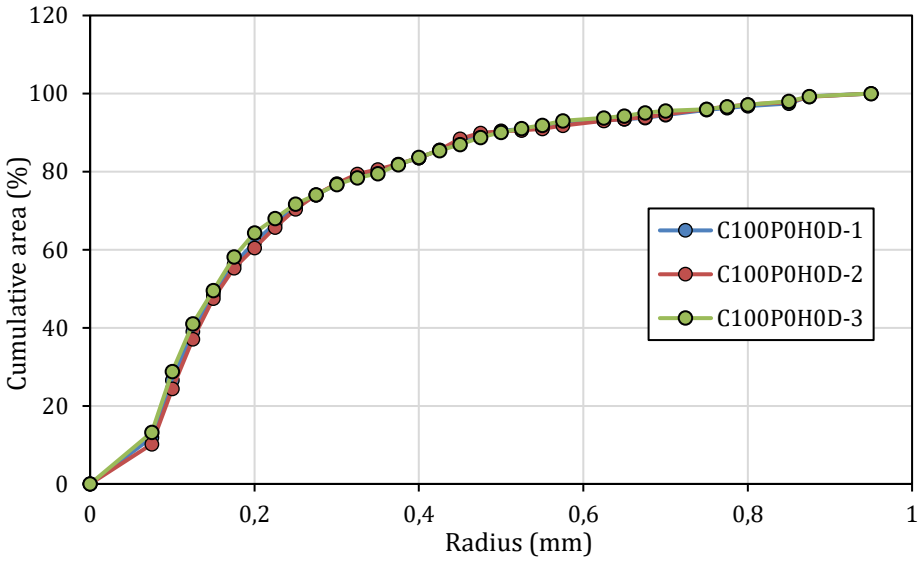

Figure 4.4: *Cumulative air bubble distribution for the three sections of C100P0H0D.*

C70P30H0P

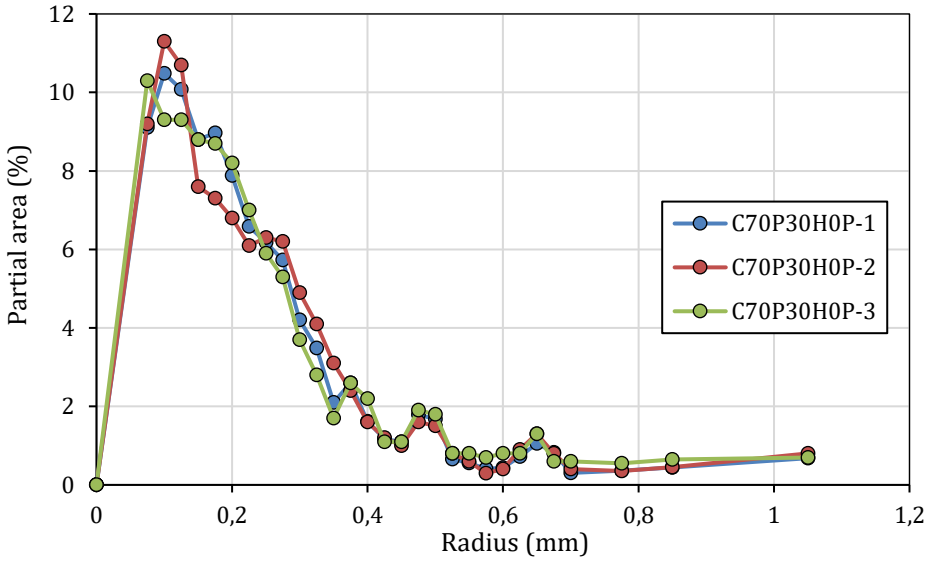

Figure 4.5: *Air bubble distribution for the three sections of C70P30H0P.*

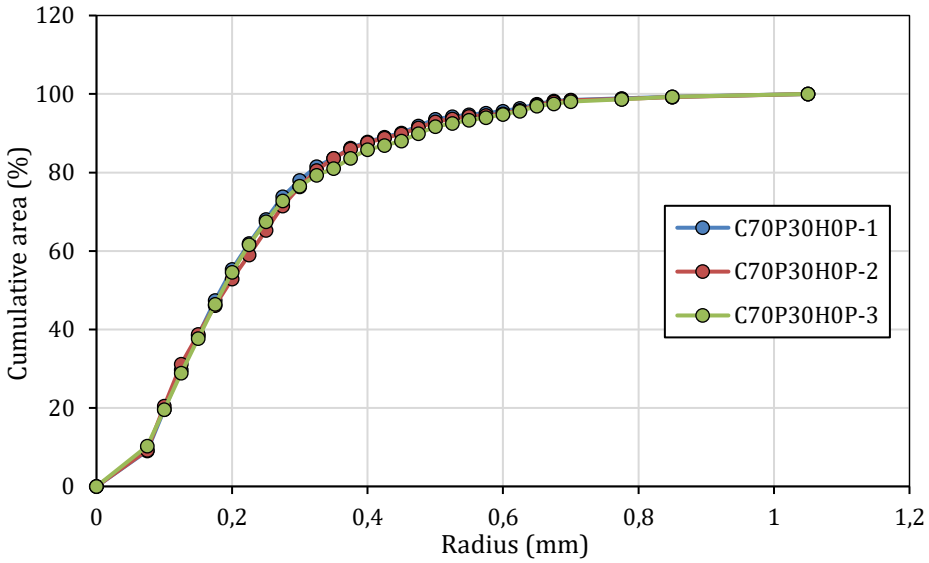

Figure 4.6: *Cumulative air bubble distribution for the three sections of C70P30H0P.*

C70P30H0D

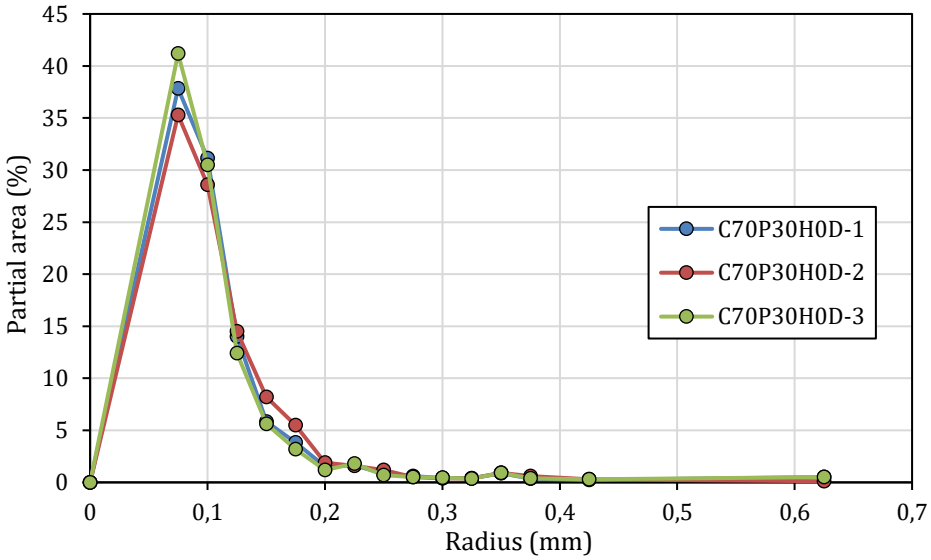

Figure 4.7: *Air bubble distribution for the three sections of C70P30H0D.*

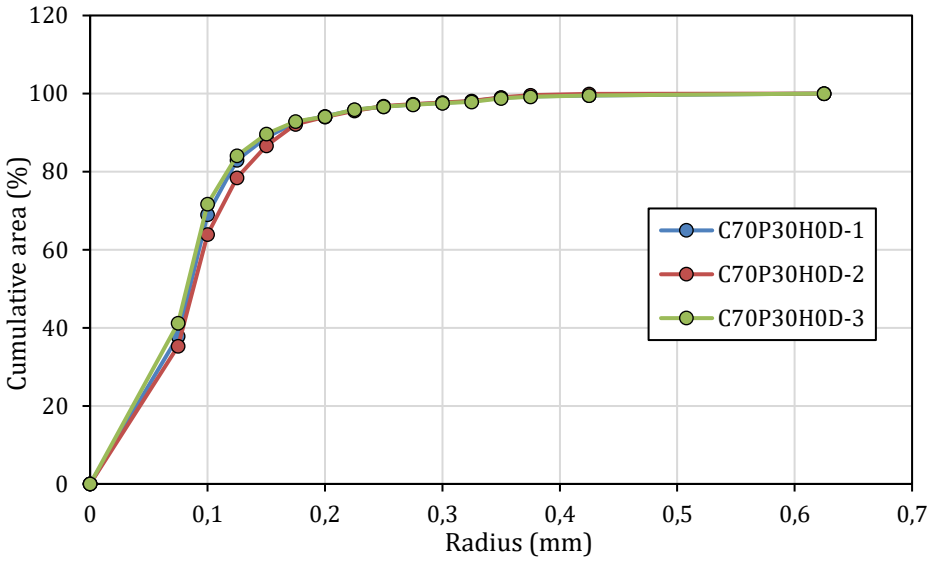

Figure 4.8: *Cumulative air bubble distribution for the three sections of C70P30H0D.*

C65P30H5P

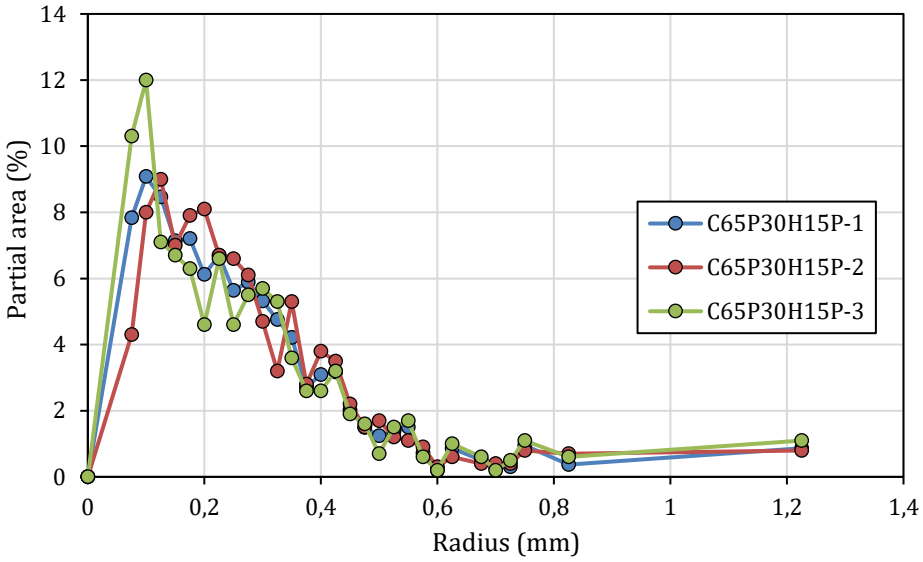

Figure 4.9: *Air bubble distribution for the three sections of C65P30H5P.*

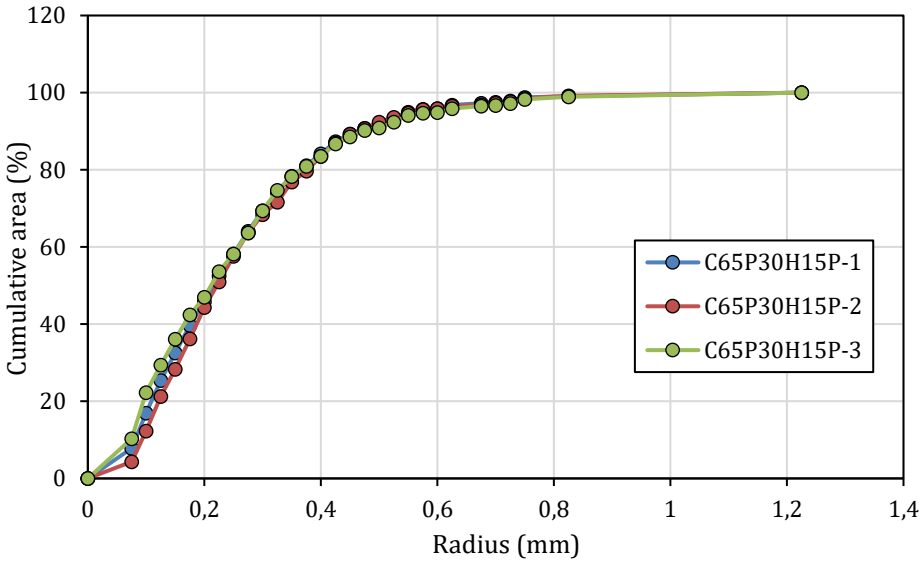

Figure 4.10: *Cumulative air bubble distribution for the three sections of C65P30H5P.*

C55P30H15P

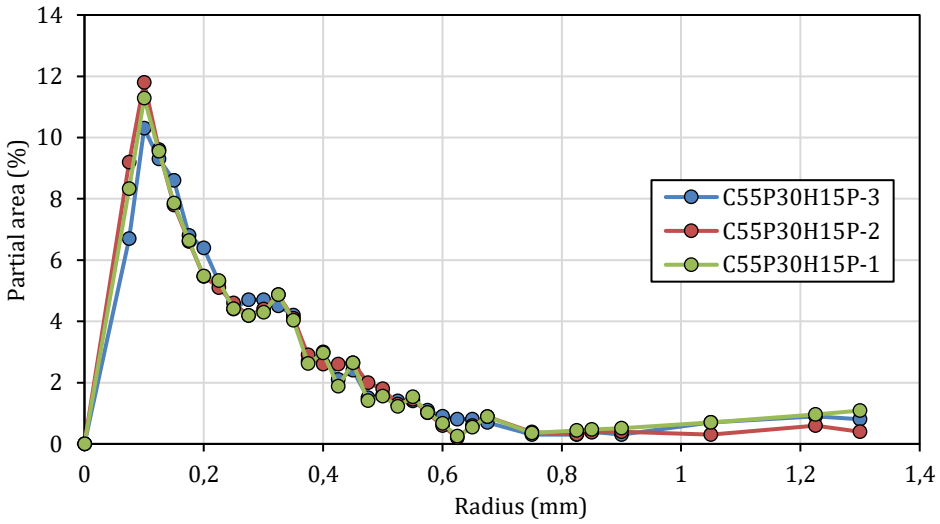

Figure 4.11: *Air bubble distribution for the three sections of C55P30H15P.*

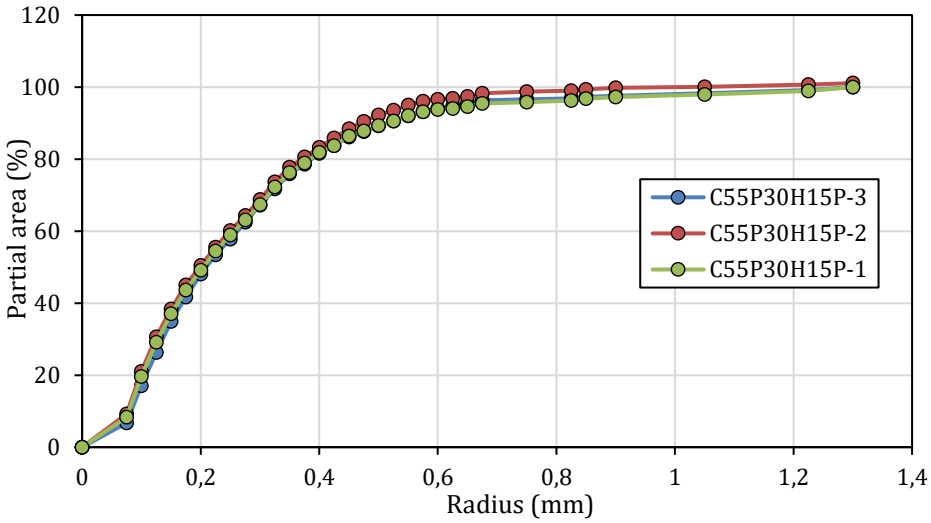

Figure 4.12: *Cumulative air bubble distribution for the three sections of C55P30H15P.*

C55P30H15D

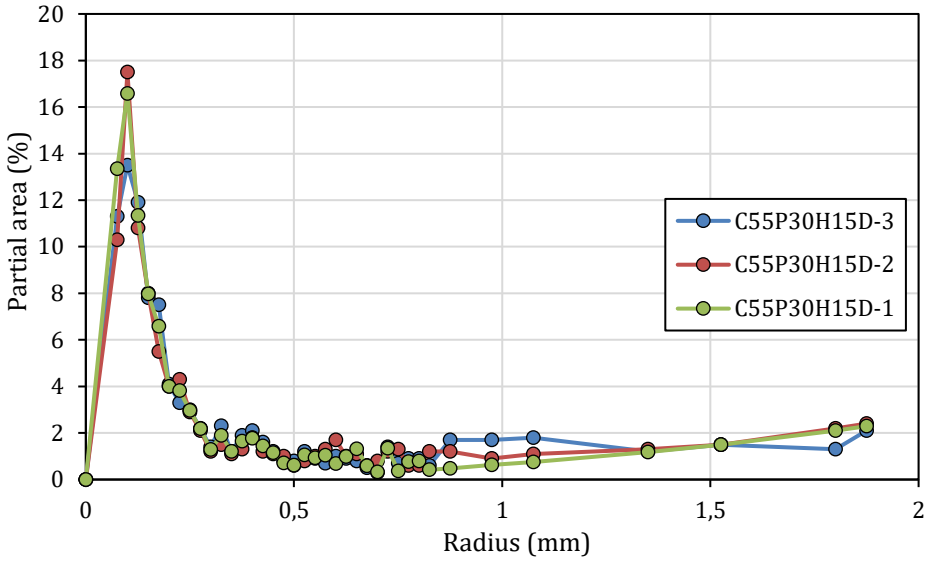

Figure 4.13: *Air bubble distribution for the three sections of C55P30H15D.*

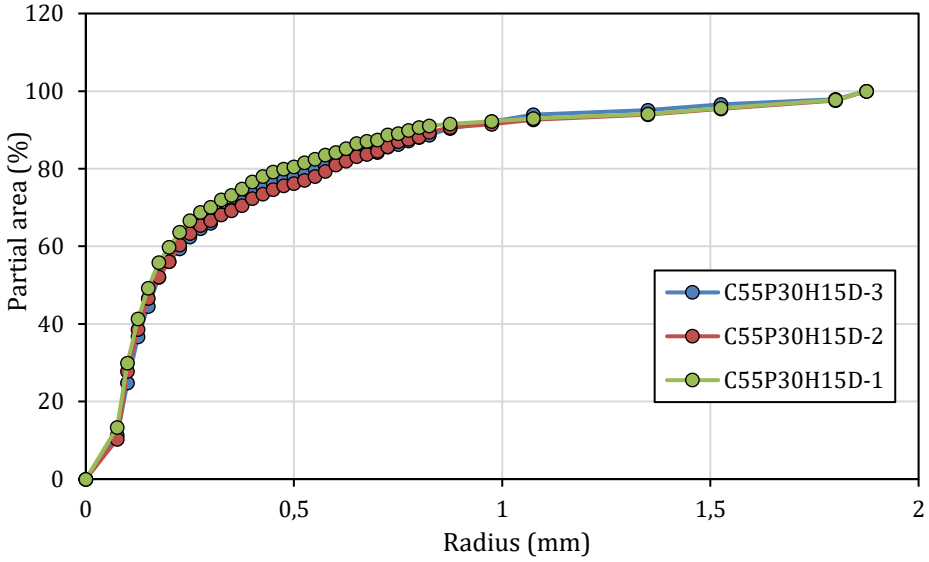

Figure 4.14: *Cumulative air bubble distribution for the three sections of C55P30H15D.*

Appendix 6: Capillary absorption coefficient of foamed concretes

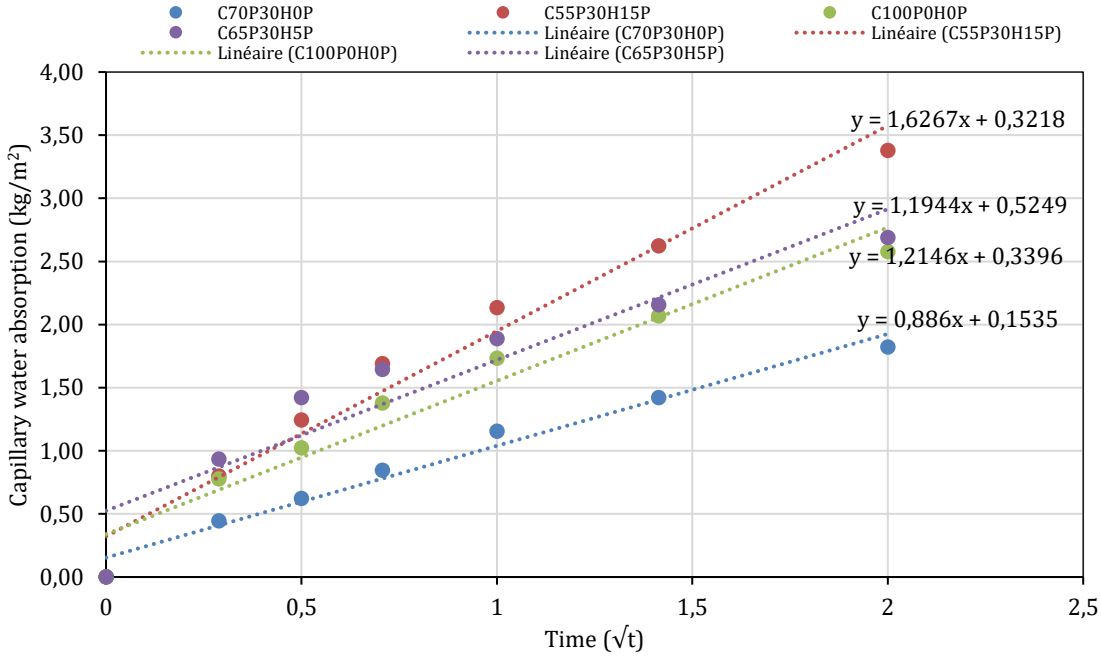

Figure 4.15: *Capillary absorption coefficient for foamed concretes using preformed method.*

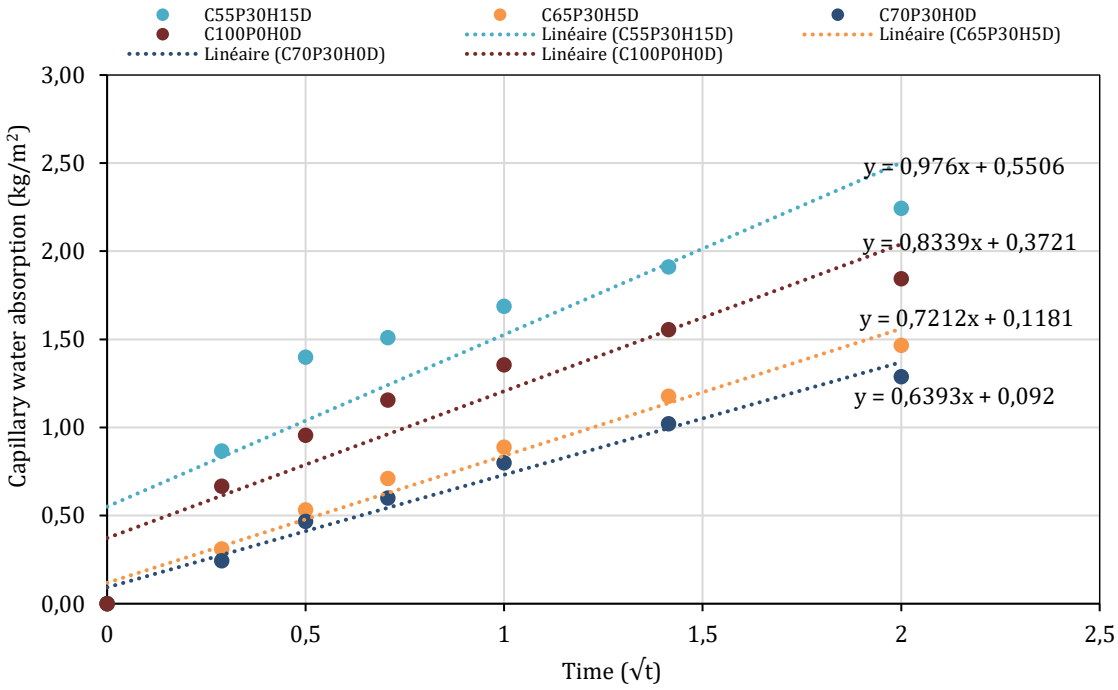

Figure 4.16: *Capillary absorption coefficient for foamed concretes using direct method.*

Appendix 7: Capillary absorption coefficient using water repellents

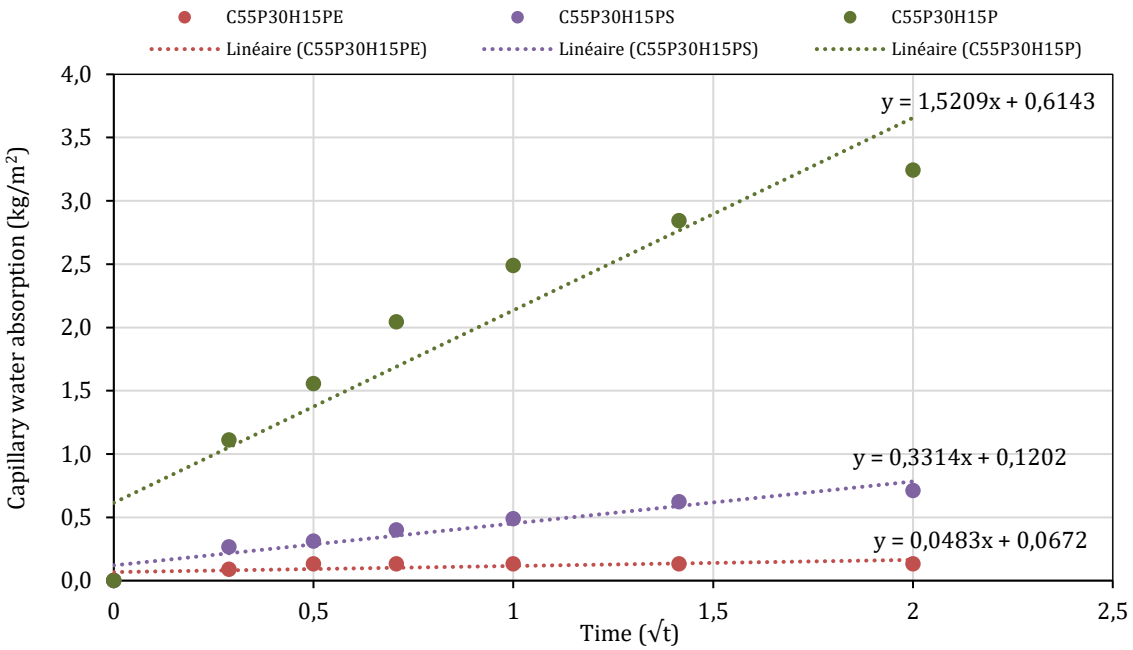

Figure 4.17: *Capillary absorption coefficient of C55P30H15P using water repellents.*

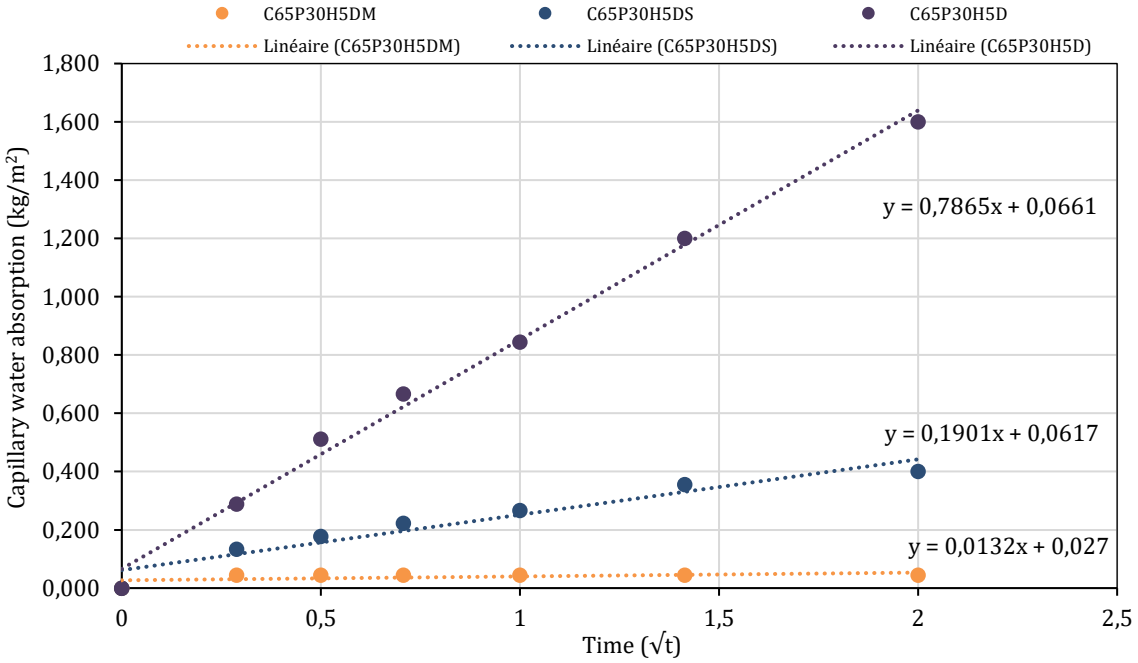

Figure 4.18: *Capillary absorption coefficient of C65P30H15D using water repellents.*

Abstract

Foamed concrete is a construction material consisting of a cementitious matrix and air bubbles network. This material offers excellent thermal performance. In addition, hemp concrete is an insulating material based on hemp aggregates which improves both the comfort and energy consumption of the habitats. But these two materials have modest mechanical performance and impermeability. Moreover, the studies that discuss the combination of these two materials are rare, so the objective of this study is to create a non-autoclaved foam concrete incorporated with hemp shiv, insulating, semi-structural and waterproof.

In this context, the research is started with a formulation of foam concrete with 100% of cement and used as a control foam concrete. In addition, another control formulation is used but by replacing 30% of portlandite cement by 10% of metakaolin and 20% of ground granulated blast-furnace slag respecting the norm NF EN-206, where metakaolin is an activator of the slag to improve the cohesion and the adhesion of the binder.

Based on these two control formulations, different cement amounts (5, 10 and 15 wt%) were replaced by hemp shiv in order to evaluate the density, mechanical and thermal properties, production cost and CO_2 emissions of these concretes. Then, the best formulations that give acceptable results to create bio-based foam concretes for semi-structural applications were chosen. Criteria that were chosen on the basis are compressive strength of at least 2 MPa (the minimum compression to achieve a self-supporting material) and thermal conductivity and density lower than 0.2 W/(m.K) and 700 kg/m^3, respectively. After that, four formulations with different amount of hemp shiv and pozzolanic additives are selected to be produced by two different methods, as preformed and direct method. Firstly, the porous structure and the cementitious matrix of these concretes are studied, then the mechanical, thermal and hydric properties of all foamed biobased concretes are investigated, and it is found that the hemp shiv particles and the pozzolanic additives have a negligible effect on the air bubble distribution of the foamed concretes produced by the preformed method, but it shows a remarkable effect on the foamed concretes produced by the direct method. Also, hemp shiv reduces the setting acceleration of concrete and reduces the mechanical strength, improves the thermal resistivity and increases the capillary absorption and adsorption of foamed concrete.

Once these concretes have been characterized, the best semi-structural (Rc > 2 MPa) and structural concretes (Rc > 17 MPa) are selected to improve their impermeability by using mass and surface water repellents. Physical and mechanical properties, and capillary absorption are studied to identify the water repellents effects on the properties and the waterproofing of bio-

based foamed concrete. Mass water repellents slightly improve the mechanical resistance of the foam concretes incorporated with hemp and the two water repellents make the foam concretes waterproof. Then, these two bio-based foamed concretes are assembled in a single semi-structural, insulator and waterproofing material, and the thermal performance of this material is studied in a model house by using a thermal numerical simulation and comparing the hygrothermal performance of this material by other insulators used in the market.

Keywords: Foamed concrete, Bio-based concrete, hemp shiv, insulating, pore distribution, waterproofing.

Résumé

Le béton mousse est un matériau de construction constitué d'une matrice cimentaire et de réseaux de bulles d'air. Ce matériau offre d'excellentes performances thermiques. Par ailleurs, le béton de chanvre est un matériau isolant à base de granulats de chanvre qui améliore le confort et la consommation énergétique des habitations. Mais ces deux matériaux présentent des performances mécaniques et une étanchéité limitée. De plus, de rares études traitent la combinaison de ces deux matériaux. L'objectif de cette étude est donc de créer un béton mousse non autoclavé incorporant des chènevottes, isolant semi-structurel et imperméable.

Dans ce contexte, la recherche a commencé par une formulation de béton mousse avec 100% de ciment et utilisée comme béton mousse témoin. De plus, une autre formulation témoin est utilisée mais en remplaçant 30% de ciment portlandite par 10% de métakaolin et 20% de laitier granulé de haut fourneau moulu respectant la norme NF EN-206, où le métakaolin est un activateur du laitier pour améliorer la cohésion et l'adhérence du liant.

Sur la base de sur ces deux formulations témoins, différentes quantités de ciment (5, 10 et 15 % en poids) ont été remplacées par de la chènevotte afin d'évaluer la densité, les propriétés mécaniques et thermiques, le coût de production et l'émission de CO_2 de ces bétons. Les meilleures formulations donnant des résultats acceptables pour créer des bétons mousses biosourcés pour des applications semi-structurelles ont été sélectionnées. Les critères qui ont été choisis sont basés sur une résistance à la compression supérieure à 2 MPa (la compression minimale pour obtenir un matériau autoporteur) et une conductivité thermique et une densité inférieure à 0,2 W/(m.K) et 800 kg/m^3, respectivement. Ensuite, quatre formulations avec différentes quantités de chanvre et d'additifs pouzzolaniques sont sélectionnées pour être produites par deux méthodes différentes de production (méthode préformée et méthode directe). Tout d'abord, la structure des pores et la matrice cimentaire de ces bétons sont étudiées, puis les propriétés mécaniques, thermiques et hydriques de tous les bétons mousses biosourcés sont analysées. Il est apparu que les particules de chanvre et les additifs pouzzolaniques ont un effet négligeable sur la distribution des bulles d'air du béton mousse produit par la méthode préformée, mais ils ont un effet remarquable sur le béton mousse produit par la méthode directe. En outre, le chanvre réduit l'accélération de la prise du béton et réduit la résistance mécanique, améliore la résistivité thermique et augmente l'absorption capillaire et l'adsorption du béton mousse.

Une fois ces bétons caractérisés, les meilleurs bétons semi-structurels (Rc > 2 MPa) et structurels (Rc > 17 MPa) sont sélectionnés pour être améliorés en termes d'imperméabilité en utilisant des hydrofuges de masse et de surface. Les propriétés physiques et mécaniques, ainsi que

l'absorption capillaire sont étudiées pour identifier les effets des hydrofuges sur les propriétés et sur l'imperméabilité du béton mousse biosourcé. Les hydrofuges de masse améliorent légèrement la résistance mécanique des bétons mousse incorporés aux chènevottes et les deux hydrofuges rendent les bétons mousse imperméables à l'eau. Ensuite, ces deux bétons mousse biosourcés sont assemblés en un seul matériau semi-structurel, isolant et imperméable, et la performance thermique de ce matériau est étudiée dans une maison modèle en utilisant une simulation numérique thermique et en comparant la performance hygrothermique de ce matériau à celle d'autres isolants traditionnellement utilisés sur le marché.

Mots-clés : Béton mousse, béton biosourcé, chènevotte, isolation, distribution des pores, étanchéité.